

# Serum metabolites in diagnostics and therapeutics

**Edited by**

Gregorio Peron and Donghai Lin

**Published in**

Frontiers in Molecular Biosciences



## FRONTIERS EBOOK COPYRIGHT STATEMENT

The copyright in the text of individual articles in this ebook is the property of their respective authors or their respective institutions or funders. The copyright in graphics and images within each article may be subject to copyright of other parties. In both cases this is subject to a license granted to Frontiers.

The compilation of articles constituting this ebook is the property of Frontiers.

Each article within this ebook, and the ebook itself, are published under the most recent version of the Creative Commons CC-BY licence. The version current at the date of publication of this ebook is CC-BY 4.0. If the CC-BY licence is updated, the licence granted by Frontiers is automatically updated to the new version.

When exercising any right under the CC-BY licence, Frontiers must be attributed as the original publisher of the article or ebook, as applicable.

Authors have the responsibility of ensuring that any graphics or other materials which are the property of others may be included in the CC-BY licence, but this should be checked before relying on the CC-BY licence to reproduce those materials. Any copyright notices relating to those materials must be complied with.

Copyright and source acknowledgement notices may not be removed and must be displayed in any copy, derivative work or partial copy which includes the elements in question.

All copyright, and all rights therein, are protected by national and international copyright laws. The above represents a summary only. For further information please read Frontiers' Conditions for Website Use and Copyright Statement, and the applicable CC-BY licence.

ISSN 1664-8714  
ISBN 978-2-8325-5765-5  
DOI 10.3389/978-2-8325-5765-5

## About Frontiers

Frontiers is more than just an open access publisher of scholarly articles: it is a pioneering approach to the world of academia, radically improving the way scholarly research is managed. The grand vision of Frontiers is a world where all people have an equal opportunity to seek, share and generate knowledge. Frontiers provides immediate and permanent online open access to all its publications, but this alone is not enough to realize our grand goals.

## Frontiers journal series

The Frontiers journal series is a multi-tier and interdisciplinary set of open-access, online journals, promising a paradigm shift from the current review, selection and dissemination processes in academic publishing. All Frontiers journals are driven by researchers for researchers; therefore, they constitute a service to the scholarly community. At the same time, the *Frontiers journal series* operates on a revolutionary invention, the tiered publishing system, initially addressing specific communities of scholars, and gradually climbing up to broader public understanding, thus serving the interests of the lay society, too.

## Dedication to quality

Each Frontiers article is a landmark of the highest quality, thanks to genuinely collaborative interactions between authors and review editors, who include some of the world's best academicians. Research must be certified by peers before entering a stream of knowledge that may eventually reach the public - and shape society; therefore, Frontiers only applies the most rigorous and unbiased reviews. Frontiers revolutionizes research publishing by freely delivering the most outstanding research, evaluated with no bias from both the academic and social point of view. By applying the most advanced information technologies, Frontiers is catapulting scholarly publishing into a new generation.

## What are Frontiers Research Topics?

Frontiers Research Topics are very popular trademarks of the *Frontiers journals series*: they are collections of at least ten articles, all centered on a particular subject. With their unique mix of varied contributions from Original Research to Review Articles, Frontiers Research Topics unify the most influential researchers, the latest key findings and historical advances in a hot research area.

Find out more on how to host your own Frontiers Research Topic or contribute to one as an author by contacting the Frontiers editorial office: [frontiersin.org/about/contact](https://frontiersin.org/about/contact)

# Serum metabolites in diagnostics and therapeutics

## Topic editors

Gregorio Peron — University of Brescia, Italy

Donghai Lin — Xiamen University, China

## Citation

Peron, G., Lin, D., eds. (2024). *Serum metabolites in diagnostics and therapeutics*. Lausanne: Frontiers Media SA. doi: 10.3389/978-2-8325-5765-5

# Table of contents

- 05 **Editorial: Serum metabolites in diagnostics and therapeutics**  
Gregorio Peron and Donghai Lin
- 08 **Targeted Metabolomic Analysis of Serum Fatty Acids for the Prediction of Autoimmune Diseases**  
Dimitris Tsoukalas, Vassileios Fragoulakis, Evangelia Sarandi, Anca Oana Docea, Evangelos Papakonstantinou, Gerasimos Tsilimidos, Chrysanthi Anamaterou, Persefoni Fragkiadaki, Michael Aschner, Aristidis Tsatsakis, Nikolaos Drakoulis and Daniela Calina
- 22 **Serum Metabolite Biomarkers Predictive of Response to PD-1 Blockade Therapy in Non-Small Cell Lung Cancer**  
Xiaoqun Nie, Liliang Xia, Fang Gao, Lixia Liu, Yi Yang, Yingying Chen, Huangqi Duan, Yaxian Yao, Zhiwei Chen, Shun Lu, Ying Wang and Chen Yang
- 33 **Serum Metabolomic Patterns in Patients With Aldosterone-Producing Adenoma**  
Yule Chen, Hanjiang Wang, Ke Wang, Guodong Zhu, Zhishang Yang, Min Wang and Wenbin Song
- 42 **Stratification of ovarian cancer borderline from high-grade serous carcinoma patients by quantitative serum NMR spectroscopy of metabolites, lipoproteins, and inflammatory markers**  
Gyuntae Bae, Georgy Berezhnoy, André Koch, Claire Cannet, Hartmut Schäfer, Stefan Kommos, Sara Brucker, Nicolas Beziere and Christoph Trautwein
- 60 **Metabolic profiling reveals altered tryptophan metabolism in patients with kawasaki disease**  
Xue Fan, Ke Li, Xin Guo, Shengyou Liao, Qi Zhang, Yangkai Xu, Hongtu Cui, Lemin Zheng and Mingguo Xu
- 74 **Differences in the lipid metabolism profile and clinical characteristics between eosinophilic and non-eosinophilic acute exacerbation of chronic obstructive pulmonary disease**  
Yating Wang, Chun Chang, Sifan Tian, Juan Wang, Xiaoyan Gai, Qiqiang Zhou, Yahong Chen, Xu Gao, Yongchang Sun and Ying Liang
- 85 **Serum metabolomics analysis of biomarkers and metabolic pathways in patients with colorectal cancer associated with spleen-deficiency and qi-stagnation syndrome or damp-heat syndrome: a prospective cohort study**  
Min Zou, Yan-Sheng Zhang, Jin-Kai Feng, Hao Tu, Ming-Bin Gui, Ya-Nan Wang, Zi-Jie Yang, Zeng-Qiang Yang, Ming Xu, Wei-Qiang Wu and Feng Gao
- 96 **Metabolomics unveils the exacerbating role of arachidonic acid metabolism in atherosclerosis**  
Sai Ma, Songqing He, Jing Liu, Wei Zhuang, Hanqing Li, Chen Lin, Lijun Wang, Jing Feng and Lei Wang



- 110 **Associations of serum cystatin C concentrations with total mortality and mortality of 12 site-specific cancers**  
Changzhi Huang, Jiayi Lu, Jing Yang, Zhenling Wang, Dong Hang and Zan Fu
- 119 **From serum metabolites to the gut: revealing metabolic clues to susceptibility to subtypes of Crohn's disease and ulcerative colitis**  
Fan Li, Zhaodi Wang, Tongyu Tang, Qi Zhao, Zhi Wang, Xiaoping Han, Zifeng Xu, Yu Chang, Hongyan Li, Sileng Hu, Chanjiao Yu, Shiyu Chang, Yue Liu and Yuqin Li



## OPEN ACCESS

EDITED AND REVIEWED BY  
Wolfram Weckwerth,  
University of Vienna, Austria

\*CORRESPONDENCE  
Gregorio Peron,  
✉ gregorio.peron@unibs.it

RECEIVED 15 November 2024  
ACCEPTED 19 November 2024  
PUBLISHED 28 November 2024

CITATION  
Peron G and Lin D (2024) Editorial: Serum  
metabolites in diagnostics and therapeutics.  
*Front. Mol. Biosci.* 11:1528799.  
doi: 10.3389/fmolb.2024.1528799

COPYRIGHT  
© 2024 Peron and Lin. This is an open-access  
article distributed under the terms of the  
[Creative Commons Attribution License \(CC  
BY\)](#). The use, distribution or reproduction in  
other forums is permitted, provided the  
original author(s) and the copyright owner(s)  
are credited and that the original publication  
in this journal is cited, in accordance with  
accepted academic practice. No use,  
distribution or reproduction is permitted  
which does not comply with these terms.

# Editorial: Serum metabolites in diagnostics and therapeutics

Gregorio Peron<sup>1\*</sup> and Donghai Lin<sup>2</sup>

<sup>1</sup>Department of Molecular and Translational Medicine, University of Brescia, Brescia, Italy, <sup>2</sup>Department of Chemical Biology, College of Chemistry and Chemical Engineering, Xiamen University, Xiamen, China

## KEYWORDS

serum, metabolites, pathogens, disease treatment, serum metabolome, molecular, mechanisms

## Editorial on the Research Topic

### Serum metabolites in diagnostics and therapeutics

The field of serum metabolomics is revolutionizing our understanding of disease mechanisms, and at the same time offers unprecedented opportunities in diagnostics and personalized medicine. This Research Topic entitled “*Serum Metabolites in Diagnostics and Therapeutics*” presents a collection of research articles that, overall, show the potential of metabolomics to capture real-time biochemical snapshots: especially this aspect makes metabolomics a valuable approach for early disease detection, therapeutic monitoring, and biomarker discovery. By examining the latest methodologies and their clinical applications, this Research Topic is intended as an integrated perspective on the advancements and clinical applications of serum metabolomics.

Serum metabolomics, which assesses small-molecule metabolites circulating in blood, directly reflects metabolic processes affected by disease, lifestyle, and genetic factors. Metabolites like amino acids, lipids, and nucleotides often reveal distinctive patterns in disease states, allowing clinicians to observe shifts linked to cellular dysfunction and pathological pathways (Qiu et al., 2023). Recent studies highlight the value of these metabolic signatures in early detection, as even minor changes in metabolite levels can indicate disease onset before clinical symptoms emerge (Al-Sulaiti et al., 2023). For instance, the literature emphasizes that metabolomics has wider applications in clinics than genomic and proteomic approaches because it provides a dynamic readout of the current physiological state (Ramautar et al., 2013). In fact, unlike genomics that reflects potential risk, metabolomics presents a functional snapshot, making it ideal for real-time monitoring.

The improvement of analytical technologies such as ultra-performance liquid chromatography (UHPLC) and high-resolution mass spectrometry (MS) has played a pivotal role in the progress of serum metabolomics. These techniques allow to efficiently separate the chemical constituents of a complex matrix like serum and detect metabolites at trace levels, being this crucial for profiling minor but diagnostically significant changes of serum metabolic composition. For instance, in a study published in this Research Topic, UHPLC-MS/MS was used to identify complex lipid profiles linked to cardiovascular and inflammatory diseases, providing new insights into vascular health. High-throughput nuclear magnetic resonance (NMR) spectroscopy is also widely used to perform serum metabolomics and especially for metabolite identification. Because it allows for robust and non-destructive analysis of samples, it is suitable for routine clinical applications. Together, UHPLC-MS and NMR allow for comprehensive metabolomic profiling and can highlight

biomarkers that could serve as early indicators for conditions like cancer, diabetes, and neurodegenerative diseases.

Computational advancements in machine learning (ML) and artificial intelligence (AI) have also catalyzed the field's growth. The interpretation of high-dimensional data generated by metabolomics is often challenging and requires sophisticated tools to identify patterns and relationships between metabolites and disease phenotypes (Ratray et al., 2018). Several studies in this Research Topic integrated AI and multivariate statistics to enhance predictive capabilities: for instance, deep learning models have been used to classify patients based on serum profiles and predict the outcomes of metabolic syndrome. This AI-driven approach enhances predictive accuracy by modeling complex, nonlinear relationships that cannot be managed with traditional statistical methods. Moreover, as metabolomic data grows, ML techniques can adaptively improve, increasing their potential applications (e.g., cancer detection and monitoring of chronic diseases).

The clinical applications of serum metabolomics extend across diagnostics, disease classification, and therapeutic management. In cancer, early detection remains crucial for improving patient outcomes (Brockhoven et al., 2023), and the analysis of serum biomarkers can represent a non-invasive and accessible alternative to biopsies. For instance, in a study of this Research Topic authors identified lipid biomarkers that can be potentially monitored for distinguishing malignant states. Also, serum metabolites may have a role as indicators of therapeutic efficacy of cancer therapies, as highlighted in another article, particularly in chemotherapy response. Furthermore, the possibility to track metabolic changes over time allows clinicians to adjust therapies based on patient-specific responses, promoting more personalized treatments that reduce adverse effects.

Similar considerations can be made for chronic diseases like diabetes and cardiovascular disease. A study published in this Research Topic explored metabolic profiles that predict treatment outcomes in patients with type 2 diabetes and identified serum markers linked to insulin resistance and glucose regulation. This highlights metabolomics as a tool not only for diagnosis but also for tracking longitudinal metabolic changes, supporting timely intervention. Similarly, in inflammatory diseases, metabolomics can detect shifts in lipid and amino acid profiles that correlate with inflammatory markers, offering insights into disease mechanisms and potential intervention points.

Despite these advancements, challenges remain in translating serum metabolomics from research into clinical practice, particularly in terms of standardization and reproducibility. The variability in metabolite measurement across different platforms and protocols can complicate the validation of biomarkers. As one article in the Research Topic advocates, harmonizing analytical protocols—standardizing sample preparation, instrument calibration, and data processing—is essential for achieving reproducible and comparable results. This standardization would not only facilitate clinical adoption but also support large-scale

biomarker validation studies, which are essential for establishing diagnostic thresholds and reference ranges in metabolomics.

Ultimately, the research presented in this Research Topic, coupled with recent findings from wider literature, highlights serum metabolomics as a cornerstone of precision diagnostics. By capturing dynamic biochemical snapshots, serum metabolomics not only allows for early disease detection but also supports personalized medicine, enabling treatment decisions that align with the patient's unique metabolic profile. The integration of AI with metabolomics, combined with the continued refinement of analytical technologies and standardization efforts, promises a future where metabolomics becomes routine in medical diagnostics and therapeutic monitoring. Continued investment in these areas is essential to unlock the full potential of serum metabolomics, transforming it from a powerful research tool into a staple of clinical practice.

To conclude, as the Guest Editors, we would like to thank all the Authors that contributed to this Research Topic by publishing their research, as well as the Reviewers and the Assistant and Academic Editors for their valuable support.

## Author contributions

GP: Writing—original draft, Writing—review and editing. DL: Writing—review and editing.

## Funding

The author(s) declare that no financial support was received for the research, authorship, and/or publication of this article.

## Conflict of interest

The authors declare that the research was conducted in the absence of any commercial or financial relationships that could be construed as a potential conflict of interest.

The author(s) declared that they were an editorial board member of *Frontiers*, at the time of submission. This had no impact on the peer review process and the final decision.

## Publisher's note

All claims expressed in this article are solely those of the authors and do not necessarily represent those of their affiliated organizations, or those of the publisher, the editors and the reviewers. Any product that may be evaluated in this article, or claim that may be made by its manufacturer, is not guaranteed or endorsed by the publisher.

## References

- Al-Sulaiti, H., Almaliti, J., Naman, C. B., Thani, A., and Yassine, H. (2023). Metabolomics approaches for the diagnosis, treatment, and better disease management of viral infections. *Metabolites* 13, 948. doi:10.3390/metabo13080948
- Brockhoven, F., Raphael, M., Currier, J., Jäderholm, C., Mody, P., Shannon, J., et al. (2023). REPRESENT recommendations: improving inclusion and trust in cancer early detection research. *Br. J. Cancer* 129, 1195–1208. doi:10.1038/s41416-023-02414-8
- Qiu, S., Cai, Y., Yao, H., Lin, C., Xie, Y., Tang, S., et al. (2023). Small molecule metabolites: discovery of biomarkers and therapeutic targets. *Signal Transduct. Target Ther.* 8, 132. doi:10.1038/s41392-023-01399-3
- Ramautar, R., Berger, R., van der Greef, J., and Hankemeier, T. (2013). Human metabolomics: strategies to understand biology. *Curr. Opin. Chem. Biol.* 17, 841–846. doi:10.1016/j.cbpa.2013.06.015
- Ratray, N. J. W., Deziel, N. C., Wallach, J. D., Khan, S. A., Vasiliou, V., Ioannidis, J. P. A., et al. (2018). Beyond genomics: understanding exposotypes through metabolomics. *Hum. Genomics* 12, 4. doi:10.1186/s40246-018-0134-x



# Targeted Metabolomic Analysis of Serum Fatty Acids for the Prediction of Autoimmune Diseases

Dimitris Tsoukalas<sup>1,2,3\*†</sup>, Vassileios Fragoulakis<sup>4†</sup>, Evangelia Sarandi<sup>2,5†</sup>, Anca Oana Docea<sup>6†</sup>, Evangelos Papakonstantinou<sup>2</sup>, Gerasimos Tsilimidos<sup>2</sup>, Chrysanthi Anamaterou<sup>2</sup>, Persefoni Fragkiadaki<sup>5</sup>, Michael Aschner<sup>7</sup>, Aristidis Tsatsakis<sup>3,5</sup>, Nikolaos Drakoulis<sup>8</sup> and Daniela Calina<sup>1</sup>

<sup>1</sup> Department of Clinical Pharmacy, Faculty of Pharmacy, University of Medicine and Pharmacy, Craiova, Romania,

<sup>2</sup> Metabolomic Medicine, Health Clinic for Autoimmune and Chronic Diseases, Athens, Greece, <sup>3</sup> E.I.Nu.M, European Institute of Nutritional Medicine, Rome, Italy, <sup>4</sup> The Golden Helix Foundation, London, United Kingdom, <sup>5</sup> Laboratory of Toxicology and Forensic Sciences, Medical School, University of Crete, Heraklion, Greece, <sup>6</sup> Department of Toxicology, Faculty of Pharmacy, University of Medicine and Pharmacy, Craiova, Romania, <sup>7</sup> Department of Molecular Pharmacology, Albert Einstein College of Medicine, The Bronx, NY, United States, <sup>8</sup> Research Group of Clinical Pharmacology and Pharmacogenomics, Faculty of Pharmacy, School of Health Sciences, National and Kapodistrian University of Athens, Athens, Greece

## OPEN ACCESS

### Edited by:

Francois-Pierre Martin,  
Nestle Institute of Health Sciences  
(NIHS), Switzerland

### Reviewed by:

Michal Jan Markuszewski,  
Medical University of Gdansk, Poland  
Gregorio Peron,  
University of Barcelona, Spain

### \*Correspondence:

Dimitris Tsoukalas  
research@metabolomicmedicine.com

<sup>†</sup>These authors have contributed  
equally to this work as co-first authors

### Specialty section:

This article was submitted to  
Metabolomics,  
a section of the journal  
Frontiers in Molecular Biosciences

**Received:** 14 August 2019

**Accepted:** 16 October 2019

**Published:** 01 November 2019

### Citation:

Tsoukalas D, Fragoulakis V, Sarandi E,  
Docea AO, Papakonstantinou E,  
Tsilimidos G, Anamaterou C,  
Fragkiadaki P, Aschner M, Tsatsakis A,  
Drakoulis N and Calina D (2019)  
Targeted Metabolomic Analysis of  
Serum Fatty Acids for the Prediction  
of Autoimmune Diseases.  
Front. Mol. Biosci. 6:120.  
doi: 10.3389/fmolb.2019.00120

Autoimmune diseases (ADs) are rapidly increasing worldwide and accumulating data support a key role of disrupted metabolism in ADs. This study aimed to identify an improved combination of Total Fatty Acids (TFAs) biomarkers as a predictive factor for the presence of autoimmune diseases. A retrospective nested case-control study was conducted in 403 individuals. In the case group, 240 patients diagnosed with rheumatoid arthritis, thyroid disease, multiple sclerosis, vitiligo, psoriasis, inflammatory bowel disease, and other AD were included and compared to 163 healthy individuals. Targeted metabolomic analysis of serum TFAs was performed using GC-MS, and 28 variables were used as input for the predictive models. The primary analysis identified 12 variables that were statistically significantly different between the two groups, and metabolite-metabolite correlation analysis revealed 653 significant correlation coefficients with 90% level of significance ( $p < 0.05$ ). Three predictive models were developed, namely (a) a logistic regression based on Principal Component Analysis (PCA), (b) a straightforward logistic regression model and (c) an Artificial Neural Network (ANN) model. PCA and straightforward logistic regression analysis, indicated reasonably well adequacy (74.7 and 78.9%, respectively). For the ANN, a model using two hidden layers and 11 variables was developed, resulting in 76.2% total predictive accuracy. The models identified important biomarkers: lauric acid (C12:0), myristic acid (C14:0), stearic acid (C18:0), lignoceric acid (C24:0), palmitic acid (C16:0) and heptadecanoic acid (C17:0) among saturated fatty acids, Cis-10-pentadecanoic acid (C15:1), Cis-11-eicosenoic acid (C20:1n9), and erucic acid (C22:1n9) among monounsaturated fatty acids and the Gamma-linolenic acid (C18:3n6) polyunsaturated fatty acid. The metabolic pathways of the candidate biomarkers are discussed in relation to ADs. The findings indicate that the metabolic profile of serum TFAs is associated with the presence of ADs and can be an adjunct tool for the early diagnosis of ADs.

**Keywords:** metabolomics, total fatty acids, biomarkers, inflammation, autoimmune diseases

## INTRODUCTION

The distinction between self and foreign is a tightly regulated process of the immune system, and defects in any of the participating mechanisms may lead to autoimmune diseases (ADs) (Menni et al., 2017). ADs incidence has increased dramatically over the last decades, currently affecting 50 million people in the US alone, especially at younger age (American Autoimmune Related Diseases Association, 2018). This rapid rise is possibly related to urbanization and higher socio-economic status, which have shifted nutritional preferences toward industrialized and low quality food with additives (Lerner et al., 2016). Twin studies unraveled key genetic determinants to ADs, especially for Major Histocompatibility Complex (MHC) haplotypes based on the findings that ADs concordance is higher in monozygotic twins (Theofilopoulos et al., 2017). However, familial association to genetic predisposition is higher in early-onset diseases suggesting that factors other than gene have an impact on ADs as well (Cooper et al., 1999; Gangemi et al., 2016; Negrei et al., 2016; Petrakis et al., 2017; Buha et al., 2018). In a recent review, the authors discuss the role of metabolic workload in immunological tolerance. Their proposed model suggests that chronic malnutrition, including high calories and nutrients intake for long periods, leads to the loss of tolerance through the generation of high pro-inflammatory T cells vs. the regulatory T cells that control inflammation (De Rosa et al., 2017). They propose that metabolic disturbance should be added to the hygiene model that has been applied to explain the rapid rise of chronic conditions (Bach, 2002). In addition, the World Health Organization (WHO) has suggested that the modifiable risk factors are the cause of chronic diseases in more than 80% of the cases (WHO, 2019). Modifiable factors are not presently satisfactorily considered within the standard medical approach (Strong et al., 2006; Tinetti et al., 2012).

Metabolomics can provide data for nutritional deficiencies, metabolic imbalance, environmental burden, and the gut microbiome. These factors can be modified through diet, lifestyle, supplements, and medication (Dahan et al., 2017). Key metabolic pathways, including the metabolism of glucose, protein and carbohydrates, fatty acids oxidation, mitochondrial function, neurotransmitters metabolism, and markers of oxidative stress and microbiome, are critically assessed through metabolomics (Lee et al., 2015). Quantification and evaluation of metabolites is the most effective method to capture time-dependent fluctuations and cellular metabolic state even prior to disease onset. Measurement of metabolites in patients with ADs and experimental ADs models have shown that there are significant metabolism fluctuations during the development of the disease (Leslie and Beyan, 2011; Hao et al., 2017). Findings from a randomized clinical trial on asthmatic children showed that urinary organic acids could be potential biomarkers to track the progression of the disease (Papamichael et al., 2018). Total fatty acids (TFAs) are valuable markers of inflammation and gain increasing attention in cases of chronic inflammation as in ADs (Serhan et al., 2007). We have previously reported the reference values of TFAs in a healthy Greek population, discussing the role of age, gender, diet, and measurement method of the levels

of TFAs (Tsoukalas et al., 2019). Given these observations, we measured serum TFAs in patients with ADs using targeted GC-MS, aiming to identify an improved combination of these biomarkers as a predictive factor for the presence of ADs (Tsoukalas et al., 2019).

## MATERIALS AND METHODS

### Subjects

A retrospective nested case-control study (Ernster, 1994) was conducted based on 5,850 subjects who visited the “Health clinic for autoimmune and chronic diseases” in Athens, Greece during the period of 3/8/2012 till 29/12/2017. All personal data were collected via the electronic platform of the clinic by trained administrative staff. The retrospective cohort study consisted of 1,950 patients for whom there were detailed records. A total of 240 patients with confirmed AD diagnosis were included in the present study, and 163 healthy individuals were assigned to the control group. Personal data of participants included age, gender, AD type, BMI, medical and nutritional history, and metabolomic analysis was performed in peripheral blood samples.

Exclusion criteria for the control group were obese ( $18.5 < \text{BMI} < 29.9$ ), athletes, pregnant or lactating women, individuals taking any supplements and/or medication, and individuals diagnosed with a chronic or acute disease.

Inclusion criteria for the control group were adults 18–60, not taking any medication or supplements, and not suffering by any chronic or acute disease. Inclusion criteria for AD patients were individuals diagnosed with thyroid AD (THY), and/or inflammatory bowel disease (IBD), and/or psoriasis (PSO), and/or rheumatoid arthritis (RA), and/or vitiligo (VIT), multiple sclerosis (MS) and/or other AD (full list of other AD and comorbidities is available in **Table S1**).

RA diagnosis was based on ACR/EULAR 2010 Rheumatoid Arthritis Classification Criteria (Kay and Upchurch, 2012).

IBD: diagnosed according to the Lennard-Jones diagnostic criteria for Ulcerative colitis and Crohn’s disease (Sherlock and Benchimol, 2017). PSO: Eligible PSO patients had to have chronic plaque type of PSO, and PASI score was used to assess the severity of the disease.

THY: As there are no international criteria for autoimmune thyroid disease classification diagnosis was performed according to levels of TSH, T3, and T4 and thyroid gland ultrasound to do disease classification.

VIT: Diagnosis performed according to Vitiligo Global Issues Consensus Conference (Kong et al., 2011).

MS: Diagnosis performed according to the McDonald 2010 diagnostic criteria (Polman et al., 2011).

Because the correlation of FA profiles to the clinical parameters of each AD is out of the scope of this paper, the clinical characteristics of patients for each AD group are not presented here but will be examined in separate studies. Also, it should be noted that in analyses such as we discuss here, matching of controls with cases is a commonly used method to control for confounding. However, there are several considerations concerning its proper use and, frequently, matching produces almost the same results with unmatching



analysis or the gain in efficiency is modest. Nonetheless, for statistically exploratory purposes, we attempted to match case and controls concerning age and gender using the Propensity Score Matching (PSM) which has become a popular approach to estimate causal treatment effects (Rose and Laan, 2009; Faresjö and Faresjö, 2010). The analysis showed that there was any gain in terms of efficiency and, thus, we decided to conduct an unmatched analysis and adjusted any potential confounder via the multivariate analysis (Figure S3).

## Ethics Approval

All procedures performed in studies involving human participants were under the ethical standards with the 1964 Helsinki declaration and its later amendments, or comparable ethical standards. Participants of the study were informed that their personal data would be processed according to the EU General Data Protection Regulation (GDPR), and fully anonymization would be used for this study. Informed consent was obtained from participants. The study has been approved by the scientific board of the “Health clinic for autoimmune and chronic diseases” and the Ethics Committee of the University of Crete (approval no. A.P. 39\_22112018).

## Chemicals

Methyl non-adeconoate (74208, Honeywell Fluka™, Honeywell, Seelze, Germany) was used as an internal standard. The calibration of the standard mixture was performed with a mixture of FA methyl esters (47885-U; Supelco-Sigma-Aldrich, St. Louis, MO, USA). All other solvents used were of the highest purity available [methanol, n-hexane (both from Merck KGaA, Darmstadt, Germany), HCl (301721) and 2,6-i-tert-butyl-4-methylphenol (BHT, B13781) (both from Sigma-Aldrich).

## Sample Preparation

The participants fasted for 12 h before their visit to the clinic. The metabolomic analysis was performed in the patients' blood samples using standard methodology (Tsoukalas et al., 2017). Briefly, peripheral blood was collected, and samples were centrifuged at  $1,500 \times g$  at  $4^\circ\text{C}$  to isolate the plasma. The plasma specimens were stored at  $-20^\circ\text{C}$  prior analysis for up to 24 h to ensure that the samples would not degrade. In the case of hemolysis of the blood samples, the blood collection was repeated.

The standard internal mixture (200  $\mu\text{l}$  methyl non-adeconoate in hexane containing BHT) was added to the 100  $\mu\text{l}$  plasma. The FAs were hydrolyzed and derivatized into methyl esters by the addition of 5% v/v methanolic HCl. Transmethylation was performed at  $90^\circ\text{C}$  for 60 min, and then the samples were brought to room temperature. The extraction of FA methyl esters was performed using hexane, and they were transferred to GC injection vials with a crimp cap.

As previously described, during the preparation of the samples lipid extraction prior to methylation was not included since with MS, the FAs can be directly identified in plasma without affecting the quantity or quality (Stellaard et al., 1990).

## Gas Chromatography-Mass Spectrometry

The carrier gas used was helium, and the injection volume was 1  $\mu\text{l}$  per sample.

The analysis was performed on an Agilent 7890A gas chromatograph (GC) coupled to a 5975C mass detector (MS quadrupole), equipped with an electron ionization (EI) source, operating in positive mode (Agilent Technologies, Santa Clara, CA, USA). The FA methyl esters were separated using an HP-5 ms capillary column (30 m  $\times$  250  $\mu\text{m}$   $\times$  0.25  $\mu\text{m}$ ). The conditions used were as follows: initial oven temperature was  $70^\circ\text{C}$ , the ramp rate was  $4^\circ\text{C}/\text{min}$ , the final temperature was  $290^\circ\text{C}$ , held for 4 min and the acquisition was in the scan mode.

## Statistical Analysis

All analyses were undertaken using IBM SPSS 22 (IBM Corp., Armonk, N.Y., USA) software<sup>1</sup> and the free R-project software (<https://www.r-project.org>). A chi-squared test with continuity correction was used to determine whether there is a significant association between gender and the presence of AD. In order to assess the normality of distributions for biomarkers, QQ-plots were applied for each one of them, while univariate analyses comparing differences between the means were conducted with a Mann-Whitney *U*-test ( $P < 0.05$ ). We further conducted a multivariate analysis of variance (MANOVA) which affords in a richer use of the information contained in the dataset and explore the effect of factors on several response variables via simultaneous hypotheses tests. In particular, the method runs the analysis on a new variable which is a linear combination of dependent variables and, thus, taking into account the potential correlation between exploratory biomarkers in our case. As an additional step, a Bonferroni correction was conducted to limit the type I error which is the probability to wrongly reject the null hypothesis at expenses of Type II errors (false negative) (Vinaixa et al., 2012). Principal Component Analysis (PCA) was applied to decompose the data into a few new variables which correspond to a linear combination of the originals. PCA is a multivariate data analysis aiming to reduce the dimension of expression data with minimum information loss, to visualize the similarities between the biological samples and to capture the most of the variation in the data set (Jolliffe et al., 2016). Outliers, the points that are distant from their own neighbors in the data set, were analyzed using a straightforward approach aiming to create a frequency of the continuous variables in a graphic form. After the outliers had been identified, the data were screened for outliers due to administrative (typo errors), and none was found. At the end, the deletion or retention of each outlier was clinically assessed. There was not any deletion since the sample was considered representative without any irregular pattern and, thus, we did not run any analysis to reduce the influence of the outliers. Next, with a binary response variable (“with” and “without” the AD) as an outcome, we built a logistic regression model including as independent variables the set of the principal components. The estimation of the model parameters is expressed via odds ratios. Since, frequently, PCA represents only a preliminary analysis of the available data,

<sup>1</sup> Available online at: <https://www.ibm.com/analytics/spss-statistics-software>



we also estimated the straightforward binary logistic regression with all the biomarkers as independent variables based on the backward selection method. Backward selection is a step-wise regression method which starts with a full model consisting of all candidate predictor variables (biomarkers). Based on the probability of the likelihood-ratio statistic, a removal testing was conducted to identify these variables that will remain in the model as statistically significant, via an iteration process (Heinze et al., 2018).

As a supplementary analysis, we employed an artificial neural network (ANN) framework to identify these biomarkers which predict better the presence of an AD. A mathematical presentation of this technique is out of the scope of the article and can be found by the interested reader elsewhere (Margarita, 2002). In short, ANN's are a family of a flexible form of equations which are often used for statistical analysis and data modeling, in which their role is perceived as an alternative to standard non-linear regression techniques. A neural network consists of a series of the so-called neurons that are interlinked to form a network, while each one of the links has a weight associated with it. ANN has an input layer, one or more hidden layers, and the output layer. An activation function is employed in the input layer, but also to the output layer to determine the outcome of the model. Differences amongst observed and predicted outcomes reinforce the model to readjust their weights of independent variables until a predetermined convergence is attained (the so-called "training" of the model). It must be mentioned that the optimal combination between the neurons and the number of layers which must be employed, remains a scientifically open question and in the most of cases, a trial-and-error approach is conducted by the researchers. In the present analysis, a Multilayer

Perceptron (MLP) feed forward neural network was used and trained with the error back propagation algorithm (Saduf, 2013). The number of neurons at the input layer was determined by the number of biomarkers used. A non-strict pre-selection of included variables was conducted based on the p-value provided by the straightforward logistic regression. We assumed two hidden layers to capture the non-linear nature of the model. A sigmoid activation function was employed in the output layer to estimate the probability of the presence (or not) of an AD as a binary outcome. Before the training of the model, all data were transformed through standardized rescaling. We separate our model to training data set, test set and holdout. Holdout or random subsampling is a technique to evaluate predictive models by partitioning the original sample into a training set to train the model, and a test set to evaluate it. Finally, Receiver Operating Characteristic (ROC) curve analysis was used to assess the accuracy of predictions based on sensitivity and specificity for all the above mentioned models (Hajian-Tilaki, 2013).

## RESULTS

### Characteristics of Patients With Autoimmune Diseases

In the present study, 403 participants were included; 240 patients with an AD (hereafter called case group) and 163 individuals in the control group. Among the patients, the majority had autoimmune thyroid disease (51.7%) while 29.7% of the total patients had more than one conditions (**Table S1**). **Figure 1** depicts the percentages of ADs per gender for those belonging to the case arm. The baseline characteristics of the case and the control group are depicted in **Table 1**. Age was also not

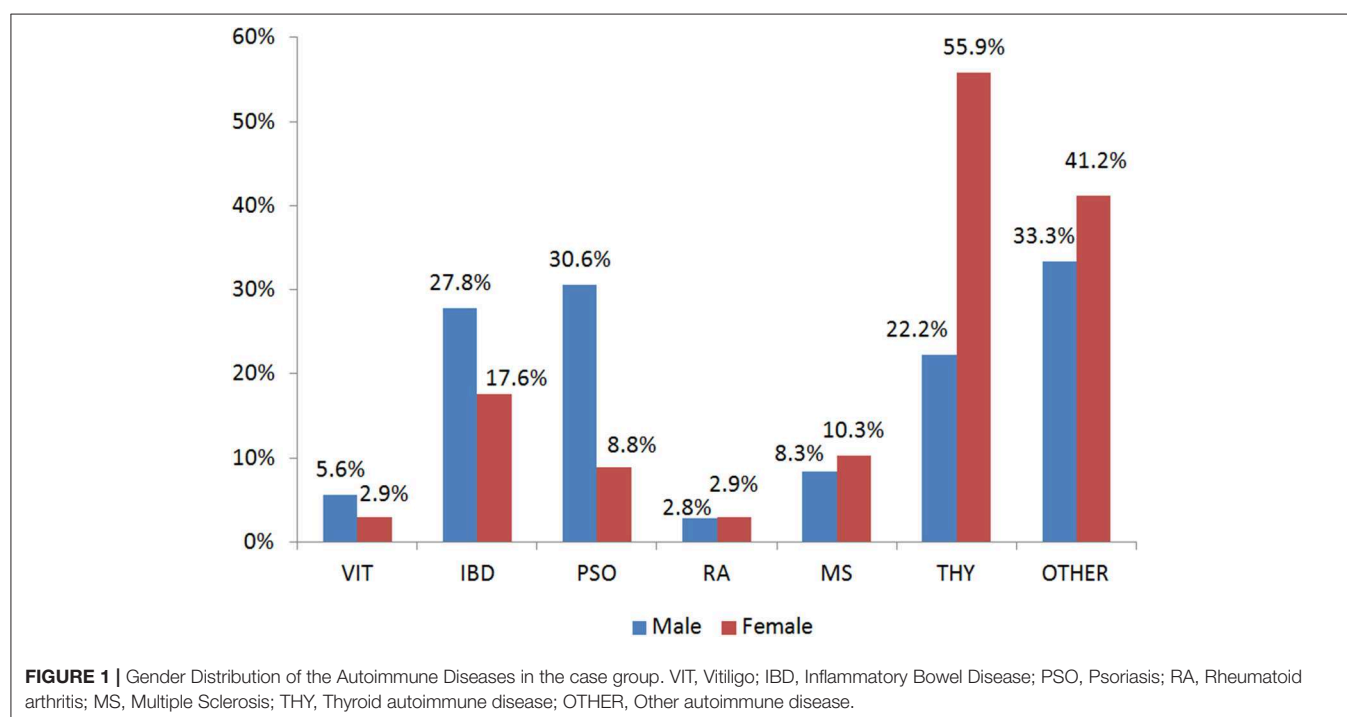


**TABLE 1** | Baseline characteristics of the case and control group.

	Case (n = 240)	Control (n = 163)
*Age (Mean ± SD)	44.43 ± 11.4	43.3 ± 9.9
*Female (%)	70.2	63.6
*BMI (Mean ± SD)	25.4 ± 5	24.9 ± 4
<sup>a</sup> Exercise n (%)	139 (56.7)	124 (75.2)
<sup>b</sup> Alcohol n (%)	108 (44.1)	43 (26.1)
THY n (%)	191(51.67)	0
RA n (%)	40 (10.81)	0
IBD n (%)	73 (19.7)	0
MS n (%)	32 (8.64)	0
PSO n (%)	62 (16.7)	0
VIT n (%)	15 (4)	0
OTHER n (%)	117 (31.67)	0

BMI, Body Mass Index; THY, Thyroid Autoimmune Disease; RA, Rheumatoid Arthritis; IBD, Inflammatory Bowel Disease; MS, Multiple Sclerosis; PSO, Psoriasis; VIT, Vitiligo;

<sup>a</sup>Exercise >3 times per week; <sup>b</sup>alcohol consumption of 3 glasses of wine per week; \* $p > 0.05$ ; \*\* $p < 0.001$ .

statistically significantly different between cases and controls ( $p > 0.05$ ), while females represented the 70.2 and 63.6% for the case and control group, respectively. The Body-Mass Index (BMI), defined as weight in kilograms divided by the square of the height in meters, was estimated at  $24.9 \pm 4$  for the control group, while was  $25.4 \pm 5$  in the cases group, indicating that there was not a statistical difference in the 95% level of significance ( $p = 0.5$ ). Concerning moderate physical exercise (3 times per week), 75.2% of total subjects answered positively in that question from the control group, while for the case group the corresponding percentage was limited to 56.7% ( $p = 0.011$ ). Moderate alcohol consumption (3 glasses of wine per week) for those belonging to the case group and control group was 44.1 and 26.1%, respectively ( $p < 0.001$ ).

## Targeted Metabolomic Profiling of Patients With Autoimmune Diseases and Healthy Controls

In total, 23 TFAs were tested on the available sample using GC-MS. Values of mean ± SD and median for each TFA, total omega-3, total omega-6, total Monounsaturated FA (MUFA), total Polyunsaturated FA (PUFA), total Saturated FA (SFA) for the two groups are listed in **Table 2**. The non-Parametric Mann-Whitney test was employed to detect differences among the variables in the two groups since Q-Q plots showed a deviation of normality. In total, 12 variables were statistically significant under the assumption of non-difference of distributions between the groups (**Table 2**). From the ratios included only total omega-6/total omega-3 was significantly different between the groups ( $p < 0.001$ ). C22:6n3, total omega 3, C18:3n6, C15:1, C20:1n9, C12:0, C15:0, C17:0, C18:0 and total omega 6/ total omega 3 ratio were statistically significantly different between the two groups after Bonferroni correction. Correlation analysis was performed in the two groups to identify metabolite-metabolite correlations with age and BMI being included as variables. Specifically, in

the case and control group, a total of 992 correlations were analyzed, among which 653 resulted in significant correlation coefficients in 90% level of significance ( $p < 0.05$ ). **Figure 2** depicts a scatter plot matrix showing the positive (blue) and negative (correlations) in the case group (left) and the control group (right). Overall, no statistically significant negative correlations were noted. Lauric acid (C12:0), pentadecanoic acid (C15:0), stearic acid (C18:0), myristoleic acid (C14:1), cis-10 pentadecanoic acid (C15:1) and arachidonic acid (C20:4n6) showed the strongest metabolite-metabolite correlations among the TFAs in the case group, while age was not correlated to any of these metabolites in any group.

Principal Component Analysis (PCA) was performed to visualize clusters within the samples. The data were screened for outliers due to administrative (typo errors), but none was identified. Due to the absence of missing data, all the available observations were included in the analysis. The Kaiser-Meyer-Olkin Measure of sampling adequacy for component analysis was estimated at 0.798, indicating reasonably well adequacy, while Bartlett's test of sphericity was statistically significant [ $X^2(253) = 5,102, p < 0.001$ ]. Analysis indicated that the first seven components, which were based on the variables shown in table 1 with correlation coefficient <75%, explained in total 70.3% of the variance, while the rest of the components explained <4.5% of the total variance each. Hence, the seven-component solution, with eigenvalues >1, was preferred as a solution for the model (**Table S2** and **Figure S1**). The component score coefficient matrix is depicted in **Table 3**. After the oblimin rotation, there was only a small correlation between each of the composite scores lower than 0.3 for all the components. **Figure 3** depicts the combination of factors, which show lower correlations, and have  $r$  coefficient < 0.030 in absolute values (pairwise score plots for components 1–7 in **Figure S2**).

## Association of TFAs and Autoimmune Disease

**Table 4** shows a binary logistic regression model which was used to test the research hypothesis regarding the relationship between the likelihood that a patient will have an AD and components 1–7 and gender. The log of the odds of a subject being affected by an AD was negative related to component one, five, six, and gender ( $p < 0.001$ ) and positive related to components two, three and seven ( $p < 0.001$ ), while the association with component four was not statistically significant (**Table 4**). The Hosmer & Lemeshow (H-L) goodness of fit test was estimated at  $X^2(8) = 29,450, p < 0.001$ , while Nagelkerke (pseudo)  $R^2$  was 0.268. The model predicts correctly 86.7 and 57.1% of those without and with an AD, respectively. The overall predictive score was also 74.7%.

## Selection of TFAs as Distinctive Markers for Autoimmune Disease

**Table 5** presents the results for the straightforward binary logistic regression model. The model initially included all the variables with a correlation <0.75 based on backward selection, while only 6 of them were statistically significant in the new model. Alcohol abstinence, myristic acid (C14:0),

**TABLE 2 |** Concentrations of FA and FA ratios in case and control groups.

	Case		Control		<i>p</i> -value
	Mean ± SD	Median	Mean ± SD	Median	
C183n3	14.6 ± 6.4	13.8	13.3 ± 10	12.2	0.006*
C205n3	50.6 ± 35	40.3	52.4 ± 74.2	35.7	0.297
<b>C226n3</b>	105.7 ± 50.9	98.2	118.9 ± 58.5	107.6	0.020
<b>Omega3</b>	178 ± 82.2	163.6	218.5 ± 129.6	194.2	<0.001*
C182n6	1597.2 ± 667.9	1534.1	1540.7 ± 573.3	1420.5	0.601
<b>C183n6</b>	24.7 ± 21.1	18.6	18.6 ± 15.7	14.8	0.001*
C203n6	107.7 ± 44.5	102.1	103.8 ± 40.9	100.1	0.558
C204n6	424.4 ± 124.7	413.9	402.9 ± 119.8	387.9	0.082
Omega6	2153.6 ± 755.9	2052.5	2065.4 ± 661.8	1937.9	0.313
C141	3.3 ± 7.7	1.9	2.1 ± 2.2	1.1	<0.001*
<b>C151</b>	28.4 ± 19.9	23.3	14.6 ± 18	6.6	<0.001*
C161n7	85.9 ± 57.9	72.7	68.7 ± 43.2	57.7	0.001*
C181n9cis	1001.6 ± 437	936.6	984.3 ± 425.1	886.2	0.516
<b>C201n9</b>	7.4 ± 3.8	6.4	5.5 ± 4.4	4.4	<0.001*
C221n9	1.5 ± 0.8	1.4	1.5 ± 2.1	1.0	<0.001*
C241n9	68.2 ± 20	65.4	69.7 ± 18.7	68.9	0.327
<b>C120</b>	8.1 ± 10.9	5.2	11.9 ± 11.7	7.2	<0.001*
C140	57.4 ± 36.8	48.9	58.5 ± 33.6	50.4	0.508
<b>C150</b>	12.5 ± 4.8	11.6	13.3 ± 5.2	12.8	0.119
C160	1740.6 ± 551.3	1631.9	1617.8 ± 363.8	1559.6	0.078
<b>C170</b>	16 ± 4.8	15.2	17 ± 4.8	16.8	0.026*
<b>C180</b>	516.2 ± 137	502.7	560.5 ± 127.5	558.9	<0.001*
C200	14.8 ± 4.3	14.4	15.3 ± 5.1	14.5	0.447
C220	37.9 ± 11.4	37.6	38.4 ± 10.8	36.5	0.700
C240	31.5 ± 10	31.5	32.8 ± 8.9	31.2	0.237
C204n6/ C205n3	11.5 ± 6.3	10.3	11.2 ± 5.7	10.1	0.901
C203n6/ C204n6	0.3 ± 0.2	0.2	0.3 ± 0.1	0.3	0.390
C18:2n6/ C20:3n6	17 ± 9.6	14.6	16.6 ± 7.9	15.7	0.677
<b>Omega6/ Omega3</b>	13.8 ± 6.4	12.7	11.1 ± 5	10.2	<0.001*
MUFA	1190.5 ± 478.9	1155.8	1140.3 ± 462	1029.8	0.188
PUFA	2330.7 ± 784.6	2274.6	2282.9 ± 702	2200.2	0.604
SFA	2433.5 ± 719	2325.6	2313.1 ± 522.3	2252.3	0.250
Total FA	5954.7 ± 1713.6	5743.7	5735.8 ± 1484.2	5538.0	0.197
BMI	25.4 ± 5	25.2	24.9 ± 4	24.4	0.502

Non-Parametric Mann-Whitney test. *Ho*, The distribution of characteristics is the same between the groups. Concentrations of fatty acids are expressed as  $\mu\text{mol/l}$ .

\* $p < 0.05$ . Omega6, Total omega6 fatty acids; Omega3, Total omega3 fatty acids; PUFA, Polyunsaturated fatty acids; MUFA, Monounsaturated fatty acids; SFA, Saturated fatty acids. Bold indicates that the variables are considered statistically significant ( $p < 0.05$ ) based on Bonferroni correction.

and lignoceric acid (C:24:0) were positively correlated to the absence of an AD. Negative correlations with the absence of ADs were found in lack of exercise, cis-10 pentadecanoic acid (C15:1) and gamma-linolenic acid (C18:3n6). The (H-L) test was  $X^2(8) = 10,374$ ,  $p = 0.240$ , while the Nagelkerke (pseudo)  $R^2$  was estimated at 0.556. Classification table indicates that the model predicts correctly 92.9 and 58.3% of those with and without an AD, respectively. The overall predictive accuracy was 78.9%. ROC analysis indicates that the area under the curve was 0.856 (0.819–0.893),  $p < 0.001$  (Figure 4).

## Validation of the Distinctive Model for Prediction of Autoimmune Disease

Artificial Neuronal Networks (ANN) analysis was employed based on the architecture of the model presented in Figure 5. Initially, we adopted 2 layers of architecture, with all available variables in the input layer to describe the non-linear nature of our data set. Due to over-fitting and the relatively limited number of our observations, we reduced our model. In the end, a model with two hidden layers and 11 variables were employed in accordance with the previous logistic model. We used 273 (67.7%) observations as training data set, 88 (21.8%) observations

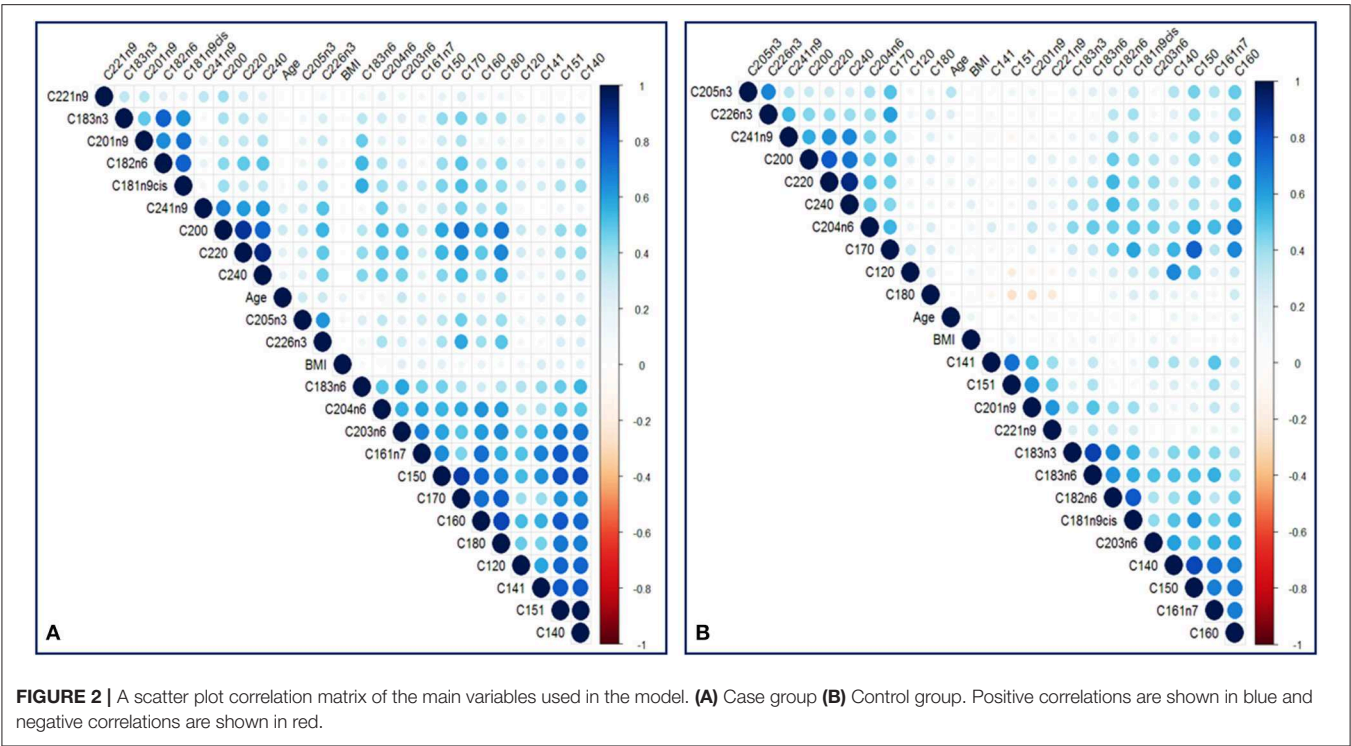


**TABLE 3 |** Component score coefficient matrix.

Component	1	2	3	4	5	6	7
C183n3	0.011	−0.005	−0.261	−0.028	−0.159	−0.052	0.189
C205n3	−0.003	−0.123	−0.011	0.500	0.041	−0.014	0.007
C226n3	−0.027	0.058	0.017	0.388	−0.015	0.008	0.048
C182n6	−0.050	0.045	−0.330	−0.036	−0.109	0.025	0.095
C183n6	0.007	−0.047	−0.303	−0.058	0.139	−0.088	0.008
C203n6	0.121	0.116	−0.017	−0.152	0.127	−0.064	−0.037
C204n6	0.076	0.132	−0.035	−0.015	−0.002	0.018	−0.092
C151	0.209	−0.128	−0.042	0.037	0.106	0.087	−0.081
C161n7	0.223	−0.064	0.023	−0.010	0.109	0.032	−0.167
C201n9	−0.049	−0.096	−0.319	0.132	0.069	0.110	−0.260
C221n9	0.062	0.023	0.034	−0.036	−0.163	−0.070	−0.682
C241n9	−0.065	0.261	0.068	0.109	0.047	0.018	−0.147
C120	0.137	−0.013	0.012	0.005	−0.284	−0.155	0.347
C140	0.227	−0.055	−0.009	0.010	−0.048	−0.035	0.095
C160	0.195	0.069	0.049	0.005	−0.063	0.045	−0.032
C170	0.069	0.085	−0.025	0.180	−0.089	−0.062	0.001
C180	0.112	0.178	0.107	−0.002	−0.132	0.014	0.199
C200	−0.011	0.272	0.011	−0.044	−0.028	−0.018	0.021
C240	−0.082	0.288	−0.079	−0.091	0.115	0.036	0.024
BMI	0.037	−0.004	0.007	−0.084	0.482	−0.058	0.091
Exercise	0.024	0.053	0.061	0.022	−0.275	0.559	−0.057
Alcohol	0.011	−0.002	−0.050	−0.024	0.146	0.691	0.101
Age	−0.024	0.047	0.037	0.141	0.455	0.031	0.051
% Variance	30,3	10,8	8,2	6,1	5,5	4,9	4,6
% Cumulative Variance	30,3	41,1	49,3	55,4	60,9	65,8	70,4

Rotation Method: Oblimin with Kaiser Normalization; in the model used only variables with Spearman correlation coefficient < 75%.

as the test set, and 42 observations (10.4%) as a holdout. The parameters of the model are presented in **Table S3**. The overall predictive accuracy of the model was estimated at 76.2%. Total predictive value of the model is presented in **Table 6**. The area under the ROC curve was estimated at 0.792 for cases and controls. The most important biomarkers which contribute to the model were Cis-11-Eicosenoic (C20:1n9), Lauric acid (C12:0), Erucic acid (C22:1n9), Cis-10-pentadecanoic acid (C15:1), Stearic acid (C18:0), Myristic acid (C14:0), Heptadecanoic acid (C17:0), Palmitic acid (C16:0) (**Figure 6**).

## DISCUSSION

In this study, we measured the levels of serum TFAs using targeted GC-MS metabolomics in patients with ADs and compared them to controls aiming to assess their potency as disease biomarkers. We hypothesized that metabolites are significantly altered in patients with ADs, including thyroid disease, rheumatoid arthritis, multiple sclerosis, vitiligo, psoriasis, and inflammatory bowel disease. In total, 28 biomarkers including 23 TFAs and demographic variables were measured in 403 individuals and data were analyzed using univariate analysis (chi-square, Man-Whitney test, and Wilcoxon Sign Rank test), as well as more advanced techniques, such as PCA analysis, logistic regression, and Artificial Neural Networks. We found that AD patients had increased levels of C14:1, C15:1, C16:1n7, C20:1n9, C22:1n9, C18:3n3, C18:3n6, and total omega-6/ total omega-3 ratio while they had lower levels of total omega-3 fatty acids, C12:0, C17:0, C18:0 in a statistically significant manner (**Table 2**). However, Bonferroni correction



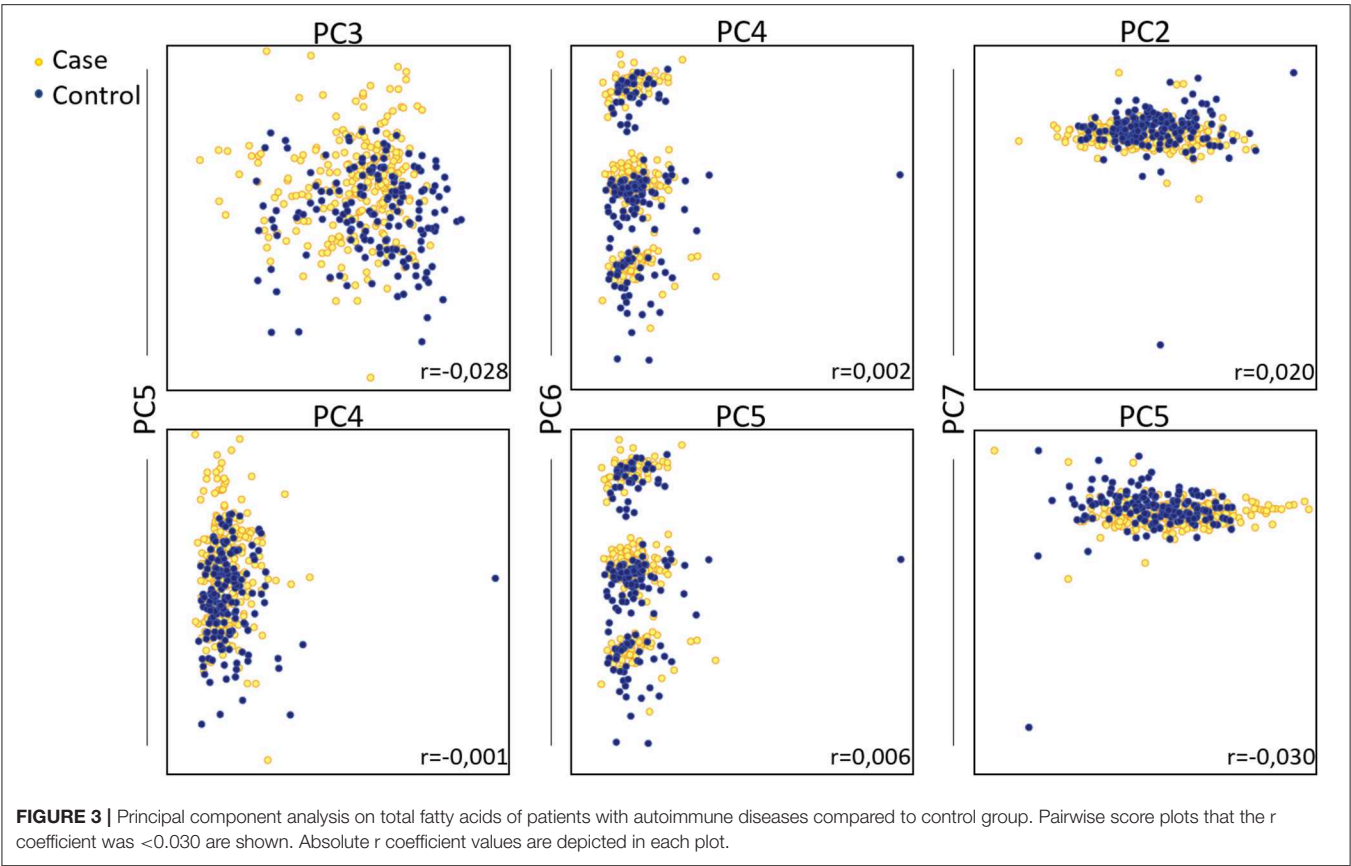


**TABLE 4 |** Association of the presence of autoimmune disease with the Principal Components Dependent.

	B	St Error	exp(B)	95% LCI	95% UCI	p-value
Factor 1	−0.285	0.141	0.752	0.570	0.992	0.044
Factor 2	0.578	0.132	1.783	1.376	2.310	0.000
Factor 3	0.570	0.136	1.769	1.354	2.310	0.000
Factor 4	0.107	0.114	1.113	0.891	1.390	0.348
Factor 5	−0.673	0.128	0.510	0.397	0.656	0.000
Factor 6	−0.294	0.118	0.745	0.591	0.940	0.013
Factor 7	0.328	0.130	1.389	1.076	1.792	0.012
Female	−0.595	0.253	0.551	0.336	0.905	0.019
Constant	−0.082	0.202	0.921			0.685

Variable: Absence of autoimmune disorder; Binary Logistic Regression LCI: Lower Confidence Interval; UCI: Upper Confidence Interval.

indicated that only the levels of C22:6n3, total omega 3, C18:3n6, C15:1, C20:1n9, C12:0, C15:0, C17:0, C18:0 and total omega 6/ total omega 3 ratio were statistically significantly different. The high inter-correlations between metabolites may partially explain the different results obtained from Mann–Whitney test and Bonferroni correction. Indeed, the metabolite-metabolite correlation patterns were markedly different between the case and the control group indicating the metabolic re-programming of ADs in line with previous studies reviewed by Seeger

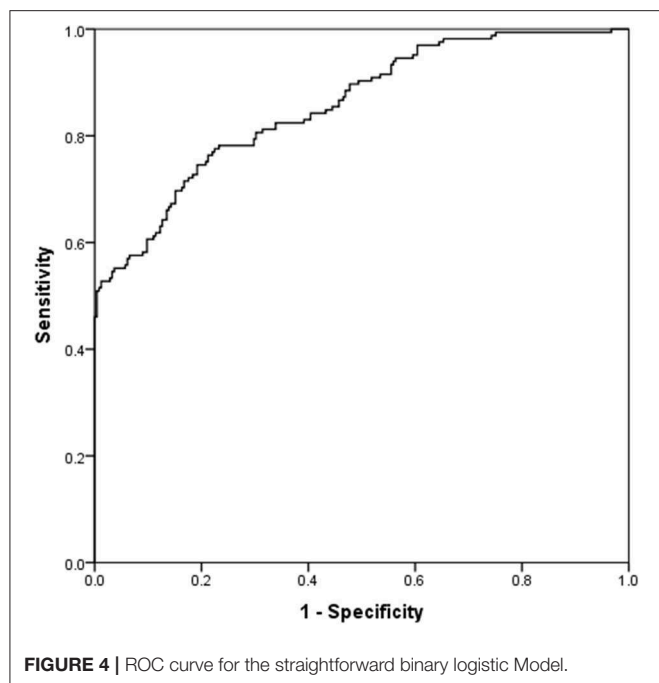
**TABLE 5 |** Association of the presence of autoimmune disease with patient's characteristics Dependent.

	B	St Error	exp(B)	95% LCI	95% UCI	p-value
C183n6	−0.039	0.010	0.961	0.943	0.980	0.000
C151	−0.299	0.055	0.741	0.666	0.825	0.000
C140	0.154	0.027	1.166	1.106	1.230	0.000
C240	0.026	0.015	1.026	0.997	1.056	0.078
No exercise	−1.002	0.309	0.367	0.200	0.673	0.001
No alcohol	0.934	0.297	2.544	1.423	4.549	0.002
Constant	−1.847	0.528	0.158			0.000

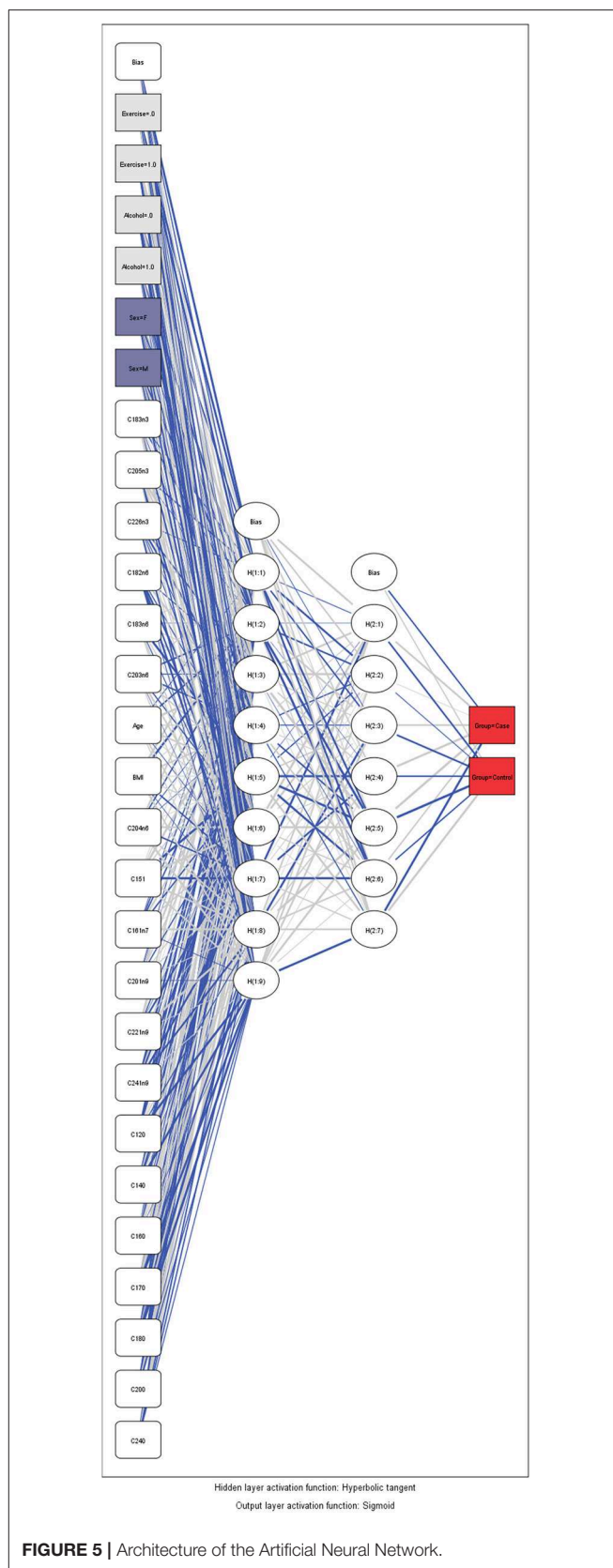
Variable: Absence of autoimmune disorder; Binary Logistic Regression Model; Stepwise Backward Method; Variable(s) entered on step 1: Exercise, Alcohol, Sex, C183n3, C205n3, C226n3, C182n6, C183n6, C203n6, C204n6, C151, C161n7, C201n9, C221n9, C241n9, C120, C140, C160, C170, C180, C200, C240, BMI.

et al. (Seeger, 2009; Amersfoort and Kuiper, 2017). Among the statistically significant correlations, lauric acid (C12:0), pentadecanoic acid (C15:0), stearic acid (C18:0), myristoleic acid (C14:1), cis-10 pentadecanoic acid (C15:1) and arachidonic acid (C20:4n6) were stronger correlated in the case than the control group ( $p < 0.001$ ).

Three predictive models were built to estimate the probability of the absence of an AD as a function of gender, age, exercise, alcohol consumption, BMI, and TFAs as biomarkers. PCA



analysis was used to reduce the representation of variables to only seven new artificial variables, and we created a new predictive model based on binary logistic regression. Furthermore, we estimated a straightforward logistic regression model with all 28 variables as potential independent biomarkers. In the end, only the statistically significant biomarkers were assessed by the model. As expected, the first model had slightly less accurate predictions (74.7 vs. 78.9%) compared to the second, since PCA reduces the portion of the information used from the initial data set. It needs to be mentioned that PCA analysis is mainly an exploratory technique aiming to investigate the data set at a first level. The main strength of this analysis – if any, depending on the data structure – is the reduction of dimension by creating artificial variables at expenses of accuracy (Jolliffe et al., 2016). However, the assumption that the principal components with highest variance will also contain the most information is a limitation of the analysis which is also observed in our study. Hence, the PCA plot does not show a considerable distinction between control and case groups and, thus, the factors of PCA do not seem sufficiently robust to be used for a satisfactory data interpretation. For the 78.9% predictive accuracy of the second model, myristic acid (C14:0), lignoceric acid (C24:0), Cis-10 pentadecanoic acid (C15:1), gamma-linolenic acid (C18:3n6), exercise and alcohol consumption were identified as the most sensitive markers. Exercise and alcohol are lifestyle variables that have a major impact on metabolism and the immune system directly. Several studies have discussed the beneficial role of physical activity not only in prevention but also for the improvement of disease progression



and the quality of life of patients (Sharif et al., 2018). More importantly, it has been shown that regular moderate exercise can increase glucose uptake and reduce insulin resistance (DeFronzo et al., 1987). The role of alcohol consumption in health and its effects on the immune system have been extensively discussed, and although several studies show that moderate alcohol consumption may be beneficial to health (Carlé et al., 2012) others demonstrate that it has a detrimental effect on the gut microbiome and immunotolerance (Wang et al., 2010; Sarkar et al., 2015; National Institute on Alcohol Abuse and Alcoholism, 2000).

ANN analysis showed that the most important predictors for the ADs were the following: Cis-11-eicosenoic (C20:1n9), lauric acid (C12:0), Erucic (C22:1n9), Cis-10 pentadecanoic acid (C15:1), stearic acid (C18:0), myristic acid (C14:0), heptadecanoic acid (C17:0), palmitic acid (C16:0) in the order of importance. The predictive accuracy of the ANN model was comparable to the straightforward binary logistic regression (76.2%). These findings indicate that the metabolic pathways of SFAs and MUFAs are significantly affected in ADs. In the group of SFAs lauric acid (C12:0), myristic acid (C14:0), stearic acid (C18:0), lignoceric acid (C24:0), palmitic acid (C16:0) and heptadecanoic acid (C17:0) can be potent biomarkers. SFAs including stearic acid (C18:0), myristic acid (C14:0) and palmitic acid (C16:0) are endogenously converted to the MUFAs oleic acid (C18:1n9cis), myristoleic acid (C14:1) and palmitoleic acid (C16:1n7), respectively. This conversion is catalyzed by the Delta-9 desaturase, and the activity of the enzyme has been associated with insulin resistance (Kurotani et al., 2012), a key player in several ADs (Giles et al., 2015; Granata et al., 2017; Medina et al.,

2018). Indeed insulin resistance has been linked to impaired desaturase activity and high levels of stearic and palmitic acid (Mayneris-Perxachs et al., 2014). Lignoceric (C24:0) is a very long chain fatty acid along with behenic acid (C22:0) and arachidic acid (C20:0). These are major components of ceramides that have been shown to have a protective role against insulin resistance and diabetes (Lemaitre et al., 2015). Heptadecanoic acid (C17:0) belongs to the odd-chain fatty acids, and although it has been widely used as a biomarker of dairy intake (Yakoob et al., 2014), there is recent evidence that it is related to metabolic diseases and gut microbiome imbalance (Jenkins et al., 2017). Insulin resistance is a common denominator in many chronic inflammatory diseases through complex molecular pathways

TABLE 6 | Classification table for artificial neural network.

		Predicted		% Correct
		Case	Control	
Training	Case	152	15	91.0%
	Control	41	65	61.3
	Overall percent	70.7%	29.3%	79.5
Testing	Case	50	4	92.6
	Control	16	18	52.9
	Overall percent	75.0%	25.0%	77.3
Holdout	Case	17	2	89.5
	Control	8	15	65.2
	Overall percent	59.5%	40.5%	76.2

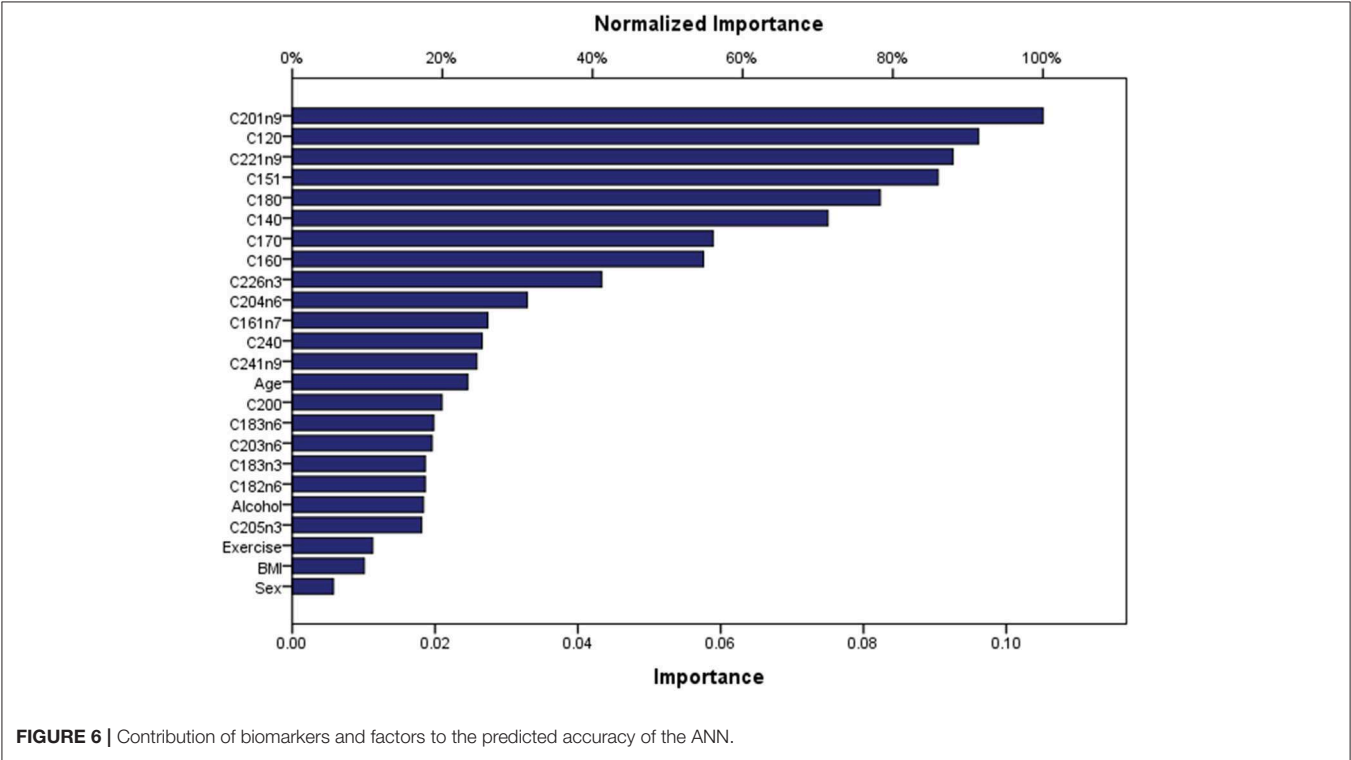


FIGURE 6 | Contribution of biomarkers and factors to the predicted accuracy of the ANN.



(Engin et al., 2018). Because insulin inhibits lipolysis of stored fat, under insulin resistant conditions, free fatty acid levels increase in blood circulation and are taken up by organs that cannot store efficiently fat such as the liver and skeletal muscles. Excess fat in these tissues generates a cascade of mechanisms that lead to local insulin resistance and inflammation (Savage et al., 2005). From a different point of view, the Western diet has been implicated in the rapid rise of ADs as a result of multiple factors that break immunotolerance (De Rosa et al., 2017; Tsoukalas et al., 2019). Therefore, biomarkers that may predict and early diagnose insulin resistance would be very helpful in the prediction of chronic diseases.

In the case of MUFAs, Cis-10-pentadecanoic acid (C15:1), Cis-11-eicosenoic acid (C20:1n9) and erucic acid (C22:1n9) were demonstrated as potent biomarkers by our predictive model. Cis-11-eicosenoic acid (C20:1n9) originates from oleic acid (C18:1n9cis) and can be elongated to produce erucic acid (C22:1n9) (Bao et al., 1998). Erucic acid intake (through canola, Wallflower, or Lorenzo's oil) has been suggested to be beneficial for peroxisomal disorders like X-linked adrenoleukodystrophy by reducing the saturated VLCFA by negative feedback (Ris   et al., 2014).

Gamma-linolenic acid (C18:3n6), the intermediate metabolite of linoleic acid (C18:2n6) conversion to dihomo-gamma-linoleic acid (C20:3n6) and Arachidonic acid (C20:4n6) was also a sensitive marker for the predictive model. Dihomo-gamma-linoleic acid (C20:3n6) and Arachidonic acid (C20:4n6) are the main precursors of the pro-inflammatory mediators. There have been several studies showing that arachidonic acid, along with other omega-6 and omega-3 fatty acids can be valuable markers in chronic inflammatory diseases because they reflect the inflammation status and the dietary preferences of the individual (Patterson et al., 2012; Tsoukalas et al., 2019). In a previous study, the authors demonstrated a strong relationship between serum fatty acid composition with the risk of type 1 diabetes-associated autoimmunity (Niinist   et al., 2017). A nested case-control analysis was performed within the Finnish Type 1 Diabetes Prediction and Prevention Study birth cohort, with 7,782 individuals. Fatty acids were associated with islet autoimmunity and primary insulin autoimmunity (higher palmitoleic acid, cis-vaccenic, arachidonic, docosapentaenoic, and docosahexaenoic acids decreased risk; higher  $\alpha$ -linoleic acid and arachidonic: docosahexaenoic and omega-6/omega-3 acid ratios increased risk). The authors concluded that the fatty acid status might play a role in the development of type 1 diabetes-associated autoimmunity, but further studies are warranted to clarify the independent role of fatty acids in the development of type 1 diabetes.

A strength of this study is the application of ANN analysis to the targeted metabolomics data. ANN or logistic regression have been employed in many areas of health care research having advantages and disadvantages (Dreiseitl and Ohno-Machado, 2002). The most profound advantage of ANN is that it does not assume any pre-specified form of relationship between response and predictive variables but, on the contrary, the model itself investigates the relationship, which is not necessarily linear. Of course, due to this feature, ANNs have some

disadvantages such as heavy mathematical computation and - more importantly- proneness to overfitting. Moreover, The ANN calculations represent a "data hungry" procedure and require an abundance of data to maximize its performance. In this light, it could be argued that the accuracy of our ANN model would have been even better in comparison with the binary logistic model if we had more data. However, this condition was not feasible for our study, but it is also not frequent in medical research, where dataset size is constrained by the complexity and the cost of large-scale experiments. As a general rule, it has been recommended that there should be approximately 10 times more training cases for each node of the model (Stathakis, 2009), but several statistical attempts have been made to reduce this numbers to smaller sample sizes (Pasini, 2015). Since our model has 9 nodes (at hidden layer 1) and 403 observations in total, this requirement is partially being fulfilled, including a fair sample size for an ANN analysis. In fact, an advantage of the present analysis is that it includes a relatively large sample of patients within the metabolomic context. As a general comment, beyond the ANN's requirements, the determination of a sample size per group is important in order to meet the criteria for a robust metabolomics analysis. Due to several complexities, there is currently no standard statistical methodology for this sample estimation (Nyamundanda et al., 2013; Trivedi et al., 2017). On a theoretical level, patient heterogeneity and other factors may play a role in the final estimation, but in practice, researchers usually include only 30–50 patients per treatment group, well below the number of subjects used in the present work.

One potential limitation of our study is that the cases (patients with ADs) had different diseases. Hence, this might be considered as a confounder and should be adjusted in statistical analysis, although this type of analysis requires a larger dataset. Our very next study will include additional variables of the population and focus on specific types of AD in order to explore more complex relationships between TFAs and pathogenesis of autoimmunity. Metabolomics is an emerging tool used for biomarker discovery as it can provide systemic understanding of the disease. However, there is some variability and inconsistencies among metabolomic studies, due to the experimental design (Kohler et al., 2017). This is a general characteristic of "omics" studies, since the small sample size results in limited statistical power especially when data require adjustment for multiple testing. In the present work, although the dataset outweighs the commonly used sample sizes, this limitation needs to be considered as the inclusion of volunteers affected by different diseases could hamper the interpretability of the results. However, many autoimmune diseases share common molecular mechanisms although different organs and cell types are involved, and, thus, probably have some common biomarkers (Arnald et al., 2016). Similarly, common biomarkers related to different diseases is observed even in a more "mature" field such as this of genomic medicine, a case that hampers the results interpretation as well (Fragoulakis et al., 2019).

The findings of the present study can be used as a baseline for studies on the metabolic fingerprint of ADs and highlight the potency of metabolomics and advanced statistical tools

in prevention, prediction, treatment response, and drug side effects monitoring.

From this study, it can be concluded that the TFAs are associated with ADs presence, which is in line with the previous studies (Simopoulos, 2002). Overall, there is growing evidence that ADs have a distinct metabolic fingerprint which can be assessed through metabolomics, permitting a personalized approach and therapy. The metabolomic profile of TFAs can provide information regarding dietary intake and endogenous synthesized fatty acids. Thus, it needs to be critically assessed by the physician considering the medical and nutritional history and the disease background as well (Trivedi et al., 2017). To this end, tailor-made interventions in nutrition and lifestyle might be of high therapeutic value in ADs.

## DATA AVAILABILITY STATEMENT

The dataset presented in this study are available from the corresponding author upon reasonable request.

## ETHICS STATEMENT

The studies involving human participants were reviewed and approved by Ethics Committee of the University of Crete (approval no. A.P. 39\_22112018) and Health Clinic for Autoimmune and Chronic Diseases. The patients/participants provided their written informed consent to participate in this study.

## REFERENCES

- American Autoimmune Related Diseases Association (2018). Available online at: <https://www.aarda.org/news-information/statistics/#1488234345468-3bf2d325-1052>.
- Amersfoort, J., and Kuiper, J. (2017). T cell metabolism in metabolic disease-associated autoimmunity. *Immunobiology* 222, 925–936. doi: 10.1016/j.imbio.2017.03.001
- Arnald, A., Julià, A., Vinaixa, M., Domènech, E., Fernández-Nebro, A., Cañete, J. D., et al. (2016). Urine metabolome profiling of immune-mediated inflammatory diseases. *BMC Med.* 14, 1–12. doi: 10.1186/s12916-016-0681-8
- Bach, J.-F. (2002). The effect of infections on susceptibility to autoimmune and allergic diseases. *N. Engl. J. Med.* 347, 911–920. doi: 10.1056/NEJMra020100
- Bao, X., Pollard, M., and Ohlrogge, J. (1998). The biosynthesis of erucic acid in developing embryos of *Brassica rapa*. *Plant Physiol.* 118, 183–190. doi: 10.1104/pp.118.1.183
- Buha, A., Matovic, V., Antonijevic, B., Bulat, Z., and Curcic, M. (2018). Overview of cadmium thyroid disrupting effects and mechanisms. *Int. J. Mol. Sci.* 19:E1501. doi: 10.3390/ijms19051501
- Carlé, A., Pedersen, I. B., Knudsen, N., Perrild, H., Ovesen, L., Rasmussen, L. B., et al. (2012). Moderate alcohol consumption may protect against overt autoimmune hypothyroidism: a population-based case-control study. *Eur. J. Endocrinol.* 167, 483–490. doi: 10.1530/EJE-12-0356
- Cooper, G. S., Miller, F. W., Pandey, J. P., and Al, C. E. T. (1999). The role of genetic factors in autoimmune disease : implications for environmental research. *Environ. Health Perspect.* 107, 693–700. doi: 10.1289/ehp.99107s5693
- Dahan, S., Segal, Y., and Shoenfeld, Y. (2017). Dietary factors in rheumatic autoimmune diseases: a recipe for therapy? *Nat. Rev. Rheumatol.* 13, 348–358. doi: 10.1038/nrrheum.2017.42

## AUTHOR CONTRIBUTIONS

DT, AD, and DC conceived and designed the study and wrote the manuscript as a special part of a Ph.D. thesis. VF conducted the analysis, prepared the figures and tables and wrote the manuscript. ES interpreted the results, wrote the manuscript, and prepared the figures. EP supervised GC-MS experiments. GT and CA involved in collecting and managing the personal data of the participants and interpreted the results. AT and PF, involved in taking ethical clearance, critically assessed the design of the study and the manuscript. MA and ND wrote the manuscript and provided valuable comments in the discussion section. All authors reviewed the manuscript.

## ACKNOWLEDGMENTS

This work was encouraged and coordinated by the European Institute of Nutritional Medicine. The authors would like to thank all the administrative, the technical and medical staff of Toxplus, the Metabolomic Medicine clinic, and the Laboratory of Toxicology for their dedicated involvement in this study. MA was supported by National Institute of Health (NIH) R01 ES10563, R01 ES07331 and R01 ES020852.

## SUPPLEMENTARY MATERIAL

The Supplementary Material for this article can be found online at: <https://www.frontiersin.org/articles/10.3389/fmolb.2019.00120/full#supplementary-material>

- De Rosa, V., La Cava, A., and Matarese, G. (2017). Metabolic pressure and the breach of immunological self-tolerance. *Nat. Immunol.* 18, 1190–1196. doi: 10.1038/ni.3851
- DeFronzo, R. A., Sherwin, R. S., and Kraemer, N. (1987). Effect of physical training on insulin action in obesity. *Diabetes* 36, 1379–1385. doi: 10.2337/diab.36.12.1379
- Dreiseitl, S., and Ohno-Machado, L. (2002). Logistic regression and artificial neural network classification models: a methodology review. *J. Biomed. Inform.* 35, 352–359. doi: 10.1016/S1532-0464(03)00034-0
- Engin, A. B., Tsatsakis, A. M., Tsoukalas, D., and Engin, A. (2018). Do flavanols-rich natural products relieve obesity-related insulin resistance? *Food Chem. Toxicol.* 112, 157–167. doi: 10.1016/j.fct.2017.12.055
- Ernst, V. L. (1994). Nested case-control studies. *Prev. Med.* 23, 587–590. doi: 10.1006/pmed.1994.1093
- Faresjö, T., and Faresjö, Å. (2010). To match or not to match in epidemiological studies - Same outcome but less power. *Int. J. Environ. Res. Public Health* 7, 325–332. doi: 10.3390/ijerph7010325
- Fragoulakis, V., Roncato, R., Fratte, C. D., Ecça, F., Bartsakoulia, M., Innocenti, F., et al. (2019). Estimating the effectiveness of DPYD genotyping in Italian individuals suffering from cancer based on the cost of chemotherapy-induced toxicity. *Am. J. Hum. Genet.* 104, 1158–1168. doi: 10.1016/j.ajhg.2019.04.017
- Gangemi, S., Gofita, E., Costa, C., Teodoro, M., Briguglio, G., Nikitovic, D., et al. (2016). Occupational and environmental exposure to pesticides and cytokine pathways in chronic diseases (Review). *Int. J. Mol. Med.* 38, 1012–1020. doi: 10.3892/ijmm.2016.2728
- Giles, J. T., Danielides, S., Szklo, M., Post, W. S., Blumenthal, R. S., Petri, M., et al. (2015). Insulin resistance in rheumatoid arthritis. Disease-related indicators and associations with the presence and progression of subclinical atherosclerosis. *Arthritis Rheumatol.* 67, 626–636. doi: 10.1002/art.38986

- Granata, M., Skarmoutsou, E., Trovato, C., Rossi, G. A., Clorinda, M., and Fabio, M. (2017). Obesity, Type 1 diabetes, and psoriasis : an autoimmune triple flip. *Pathobiology* 84, 71–79. doi: 10.1159/000447777
- Hajian-Tilaki, K. (2013). Receiver Operating Characteristic (ROC) curve analysis for medical diagnostic test evaluation. *Casp. J. Intern. Med.* 4:627–635. Available online at: <http://caspij.com/article-1-193-en.html&sw=Receiver+Operating+Characteristic+%28roc%29+Curve+Analysis+for+Medical+Dia>
- Hao, J., Yang, T., Zhou, Y., Gao, G.-Y., Xing, F., Peng, Y., et al. (2017). Serum metabolomics analysis reveals a distinct metabolic profile of patients with primary biliary cholangitis. *Sci. Rep.* 7:784. doi: 10.1038/s41598-017-00944-9
- Heinze, G., Wallisch, C., and Dunkler, D. (2018). Variable selection – A review and recommendations for the practicing statistician. *Biometrical J.* 60, 431–449. doi: 10.1002/bimj.201700067
- Jenkins, B. J., Seyssel, K., Chiu, S., Pan, P. H., Lin, S. Y., Stanley, E., et al. (2017). Odd chain fatty acids; new insights of the relationship between the gut microbiota, dietary intake, biosynthesis and glucose intolerance. *Sci. Rep.* 7, 1–8. doi: 10.1038/srep44845
- Jolliffe, I. T., Cadima, J., and Cadima, J. (2016). Principal component analysis : a review and recent developments. *Philos. Trans. R. Soc.* 374:16. doi: 10.1098/rsta.2015.0202
- Kay, J., and Upchurch, K. S. (2012). ACR/EULAR 2010 rheumatoid arthritis classification criteria. *Rheumatology* 51, 5–9. doi: 10.1093/rheumatology/kes279
- Kohler, I., Hankemeier, T., van der Graaf, P. H., Knibbe, C. A. J., and van Hasselt, J. G. C. (2017). Integrating clinical metabolomics-based biomarker discovery and clinical pharmacology to enable precision medicine. *Eur. J. Pharm. Sci.* 109, S15–S21. doi: 10.1016/j.ejps.2017.05.018
- Kong, B. Y., Menzies, A. M., Saunders, A. B., Liniker, E., Ramanujam, S., Guminski, A., et al. (2011). Revised classification/nomenclature of vitiligo and related issues: the vitiligo global issues consensus conference. *Pigment Cell Melanoma Res.* 25, E1–E13. doi: 10.1111/j.1755-148X.2012.00997.x
- Kurotani, K., Sato, M., Ejima, Y., Nanri, A., Yi, S., Pham, N. M., et al. (2012). High levels of stearic acid, palmitoleic acid, and dihomo- $\gamma$ -linolenic acid and low levels of linoleic acid in serum cholesterol ester are associated with high insulin resistance. *Nutr. Res.* 32, 669–675.e3. doi: 10.1016/j.nutres.2012.07.004
- Lee, S. J., Woo, S., Ahn, S. H., Lim, D. K., Hong, J. Y., Park, J. H., et al. (2015). Functional interpretation of metabolomics data as a new method for predicting long-term side effects: treatment of atopic dermatitis in infants. *Sci. Rep.* 4:7408. doi: 10.1038/srep07408
- Lemaitre, R. N., Fretts, A. M., Sitlani, C. M., Biggs, M. L., Mukamal, K., King, I. B., et al. (2015). Plasma phospholipid very-long-chain saturated fatty acids and incident diabetes in older adults : the Cardiovascular Health Study 1 – 4. *Am. J. Clin. Nutr.* 101, 1047–1054. doi: 10.3945/ajcn.114.101857
- Lerner, A., Jeremias, P., and Matthias, T. (2016). The world incidence and prevalence of autoimmune diseases is increasing. *Int. J. Celiac Dis.* 3, 151–155. doi: 10.12691/ijcd-3-4-8
- Leslie, R. D., and Beyan, H. (2011). Metabolomics makes a mark: early changes associated with autoimmune diabetes. *Diabetes* 60, 2688–2690. doi: 10.2337/db11-1177
- Margarita, S. (2002). Introduction to neural networks in healthcare. *Open Clin.* Available online at: [https://www.researchgate.net/publication/228820949\\_Introduction\\_to\\_neural\\_networks\\_in\\_healthcare](https://www.researchgate.net/publication/228820949_Introduction_to_neural_networks_in_healthcare)
- Mayneris-Perxachs, J., Guerendian, M., Castellote, A. I., Estruch, R., Covas, M. I., Fitó, M., et al. (2014). Plasma fatty acid composition, estimated desaturase activities, and their relation with the metabolic syndrome in a population at high risk of cardiovascular disease. *Clin. Nutr.* 33, 90–97. doi: 10.1016/j.clnu.2013.03.001
- Medina, G., Vera-Lastra, O., Peralta-Amaro, A. L., Jiménez-Arellano, M. P., Saavedra, M. A., Cruz-Domínguez, M. P., et al. (2018). Metabolic syndrome, autoimmunity and rheumatic diseases. *Pharmacol. Res.* 133, 277–288. doi: 10.1016/j.phrs.2018.01.009
- Menni, C., Zierer, J., Valdes, A. M., and Spector, T. D. (2017). Mixing omics: Combining genetics and metabolomics to study rheumatic diseases. *Nat. Rev. Rheumatol.* 13, 174–181. doi: 10.1038/nrrheum.2017.5
- National Institute on Alcohol Abuse and Alcoholism (2000) “Chapter 4: Alcohol and the immune system,” in 10th Special Report to the U.S. Congress on Alcohol and Health, 214–239.
- Negrei, C., Bojinca, V., Balanescu, A., Bojinca, M., Baconi, D., Spandidos, D. A., et al. (2016). Management of rheumatoid arthritis : Impact and risks of various therapeutic approaches (Review). *Exp. Ther. Med.* 11, 1177–1183. doi: 10.3892/etm.2016.3045
- Niinistö, S., Takkinen, H. M., Erlund, I., Ahonen, S., Toppari, J., Ilonen, J., et al. (2017). Fatty acid status in infancy is associated with the risk of type 1 diabetes-associated autoimmunity. *Diabetologia* 60, 1223–1233. doi: 10.1007/s00125-017-4280-9
- Nyamundanda, G., Gormley, I. C., Fan, Y., Gallagher, W. M., and Brennan, L. (2013). MetSizeR: Selecting the optimal sample size for metabolomic studies using an analysis based approach. *BMC Bioinformatics* 14, 1–8. doi: 10.1186/1471-2105-14-338
- Papamichael, M. M., Katsardis, C., Erbas, B., Itsiopoulos, C., and Tsoukalas, D. (2018). Urinary organic acids as biomarkers in the assessment of pulmonary function in children with asthma. *Nutr. Res.* 61, 31–40. doi: 10.1016/j.nutres.2018.10.004
- Pasini, A. (2015). Artificial neural networks for small dataset analysis. *J. Thorac. Dis.* 7, 953–960. doi: 10.3978/j.issn.2072-1439.2015.04.61
- Patterson, E., Wall, R., Fitzgerald, G., Ross, R., and Stanton, C. (2012). Health implications of high dietary omega-6 polyunsaturated fatty acids. *J. Nutr. Metab.* 2012:539426. doi: 10.1155/2012/539426
- Petrakis, D., Vassilopoulou, L., Mamoulakis, C., Tsiaoussis, J., Makrigrannakis, A., and Tsatsakis, A. M. (2017). Endocrine disruptors leading to obesity and related diseases. *Int. J. Environ. Res. Public Health* 14:E1282. doi: 10.3390/ijerph14101282
- Polman, C. H., Reingold, S. C., Banwell, B., Clanet, M., Cohen, J. A., Filippi, M., et al. (2011). Diagnostic criteria for multiple sclerosis: 2010 Revisions to the McDonald criteria. *Ann. Neurol.* 69, 292–302. doi: 10.1002/ana.22366
- Risé, P., Paroni, R., and Petroni, A. (2014). “Peroxisomal pathways, their role in neurodegenerative disorders and therapeutic strategies,” in *Omega-3 Fatty Acids in Brain and Neurological Health*, eds W. Ronald Ross and F. De Meester (Academic Press), 19–30. doi: 10.1016/B978-0-12-410527-0.00003-X
- Rose, S., and Laan, M. J. (2009). Why match? investigating matched case-control study designs with causal effect estimation. *Int. J. Biostat.* 5:1. doi: 10.2202/1557-4679.1127
- Saduf, M. A. W. (2013). Comparative study of back propagation learning algorithms for neural networks. *Int. J. Adv. Res. Comput. Sci. Softw. Eng.* 3, 1151–1156. Available online at: <https://pdfs.semanticscholar.org/c804/342a840fc2eb3a3415e249b67145019c5b55.pdf>
- Sarkar, D., Jung, K. M., and Wang, J. (2015). Alcohol and the immune system. *Alcohol Res.* 37, 153–155.
- Savage, D. B., Petersen, K. F., and Shulman, G. I. (2005). Mechanisms of insulin resistance in humans and possible links with inflammation. *Hypertension* 45, 828–833. doi: 10.1161/01.HYP.0000163475.04421.e4
- Seeger, K. (2009). Metabolic changes in autoimmune diseases. *Curr. Drug Discov. Technol.* 6, 256–261. doi: 10.2174/157016309789869074
- Serhan, C. N., Brain, S. D., Buckley, C. D., Gilroy, D. W., Haslett, C., O'Neill, L. A. J., et al. (2007). Resolution of inflammation: state of the art, definitions and terms. *FASEB J.* 21, 325–332. doi: 10.1096/fj.06-7227rev
- Sharif, K., Wataid, A., Bragazzi, N. L., Lichtbroun, M., Amital, H., and Shoenfeld, Y. (2018). Physical activity and autoimmune diseases: Get moving and manage the disease. *Autoimmun. Rev.* 17, 53–72. doi: 10.1016/j.autrev.2017.11.010
- Sherlock, M. E., and Benchimol, E. I. (2017). Classification of inflammatory bowel disease in children. *Pediatr. Inflamm. Bowel Dis. Third Ed.*, 181–191. doi: 10.1007/978-3-319-49215-5\_15
- Simopoulos, A. P. (2002). Omega-3 fatty acids in inflammation and autoimmune diseases. *J. Am. Coll. Nutr.* 21, 495–505. doi: 10.1080/07315724.2002.10719248
- Stathakis, D. (2009). How many hidden layers and nodes? *Int. J. Remote Sens.* 30, 2133–2147. doi: 10.1080/01431160802549278
- Stellaard, F., Brink, H. J., Kok, R. M., Van Den Heuvel, L., and Jakobs, C. (1990). Stable isotope dilution analysis of very long chain fatty acids in plasma, urine and amniotic fluid by electron capture negative ion mass fragmentography. *Clin. Chim. Acta* 192, 133–144. doi: 10.1016/0009-8981(90)90077-6
- Strong, K., Mathers, C., Epping-Jordan, J., and Beaglehole, R. (2006). Preventing chronic disease: a priority for global health. *Int. J. Epidemiol.* 35, 491–492. doi: 10.1093/ije/dyi315
- Theofilopoulos, A. N., Kono, D. H., and Baccala, R. (2017). The multiple pathways to autoimmunity. *Nat. Immunol.* 18, 716–724. doi: 10.1038/ni.3731
- Tinetti, M. E., Fried, T. R., and Boyd, C. M. (2012). Designing health care for the most common chronic

- condition—multimorbidity. *JAMA* 307, 2493–2494. doi: 10.1001/jama.2012.5265
- Trivedi, D. K., Hollywood, K. A., and Goodacre, R. (2017). Metabolomics for the masses: the future of metabolomics in a personalized world. *New Horizons Transl. Med.* 3, 294–305. doi: 10.1016/j.nhtm.2017.06.001
- Tsoukalas, D., Alegakis, A., Fragkiadaki, P., Papakonstantinou, E., Nikitovic, D., Karataraki, A., et al. (2017). Application of metabolomics: focus on the quantification of organic acids in healthy adults. *Int. J. Mol. Med.* 40, 112–120. doi: 10.3892/ijmm.2017.2983
- Tsoukalas, D., Alegakis, A. K., Fragkiadaki, P., Papakonstantinou, E., Tsilimidos, G., Geraci, F., et al. (2019). Application of metabolomics part II: focus on fatty acids and their metabolites in healthy adults. *Int. J. Mol. Med.* 43, 233–242. doi: 10.3892/ijmm.2018.3989
- Vinaixa, M., Samino, S., Saez, I., Duran, J., Guinovart, J. J., and Yanes, O. (2012). A guideline to univariate statistical analysis for LC/MS-based untargeted metabolomics-derived data. *Metabolites* 2, 775–795. doi: 10.3390/metabo2040775
- Wang, H. J., Zakhari, S., and Jung, M. K. (2010). Alcohol, inflammation, and gut-liver-brain interactions in tissue damage and disease development. *World J. Gastroenterol.* 16, 1304–1313. doi: 10.3748/wjg.v16.i11.1304
- WHO (2019). *Fact sheets. Non communicable diseases*. WHO. Available online at: <https://www.who.int/news-room/fact-sheets/detail/noncommunicable-diseases>
- Yakoob, M. Y., Shi, P., Hu, F. B., Campos, H., Rexrode, K. M., Orav, J. E., et al. (2014). Circulating biomarkers of dairy fat and incident type 2 diabetes in two us prospective cohorts. *Am. J. Clin. Nutr.* 100, 1437–1447. doi: 10.3945/ajcn.114.083097

**Conflict of Interest:** The authors declare that the research was conducted in the absence of any commercial or financial relationships that could be construed as a potential conflict of interest.

Copyright © 2019 Tsoukalas, Fragoulakis, Sarandi, Docea, Papakonstantinou, Tsilimidos, Anamaterou, Fragkiadaki, Aschner, Tsatsakis, Drakoulis and Calina. This is an open-access article distributed under the terms of the Creative Commons Attribution License (CC BY). The use, distribution or reproduction in other forums is permitted, provided the original author(s) and the copyright owner(s) are credited and that the original publication in this journal is cited, in accordance with accepted academic practice. No use, distribution or reproduction is permitted which does not comply with these terms.





# Serum Metabolite Biomarkers Predictive of Response to PD-1 Blockade Therapy in Non-Small Cell Lung Cancer

Xiaoqun Nie<sup>1†</sup>, Liliang Xia<sup>2†</sup>, Fang Gao<sup>1†</sup>, Lixia Liu<sup>1</sup>, Yi Yang<sup>2</sup>, Yingying Chen<sup>3</sup>, Huangqi Duan<sup>3</sup>, Yaxian Yao<sup>2</sup>, Zhiwei Chen<sup>2</sup>, Shun Lu<sup>2\*</sup>, Ying Wang<sup>3\*</sup> and Chen Yang<sup>1\*</sup>

<sup>1</sup>CAS-Key Laboratory of Synthetic Biology, CAS Center for Excellence in Molecular Plant Sciences, Chinese Academy of Sciences, Shanghai, China, <sup>2</sup>Department of Shanghai Lung Cancer, Shanghai Chest Hospital, Shanghai Jiao Tong University, Shanghai, China, <sup>3</sup>Department of Immunology and Microbiology, Shanghai Institute of Immunology, Shanghai Jiao Tong University School of Medicine, Shanghai, China

## OPEN ACCESS

### Edited by:

Donghai Lin,  
Xiamen University, China

### Reviewed by:

Jianbo Wan,  
University of Macau, China  
Kaifeng Hu,  
Chengdu University of Traditional  
Chinese Medicine, China

### \*Correspondence:

Chen Yang  
cyang@cemps.ac.cn  
Ying Wang  
ywang@sibs.ac.cn  
Shun Lu  
shunlu@sjtu.edu.cn

<sup>†</sup>These authors have contributed  
equally to this work

### Specialty section:

This article was submitted to  
Metabolomics,  
a section of the journal  
Frontiers in Molecular Biosciences

**Received:** 10 March 2021

**Accepted:** 10 May 2021

**Published:** 21 May 2021

### Citation:

Nie X, Xia L, Gao F, Liu L, Yang Y,  
Chen Y, Duan H, Yao Y, Chen Z, Lu S,  
Wang Y and Yang C (2021) Serum  
Metabolite Biomarkers Predictive of  
Response to PD-1 Blockade Therapy  
in Non-Small Cell Lung Cancer.  
Front. Mol. Biosci. 8:678753.  
doi: 10.3389/fmolb.2021.678753

**Background:** Despite remarkable success of immunotherapies with checkpoint blockade antibodies targeting programmed cell death protein 1 (PD-1), the majority of patients with non-small-cell lung cancer (NSCLC) have yet to receive durable benefits. We used the metabolomic profiling of early on-treatment serum to explore predictors of clinical outcomes of anti-PD-1 treatment in patients with advanced NSCLC.

**Methods:** We recruited 74 Chinese patients who had stage IIIB/IV NSCLC-proven tumor progression and were treated with PD-1 inhibitor. The study was comprised of a discovery cohort of patients treated with nivolumab and two validation cohorts of patients receiving tislelizumab or nivolumab. Serum samples were collected 2–3 weeks after the first infusion of PD-1 inhibitor. Metabolomic profiling of serum was performed using ultrahigh performance lipid chromatograph-mass spectrometry. The serum metabolite biomarkers were identified using an integral workflow of nontargeted metabolomic data analysis.

**Results:** A serum metabolite panel consisting of hypoxanthine and histidine was identified and validated as a predictor of response to PD-1 blockade treatment in patients with advanced NSCLC. High levels of both hypoxanthine and histidine in early on-treatment serum were associated with improved progression-free survival [hazard ratio (HR) = 0.078, 95% confidence interval (CI), 0.027–0.221,  $p < 0.001$ ] and overall survival (HR = 0.124, 95% CI, 0.039–0.397,  $p < 0.001$ ) in the discovery cohort. The serum metabolite panel showed a high sensitivity and specificity in distinguishing responders and non-responders in the validation cohorts 1 and 2, with an area under the receiver-operating characteristic curve of 0.933 and 1.000, respectively. High levels of serum hypoxanthine and histidine were correlated with improved progression-free survival in the validation cohort 1 (HR = 0.137, 95% CI, 0.040–0.467,  $p = 0.001$ ) and in the validation cohort 2 (HR = 0.084, 95% CI, 0.009–0.762,  $p = 0.028$ ).

**Conclusion:** Our results revealed that hypoxanthine and histidine in early on-treatment serum are predictive biomarkers of response to PD-1 blockade therapy in patients with

advanced NSCLC. The serum biomarker panel would enable early identification of NSCLC patients who may benefit from PD-1 blockade therapy.

**Keywords:** immune checkpoint inhibitors, non-small cell lung cancer, serum metabolomics, metabolite biomarker, non-targeted metabolomics

## INTRODUCTION

Non-small cell lung cancer (NSCLC) is the leading cause of cancer-related mortality worldwide and generally has a poor prognosis (Bray et al., 2018). During the past several years, major advances have been made in cancer treatment through the use of immune checkpoint inhibitors (ICIs) (Ribas and Wolchok, 2018). ICIs targeting programmed cell death protein 1 (PD-1) or its ligand PD-L1 have demonstrated improved clinical efficacy in both second-line and first-line treatment of advanced NSCLC when compared to conventional chemotherapy (Sui et al., 2018). At present, two anti-PD-1 antibodies nivolumab and pembrolizumab as well as several anti-PD-L1 antibodies have been approved by the United States Food and Drug Administration (FDA) for treatment of multiple cancer types including NSCLC (Ribas and Wolchok, 2018). Recently, an anti-PD-1 antibody tislelizumab has been approved in China for treatment of NSCLC and other cancers (Liu and Wu, 2020). These PD-1/PD-L1 inhibitors block the binding of PD-1 to its PD-L1 ligand and restore the capacity of cytotoxic T cells to recognize and kill cancer cells. Current PD-1/PD-L1 blockade therapies have shown durable disease control and improved survival in patients with advanced NSCLC (Rangachari and Costa, 2019). However, only subsets of patients are benefiting from the anti-PD-1/PD-L1 therapies. For example, only 10–30% of patients with NSCLC have objective tumor responses to treatment with nivolumab (Borghaei et al., 2015; Topalian et al., 2019). The mechanistic basis for the variation in response patterns remains poorly explained. In addition, some patients experience severe autoimmune adverse events (Friedman et al., 2016; Spain et al., 2016). Given the distinct response patterns, combined with potentially severe toxicity and high costs, there is an urgent need to identify biomarkers that can predict which patients are likely to benefit from PD-1/PD-L1 blockade therapies.

So far, PD-L1 expression, which is assayed by immunohistochemistry (IHC) staining on tumor specimens, is the most commonly used biomarker for selecting patients treated with anti-PD-1/PD-L1 antibodies (Topalian et al., 2015). However, PD-L1 expression was not consistently associated with tumor responses and patient survival. For example, only 44.8% of PD-L1-positive NSCLCs are responsive to pembrolizumab in a first-line treatment (Garon et al., 2015). A proportion of PD-L1-negative patients with NSCLC or other cancers also benefits from anti-PD-1 therapy (Robert et al., 2015). Several other biomarkers, which include tumor mutational load, mismatch-repair deficiency, neoantigens, density of tumor-infiltrating lymphocytes, and the diversity of gut microbiome, have been reported to correlate with the clinical outcomes (Le et al., 2015; Rizvi et al., 2015; Berghoff et al., 2016; McGranahan et al., 2016; Jin et al., 2019). However, these proposed biomarkers are not perfectly predictive. Moreover, most of them are based on tumor assays, which require invasive sampling, and are not practical for

monitoring tumor response during treatment. Recently, circulating blood biomarkers for prediction of immunotherapeutic responses have attracted increasing attention because they can be minimally invasively obtained from patients and trended over time (Li, Bullock, et al., 2019).

Tumor-infiltrating immune cells typically experience metabolic stress as a result of the dysregulated metabolic activity of tumor cells, which can result in immunosuppression and tumor immune evasion (Herbel et al., 2016). Cumulative evidence indicates that combination of ICIs with interventions targeting the metabolic circuits that impede antitumor immunity may be a promising strategy to improve clinical efficacy (Li, Wenes, et al., 2019). Metabolic biomarkers of immunotherapeutic responses can not only guide the therapeutic decisions but also lead to identification of novel metabolic targets for combination therapies. Advances in mass spectrometry (MS)-based metabolomics have allowed the discovery of new biomarkers for cancer diagnosis and customized treatment (Crutchfield et al., 2016). However, up to now, only a few metabolomics studies have been performed to investigate the changes in serum metabolites after anti-PD-1 treatment (Li H, et al., 2019), the gut microbiota-derived metabolites in responsive patients (Frankel et al., 2017), and the correlation between plasma metabolites and T cell markers (Hatae et al., 2020). Metabolic biomarkers that can reliably predict outcomes of anti-PD-1/PD-L1 treatments remain to be uncovered.

In this study, by comprehensively profiling metabolites in early on-treatment serum from a discovery cohort, we identified a metabolite panel consisting of hypoxanthine and histidine as a predictor of NSCLC response to PD-1 blockade, which was then validated in independent patient cohorts. High levels of the serum metabolite biomarkers were found to correlate with improved survival of patients with NSCLC receiving PD-1 blockade therapy.

## MATERIALS AND METHODS

### Patients

Patients of this study were recruited from Shanghai Chest Hospital affiliated to Shanghai Jiao Tong University (Shanghai, China). All the participants had histologically proven stage IIIB/IV NSCLC (**Table 1**). Serum samples from a patient cohort treated with nivolumab were used as a discovery set to identify potential serum biomarkers of response to PD-1 blockade therapy. The potential metabolite biomarkers were validated in a patient cohort receiving tislelizumab and another cohort treated with nivolumab. The patients treated with nivolumab had squamous or non-squamous cell carcinoma and had received one to two prior systemic

**TABLE 1 |** Clinical characteristics of discovery and validation sets and efficacy of anti-PD-1 therapy.

Characteristics <sup>a</sup>	Discovery set (n = 43)	Validation set 1 (n = 21)	Validation set 2 (n = 10)
Age, year	63 (41–74)	60.4 (54–72)	64.5 (46–78)
Sex			
Male	33 (77%)	14 (67%)	9 (90%)
Female	10 (23%)	7 (33%)	1 (10%)
Smoking status			
Smoker	31 (72%)	11 (52%)	8 (80%)
Non-smoker	12 (28%)	10 (48%)	2 (20%)
Histology			
Squamous	17 (40%)	0	7 (70%)
Non-squamous	26 (60%)	21 (100%)	3 (30%)
Disease stage			
III	6 (14%)	1 (5%)	1 (10%)
IV	37 (86%)	20 (95%)	9 (90%)
Metastasis			
Yes	37 (86%)	20 (95%)	9 (90%)
No	6 (14%)	1 (5%)	1 (10%)
Previous chemotherapy treatment			
Cisplatin based	28 (62%)	-	5 (36%)
Carboplatin based	12 (27%)	-	6 (43%)
Others	3 (7%)	-	3 (21%)
No previous treatment	0	-	0
Unknown	2 (4%)	-	0
Radiotherapy			
Yes	15 (35%)	4 (19%)	8 (80%)
No	27 (63%)	9 (43%)	2 (20%)
Unknown	1 (2%)	8 (38%)	0
Clinical benefit to PD-1 blockade			
Durable clinical benefit	23 (53%)	13 (62%)	4 (40%)
No clinical benefit	20 (47%)	8 (38%)	6 (60%)
RECIST response to PD-1 blockade			
Complete response	0	0	0
Stable disease	18 (42%)	6 (29%)	6 (60%)
Partial response	8 (19%)	13 (62%)	0
Progression disease	17 (39%)	2 (9%)	4 (40%)
Progression-free survival since PD-1 blockade, days	152 (24–645)	369 (42–770)	87 (27–429)
Overall survival since PD-1 blockade, days	573 (33–648)	596 (86–769)	366 (144–429)

<sup>a</sup>Data are expressed as number (%) or median (range).

therapies and proved progression before PD-1 blockade therapy. The patients receiving tislelizumab all had non-squamous cell carcinoma, and tislelizumab was used as first-line therapy in combination with chemotherapy. All the participants in this study were followed up until disease progression or death. Patients received nivolumab (240 mg) every 2 weeks, and tislelizumab (200 mg) was administered every 3 weeks. Peripheral blood samples were collected after administration of nivolumab or tislelizumab. Disease severity was measured by computed tomography or magnetic resonance imaging and evaluated for therapeutic response using Response Evaluation Criteria in Solid Tumors 1.1 (RECIST 1.1). Clinical response to the treatment with nivolumab or tislelizumab was evaluated every 8 weeks and was confirmed by a subsequent assessment no less than 4 weeks thereafter. Electronic medical charts were reviewed independently by two investigators to assign clinical response groups. Responders were defined by freedom from disease, stable disease, or decreased tumor volume for more than 6 months, and non-responders were defined by tumor growth or a clinical benefit lasting 6 months or less (Hodi et al., 2018). Patients gave their written informed consent to participate in the

research, which had received approval from the Ethics Committee of Shanghai Chest Hospital. All the procedures were conducted in accordance with the Declaration of Helsinki.

## Sample Preparation

Serum was collected after centrifugation of peripheral blood at 1500 g for 10 min and immediately stored at  $-80^{\circ}\text{C}$ . The samples were thawed on ice. Then 100  $\mu\text{l}$  of samples were mixed with 50  $\mu\text{l}$  of internal standard (6  $\mu\text{g}/\text{ml}$  2-chloro-L-phenylalanine in water) and 350  $\mu\text{l}$  of methanol. After vortex for 1 min, the samples were centrifuged at 14,000 g for 15 min, and the supernatant was used for LC-MS analysis. Quality control (QC) samples were prepared by mixing aliquots of serum samples from a subset of the cohort and using the same procedure as the samples studied.

## Liquid Chromatography-Mass Spectrometry Analysis

Metabolites were profiled using ultrahigh performance lipid chromatography-mass spectrometry (UHPLC-MS). Samples were injected onto a UHPLC system (Acquity, Waters)



coupled to a Q Exactive hybrid quadrupole-orbitrap mass spectrometer (Thermo Fisher). The sample injection order was randomized, and QC and blank samples (80% methanol in water) were regularly injected throughout the run. The injection volume was 10  $\mu$ l. Metabolites were separated with a Luna NH2 column (50 mm  $\times$  2 mm, 5  $\mu$ m particle size, Phenomenex) (Yuan et al., 2012). The column was maintained at 15°C with a solvent flow rate of 0.3 ml/min. Solvent A was 20 mM ammonium acetate adjusted to pH 9.0 with ammonium hydroxide, and solvent B was acetonitrile. The gradient of B was as follows: 0 min, 85%; 3 min, 30%; 12 min, 2%; 15 min, 2%; 16 min, 85%; 23 min, 85% B. The mass spectrometer was run in both electrospray ionization positive (ESI<sup>+</sup>) and negative (ESI<sup>-</sup>) modes. The key parameters were as follows: ionization voltage, +3.8 kV/−3.8 kV; sheath gas pressure, 35 arbitrary units; capillary temperature, 320°C. The mass spectrometer was run in full scan mode at an *m/z* 70–1000 scan range and 70,000 resolution. MS/MS spectra were acquired with 15–35-eV collision energy.

## Data Processing

Data processing was performed using an integral workflow of nontargeted metabolomic data analysis (Dunn et al., 2011). Briefly, data were processed by R package XCMS, followed by quality checks and signal drift correction to generating a data matrix that consisted of retention time, *m/z* value, and peak intensity. The peak area of each metabolite was normalized to sum of areas of all metabolites present in the sample, and then unit-variance scaled before further statistical analysis (Gorrochategui et al., 2016). The accurate mass and acquired MS/MS spectra were used for metabolite identification by matching with in-house spectral libraries and online databases (mzCloud, MoNA, and HMDB) (Kind et al., 2018). Quantitation of serum metabolites was performed by using a targeted analysis and external calibration curves as reported previously (Roberts et al., 2012).

## Statistical Analysis

Multivariate statistical analysis of metabolomic data was performed using the SIMCA software (Umetrics). Unsupervised principal component analysis was conducted to visualize grouping trends and the clustering of QC samples. A supervised model of orthogonal partial least-squares-discriminant analysis (OPLS-DA) was applied to identify the metabolites contributing to class separation according to corresponding variable importance in the projection (VIP). The OPLS-DA parameters, R2Y and Q2, were used for evaluating the goodness of the model fit. The risk of overfitting of the OPLS-DA model was evaluated by performing 200 permutation tests.

Univariate statistical analysis of marker metabolites was performed using the Multi Experimental Viewer software (<http://www.tm4.org>). A nonparametric Wilcoxon-Mann-Whitney test was conducted, and a *p* value < 0.05 was considered a priori to be statistically significant. The metabolites with false discovery rate (FDR) values less than 0.05 and VIP values greater than 1.0 were defined as putative marker metabolites. The biomarker model was built by binary

logistic regression using forward stepwise method. To evaluate the classification performance, receiver operating characteristic (ROC) analysis was conducted and the area under the ROC curve (AUC) was computed by using the MedCalc software (<https://www.medcalc.org/>).

The Kaplan-Meier method was used to estimate progression-free and overall survival, with the differences between the groups calculated with the log-rank test. Hazard ratios (HRs) from univariate Cox regression were used to determine the association between marker metabolites and survival. Multivariate Cox regression was conducted to adjust for patient characteristics by using the SPSS software (SPSS Inc.).

## RESULTS

### Study Population

The characteristics of the study cohorts are summarized in **Table 1**. To identify potential serum biomarkers of clinical response to PD-1 blockade, we collected serum samples from a discovery cohort of 43 patients with advanced NSCLC treated with the anti-PD-1 antibody nivolumab. The potential biomarkers were confirmed in two independent validation sample sets. A validation cohort was comprised of 21 patients with advanced NSCLC treated with another PD-1 inhibitor, tislelizumab. Another cohort for biomarker validation includes 10 patients with NSCLC treated with nivolumab. Nivolumab-treated patients had squamous or non-squamous cell carcinoma, whereas all the patients receiving tislelizumab had non-squamous cell carcinoma. The patients were treated with nivolumab as the second-line or third-line therapy, whereas tislelizumab was used in the first-line combination therapy of the patients. We defined responsive and non-responsive patients based on the following criteria (Hodi et al., 2018): patients with durable clinical benefit (defined as no progression event or death within the first 6 months of PD-1 blockade) were classified as responders; patients with no durable clinical benefit (progression event or death within the first 6 months of PD-1 blockade) were classified as non-responders. No significant difference was observed in age, sex, disease history, disease stage, smoking history, and prior treatments between responders and non-responders in nivolumab- or tislelizumab-treated patients (**Supplementary Table S1**).

### Identification of Potential Metabolite Biomarkers of Response to PD-1 Blockade

We collected serum samples from the discovery cohort 2 weeks after the first infusion of nivolumab. Among the patients in the discovery cohort (*n* = 43), 21 being evaluated as partial response or stable disease were classified as responders, and 22 with disease progression were classified as non-responders. By using ultrahigh performance lipid chromatography-mass spectrometry (UHPLC-MS), a total of 1,566 metabolite peaks were detected, including 803 in the negative and 763 in the positive ionization modes. The quality control samples are clustered in the score plot of principal component analysis (PCA), indicating the good

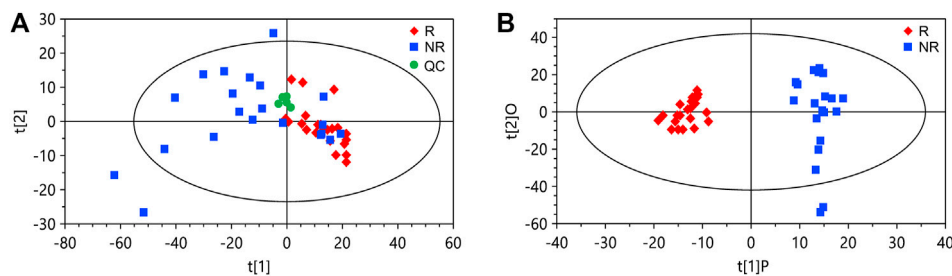


**FIGURE 1 |** Principal component analysis (PCA) and orthogonal partial least squares discriminant analysis (OPLS-DA) of the data from the discovery set. **(A)** PCA score plot. **(B)** OPLS-DA score plot. The cumulative  $R^2Y$  and  $Q^2Y$  of the OPLS-DA model are 0.92 and 0.67, respectively. R, responders; NR, non-responders; QC, quality control.

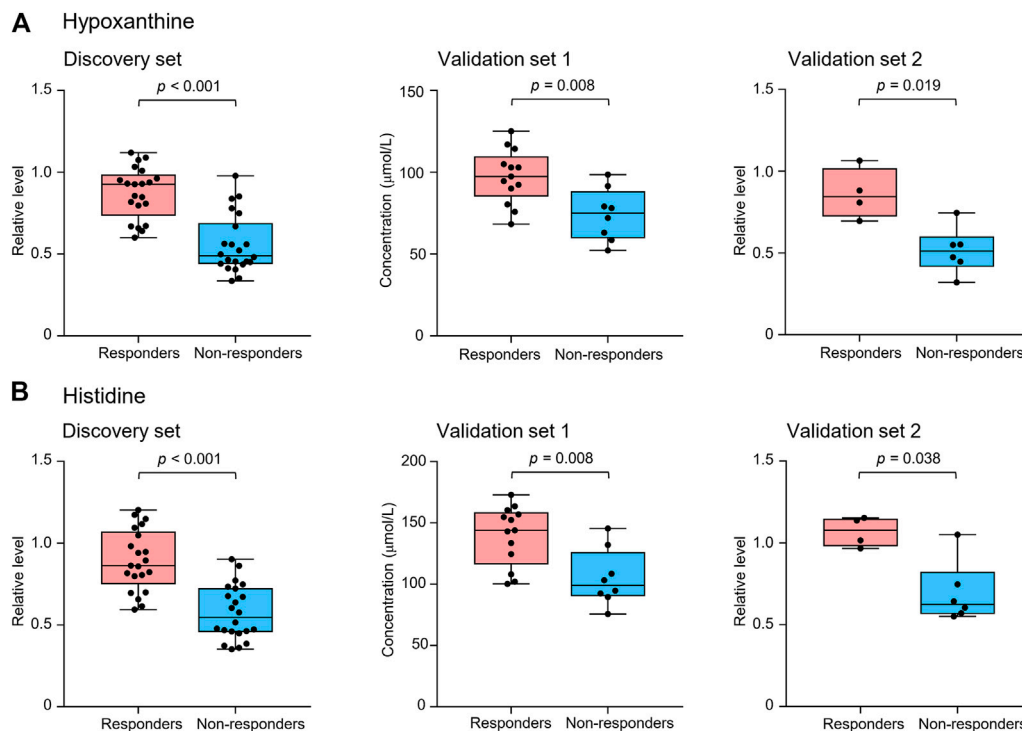


**FIGURE 2 |** Serum levels of potential marker metabolites hypoxanthine **(A)** and histidine **(B)** at early on-treatment in responders and non-responders of the discovery set and validation sets 1 and 2. The box plots depict the minimum and maximum values (whiskers), the upper and lower quartiles, and the median. Groups were compared by Wilcoxon-Mann-Whitney test with Benjamini-Hochberg-based adjustment for multiple comparisons.

reproducibility of the metabolomics analysis (**Figure 1A**). The PCA of the discovery set also demonstrated a tendency of difference in metabolomic profiles between responders and non-responders. For screening of potential marker metabolites, orthogonal partial least squares discriminant analysis (OPLS-DA) was applied. The OPLS-DA score plot of the discovery set revealed a clear separation between responders and non-responders without overfitting (**Figure 1B**). The validity of the OPLS-DA model was confirmed using permutation tests (**Supplementary Figure S1**). A subsequent univariate analysis was performed, resulting in identification of 185 metabolite peaks

with a variable importance in the project (VIP)  $> 1.0$ ,  $p < 0.05$ , and a false discovery rate (FDR)  $< 0.05$  as important variables contributing to class separation.

Metabolite identification was performed by matching accurate mass and tandem MS/MS spectra with in-house spectral libraries and online databases and by confirmation with authentic standards. Thus, six candidates of marker metabolites were obtained, including cystine, threonine, histidine, 3-oxotetradecanoic acid, 1,7-dimethyluric acid, and hypoxanthine (**Supplementary Table S2**). Binary logistic regression was performed to construct the best model using

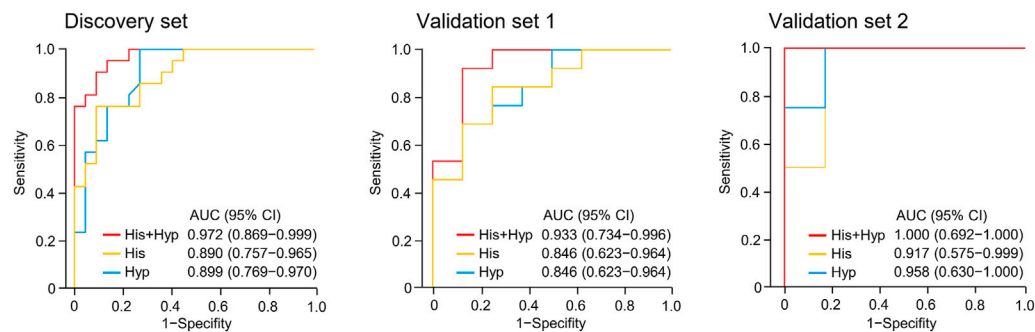


**FIGURE 3 |** Receiver operating characteristic (ROC) analysis of hypoxanthine and/or histidine in the discovery set and validation sets 1 and 2. Hyp, hypoxanthine; His, histidine; AUC, area under the curve.

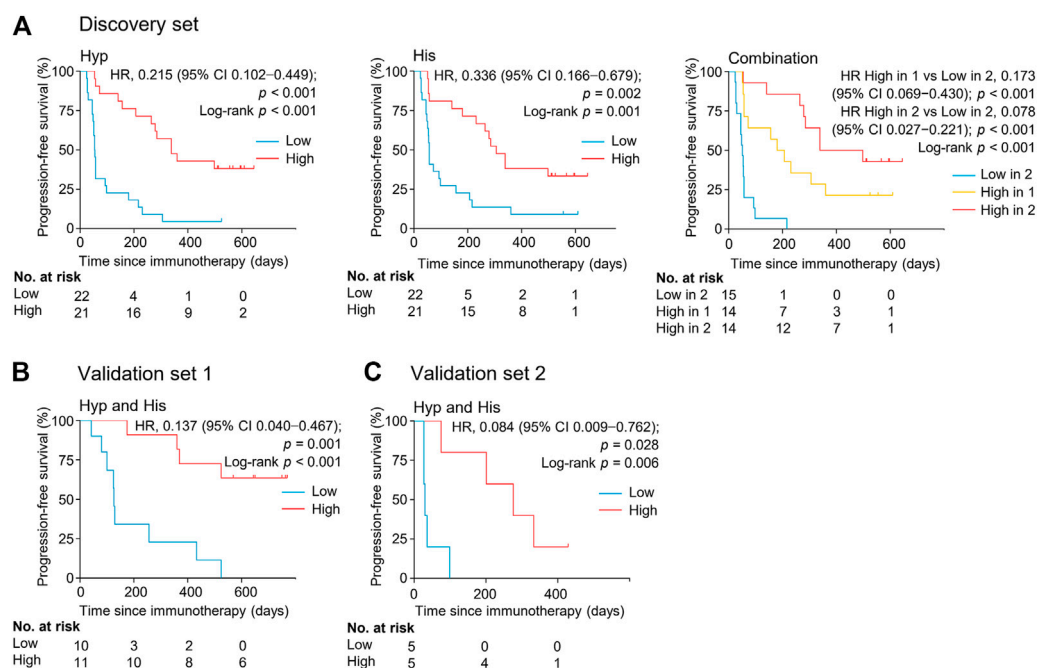


**FIGURE 4 |** Serum levels of metabolite biomarkers at early on-treatment associate with progression-free survival in the discovery set (A), validation set 1 (B), and validation set 2 (C). Kaplan-Meier analysis for progression-free survival in NSCLC patients by serum levels of hypoxanthine and/or histidine. His, histidine; Hyp, hypoxanthine; HR, hazard ratio.

the six metabolites (Supplementary Table S3). Therefore, the combination of hypoxanthine and histidine was identified as the best biomarker panel to distinguish responders and non-responders to nivolumab treatment. Responders had significantly higher levels of both marker metabolites in early on-treatment serum than non-responders ( $p < 0.001$  and  $p < 0.001$ , respectively) (Figure 2). By contrast, the PD-L1 expression in pretreatment tumors was not significantly different ( $p = 0.116$ ) between responders and non-responders in the discovery cohort (Supplementary Table S1). The receiver operating characteristic (ROC) analysis showed that the metabolite panel performs better than each metabolite in discrimination of responders and non-

responders (Figure 3). The area under the curve (AUC) for the metabolite panel was 0.972 [95% confidence interval (CI), 0.869–0.999], with sensitivity of 95% and specificity of 86%.

### High Marker Metabolite Levels Correlate With Improved Patient Survival

The association between the marker metabolites and the clinical outcome of nivolumab treatment was examined. Metabolite levels were dichotomized into high and low categorical variables based on the median value in the analyzed samples. We found that the serum levels of hypoxanthine and histidine at early on-treatment

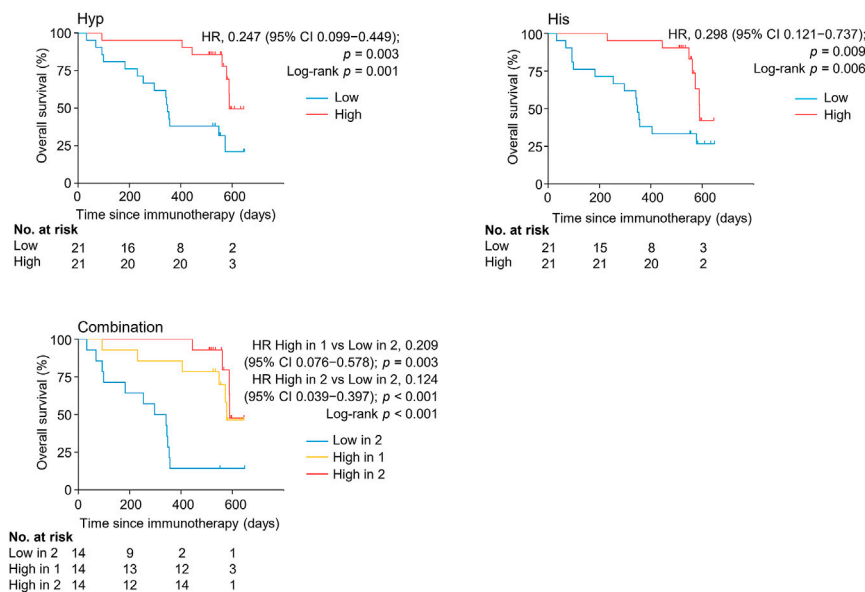


**FIGURE 5 |** Kaplan-Meier estimates of overall survival by serum levels of hypoxanthine and/or histidine in the discovery set. His, histidine; Hyp, hypoxanthine; HR, hazard ratio.

were significantly associated with progression-free survival (PFS) [hazard ratio (HR) = 0.215, 95% CI, 0.102–0.449,  $p < 0.001$ ; HR = 0.336, 95% CI, 0.166–0.679,  $p = 0.002$ , respectively] (**Figure 4**, **Supplementary Table S4**). The combination of both metabolites and the association with PFS demonstrated an additive effect (HR = 0.078, 95% CI, 0.027–0.221,  $p < 0.001$ ) (**Figure 4**, **Supplementary Table S4**). The median PFS of patients with high levels of one or both metabolites were 180 days (95% CI, 57–360 days) and 339 days (95% CI, 264–498 days), respectively, whereas patients with low levels of both metabolites had a median PFS of 51 days (95% CI, 27–57 days) ( $p < 0.001$ ) (**Figure 4**). The combination of both metabolites remained an independent factor for PFS in the multivariate analysis (**Supplementary Table S4**).

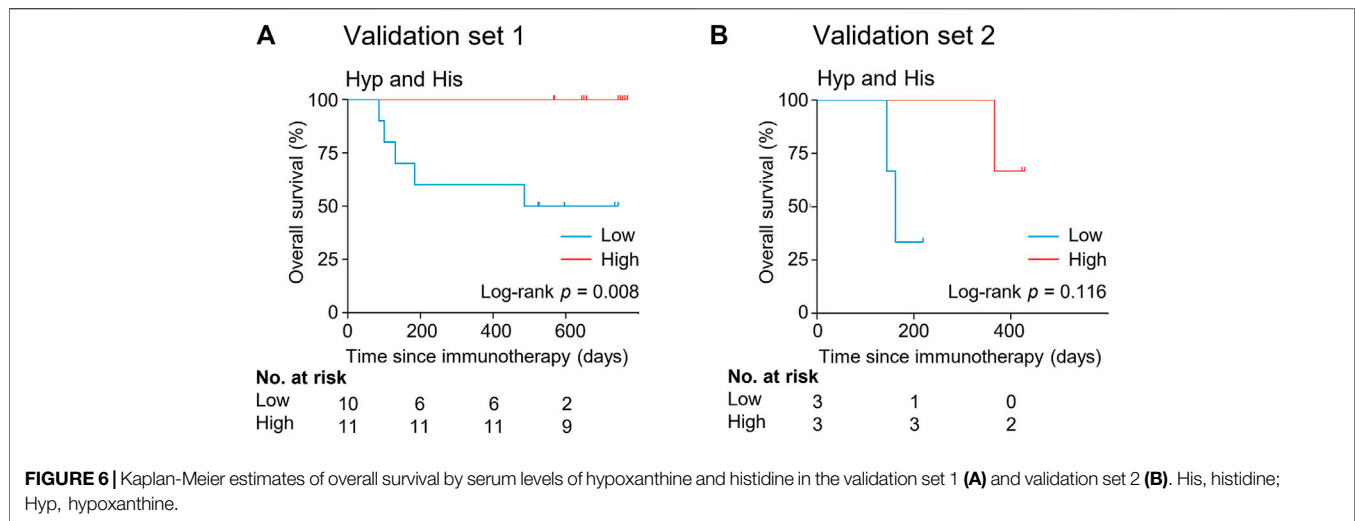
The levels of serum hypoxanthine and histidine were also significantly and independently correlated with overall survival (OS) (HR = 0.124, 95% CI, 0.039–0.397,  $p < 0.001$ ) (**Figure 5**, **Supplementary Table S5**). Patients with high levels of both metabolites had a longer overall survival (median OS of 589 days, 95% CI, 56–589 days) than did patients with low levels of both metabolites (median OS of 297 days, 95% CI 93–354 days) ( $p < 0.001$ ). Thus, hypoxanthine and histidine in early on-treatment serum were identified as the potential biomarkers predictive of clinical outcomes in patients with NSCLC receiving PD-1 blockade therapy.

## Validation of Serum Metabolite Biomarkers Predictive of Response to PD-1 Blockade

The potential metabolite biomarkers were evaluated in two independent validation sample sets. Serum samples were collected from a validation cohort 3 weeks after the first infusion of tislelizumab. This cohort consisted of 13

responders and eight non-responders (validation set 1) (**Table 1**). We determined the absolute concentrations of hypoxanthine and histidine in serum (**Figure 2**), and the measurements were highly reproducible. The logistic regression model of the metabolite panel for predicting response to PD-1 blockade was constructed as follows:  $\text{logit}(p = \text{Responder}) = 0.114 \times (\text{Hyp}) + 0.079 \times (\text{His}) - 19.548$ . In this equation, ( $p = \text{Responder}$ ) is the predicted probability of NSCLC patients benefiting from PD-1 blockade therapy, (Hyp) and (His) are the serum concentrations of hypoxanthine and histidine, respectively, at early on-treatment. The cutoff value of ( $p = \text{Responder}$ ) was 0.798. By using this model, the AUC was determined as 0.933 (95% CI, 0.734–0.996) for the validation set 1, with sensitivity of 92% and specificity of 88%, which indicates that the metabolite panel performed well in distinguishing responders and non-responders (**Figure 3**). A positive association between levels of the serum metabolite panel and PFS was highly statistically significant and independent (HR = 0.137, 95% CI, 0.040–0.467,  $p = 0.001$ ) (**Figure 4**, **Supplementary Table S6**). Patients with high levels of hypoxanthine and histidine had a median PFS of 569 days (95% CI, 360–750 days), whereas the median PFS for patients with low levels of both metabolites was 126 days (95% CI, 42–256 days) ( $p < 0.001$ ). Moreover, we found that high levels of the serum metabolite panel were significantly associated with improved overall survival of patient in the validation set 1 ( $p = 0.008$ ) (**Figure 6**).

Another validation cohort was comprised of 10 patients with NSCLC treated with nivolumab (validation set 2) (**Table 1**). Serum samples were collected from these patients 2 weeks after the first infusion of nivolumab. Similar to the results of the discovery set and validation set 1, serum level of the two



marker metabolites had a high sensitivity and specificity in discrimination of responders and non-responders of the validation set 2 (Figure 3). Responders had significantly higher levels of hypoxanthine and histidine in serum than non-responders ( $p = 0.019$  and  $p = 0.038$ , respectively) (Figure 2), which were verified by the enzyme-based assays (Supplementary Figure S2) (Liu et al., 2009; Sun et al., 2012). We found that high levels of the serum metabolite panel were correlated with improved PFS in the validation set 2 (HR = 0.084, 95% CI, 0.009–0.762,  $p = 0.028$ ) (Figure 4, Supplementary Table S6). Patients with high levels of the serum metabolite panel outlived patients with low levels of both metabolites, although the statistical significance cutoff was not met ( $p = 0.116$ ) (Figure 6). Thus, the results from the two independent validation sets confirmed the serum metabolite panel as predictive biomarkers of NSCLC response to PD-1 blockade therapy.

## DISCUSSION

Immunotherapies with checkpoint blockade antibodies targeting PD-1, PD-L1, and cytotoxic T-lymphocyte antigen 4 (CTLA-4) have remarkably improved the outcome of patients with advanced NSCLC and other cancers (Ribas and Wolchok, 2018). However, a substantial number of patients do not receive any clinical benefit, and robust predictors of therapeutic response are currently lacking. Though several tumor-derived and immune cell-derived biomarkers have been proposed, the demonstrated biomarker profiles often overlap between responders and non-responders and require invasive sampling from patients (Zhang et al., 2019). In the present study, we identified the serum metabolite biomarkers predictive of response to anti-PD-1 treatment in patients with advanced NSCLC based on metabolomic profiling using UHPLC-MS. The metabolomic profile of early on-treatment serum was found to be highly predictive of therapeutic responses, whereas the pretreatment serum metabolome was influenced by the initial

states in patients including the treatments prior to PD-1 blockade, thereby making it less suitable for use. Indeed, we failed to identify reliable biomarkers from the pretreatment serum metabolomic data of the discovery cohort possibly due to the heterologous treatments prior to PD-1 blockade. Hypoxanthine and histidine in early on-treatment serum were identified and validated in independent patient cohorts as the predictive biomarkers of clinical outcomes of PD-1 block therapy. To our knowledge, this is the first report of the validated serum metabolite biomarkers predictive of response to immune checkpoint blockade therapies in lung cancer. This biomarker panel would enable the identification of patients who may benefit from continuing after the first administration of anti-PD-1 antibodies. Moreover, blood collection for these biomarkers is minimally invasive compared with the collection of tumor tissues. For clinical praxis, the nontargeted metabolomic approach can be replaced by a targeted MS analysis or sensitive enzyme-based assays specifically for the metabolite biomarkers, which could simplify the process and reduce the measurement costs and thus allow a more affordable, large-scale analysis (Cui et al., 2018).

The identified metabolite biomarkers, hypoxanthine and histidine, have values beyond their ability to predict the response to PD-1 blockade. They also offer novel insight into mechanisms of therapeutic resistance and suggest metabolic targets for interventions in combination with PD-1 blockade to improve clinical efficacy. Hypoxanthine is a key intermediate in adenosine metabolism, which can be synthesized from adenosine through sequential activities of adenosine deaminase (ADA) and purine nucleoside phosphorylase (PNP) (Boison and Yegutkin, 2019). We found that hypoxanthine levels were significantly higher in responders than in non-responders, which suggests a role of the adenosine-hypoxanthine metabolism in therapeutic resistance to PD-1 blockade. Previous studies have demonstrated that adenosine is implicated in the suppression of T cell-mediated antitumor responses, and the adenosine pathway has become an important therapeutic target in cancer (Li X et al., 2019). Several clinical trials have been initiated to test the efficacy of combined



adenosine pathway inhibitors with PD-1/PD-L1 blockade in several cancers including NSCLC (Boison and Yegutkin, 2019). So far, much effort has been made to target adenosine-producing enzymes CD39 and CD73 and adenosine receptor A<sub>2A</sub>R for enhancing antitumor immunity (Arab and Hadjati, 2019). However, adenosine levels depend on the complex interplay between several adenosine-producing and -degrading pathways (Arab and Hadjati, 2019). Conversion of adenosine to hypoxanthine *via* ADA and PNP represents a currently underappreciated route that could regulate adenosine levels. Our finding prompts the intriguing question of whether increasing ADA and PNP activities for hypoxanthine synthesis from adenosine could improve antitumor immunity. In fact, ADA deficiency has been shown to result in tumor progression, and ADA activity of T cells has been suggested as an indicator of immune competence in patients with head and neck squamous cell carcinoma (Theodoraki et al., 2018).

Cancer cells increase uptake of amino acids, thereby depleting these resources for immune cells in the TME (Pavlova and Thompson, 2016). The amino acid transport and metabolism in T cells are also repressed by PD-1 ligation (Patsoukis et al., 2015). Thus, increased availability of amino acids may support the growth and function of T cells in the presence of PD-1 inhibitor. This may partially explain why responders had higher levels of serum histidine than non-responders among the patients receiving anti-PD-1 therapy. Moreover, high levels of histidine can increase the production of histamine through the reaction catalyzed by histidine decarboxylase (HDC). Histamine is an inhibitor of NADPH oxidase (NOX2) and has been approved in Europe in conjunction with interleukin-2 for relapse prevention in patients with acute myeloid leukemia (Stadtmauer, 2002). A recent study has shown that histamine targets myeloid-derived suppressor cells and improves the anti-tumor efficacy of PD-1/PD-L1 checkpoint blockade in mouse models (Grauers Wiktorin et al., 2019). Thus, our finding raises the possibility that supplementation of histamine/histidine and increasing HDC activity might be attractive strategies to enhance immunotherapy.

In conclusion, we report that the identification of metabolite biomarkers in early on-treatment serum constitutes a predictive tool for selecting NSCLC patients who stand to gain clinical benefit from anti-PD-1 therapy. Despite these provocative results, several limitations exist with this study. The patient cohorts in the current study were admittedly small and results need to be validated in large cohorts. Although the validation set one was comprised of patients receiving PD-1 inhibitor in combination with chemotherapy, the metabolite biomarkers need to be validated in more patient cohorts treated with combination therapy that is becoming a promising treatment strategy for NSCLC (Dong et al., 2019). Further studies are required to evaluate the serum metabolite panel for predicting clinical outcome of anti-PD-1 therapy in other cancer types. Our findings also warrant follow-

up studies to check the ability of the serum metabolite biomarkers to predict the response to drugs targeting other immune-related proteins, such as PD-L1 and CTLA-4.

## DATA AVAILABILITY STATEMENT

The original contributions presented in the study are included in the article/**Supplementary Material**, further inquiries can be directed to the corresponding authors.

## ETHICS STATEMENT

The studies involving human participants were reviewed and approved by the Ethics Committee of Shanghai Chest Hospital. The patients/participants provided their written informed consent to participate in this study.

## AUTHOR CONTRIBUTIONS

CY, YW, and SL designed the research; XN, LX, and FG performed the research; LL contributed analytic tools; YIY, YC, HD, YAY, and ZC contributed patient recruitment and medical records; XN, LX, FG, CY, YW, and SL analyzed data; and XN, CY, YW, and SL wrote the paper.

## FUNDING

This study was supported by grants from the National Key R&D Program of China (2016YFC1303303), National Natural Science Foundation of China (82030045, 81802264, 31925001, 31921006, 31900044, 82073152), Shanghai Science and Technology Commission Program (19411950500), and the Chinese Academy of Sciences (XDB27020201).

## ACKNOWLEDGMENTS

The authors thank X. Xu and W. Hu for technical assistance on hybrid quadrupole-orbitrap MS and G. P. Zhao for helpful discussions.

## SUPPLEMENTARY MATERIAL

The Supplementary Material for this article can be found online at: <https://www.frontiersin.org/articles/10.3389/fmolb.2021.678753/full#supplementary-material>

## REFERENCES

- Arab, S., and Hadjati, J. (2019). Adenosine Blockage in Tumor Microenvironment and Improvement of Cancer Immunotherapy. *Immune Netw.* 19 (4), e23. doi:10.4110/in.2019.19.e23
- Berghoff, A. S., Fuchs, E., Ricken, G., Mlecnik, B., Bindea, G., Spanberger, T., et al. (2016). Density of Tumor-Infiltrating Lymphocytes Correlates with Extent of Brain Edema and Overall Survival Time in Patients with Brain Metastases. *Oncoimmunology*. 5 (1), e1057388. doi:10.1080/2162402X.2015.1057388
- Boison, D., and Yegutkin, G. G. (2019). Adenosine Metabolism: Emerging Concepts for Cancer Therapy. *Cancer Cell*. 36 (6), 582–596. doi:10.1016/j.ccell.2019.10.007
- Borghaei, H., Paz-Ares, L., Horn, L., Spigel, D. R., Steins, M., Ready, N. E., et al. (2015). Nivolumab versus Docetaxel in Advanced Nonsquamous Non-small-cell Lung Cancer. *N. Engl. J. Med.* 373 (17), 1627–1639. doi:10.1056/NEJMoa1507643
- Bray, F., Ferlay, J., Soerjomataram, I., Siegel, R. L., Torre, L. A., and Jemal, A. (2018). Global Cancer Statistics 2018: GLOBOCAN Estimates of Incidence and Mortality Worldwide for 36 Cancers in 185 Countries. *CA: A Cancer J. Clinicians* 68 (6), 394–424. doi:10.3322/caac.21492
- Crutchfield, C. A., Thomas, S. N., Sokoll, L. J., and Chan, D. W. (2016). Advances in Mass Spectrometry-Based Clinical Biomarker Discovery. *Clin. Proteom.* 13, 1. doi:10.1186/s12014-015-9102-9
- Cui, L., Lu, H., and Lee, Y. H. (2018). Challenges and Emergent Solutions for LC-MS/MS Based Untargeted Metabolomics in Diseases. *Mass. Spec. Rev.* 37 (6), 772–792. doi:10.1002/mas.21562
- Dong, J., Li, B., Lin, D., Zhou, Q., and Huang, D. (2019). Advances in Targeted Therapy and Immunotherapy for Non-small Cell Lung Cancer Based on Accurate Molecular Typing. *Front. Pharmacol.* 10 (10), 230. doi:10.3389/fphar.2019.00230
- Dunn, W. B., Broadhurst, D., Broadhurst, D., Begley, P., Zelena, E., Francis-McIntyre, S., et al. (2011). Procedures for Large-Scale Metabolic Profiling of Serum and Plasma Using Gas Chromatography and Liquid Chromatography Coupled to Mass Spectrometry. *Nat. Protoc.* 6 (7), 1060–1083. doi:10.1038/nprot.2011.335
- Frankel, A. E., Coughlin, L. A., Kim, J., Froehlich, T. W., Xie, Y., Frenkel, E. P., et al. (2017). Metagenomic Shotgun Sequencing and Unbiased Metabolomic Profiling Identify Specific Human Gut Microbiota and Metabolites Associated with Immune Checkpoint Therapy Efficacy in Melanoma Patients. *Neoplasia*. 19 (10), 848–855. doi:10.1016/j.neo.2017.08.004
- Friedman, C. F., Proverbs-Singh, T. A., and Postow, M. A. (2016). Treatment of the Immune-Related Adverse Effects of Immune Checkpoint Inhibitors. *JAMA Oncol.* 2 (10), 1346–1353. doi:10.1001/jamaoncol.2016.1051
- Garon, E. B., Rizvi, N. A., Hui, R., Leighl, N., Balmanoukian, A. S., Eder, J. P., et al. (2015). Pembrolizumab for the Treatment of Non-small-cell Lung Cancer. *N. Engl. J. Med.* 372 (21), 2018–2028. doi:10.1056/NEJMoa1501824
- Gorrochategui, E., Jaumot, J., Lacorte, S., and Tauler, R. (2016). Data Analysis Strategies for Targeted and Untargeted LC-MS Metabolomic Studies: Overview and Workflow. *Trac Trends Anal. Chem.* 82, 425–442. doi:10.1016/j.trac.2016.07.004
- Grauers Wiktorin, H., Nilsson, M. S., Kiffin, R., Sander, F. E., Lenox, B., Rydström, A., et al. (2019). Histamine Targets Myeloid-Derived Suppressor Cells and Improves the Anti-tumor Efficacy of PD-1/pd-L1 Checkpoint Blockade. *Cancer Immunol. Immunother.* 68 (2), 163–174. doi:10.1007/s00262-018-2253-6
- Hatae, R., Chamoto, K., Kim, Y. H., Sonomura, K., Taneishi, K., Kawaguchi, S., et al. (2020). Combination of Host Immune Metabolic Biomarkers for the PD-1 Blockade Cancer Immunotherapy. *JCI Insight*. 5 (2), e133501. doi:10.1172/jci.insight.133501
- Herbel, C., Patsoukis, N., Bardhan, K., Seth, P., Weaver, J. D., and Boussiotis, V. A. (2016). Clinical Significance of T Cell Metabolic Reprogramming in Cancer. *Clin. Translational Med.* 5 (1), 29. doi:10.1186/s40169-016-0110-9
- Hodi, F. S., Ballinger, M., Lyons, B., Soria, J.-C., Nishino, M., Tabernero, J., et al. (2018). Immune-Modified Response Evaluation Criteria in Solid Tumors (imRECIST): Refining Guidelines to Assess the Clinical Benefit of Cancer Immunotherapy. *Jco* 36 (9), 850–858. doi:10.1200/jco.2017.75.1644
- Jin, Y., Dong, H., Xia, L., Yang, Y., Zhu, Y., Shen, Y., et al. (2019). The Diversity of Gut Microbiome Is Associated with Favorable Responses to Anti-programmed Death 1 Immunotherapy in Chinese Patients with NSCLC. *J. Thorac. Oncol.* 14 (8), 1378–1389. doi:10.1016/j.jtho.2019.04.007
- Kind, T., Tsugawa, H., Cajka, T., Ma, Y., Lai, Z., Mehta, S. S., et al. (2018). Identification of Small Molecules Using Accurate Mass MS/MS Search. *Mass. Spec. Rev.* 37 (4), 513–532. doi:10.1002/mas.21535
- Le, D. T., Uram, J. N., Wang, H., Bartlett, B. R., Kemberling, H., Eyring, A. D., et al. (2015). PD-1 Blockade in Tumors with Mismatch-Repair Deficiency. *N. Engl. J. Med.* 372 (26), 2509–2520. doi:10.1056/NEJMoa1500596
- Li, H., Bullock, K., Gurjao, C., Braun, D., Shukla, S. A., Bossé, D., et al. (2019). Metabolomic Adaptations and Correlates of Survival to Immune Checkpoint Blockade. *Nat. Commun.* 10 (1), 4346. doi:10.1038/s41467-019-12361-9
- Li, X., Wenes, M., Romero, P., Huang, S. C.-C., Fendt, S.-M., and Ho, P.-C. (2019). Navigating Metabolic Pathways to Enhance Antitumour Immunity and Immunotherapy. *Nat. Rev. Clin. Oncol.* 16 (7), 425–441. doi:10.1038/s41571-019-0203-7
- Liu, S.-Y., and Wu, Y.-L. (2020). Tislelizumab: an Investigational Anti-PD-1 Antibody for the Treatment of Advanced Non-small Cell Lung Cancer (NSCLC). *Expert Opin. Investig. Drugs*. 29 (12), 1355–1364. doi:10.1080/13543784.2020.1833857
- Liu, X., Chen, R., Shang, Y., Jiao, B., and Huang, C. (2009). Superoxide Radicals Scavenging and Xanthine Oxidase Inhibitory Activity of Magnesium Lithospermate B from *Salvia Miltiorrhiza*. *J. Enzyme Inhib. Med. Chem.* 24 (3), 663–668. doi:10.1080/14756360802323829
- McGranahan, N., Furness, A. J. S., Rosenthal, R., Ramskov, S., Lyngaa, R., Saini, S. K., et al. (2016). Clonal Neoantigens Elicit T Cell Immunoreactivity and Sensitivity to Immune Checkpoint Blockade. *Science*. 351 (6280), 1463–1469. doi:10.1126/science.aaf1490
- Patsoukis, N., Bardhan, K., Chatterjee, P., Sari, D., Liu, B., Bell, L. N., et al. (2015). PD-1 Alters T-Cell Metabolic Reprogramming by Inhibiting Glycolysis and Promoting Lipolysis and Fatty Acid Oxidation. *Nat. Commun.* 6, 6692. doi:10.1038/ncomms7692
- Pavlova, N. N., and Thompson, C. B. (2016). The Emerging Hallmarks of Cancer Metabolism. *Cel Metab.* 23 (1), 27–47. doi:10.1016/j.cmet.2015.12.006
- Rangachari, D., and Costa, D. B. (2019). From Hope to Reality: Durable Overall Survival with Immune Checkpoint Inhibitors for Advanced Lung Cancer. *J Clin Oncol.* 37 (28), 2511–2513. doi:10.1200/JCO.19.01207
- Ribas, A., and Wolchok, J. D. (2018). Cancer Immunotherapy Using Checkpoint Blockade. *Science*. 359 (6382), 1350–1355. doi:10.1126/science.aar4060
- Rizvi, N. A., Hellmann, M. D., Snyder, A., Kvistborg, P., Makarov, V., Havel, J. J., et al. (2015). Mutational Landscape Determines Sensitivity to PD-1 Blockade in Non-small Cell Lung Cancer. *Science*. 348 (6230), 124–128. doi:10.1126/science.aaa1348
- Robert, C., Long, G. V., Brady, B., Dutriaux, C., Maio, M., Mortier, L., et al. (2015). Nivolumab in Previously Untreated Melanoma without BRAF Mutation. *N. Engl. J. Med.* 372 (4), 320–330. doi:10.1056/NEJMoa1412082
- Roberts, L. D., SouzaFau - Gerszten, A., Robert, E., Gerszten Re Fau - Clish, Clary, B., and Clish, C. B. (2012). Targeted Metabolomics. *Curr. Protoc. Mol. Biol.* 98 (30), 1–24. doi:10.1002/0471142727.mb3002s98
- Spain, L., Diem, S., and Larkin, J. (2016). Management of Toxicities of Immune Checkpoint Inhibitors. *Cancer Treat. Rev.* 44, 51–60. doi:10.1016/j.ctrv.2016.02.001
- Stadtmauer, E. A. (2002). Histamine Dihydrochloride and Interleukin-2 in the Treatment of Acute Myeloid Leukemia. *Semin. Oncol.* 29 (3 Suppl. 7), 47–51. doi:10.1053/sonc.2002.33084
- Sui, H., Ma, N., Wang, Y., Li, H., Liu, X., Su, Y., et al. (2018). Anti-PD-1/PD-L1 Therapy for Non-small-cell Lung Cancer: Toward Personalized Medicine and Combination Strategies. *J. Immunol. Res.* 2018, 1–17. doi:10.1155/2018/6984948
- Sun, S.-K., Tu, K.-X., and Yan, X.-P. (2012). An Indicator-Displacement Assay for Naked-Eye Detection and Quantification of Histidine in Human Urine. *Analyst*. 137 (9), 2124–2128. doi:10.1039/c2an35126a
- Theodoraki, M.-N., Hoffmann, T. K., Jackson, E. K., and Whiteside, T. L. (2018). Exosomes in HNSCC Plasma as Surrogate Markers of Tumour Progression and Immune Competence. *Clin. Exp. Immunol.* 194 (1), 67–78. doi:10.1111/cei.13157
- Topalian, S. L., Drake, C. G., and Pardoll, D. M. (2015). Immune Checkpoint Blockade: a Common Denominator Approach to Cancer Therapy. *Cancer Cell*. 27 (4), 450–461. doi:10.1016/j.ccell.2015.03.001



- Topalian, S. L., Hodi, F. S., Brahmer, J. R., Gettinger, S. N., Smith, D. C., McDermott, D. F., et al. (2019). Five-Year Survival and Correlates Among Patients with Advanced Melanoma, Renal Cell Carcinoma, or Non-small Cell Lung Cancer Treated with Nivolumab. *JAMA Oncol.* 5 (10), 1411–1420. doi:10.1001/jamaoncol.2019.2187
- Yuan, M., Breitkopf, S. B., Yang, X., and Asara, J. M. (2012). A Positive/negative Ion-Switching, Targeted Mass Spectrometry-Based Metabolomics Platform for Bodily Fluids, Cells, and Fresh and Fixed Tissue. *Nat. Protoc.* 7 (5), 872–881. doi:10.1038/nprot.2012.024
- Zhang, M., Yang, J., Hua, W., Li, Z., Xu, Z., and Qian, Q. (2019). Monitoring Checkpoint Inhibitors: Predictive Biomarkers in Immunotherapy. *Front. Med.* 13 (1), 32–44. doi:10.1007/s11684-018-0678-0

**Conflict of Interest:** The authors declare that the research was conducted in the absence of any commercial or financial relationships that could be construed as a potential conflict of interest.

Copyright © 2021 Nie, Xia, Gao, Liu, Yang, Chen, Duan, Yao, Chen, Lu, Wang and Yang. This is an open-access article distributed under the terms of the Creative Commons Attribution License (CC BY). The use, distribution or reproduction in other forums is permitted, provided the original author(s) and the copyright owner(s) are credited and that the original publication in this journal is cited, in accordance with accepted academic practice. No use, distribution or reproduction is permitted which does not comply with these terms.



# Serum Metabolomic Patterns in Patients With Aldosterone-Producing Adenoma

Yule Chen<sup>1,2†</sup>, Hanjiang Wang<sup>1†</sup>, Ke Wang<sup>1,2</sup>, Guodong Zhu<sup>1,2</sup>, Zhishang Yang<sup>1,2</sup>, Min Wang<sup>1</sup> and Wenbin Song<sup>1,2\*</sup>

<sup>1</sup>Department of Urology, The First Affiliated Hospital of Xi'an Jiaotong University, Xi'an, China, <sup>2</sup>Oncology Research Laboratory, Key Laboratory of Environment and Genes Related to Diseases, Ministry of Education, Xi'an, China

## OPEN ACCESS

### Edited by:

Peter Igaz,  
Semmelweis University, Hungary

### Reviewed by:

Ariadni Spyroglou,  
University Hospital Zürich, Switzerland  
Adina F. Turcu,  
University of Michigan, United States

### \*Correspondence:

Wenbin Song  
drswb1206@aliyun.com

<sup>†</sup>These authors have contributed  
equally to this work

### Specialty section:

This article was submitted to  
Metabolomics,  
a section of the journal  
Frontiers in Molecular Biosciences

**Received:** 18 November 2021

**Accepted:** 21 February 2022

**Published:** 08 April 2022

### Citation:

Chen Y, Wang H, Wang K, Zhu G,  
Yang Z, Wang M and Song W (2022)  
Serum Metabolomic Patterns in  
Patients With Aldosterone-  
Producing Adenoma.  
Front. Mol. Biosci. 9:816469.  
doi: 10.3389/fmolb.2022.816469

Aldosterone-producing adenoma (APA), the main cause of endocrine hypertension, has recently been reported to be associated with other diseases, such as metabolic syndrome, but the detailed mechanism underlying this association remains unclear. Here, we used untargeted metabolomics and compared the abundance of serum metabolites between essential hypertension (EHT) and APA patients, as well as the serum metabolites of APA patients before and after adrenalectomy. Our results revealed 44 differential metabolites between APA and EHT patients and 39 differential metabolites between pre- and postoperative APA patients. Several metabolites involved in cardiovascular disease, obesity, and diabetes were dysregulated in APA patients compared to EHT patients, including arachidonic acid metabolites [e.g., 5(S)-HpETE and 12-HETE], amino acids (e.g., L-carnitine, taurine, and L-arginine), nucleotide metabolites (e.g., hypoxanthine) and cholesterol 3-sulfate. Importantly, the levels of hypoxanthine and cholesterol 3-sulfate, two metabolites that promote the development of atherosclerotic lesions and obesity, were originally increased in APA patients, but those elevated levels were reversed by adrenalectomy. Conversely, levels of L-carnitine and (3-carboxypropyl) trimethylammonium cation, two metabolites participating in lipid metabolism, were decreased in APA patients but increased postoperatively. We conclude that APA might participate in cardiovascular and metabolic diseases by regulating serum metabolites.

**Keywords:** aldosterone-producing adenoma, metabolomics, serum, hypertension, adrenalectomy

## INTRODUCTION

The renin-angiotensin-aldosterone system (RAAS) is an orchestrated hormonal cascade, that is, important for maintaining the homeostasis of fluids, electrolytes, and blood pressure; dysregulation of this cascade leads to cardiovascular disorders (Nappi and Sieg, 2011). Primary aldosteronism (PA), characterized as an overproduction of aldosterone under suppressed renin conditions (Gomez-Sanchez et al., 2020), is one of the most common causes of secondary hypertension, with a prevalence of 20% among patients with resistant hypertension (Byrd et al., 2018). Aldosterone-producing adenoma (APA) is one of the major subtypes of PA and can be cured by adrenalectomy (Funder, 2019). Elevated aldosterone results in low-renin hypertension, hypokalemia, and damage to target organs. It has been shown that patients with PA have a higher cardiovascular mortality than patients with essential hypertension (EHT), and this phenomenon was not explained by blood pressure

because the patients were matched for cardiovascular risk (Reincke et al., 2012). In addition, PA-directed therapy reduced the excess morbidity (Loh and Sukor, 2020). Importantly, emerging evidence has indicated that patients with PA not only have an increased risk of cardiovascular events but also have increased risks of diabetes and metabolic syndrome (Monticone et al., 2018). Thus, aldosterone in PA patients might play a wide range of roles in the human body. However, the details of the underlying mechanism remain unclear.

In recent decades, much effort has been exerted to improve our understanding of PA. Metabolomics, a high-throughput approach, has been adopted to describe the metabolic features of PA using tumor or urinary samples from APA patients to reveal the characteristics or improve the diagnosis of PA (Spyroglou et al., 2021). However, serum is an ideal sample for disease diagnosis, disease monitoring, and mechanistic investigations and not only reflects the changes at the genomic and proteomic levels but also is influenced by environmental factors (Hashim et al., 2019). Thus, in this study, we preliminarily investigated the effects of APA on human disease using untargeted metabolomics of serum samples from EHT patients and APA patients before and after adrenalectomy.

## MATERIALS AND METHODS

### Patients

We recruited a total of 11 patients with APA who had undergone unilateral retroperitoneal laparoscopic adrenalectomy in the Department of Urology at the First Affiliated Hospital of Xi'an Jiaotong University between January 2020 and May 2020. Serum renin and aldosterone were tested, and the aldosterone-renin ratio (ARR) was calculated to screen for APA. All patients had been diagnosed with unilateral cortical adenoma of the adrenal gland via enhanced computed tomography (CT). The diagnosis was confirmed by conducting an intravenous saline infusion test. Two of the patients aged <35 years were not recommended for adrenal vein sampling (AVS). The other patients were recommended for this procedure, but 3 patients refused it. Thus, in total, 6 patients underwent AVS, and the results were consistent with those of the CT scan. Eight patients had hypokalemia. No patients had abnormalities on cortisol or catecholamine tests. Three days after the adrenalectomy the serum aldosterone ARR and potassium levels were reexamined. We also recruited 9 patients with EHT admitted to the Department of Cardiovascular Medicine at the First Affiliated Hospital of Xi'an Jiaotong University as controls. EHT was defined as hypertension with no secondary hypertension cause, such as aberrant adrenal hormone levels, an adrenal mass, chronic kidney disease, renal artery stenosis, or hyperthyroidism. All patients agreed to participate in this study.

### Serum Collection

The EHT and preoperative APA patients were phlebotomized on the second day of hospitalization on an empty stomach. On the third day after adrenalectomy, the APA patients underwent a

second blood draw. The peripheral blood sample was kept at 4°C for 2 h until it coagulated, followed by centrifugation at 2000 rpm for 10 min. The supernatant was collected and subjected to metabolomics analysis. One patient did not undergo postoperative phlebotomization because of a fever after adrenalectomy. Finally, 9 EHT samples and 11 preoperative APA samples were used to analyze the differential serum metabolites between EHT and APA patients. Additionally, 10 pairs of preoperative and postoperative samples were used to analyze the differential serum metabolites before and after adrenalectomy.

### Metabolite Extraction

To extract metabolites from the serum samples, 400  $\mu$ L of cold extraction solvent methanol/acetonitrile/ $H_2O$  (2:2:1, v/v/v) was added to 100 mg of sample and adequately vortexed. After vortexing, the samples were incubated on ice for 20 min and then centrifuged at 14,000 g for 20 min at 4°C. The supernatant was collected and dried in a vacuum centrifuge at 4°C. For LC-MS analysis, the samples were redissolved in 100  $\mu$ L of acetonitrile/water (1:1, v/v) solvent and transferred to LC vials.

### LC-MS Analysis

For untargeted metabolomics of polar metabolites, extracts were analyzed using a quadrupole time-of-flight mass spectrometer (Sciex TripleTOF 6600) coupled to hydrophilic interaction chromatography via electrospray ionization (performed by Shanghai Applied Protein Technology Co., Ltd.). LC separation was performed on an ACQUITY UPLC BEH Amide column [2.1 mm  $\times$  100 mm, 1.7  $\mu$ m particle size (Waters, Ireland) using a gradient] of solvent A (25 mM ammonium acetate and 25 mM ammonium hydroxide in water) to solvent B (acetonitrile). The gradient was 85% B for 1 min and was linearly reduced to 65% B over 11 min and then reduced to 40% over 0.1 min and kept at that level for 4 min; then, the gradient was increased to 85% over 0.1 min, and a 5-min re-equilibration period was employed. The flow rate was 0.4 ml/min, the column temperature was 25°C, the auto sampler temperature was 5°C, and the injection volume was 2  $\mu$ L. The mass spectrometer was operated in both negative ion and positive ionization modes. The ESI source conditions were set as follows: ion source gas 1 (Gas 1) as 60, ion source gas 2 (gas 2) as 60, curtain gas (CUR) as 30, source temperature of 600°C, and IonSpray Voltage Floating (ISVF) of  $\pm$  5500 V. For MS acquisition, the instrument was set to acquire over the m/z range of 60–1000 Da, and the accumulation time for the TOF MS scan was set at 0.20 s/spectra. In auto MS/MS acquisition, the instrument was set to acquire over the m/z range of 25–1000 Da, and the accumulation time for the product ion scan was set at 0.05 s/spectra. The product ion scan was acquired using information-dependent acquisition (IDA) with the high-sensitivity mode selected. The parameters were set as follows: the collision energy (CE) was fixed at 35 V with  $\pm$  15 eV, a declustering potential (DP) was set at 60 V (+) and –60 V (–) to exclude isotopes within 4 Da, and the candidate ions to monitor per cycle were set at 10.

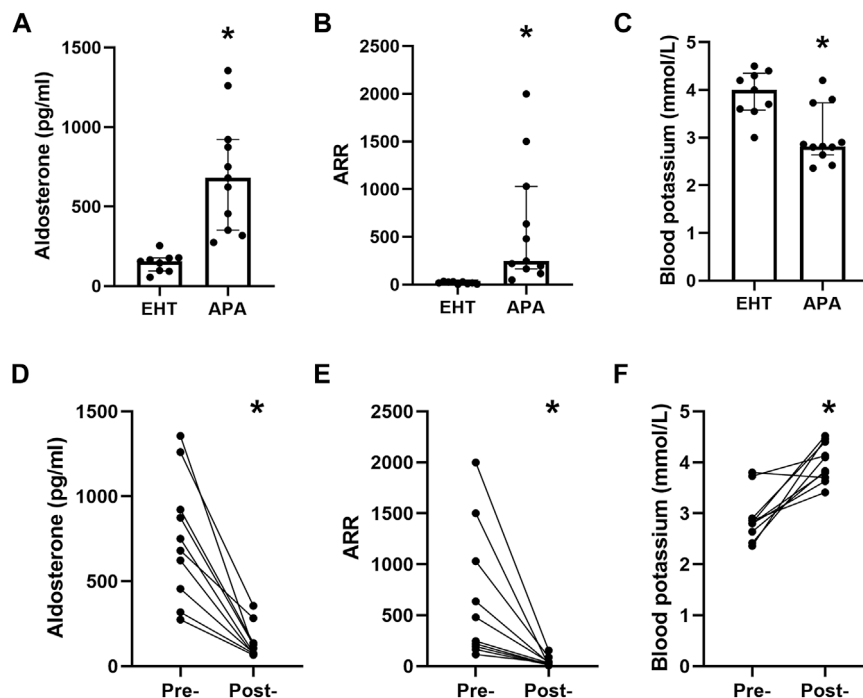


**FIGURE 1 |** Baseline characteristics of the participants. **(A)** Serum aldosterone levels of the EHT and APA patients. **(B)** The aldosterone-to-renin ratio (ARR) of EHT and APA patients. **(C)** Serum levels of potassium in EHT and APA patients. **(D)** Preoperative and postoperative serum aldosterone levels. **(E)** Preoperative and postoperative serum ARRs. **(F)** Preoperative and postoperative serum potassium levels.  $*p < 0.05$ .

## Data Processing and Statistical Analysis

Processing of LC-MS data was carried out by Shanghai Applied Protein Technology Co., Ltd. The raw MS data (wiff.scan files) were converted to MzXML files using ProteoWizard MSConvert before being imported into freely available XCMS software. To select the peaks, the following parameters were used: centWave  $m/z = 25$  ppm, peak width = c (10, 60), prefilter = c (10, 100). For peak grouping, bw = 5, mzwid = 0.025, and minfrac = 0.5 were used. Of the extracted ion features, only the variables with more than 50% of nonzero measurement values in at least one group were retained. Compound identification of metabolites by MS/MS spectra was conducted with an in-house database established with available authentic standards. After normalization to the total peak intensity, the processed data were uploaded before being imported into SIMCA-P (version 14.1, Umetrics, Umea, Sweden), where they were subjected to multivariate data analysis, including Pareto-scaled principal component analysis (PCA) and orthogonal partial least-squares discriminant analysis (OPLS-DA). Sevenfold cross-validation and response permutation testing were used to evaluate the robustness of the model. The variable importance in the projection (VIP) value of each variable in the OPLS-DA model was calculated to indicate its contribution to the classification. The normality of the distributions and the homogeneity of variances were checked using the Shapiro-Wilk test and Levene's test, respectively. For comparisons between the EHT and APA groups, the  $p$  value of normally distributed samples was calculated using Student's  $t$ -test (equal variances) or a two-tailed Welch's  $t$ -test (unequal variances), and the  $p$  value

of non-normally distributed samples was calculated using the Mann-Whitney  $U$  test. For comparisons between the preoperative and postoperative APA groups, the  $p$  value was calculated using a dependent  $t$ -test (normal distribution) or Wilcoxon signed-rank test (non-normal distribution). Metabolites with VIP  $> 1$  in OPLS-DA analysis and  $p < 0.05$  were defined as significantly differential metabolites. Metabolites with VIP values  $> 1$  and  $0.05 \leq p < 0.1$  were defined as differential metabolites because the difference approached statistical significance (Carrillo et al., 2016). A Kyoto Encyclopedia of Genes and Genomes (KEGG) analysis was performed to evaluate the enrichment of metabolites in various pathways.

The baseline patient data (e.g., age, serum aldosterone) were analyzed using GraphPad Prism 8.0. Quantitative data are presented as the median and interquartile range. Differences in mean values between two groups were analyzed with the Wilcoxon test. The differences in count data between two groups were analyzed using the  $\chi^2$  test.

## RESULTS

### Clinical Characteristics of Participants

We did not find any significant difference in sex, body mass index (BMI), or blood pressure between the EHT and APA groups, though they did differ in age (**Supplementary Table S1**). The serum aldosterone levels and ARR in the APA group were

**TABLE 1** | Differential metabolites between APA and EHT patients.

Positive ion mode				Negative ion mode			
Name	VIP	Fold change (APA vs EHT)	p value	Name	VIP	Fold change (APA vs EHT)	p value
<b>Glycerophosphocholine</b>	4.39	0.22	0.00	<b>(+)-12-HETE</b>	7.36	0.11	0.00
<b>L-Histidine</b>	2.13	0.29	0.00	<b>L-Glutamate</b>	5.55	0.41	0.00
<b>N6-Methyl-L-lysine</b>	1.34	0.37	0.05	<b>Succinate</b>	1.36	0.52	0.00
<b>Trigonelline</b>	1.18	0.45	0.01	<b>L-Aspartate</b>	1.77	0.59	0.00
<b>D-Proline</b>	3.60	0.48	0.00	<b>1-Oleoyl-L-<math>\alpha</math>-lysophosphatidic acid</b>	1.31	0.59	0.01
<b>L-Glutamate</b>	1.53	0.50	0.00	<b>Hydroxyisocaproic acid</b>	2.36	0.64	0.02
<b>Betaine</b>	2.73	0.51	0.00	<b>D-Quinovose</b>	1.88	0.66	0.05
<b>Ornithine</b>	1.21	0.53	0.01	<b>2-Hydroxy-3-methylbutyric acid</b>	2.96	0.66	0.05
<b>2-Methylbutyrocarnitine</b>	1.64	0.55	0.02	<b>Ammelide</b>	1.17	0.81	0.00
<b>L-Lysine</b>	1.36	0.55	0.03	<b>Hypoxanthine</b>	7.53	1.49	0.02
<b>L-Glutamine</b>	3.60	0.62	0.00	<b>3-Hydroxycaproic acid</b>	2.70	1.52	0.02
<b>1-Stearoyl-2-hydroxy-sn-glycero-3-phosphocholine</b>	1.80	0.62	0.01	<b>Bisindolylmaleimide I</b>	2.82	2.35	0.03
<b>(3-Carboxypropyl) trimethylammonium cation</b>	2.59	0.62	0.00	<b>pregnenolone sulfate</b>	4.36	2.38	0.04
<b>L-Citrulline</b>	1.06	0.66	0.02	<b>5(S)-HpETE</b>	2.95	32.38	0.00
<b>L-Leucine</b>	2.07	0.68	0.02	Phenol	6.98	0.51	0.06
<b>1-Oleoyl-sn-glycero-3-phosphocholine</b>	5.60	0.68	0.05	D-Sorbitol	1.14	0.57	0.08
<b>Nicotinamide</b>	1.56	0.73	0.04	L-Iditol	2.14	0.65	0.05
<b>L-Carnitine</b>	10.97	0.77	0.00	Capric acid	1.28	0.75	0.07
<b>Taurine</b>	1.75	0.83	0.02	L-Proline	2.01	0.81	0.09
<b>Sphingomyelin (d18:1/18:0)</b>	2.22	1.34	0.02	L-Glutamine	1.10	0.87	0.09
<b>Hypoxanthine</b>	2.26	1.55	0.02	2-Oxoadipic acid	8.58	1.03	0.08
<b>Thioetheramide-PC</b>	1.03	1.56	0.04	Cholesterol 3-sulfate	8.38	1.39	0.07
<b>L-Arginine</b>	4.99	0.57	0.05				

All significantly differential metabolites ( $VIP > 1$ ,  $p < 0.05$ ) are shown in bold and differential metabolites ( $VIP > 1$ ,  $0.05 \leq p < 0.1$ ) are shown in regular font. Bold values represents the significant differential metabolites.

significantly higher than those in the EHT group (Figures 1A,B). The level of serum potassium in the APA group was significantly lower than that in the EHT group (Figure 1C). Three days after adrenalectomy, serum aldosterone levels and ARR were significantly decreased, and all patients with hypokalemia had normal potassium levels (Figures 1D–F).

## Differential Metabolites Between EHT and APA Patients

The PCA indicated good clustering of the QC group, and no extreme outliers were observed (Supplementary Figure S1A). The OPLS-DA analysis indicated clear separation between the EHT and APA groups in both positive and negative ion modes (Supplementary Figure S1B). The results of the permutation test strongly indicated that original models in both positive ( $R^2 = 0.6675$ ,  $Q^2 = -0.3839$ ) and negative ( $R^2Y = 0.9786$ ,  $Q^2 = -0.1739$ ) ion modes were valid (Supplementary Figure S1C).

In our study, a total of 164 and 168 known biochemical compounds were identified by LC–MS analysis in positive ion and negative ion modes, respectively. Based on our selection criteria, we detected 22 significantly differential metabolites between the EHT and APA groups ( $VIP > 1$ ,  $p < 0.05$ ) and one differential metabolite ( $VIP > 1$ ,  $0.05 \leq p < 0.1$ ) in the positive ion mode, and we identified 14 significantly differential metabolites ( $VIP > 1$ ,  $p < 0.05$ ) and 8 differential metabolites ( $VIP > 1$ ,  $0.05 \leq p < 0.1$ ) between the EHT and APA groups in the negative ion

mode. All significantly differential metabolites and differential metabolites are listed in Table 1. Combining the results from both positive and negative ion modes revealed that 10 metabolites exhibited higher abundance in the APA group, while 34 metabolites exhibited lower abundance in the APA group than in the EHT group. Among the metabolites abundant in the APA group, 5(S)-HpETE showed the largest fold change and was 32-fold higher in the APA group than in the EHT group. Among the metabolites abundant in the EHT group, 12-HETE showed the largest fold change and was 9-fold higher in the EHT group than in the APA group (Figure 2A, Table 1).

A KEGG enrichment analysis was conducted on all significantly differential metabolites detected by both positive and negative ion modes. The results indicated that the significantly differential metabolites were enriched in several pathways, such as those involving GABAergic synapses, arginine synthesis, and ABC transporters (Figure 2B).

## Differential Metabolites Between the Preoperative and Postoperative Serum of APA Patients

The PCA indicated good clustering of the QC group, and no extreme outliers were observed (Supplementary Figure S2A). The OPLS-DA analysis indicated clear separation between the preoperative and postoperative groups, in both positive and negative ion modes (Supplementary Figure S2B). The results

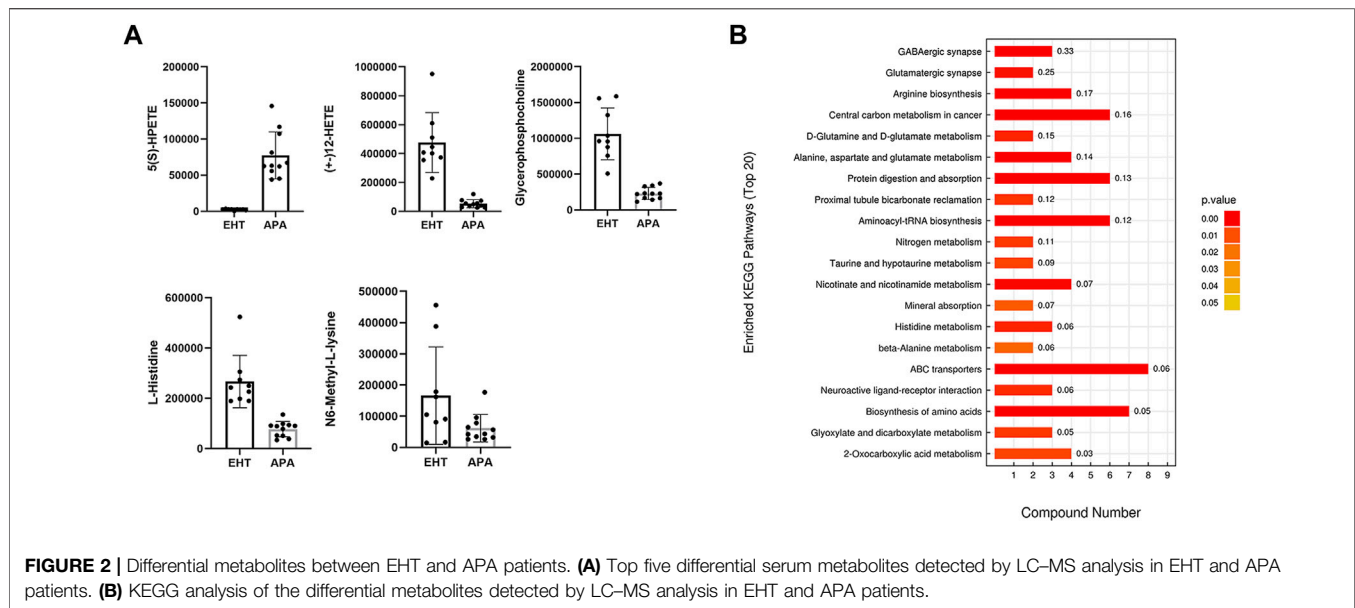
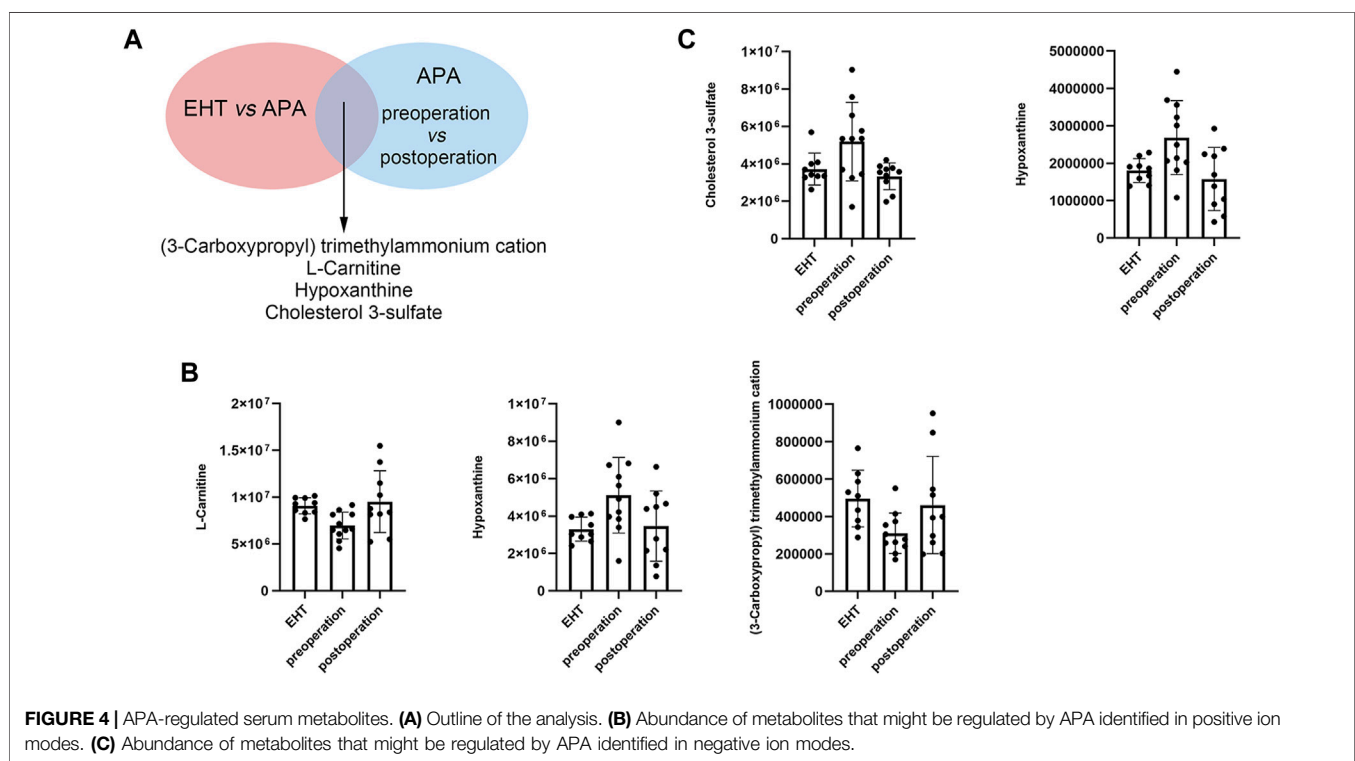
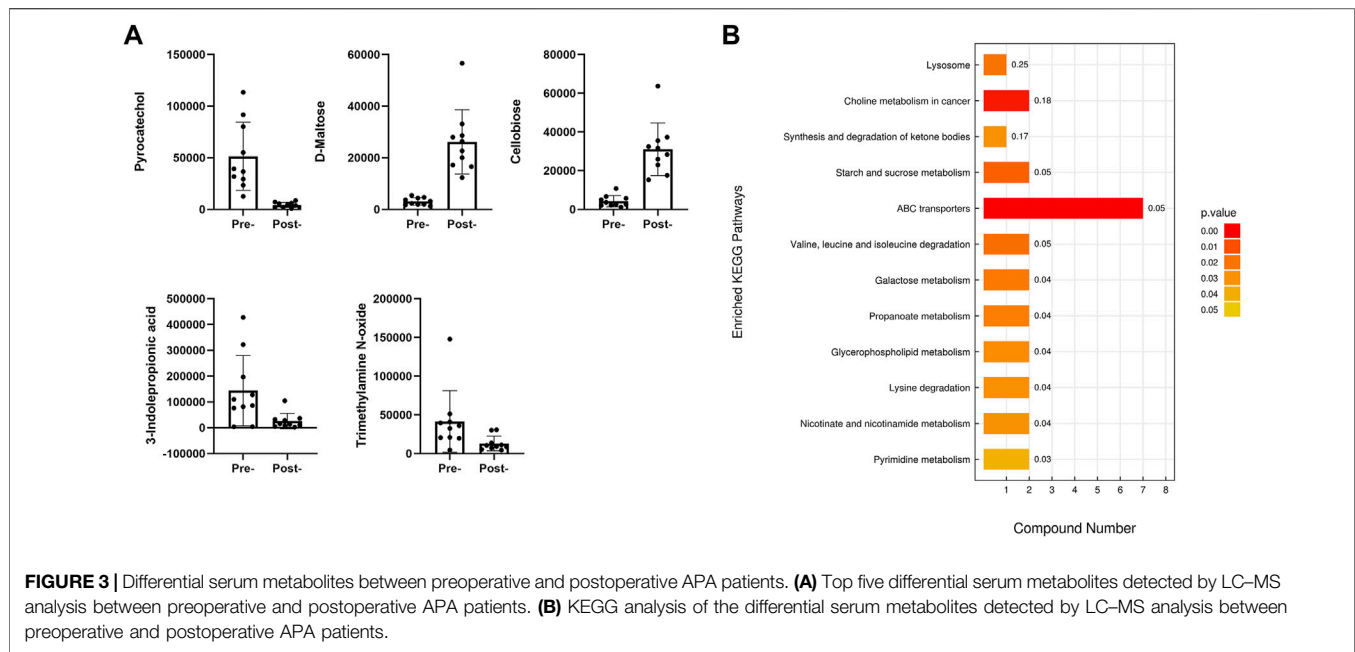


**TABLE 2 |** Differential metabolites between preoperative and postoperative APA patients.

Positive ion mode				Negative ion mode			
Name	VIP	Fold change (postoperative vs. preoperative)	p value	Name	VIP	Fold change (postoperative vs. preoperative)	p value
Trimethylamine N-oxide	1.70	0.32	0.04	<b>Pyrocatechol</b>	1.95	0.08	0.00
Trigonelline	2.21	0.33	0.00	<b>3-Indolepropionic acid</b>	2.68	0.18	0.02
Nicotinamide	3.71	0.38	0.00	<b>Indoxyl sulfate</b>	10.53	0.48	0.03
L-Lysine	2.18	0.48	0.01	<b>Hypoxanthine</b>	9.58	0.55	0.00
Allopurinol riboside	2.86	0.50	0.01	<b>Cholesterol 3-sulfate</b>	13.22	0.60	0.00
Inosine	5.45	0.53	0.01	<b>1-Palmitoyl-2-hydroxy-sn-glycero-3-phosphoethanolamine</b>	1.34	0.76	0.01
Uracil	1.09	0.60	0.00	<b>Taurine</b>	1.90	1.25	0.05
Hypoxanthine	15.68	0.63	0.02	<b>D-Mannose</b>	1.24	1.50	0.01
Phthalic acid Mono-2-ethylhexyl Ester	1.70	0.64	0.03	<b>D-Lyxose</b>	1.62	1.57	0.01
Glycerophosphocholine	3.58	0.65	0.03	<b>Methylmalonic acid</b>	1.45	1.77	0.00
L-Citrulline	1.36	0.66	0.01	<b>D-Threitol</b>	1.02	1.98	0.00
1-Palmitoyllysophosphatidylcholine	1.23	0.67	0.01	<b>myo-Inositol</b>	1.33	2.15	0.02
1-Palmitoyl-2-hydroxy-sn-glycero-3-phosphoethanolamine	1.66	0.74	0.01	<b>Acetoacetic acid</b>	1.33	2.21	0.00
1-Stearoyl-2-oleoyl-sn-glycerol 3-phosphocholine (SOPC)	13.56	1.24	0.05	<b>D-Maltose</b>	1.28	8.55	0.00
L-Carnitine	16.64	1.40	0.03	Chenodeoxycholate	1.49	0.31	0.07
Phe-Ile	1.26	2.04	0.01	Allantoin	1.97	0.84	0.07
Cellobiose	1.99	7.37	0.00	DL-3-Phenyllactic acid	1.32	1.66	0.06
N1-Methyl-2-pyridone-5-carboxamide	3.32	0.50	0.06				
Decanoyl-L-carnitine	2.99	0.64	0.09				
1-Oleoyl-sn-glycero-3-phosphocholine	8.81	0.72	0.05				
1-Palmitoyl-sn-glycero-3-phosphocholine	2.38	0.81	0.08				
Betaine	1.75	0.83	0.08				
(3-Carboxypropyl) trimethylammonium cation	3.34	1.61	0.06				

All significantly differential metabolites ( $VIP > 1$ ,  $p < 0.05$ ) are shown in bold and differential metabolites ( $VIP > 1$ ,  $0.05 \leq p < 0.1$ ) are shown in regular font. Bold values represents the significant differential metabolites.





of the permutation test strongly indicated that the original models of both positive ( $R^2 = 0.9196$ ,  $Q^2 = -0.2122$ ) and negative ( $R^2Y = 0.8224$ ,  $Q^2 = -0.3506$ ) ion modes were valid (**Supplementary Figure S2C**).

Based on our selection criteria, we detected 17 significantly differential metabolites ( $VIP > 1$ ,  $p < 0.05$ ) and 6 differential metabolites ( $VIP > 1$ ,  $0.05 \leq p < 0.1$ ) between the preoperative

and postoperative groups in the positive ion mode, and we identified 14 significantly differential metabolites ( $VIP > 1$ ,  $p < 0.05$ ) and 3 differential metabolites ( $VIP > 1$ ,  $0.05 \leq p < 0.1$ ) between the preoperative and postoperative groups in the negative ion mode. All significantly differential metabolites and differential metabolites are listed in **Table 2**.

Combining the results of both positive and negative ion modes revealed that 10 metabolites exhibited higher abundance in the preoperative APA group, while 34 metabolites exhibited higher abundance in the postoperative APA group. Among the metabolites abundant in the preoperative APA group, cellobiose showed the largest fold change and was 8.5-fold higher in the preoperative APA group than in the postoperative APA group. Among the metabolites abundant in the postoperative APA group, pyrocatechol showed the largest fold change and was 12.5-fold higher in the postoperative APA group than in the preoperative APA group (**Figure 3A**).

A KEGG enrichment analysis was conducted including all significantly differential metabolites detected by both positive and negative ion modes. The results indicated that the significantly differential metabolites were enriched in 12 pathways, such as those involving ABC transporters and lysine degradation (**Figure 3B**).

### APA-Regulated Serum Metabolites

Next, we conducted a conjoint analysis by combining the significantly differential metabolites and differential metabolites between the serum of the EHT and APA groups and those between the serum of the preoperative and postoperative APA patients (**Figure 4A**). The results indicated that hypoxanthine and cholesterol 3-sulfate levels were increased in APA patients compared with those in EHT patients and were decreased postoperatively (**Figures 4B,C**). Conversely, L-carnitine and (3-carboxypropyl) trimethylammonium cation levels were decreased in APA patients compared with those in EHT patients and were increased postoperatively (**Figures 4B,C**). In particular, a change in hypoxanthine levels was detected in both positive and negative ion modes (**Figures 4B,C**).

## DISCUSSION

Early studies on PA metabolomics mainly focused on steroid profiling, which indicated elevated 18-hydroxycortisol and 18-oxocortisol levels in APA patients (Spyrogliou et al., 2021). Recently, Alessandro Lana et al. performed metabolic profiling to distinguish between EHT and APA patients and between APA and bilateral adrenal hyperplasia (BAH) patients.

They found that purine nucleosides and the related catabolites deoxyadenosine and uric acid were considerably different between EHT and PA patients; however, the adenosine deamination catabolites (deoxyinosine, hypoxanthine, and IMP), free amino acids (histidine and taurine), and the pyrimidine diphosphate CDP exhibited higher discriminatory power when comparing APA and BAH groups in a sex-independent manner (Lana et al., 2019). Another study focusing on distinct signatures of KCNJ5 and CACNA1D mutant APAs was performed by Murakami and colleagues. They revealed that purine metabolism is activated in KCNJ5 mutant APA (Murakami et al., 2019).

In the current study, we compared the abundance of serum metabolites in EHT and APA patients using untargeted metabolomics. The results revealed 34 decreased and 10

increased metabolites in APA patients compared with EHT patients. KEGG analysis of the differential metabolites between APA and EHT patients found that they were enriched in several pathways involved in central carbon metabolism, amino acid metabolism, and ABC transporters, indicating that APA might have a broad effect on human metabolism. Among these metabolites, we observed differences in two arachidonic acid catabolites, 5(S)-HpETE and 12-HETE, between EHT and APA patients. Since arachidonic acid is widely involved in inflammation, obesity, diabetes, hypercholesterolemia, and cardiovascular disease, it is possible that APA facilitates cardiovascular and metabolic diseases via changes in arachidonic acid metabolism (Sonnweber et al., 2018). Furthermore, both 5(S)-HpETE and 12-HETE levels showed clear separation between APA and EHT patients, indicating that these metabolites might be used as biomarkers to screen for APA.

We also found that APA patients had lower levels of several amino acids (e.g., L-histidine, D-proline, L-glutamate, ornithine, L-lysine, L-glutamine, L-citrulline, L-leucine, L-carnitine, taurine, L-arginine, L-aspartate) than those of EHT patients; some of these amino acids have been reported to play a protective role against cardiovascular diseases. For example, L-arginine was found to improve artery diameter and endothelial function in humans and improve endothelial function and reduce atherosclerotic plaques in animal models (Zaric et al., 2020), while taurine supplementation improved left ventricular function and reduced atherosclerotic lesion formation (Zaric et al., 2020). Thus, amino acid metabolism might be another mechanism underlying APA-mediated cardiovascular risks.

We also compared serum metabolites in preoperative and postoperative patients with APA. The results indicated 25 downregulated and 14 upregulated metabolites after the operation. KEGG analysis of the differential metabolites showed that they were enriched in pathways involved in ABC transporters, pyrimidine metabolism, and lysine degradation. Using a conjoint analysis that combined the differential serum metabolites of the EHT and APA groups and of the preoperative and postoperative APA patients, we found that hypoxanthine and cholesterol 3-sulfate levels were increased in APA patients compared with those in EHT patients but decreased postoperatively. Conversely, L-carnitine and (3-carboxypropyl) trimethylammonium cation levels were decreased in APA patients compared with those in EHT patients but increased postoperatively. Most of these metabolites have been found to be associated with metabolic syndrome or cardiovascular diseases. For example, cholesterol 3-sulfate is present on a variety of cells and in human low-density lipoproteins and is believed to participate in platelet adhesion and atherosclerotic lesions (Merten et al., 2001). Hypoxanthine is a product of purine metabolism and is associated with obesity and smoking (Furuhashi et al., 2020). L-carnitine transports long-chain fatty acids into the mitochondrial matrix, thus allowing the cells to degrade fat (Pekala et al., 2011). L-carnitine supplementation thus provides a protective effect against overweight (Askarpour et al., 2020) and cardiovascular events (Wang et al., 2018). (3-Carboxypropyl) trimethylammonium is derived from betaine,

a dietary compound that participates in lipid metabolism (Airaksinen et al., 2018). However, we did not observe any changes in levels of 5(S)-HpETE or 12-HETE, possibly due to the short interval (only 3 d) between the adrenalectomy and postoperative blood sampling.

The main limitation of our study was its small sample size. Further studies with larger sample sizes are needed to validate the differential metabolites and to investigate their clinical significance. In addition, postoperative serum samples were collected only 3 d after adrenalectomy. This might miss potential metabolites regulated by APA. Thus, longer follow-up times are also needed in future studies. Finally, the age difference between APA and EHT patients might affect the accuracy of the results.

## CONCLUSION

In this study, we identified differential serum metabolites between patients with EHT and APA, as well as differential serum metabolites between APA patients pre- and post-adrenalectomy. We found that several metabolites involved in cardiovascular diseases, obesity, and diabetes were dysregulated in APA patients compared to those in EHT patients. In particular, APA patients had higher hypoxanthine and cholesterol 3-sulfate levels but lower L-carnitine and (3-carboxypropyl) trimethylammonium cations levels than EHT patients. The abnormality of the concentrations of these metabolites was reversed by adrenalectomy. We conclude that APA might influence cardiovascular and metabolic diseases by regulating these metabolites.

## DATA AVAILABILITY STATEMENT

The original contributions presented in the study are included in the article/**Supplementary Material**, further inquiries can be directed to the corresponding author.

## REFERENCES

- Airaksinen, K., Jokkala, J., Ahonen, I., Auriola, S., Kolehmainen, M., Hanhineva, K., et al. (2018). High-Fat Diet, Betaine, and Polydextrose Induce Changes in Adipose Tissue Inflammation and Metabolism in C57BL/6J Mice. *Mol. Nutr. Food Res.* 62, e1800455. doi:10.1002/mnfr.201800455
- Askarpour, M., Hadi, A., Miraghajani, M., Symonds, M. E., Sheikhi, A., and Ghaedi, E. (2020). Beneficial Effects of L-Carnitine Supplementation for Weight Management in Overweight and Obese Adults: An Updated Systematic Review and Dose-Response Meta-Analysis of Randomized Controlled Trials. *Pharmacol. Res.* 151, 104554. doi:10.1016/j.phrs.2019.104554
- Byrd, J. B., Turcu, A. F., and Auchus, R. J. (2018). Primary Aldosteronism. *Circulation* 138, 823–835. doi:10.1161/circulationaha.118.033597
- Carrillo, J. A., He, Y., Li, Y., Liu, J., Erdman, R. A., Sonstegard, T. S., et al. (2016). Integrated Metabolomic and Transcriptome Analyses Reveal Finishing Forage Affects Metabolic Pathways Related to Beef Quality and Animal Welfare. *Sci. Rep.* 6, 25948. doi:10.1038/srep25948
- Funder, J. W. (2019). Primary Aldosteronism. *Hypertension* 74, 458–466. doi:10.1161/hypertensionaha.119.12935

## ETHICS STATEMENT

The studies involving human participants were reviewed and approved by the Ethics Committee of the First Affiliated Hospital of Xi'an Jiaotong University. The patients/participants provided their written informed consent to participate in this study.

## AUTHOR CONTRIBUTIONS

WS supervised the study and revised the manuscript. YC designed the study. HW wrote the manuscript. KW prepared the serum samples. GZ analyzed the data. ZY collected the clinical data. MW conducted the phlebotomization. All authors read and approved the final manuscript.

## FUNDING

This study was supported by National Natural Science Foundation of China grants (No. 81672539 and No. 82173292).

## SUPPLEMENTARY MATERIAL

The Supplementary Material for this article can be found online at: <https://www.frontiersin.org/articles/10.3389/fmolb.2022.816469/full#supplementary-material>

**Supplementary Figure S1** | PCA and OPLS-DA score plots of EHT and APA patients. **(A)** PCA score plot of the serum of EHT and APA patients. **(B)** OPLS-DA score plot of the serum of EHT and APA patients. **(C)** Permutation plots for the OPLS-DA model showing R<sup>2</sup> and Q<sup>2</sup> values.

**Supplementary Figure S2** | PCA and OPLS-DA score plots of preoperative and postoperative APA patients. **(A)** PCA score plot of the serum of preoperative and postoperative APA patients. **(B)** OPLS-DA score plot of the serum of preoperative and postoperative APA patients. **(C)** Permutation plots for the OPLS-DA model showing R<sup>2</sup> and Q<sup>2</sup> values.

**Supplementary Table S1** | Baseline characteristics of the participants.

- Furuhashi, M., Koyama, M., Higashiura, Y., Murase, T., Nakamura, T., Matsumoto, M., et al. (2020). Differential Regulation of Hypoxanthine and Xanthine by Obesity in a General Population. *J. Diabetes Investig.* 11, 878–887. doi:10.1111/jdi.13207
- Gomez-Sanchez, C. E., Gomez-Sanchez, C. M., and Oki, K. (2020). Aldosterone-Producing Adenomas: More Than Meets the Eye. *Hypertension* 75, 927–929. doi:10.1161/HYPERTENSIONAHA.119.14534
- Hashim, N. A. A., Ab-Rahim, S., Suddin, L. S., Saman, M. S. A., and Mazlan, M. (2019). Global Serum Metabolomics Profiling of Colorectal Cancer. *Mol. Clin. Oncol.* 11, 3–14. doi:10.3892/mco.2019.1853
- Lana, A., Alexander, K., Castagna, A., D'Alessandro, A., Morandini, F., Pizzolo, F., et al. (2019). Urinary Metabolic Signature of Primary Aldosteronism: Gender and Subtype-specific Alterations. *Proteomics Clin. Appl.* 13, e1800049. doi:10.1002/prca.201800049
- Loh, H. H., and Sukor, N. (2020). Associations between Primary Aldosteronism and Diabetes, Poor Bone Health, and Sleep Apnea-What Do We Know So Far? *J. Hum. Hypertens.* 34, 5–15. doi:10.1038/s41371-019-0294-8
- Merten, M., Dong, J. F., Lopez, J. A., and Thiagarajan, P. (2001). Cholesterol Sulfate. *Circulation* 103, 2032–2034. doi:10.1161/01.cir.103.16.2032

- Monticone, S., D'Ascenzo, F., Moretti, C., Williams, T. A., Veglio, F., Gaita, F., et al. (2018). Cardiovascular Events and Target Organ Damage in Primary Aldosteronism Compared with Essential Hypertension: a Systematic Review and Meta-Analysis. *Lancet Diabetes Endocrinol.* 6, 41–50. doi:10.1016/s2213-8587(17)30319-4
- Murakami, M., Rhayem, Y., Kunzke, T., Sun, N., Feuchtinger, A., Ludwig, P., et al. (2019). *In Situ* metabolomics of Aldosterone-Producing Adenomas. *JCI Insight* 4, e130356. doi:10.1172/jci.insight.130356
- Nappi, J., and Sieg, A. (2011). Aldosterone and Aldosterone Receptor Antagonists in Patients with Chronic Heart Failure. *Vhrm* 7, 353–363. doi:10.2147/vhrm.s13779
- Pekala, J., Patkowska-Sokola, B., Bodkowski, R., Jamroz, D., Nowakowski, P., Lochynski, S., et al. (2011). L-carnitine - Metabolic Functions and Meaning in Humans Life. *Cdm* 12, 667–678. doi:10.2174/138920011796504536
- Reincke, M., Fischer, E., Gerum, S., Merkle, K., Schulz, S., Pallauf, A., et al. (2012). Observational Study Mortality in Treated Primary Aldosteronism. *Hypertension* 60, 618–624. doi:10.1161/hypertensionaha.112.197111
- Sonnweber, T., Pizzini, A., Nairz, M., Weiss, G., and Tancevski, I. (2018). Arachidonic Acid Metabolites in Cardiovascular and Metabolic Diseases. *Int. J. Mol. Sci.* 19, 3285. doi:10.3390/ijms19113285
- Spyroglou, A., Piaditis, G. P., Kaltsas, G., and Alexandraki, K. I. (2021). Transcriptomics, Epigenetics, and Metabolomics of Primary Aldosteronism. *Cancers (Basel)* 13, 5582. doi:10.3390/cancers13215582
- Wang, Z.-Y., Liu, Y.-Y., Liu, G.-H., Lu, H.-B., and Mao, C.-Y. (2018). l-Carnitine and Heart Disease. *Life Sci.* 194, 88–97. doi:10.1016/j.lfs.2017.12.015
- Zaric, B. L., Radovanovic, J. N., Gluvic, Z., Stewart, A. J., Essack, M., Motwalli, O., et al. (2020). Atherosclerosis Linked to Aberrant Amino Acid Metabolism and Immunosuppressive Amino Acid Catabolizing Enzymes. *Front. Immunol.* 11, 551758. doi:10.3389/fimmu.2020.551758

**Conflict of Interest:** The authors declare that the research was conducted in the absence of any commercial or financial relationships that could be construed as a potential conflict of interest.

**Publisher's Note:** All claims expressed in this article are solely those of the authors and do not necessarily represent those of their affiliated organizations, or those of the publisher, the editors, and the reviewers. Any product that may be evaluated in this article, or claim that may be made by its manufacturer, is not guaranteed or endorsed by the publisher.

Copyright © 2022 Chen, Wang, Wang, Zhu, Yang, Wang and Song. This is an open-access article distributed under the terms of the Creative Commons Attribution License (CC BY). The use, distribution or reproduction in other forums is permitted, provided the original author(s) and the copyright owner(s) are credited and that the original publication in this journal is cited, in accordance with accepted academic practice. No use, distribution or reproduction is permitted which does not comply with these terms.



## OPEN ACCESS

## EDITED BY

Donghai Lin,  
Xiamen University, China

## REVIEWED BY

Daniele Vergara,  
University of Salento, Italy  
Yahui Wang,  
Washington University in St. Louis,  
United States  
Lin Shi,  
Shaanxi Normal University, China

## \*CORRESPONDENCE

Christoph Trautwein,  
✉ christoph.trautwein@med.uni-  
tuebingen.de

## SPECIALTY SECTION

This article was submitted to  
Metabolomics, a section of the journal  
Frontiers in Molecular Biosciences

RECEIVED 08 February 2023

ACCEPTED 30 March 2023

PUBLISHED 19 April 2023

## CITATION

Bae G, Berezhnoy G, Koch A, Cannet C,  
Schäfer H, Kommos S, Brucker S,  
Beziere N and Trautwein C (2023),  
Stratification of ovarian cancer borderline  
from high-grade serous carcinoma  
patients by quantitative serum NMR  
spectroscopy of metabolites,  
lipoproteins, and inflammatory markers.  
*Front. Mol. Biosci.* 10:1158330.  
doi: 10.3389/fmolb.2023.1158330

## COPYRIGHT

© 2023 Bae, Berezhnoy, Koch, Cannet,  
Schäfer, Kommos, Brucker, Beziere and  
Trautwein. This is an open-access article  
distributed under the terms of the  
Creative Commons Attribution License  
(CC BY). The use, distribution or  
reproduction in other forums is  
permitted, provided the original author(s)  
and the copyright owner(s) are credited  
and that the original publication in this  
journal is cited, in accordance with  
accepted academic practice. No use,  
distribution or reproduction is permitted  
which does not comply with these terms.

# Stratification of ovarian cancer borderline from high-grade serous carcinoma patients by quantitative serum NMR spectroscopy of metabolites, lipoproteins, and inflammatory markers

Gyuntae Bae<sup>1</sup>, Georgy Berezhnoy<sup>1</sup>, André Koch<sup>2</sup>, Claire Cannet<sup>3</sup>,  
Hartmut Schäfer<sup>3</sup>, Stefan Kommos<sup>2</sup>, Sara Brucker<sup>2</sup>,  
Nicolas Beziere<sup>1,4</sup> and Christoph Trautwein<sup>1\*</sup>

<sup>1</sup>Werner Siemens Imaging Center, Department of Preclinical Imaging and Radiopharmacy, University Hospital Tübingen, Tübingen, Germany, <sup>2</sup>Department of Women's Health, University Hospital Tübingen, Tübingen, Germany, <sup>3</sup>Bruker BioSpin GmbH, Ettlingen, Germany, <sup>4</sup>Cluster of Excellence CMFI (EXC 2124) "Controlling Microbes to Fight Infections", Eberhard Karls University of Tübingen, Tübingen, Germany

**Background:** Traditional diagnosis is based on histology or clinical-stage classification which provides no information on tumor metabolism and inflammation, which, however, are both hallmarks of cancer and are directly associated with prognosis and severity. This project was an exploratory approach to profile metabolites, lipoproteins, and inflammation parameters (glycoprotein A and glycoprotein B) of borderline ovarian tumor (BOT) and high-grade serous ovarian cancer (HGSOC) for identifying additional useful serum markers and stratifying ovarian cancer patients in the future.

**Methods:** This project included 201 serum samples of which 50 were received from BOT and 151 from high-grade serous ovarian cancer (HGSOC), respectively. All the serum samples were validated and phenotyped by <sup>1</sup>H-NMR-based metabolomics with *in vitro* diagnostics research (IVDr) standard operating procedures generating quantitative data on 38 metabolites, 112 lipoprotein parameters, and 5 inflammation markers. Uni- and multivariate statistics were applied to identify NMR-based alterations. Moreover, biomarker analysis was carried out with all NMR parameters and CA-125.

**Results:** Ketone bodies, glutamate, 2-hydroxybutyrate, glucose, glycerol, and phenylalanine levels were significantly higher in HGSOC, while the same tumors showed significantly lower levels of alanine and histidine. Furthermore, alanine and histidine and formic acid decreased and increased, respectively, over the clinical stages. Inflammatory markers glycoproteins A and B (GlycA and GlycB) increased significantly over the clinical stages and were higher in HGSOC, alongside significant changes in lipoproteins. Lipoprotein subfractions of VLDLs, IDLs, and LDLs increased significantly in HGSOC and over the clinical stages, while total plasma apolipoprotein A1 and A2 and a subfraction of HDLs decreased significantly over the clinical stages. Additionally, LDL triglycerides



significantly increased in advanced ovarian cancer. In biomarker analysis, glycoprotein inflammation biomarkers behaved in the same way as the established clinical biomarker CA-125. Moreover, CA-125/GlycA, CA-125/GlycB, and CA-125/GlycS are potential biomarkers for diagnosis, prognosis, and treatment response of epithelial ovarian cancer (EOC). Last, the quantitative inflammatory parameters clearly displayed unique patterns of metabolites, lipoproteins, and CA-125 in BOT and HGSOC with clinical stages I–IV.

**Conclusion:**  $^1\text{H}$ -NMR-based metabolomics with commercial IVDr assays could detect and identify altered metabolites and lipoproteins relevant to EOC development and progression and show that inflammation (based on glycoproteins) increased along with malignancy. As inflammation is a hallmark of cancer, glycoproteins, thereof, are promising future serum biomarkers for the diagnosis, prognosis, and treatment response of EOC. This was supported by the definition and stratification of three different inflammatory serum classes which characterize specific alternations in metabolites, lipoproteins, and CA-125, implicating that future diagnosis could be refined not only by diagnosed histology and/or clinical stages but also by glycoprotein classes.

#### KEYWORDS

metabolomics, tumor progression, metastasis, glycoprotein, CA-125, biomarker, diagnostics, precision medicine

## 1 Introduction

Ovarian cancer (OC) has been considered highly life-threatening (Clarke-Pearson, 2009), and worldwide, OC incidents and deaths are 88.01% and 84.20%, respectively (Zhou et al., 2021). To date, more than 30 different histology types of OC have been described, and epithelial OC (EOC) that starts to proliferate in the epithelial layer covering the ovary is the most common and accounts for more than 95% of OC malignancy (Desai et al., 2014; Kaku et al., 2003). Furthermore, EOC is classified into five subtypes, of which high-grade serous ovarian cancer (HGSOC) is the most frequently diagnosed (Prat and FIGO Committee on Gynecologic Oncology, 2014).

OC relies on a variety of energy metabolites to develop; in particular, OC has high propensity on Warburg and reverse Warburg effects (Schwartz et al., 2017; Li et al., 2019; Wang and Li, 2020). As Otto Warburg demonstrated, neoplasms showed highly increased metabolic rates that were characterized by a high uptake of glucose as a primary energy source and the production of an excessive amount of lactate even in the presence of oxygen (Warburg et al., 1927). This process is called the Warburg effect, involving the alteration of metabolic enzymes such as hexokinase 2 (HK2) (Wang et al., 2014), pyruvate kinase type M2 (PKM2) (Wong et al., 2015), glucose transporter 1 (GLUT1) (Mayer et al., 2014), lactate dehydrogenase (LDH), and lactate transporter [monocarboxylate transporter (MCTs)] (Fantin et al., 2006). On the other hand, the reverse Warburg effect reflects that adjacent cancer cells are metabolically supported by cancer-associated fibroblasts (CAFs), which can undergo HIF-1 $\alpha$ -induced autophagosomal degradation and aerobic glycolysis. Following this, lactate, 3-hydroxybutyrate, and glutamines are released into the tumor microenvironment (TME). In turn, the cancer cells utilize lactate and 3-hydroxybutyrate and glutamine for adenosine triphosphate (ATP) and glutathione production, respectively (Fu et al., 2017; Thuwajit et al., 2018; Wilson et al., 2019). Furthermore,

OC patients end up with cachexia, anorexia, and death due to increased resting metabolism alongside peritoneal metastasis and progression (Archid et al., 2019; Hilal et al., 2017).

In addition to energy production by polar metabolites, cancer cells also utilize lipids to survive and proliferate (Butler et al., 2020). The consequence of altered lipid metabolic pathways, increased *de novo* lipogenesis and lipolysis *via* exogenous (dietary) and endogenous uptakes, respectively, allows cancer cells to enhance membrane biogenesis and ATP production (Butler et al., 2020) and then evades apoptosis (Swinnen et al., 2006; Menendez and Lupu, 2007; DeBerardinis et al., 2008). The two major sources to obtain such supplies endogenously are the omentum majus adipocytes, especially in OC (Nieman et al., 2011), and lipoproteins that are mainly synthesized by the liver carrying cholesterols (CL) and triglycerides (TG) to cancer cells (Brown, 2007; Maran et al., 2021). Moreover, inflammation is related to EOC initiation and progression. Some sources of inflammation are retrograde menstruation, obesity, ovulation, polycystic ovary syndrome (PCOS), talc exposure, infections (Savant et al., 2018), postmenopausal event (Jia et al., 2018), and dysbiotic microbiome (Wang et al., 2020). As a result, systemic inflammation occurs alongside changes in lipoproteins, which promotes carcinogenesis and malignant metastasis (Greten and Grivennikov, 2019; Georgila et al., 2019).

Detection of OC at an early stage (clinical stage I or II) is a crucial step for curing OC. Approximately, the chance to diagnose OC at the early stage is about 20%, and it allows to increase the 5- and 10-year overall survival of the patients by 71.4% and 53%, respectively (Kim et al., 2018; Peres et al., 2019). However, to date, an early-stage diagnosis is hard to achieve due to an unclear understanding of OC development and tumor pathogenesis (Bast et al., 2009; Bowtell et al., 2015).

Until now, in addition to conventional strategies to determine OC development, there is no specific way to diagnose and detect OC at the early stage among women who are exposed to inevitable risks,

such as aging (Setiawan et al., 2012) and menopausal status (Nichols et al., 2006). A conventional diagnostic approach is blood test of the cancer antigen marker CA-125 (Gupta and Lis, 2009) and transvaginal ultrasound (van Nagell and Hoff, 2013). Yet, each diagnostic test has a drawback; CA-125 is influenced by a number of OC-unrelated conditions (Kobayashi et al., 2012), and transvaginal ultrasound cannot distinguish between benign tumor and cancer (van Nagell and Hoff, 2013), thus providing a low specification. Moreover, other imaging approaches, including computed tomography (Iyer and Lee, 2010), magnetic resonance imaging (Prayer et al., 1993; Low et al., 1995), and positron emission tomography/computed tomography (Yamamoto et al., 2008; Karantanis et al., 2012), are not sensitive to diagnose ovarian tumor and cancer. In other words, morphological changes and biological properties are not enough to evaluate the disease progression in OC. Hence, discovering additional biomarkers is, indeed, one of the clinical needs.

In this project, metabolite and lipoprotein profiles of borderline ovarian tumor and HGSOc patients' serum were investigated alongside inflammatory markers by commercially available quantitative IVDr NMR standard operating procedures (SOPs) as provided by Bruker BioSpin. Uni- and multivariate statistics were applied to identify NMR-based alterations based on patients' diagnosed histology and clinical stage. The correlation of glycoproteins and OC cancer antigen markers [CA-125, carcinoembryonic antigen (CEA), and carbohydrate antigen 19-9 (CA 19-9)] was studied for the first time.

## 2 Materials and methods

### 2.1 Patients' clinical information and sample collection and storage

Table 1 describes clinical and pathological characteristics of the patients. A total of 201 serum samples in 2 mL aliquots (50 of BOT and 151 of HGSOc) with patients' information were provided by the biobank (freezer at  $-80^{\circ}\text{C}$ ) of Women's Health at Universitätsklinikum Tübingen. All patients gave written consent, and samples were collected under the ethical approval number 208/2021BO2. A graphical summary of the key findings of this study is provided within Figure 1.

### 2.2 $^1\text{H}$ -NMR spectroscopy equipment and spectra acquisition

$^1\text{H}$ -NMR spectroscopy (Bruker Avance III HD 14.10 T) was operated at 600 MHz with a triple-resonance (TXI) room temperature 5 mm probe at 310 K. All samples were measured, quantified and analyzed in a similar scheme (Figure 2).

### 2.3 Sample preparation for Bruker Avance IVDr NMR analysis

The serum was thawed at room temperature for 30 min. Following this, the serum samples were then placed inside a box

TABLE 1 Summary of patient characteristics.

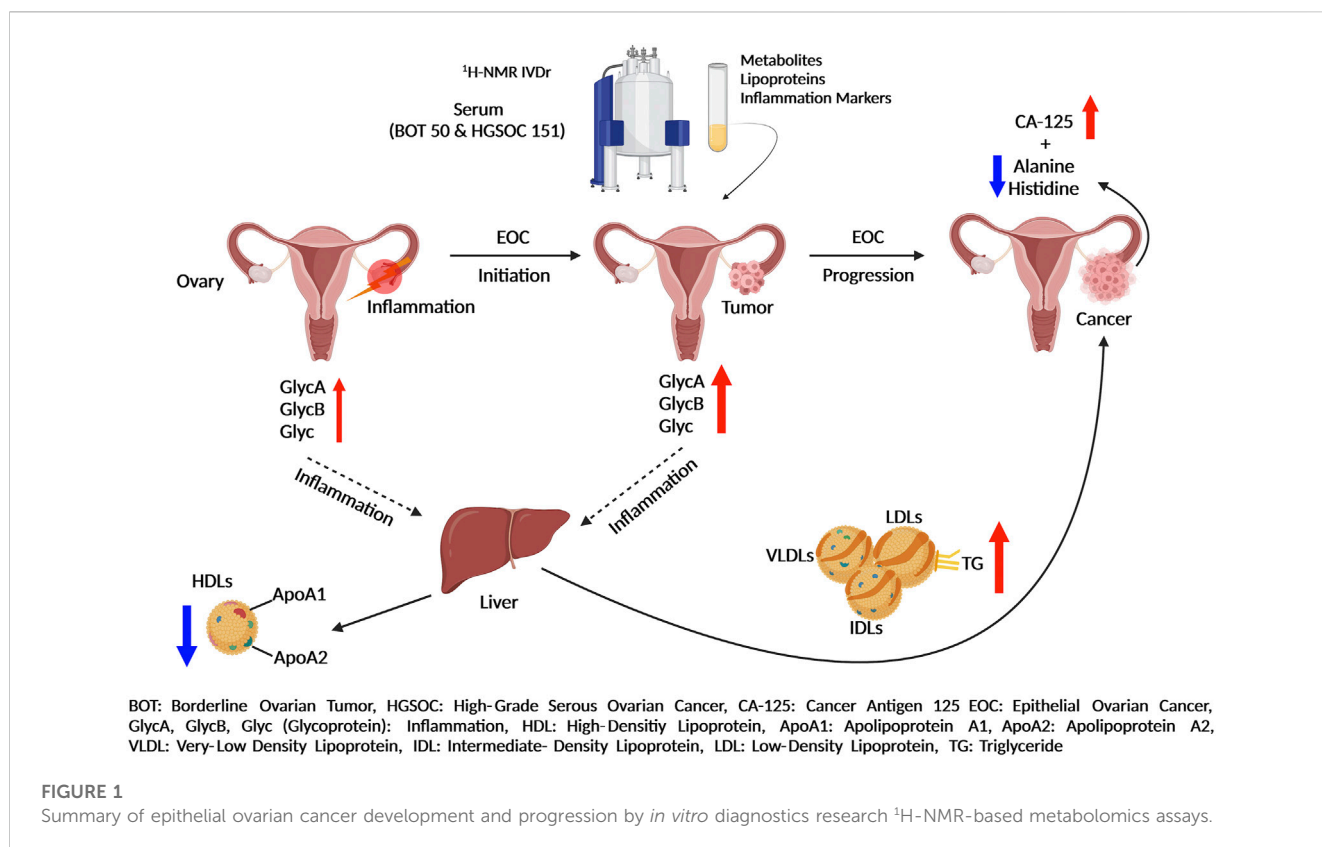
Number of patients	201
Age (mean, minimum, and maximum)	58.75 (18–87)
Gender	Female
Cancer type	Ovarian cancer
Histology	
High-grade serous ovarian cancer	151 (75%)
Endometrioid borderline tumor	2 (1%)
Mucinous borderline tumor	16 (8%)
Serous borderline tumor	29 (14%)
N/A but diagnosed as borderline tumor	3 (2%)
Tumor grading	
GB	50 (25%)
G3	151 (75%)
FIGO stage	
I	43 (21%)
II	13 (6.5%)
III	81 (40%)
III-IV	1 (0.5%)
IV	33 (16%)
N/A	30 (15%)
Treatment status	
Pre-treated	25 (12%)
Untreated	150 (75%)
N/A	26 (13%)

N/A: not applicable; FIGO: International Federation of Gynecology and Obstetrics.

with ice to prevent degradation. The next steps were performed according to the Bruker IVDr NMR SOP in brief by adding 400  $\mu\text{L}$  of Bruker Plasma Buffer and 400  $\mu\text{L}$  of the serum into a 1.5 mL Eppendorf tube and then transferring 600  $\mu\text{L}$  of the solution into a 5 mm NMR tube for measurement.

### 2.4 Quantification of the measured serum and evaluation of quality control

All the serums were measured with a nuclear Overhauser spectroscopy experiment (1D-NOESY) for 4 min to quantify polar 40 metabolites and 112 lipoproteins by small-molecule metabolites (B.I.QUANT-PS<sup>TM</sup>) and Bruker IVDr Lipoprotein Subclass Analysis (B.I.LISA<sup>TM</sup>), respectively (Bruker.com, 2022a). The inflammatory analytes GlycA, GlycB, and Glyc (addition of GlycA and GlycB) were measured with a sequence of pulse gradient perfect echo experiment (1D-PGPE) and quantified by PhenoRisk PACS<sup>TM</sup> RuO\* (Bruker.com, 2022b). Each serum was subject to a quality control test by B.I. methods (Bruker.com, 2022b).



## 2.5 Chemometrics

This is an exploratory study without prior sample size calculation. Statistical analysis was performed using the MetaboAnalyst 5.0 toolbox (Xia et al., 2009). The quantified analytes were normalized to the sample volume. The missing values of metabolites were replaced by LoDs (1/5 of the minimum positive value of each variable), and the missing values of lipoproteins were estimated by k-nearest neighbors (KNN) feature-wise. Additionally, the estimation of the missing value of metabolites and lipoproteins was carried out using the KNN for correlation between metabolites, lipoproteins, inflammation, and CA-125 markers. Serum samples that appeared as outliers by principal component analysis (PCA) and failed to pass an NMR experiment quality test were excluded. Of note, all pre-treated patients (radiotherapy and/or chemotherapy) were excluded from statistical analysis. Moreover, all patients with missing and non-absolute levels of cancer antigen markers, such as CA-125, CEA, and CA 19-9, were excluded from comparative and correlation analysis.

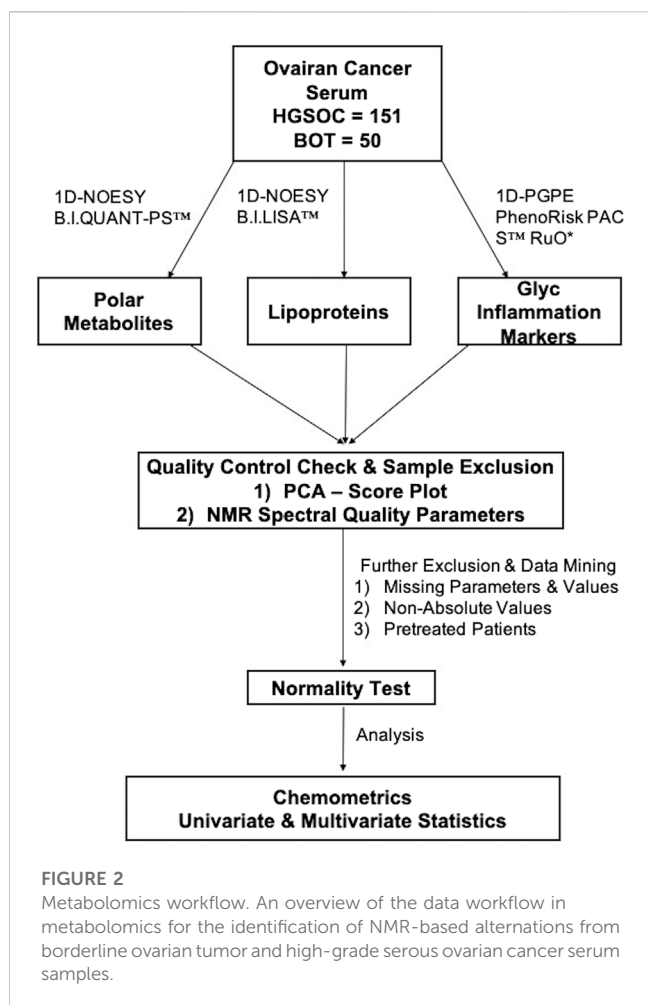
## 2.6 Comparative statistics

It was performed using Prism software 9. Normally distributed data were subject to an unpaired t-test and ordinary ANOVA tests after the F-test. Skewed data were statistically analyzed with Mann-Whitney and

Kruskal-Wallis tests. A value of  $p < 0.05$  was considered significant. Of note, a false discovery rate (FDR) was applied to correct the  $p$ -value.

## 2.7 Univariate and multivariate analyses

A volcano plot was used only for two group-based comparisons, to analyze altered metabolites and lipoproteins. A value of  $p < 0.05$  and fold change (FC) cutoff  $>1.2$  were considered statistically and biologically significant. In multivariate analysis, a PCA score plot, PCA biplot, and sparse partial least square discriminant analysis (sPLSDA) score plot were used to observe the clusters and separation based on the respective comparison. Correlation analysis is independent of the group. The data were log-transformed, pareto-scaled, and then, analyzed by Spearman's correlation with the PatternHunter tool of MetaboAnalyst 5.0 for skewed data. Moreover, correlation analysis was performed to observe the correlation between Glyc NMR parameters and cancer antigen markers (CEA and CA 19-9), the data of which were log-transformed. Last, a k-means clustering plot was performed based on the quantitative inflammatory parameters (GlycA, GlycB, and Glyc), and then, we further analyzed the NMR-based alternation of metabolites and lipoproteins with the CA-125 marker by the sPLSDA score plot and comparative statistics. Of note, all of these parameters were also log-transformed and pareto-scaled.



## 2.8 Biomarker analysis

Inflammation markers (GlycA, GlycB, and Glyc) were subject to a comparative statistical analysis and classical univariate receiver operating characteristic (ROC) curve analysis, to observe how accurate these markers are in distinguishing OC patients. Furthermore, all NMR parameters and CA-125 were log-transformed and pareto-scaled, and biomarker analysis was carried out based on the principle “compute and include metabolite ratios.”

## 3 Results

### 3.1 Polar metabolites and lipoproteins vary in histology of ovarian cancer with clinical stages I–IV

Volcano analysis and comparative statistics were carried out. In the volcano plot, ketone bodies, glutamate, and glycerol were upregulated in HGSOC compared to BOT (Figure 3A). The rest of the metabolites were found significant by comparative statistics; alanine and histidine were significantly higher in BOT (Figure 3A), and glucose, 2-hydroxybutyric acid (Supplementary Figure S1), and phenylalanine (Figure 3A) were significantly higher in

HGSOC. A multivariate analysis was further performed to observe any discernible patterns in the metabolite profiles of BOT and HGSOC. HGSOCs were closely clustered to BOT (Supplementary Figure S9A), yet they tended to be separate from BOTs, which was due to glucose and lactic acid relevant to OC development.

In terms of the clinical stages, acetoacetic acid, formic acid, and histidine were significantly different between OC with stages I–IV. Acetoacetic acid was observed to be significantly lower in OC with stage I than in OC with stages II and IV (Supplementary Figure S1), while alanine was significantly higher in OC with stages I and III than OC with stage IV (Figure 3A). Formic acid (Supplementary Figure S1) and histidine (Figure 3A) increased and decreased over the clinical stage, respectively.

From the quantitative lipoprotein panel, the parameters L1TG, L2TG, L4TG, L5TG, IDAB, IDPN, H2TG, L3TG, L3TG, V4PL, V4CH, H1TG, V4TG, V4FC, VLAB, VLPN, IDCH, and IDFC were upregulated in HGSOC compared to BOT (Figure 3B). It can be estimated that these increased lipoproteins carry TG, phospholipids, CL, and free CL to the OC, and at the same time, TG are transported back to the liver by H1TG and H2TG. Moreover, total TG (TPTG), total cholesterol (TPCH), high-density lipoprotein cholesterol (HDCH), and low-density lipoprotein cholesterol (LDCH) were not significant between HGSOC and BOT (Supplementary Figure S2). The multivariate analysis showed that HGSOC and BOT were clustered next to each other, and the separation was driven by TBPn and LDPN (Supplementary Figures S9C, S9D). Indeed, lipoproteins seemed to facilitate OC development.

In the clinical stage-based comparison, H3FC, H4A1, H4A2, H4FC, HDA1, HDCH, HDTG, TPA1, TPA2, V5TG, and ABA1 showed significant changes, while the rest of the lipoproteins were observed the same way as in the histology-based comparison (Supplementary Figure S3). High-density lipoproteins (HDLs) apolipoprotein A-1 (ApoA1) and apolipoprotein A-2 (ApoA2), and low-density lipoproteins (LDLs), very-low-density lipoproteins (VLDLs), and intermediate-density lipoproteins (IDLs) tended to decrease and increase, respectively, over the clinical stage. Moreover, H1TG, H2TG, and HDTG increased over the clinical stage (Supplementary Figure S3).

### 3.2 Glycoprotein inflammation markers of borderline ovarian tumor and high-grade serous ovarian cancer stages I–IV vary according to each other

Inflammation markers such as glycoprotein A (GlycA), glycoprotein B (GlycB), and overall Glyc were significantly higher in HGSOC than in BOT (Figure 4), indicating that inflammation occurred during OC development. The inflammation based on Glyc results also increased over the clinical stages where significance was observed between stages I vs. IV, I vs. III, II vs. IV, and III vs. IV (Figure 4). The multivariate analysis clearly showed that glycoprotein-assessed inflammation varied between the diagnosed histology, and the altered inflammation was indeed related to their tumor progression (Supplementary Figures S9E, S9F).



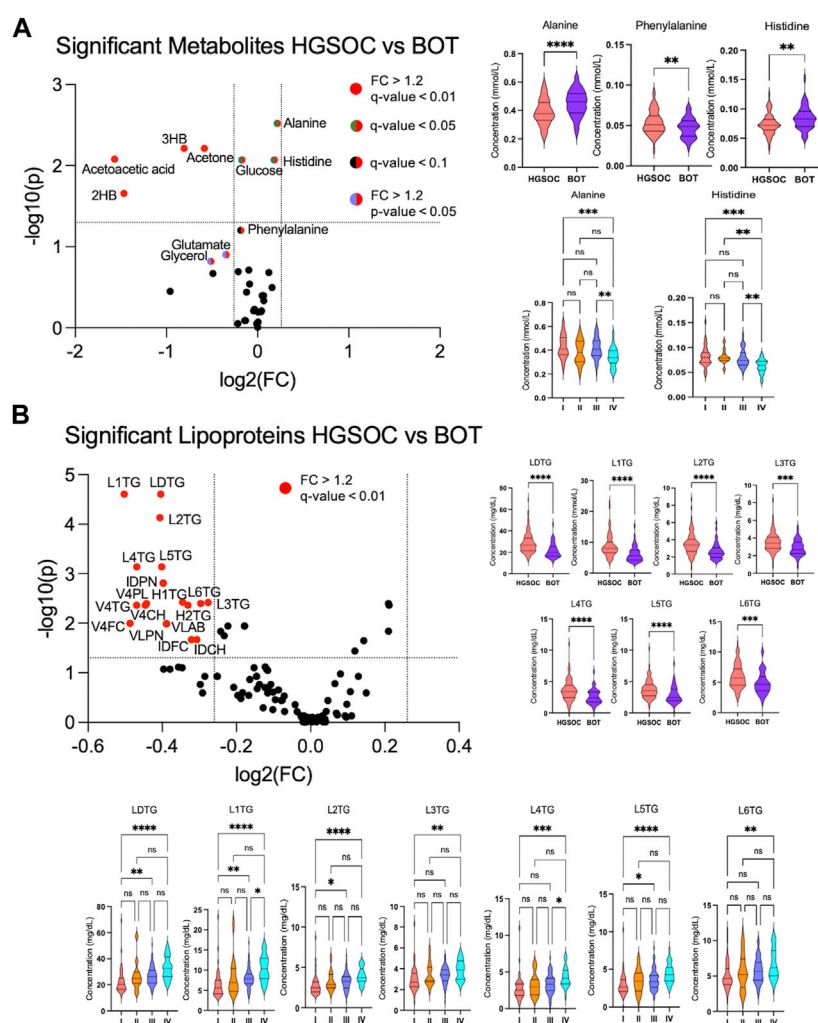


FIGURE 3

Altered metabolites and lipoproteins in borderline ovarian tumor (BOT) and high-grade serous ovarian cancer (HGSOC) with clinical stages I–IV. From left: (A, B) volcano plot showing statistically and biologically significant metabolites and lipoproteins in the histology of ovarian cancer; red plots indicate upregulation in high-grade serous ovarian cancer (fold change  $>1.2$  and  $p\text{-value} < 0.05$ ). From right: (A, B) violin plots by comparative statistics showing significantly altered alanine (FDR  $< 0.01$ ), phenylalanine (FDR  $< 0.1$ ), and histidine (FDR  $< 0.01$ ) in high-grade serous ovarian cancer (\*\*  $< 0.01$  and \*\*\*\*  $< 0.0001$ ) and significantly altered alanine and histidine over the clinical stages ( $q\text{-value} = ** < 0.01$  and \*\*\*  $< 0.001$ ). From right: (B and bottom) violin plots displaying significantly altered lipoproteins in high-grade serous ovarian cancer (FDR  $< 0.01$ , \*\*\*  $< 0.001$ , and \*\*\*\*  $< 0.0001$ ) and over the clinical stages ( $q\text{-value} = * < 0.05$ , \*\*  $< 0.01$ , \*\*\*  $< 0.001$ , and \*\*\*\*  $< 0.0001$ ).

### 3.3 Glycoprotein inflammation markers predict effectiveness of the treatment and are promising add-ons for diagnosis and prognosis of ovarian cancer

In order to see whether GlycA, GlycB, and the sum of Glyc possess potential for diagnosis and prognosis, comparative statistical analysis was carried out in a treatment-based comparison. The inflammation markers were not significant between the treatment statuses (Supplementary Figure S4). No significant change was further confirmed by cross-validation with the “leave one out cross-validation” method (LOOCV); Q2 was negative (Supplementary Table S16), which means that the group was not predictive at all, and PLS-DA (partial least square

discriminant analysis) would not provide important information (Szymańska et al., 2012). Additionally, the cancer antigen marker CA-125 that is used to investigate the effectiveness of radiotherapy (Aliomar et al., 2013) and chemotherapy (Wang et al., 2019) was subject to comparative statistics. Hereby, the result shows non-significance between the overall groups (Supplementary Figure S4), yet it was significant in comparing BOT vs. HGSOC and clinical stages (Figure 4). Biomarker analysis shows that the inflammation markers were able to distinguish between BOT vs. HGSOC (Supplementary Figure S7) and I–II vs. III–IV (Supplementary Figure S5), as CA-125. In this study, all NMR parameters alone were not good enough to classify both histology and clinical stage of OC (Supplementary Tables S24, S25). However, we could see that



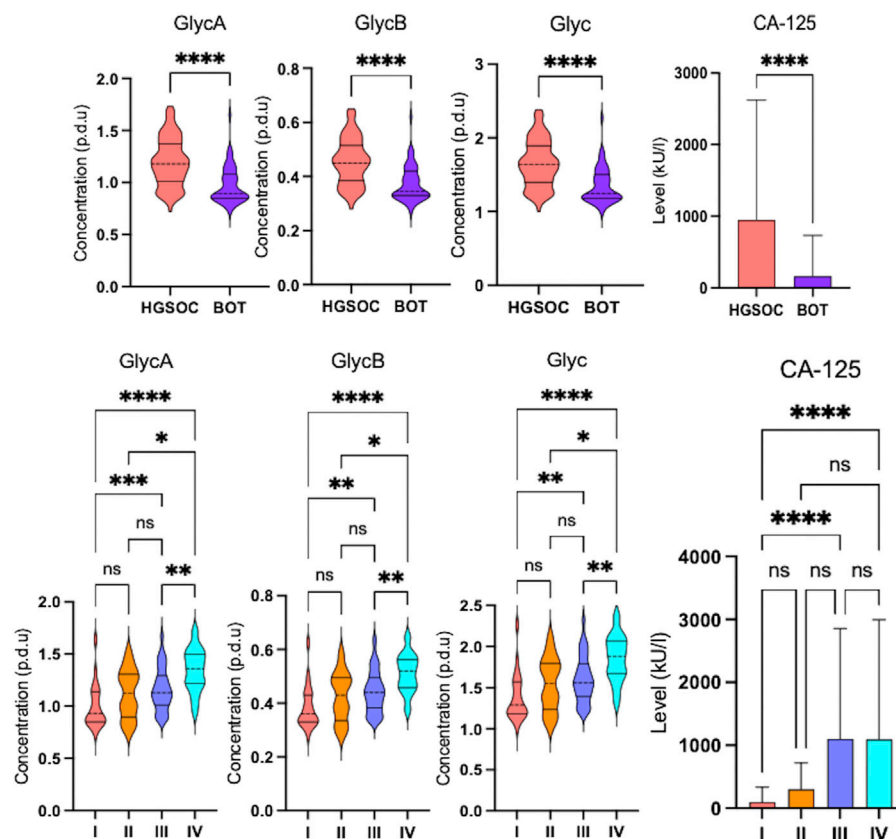


FIGURE 4

Altered glycoprotein inflammation and cancer antigen-125 markers in ovarian cancer serum samples. Violin and box plots showing significant increase in glycoprotein inflammation and cancer antigen-125 markers over the clinical stages (q-value = \* $<0.05$ , \*\* $<0.01$ , \*\*\* $<0.001$ , and \*\*\*\* $<0.0001$ ) that they are higher in high-grade serous ovarian cancer than in borderline ovarian tumor (FDR  $<0.001$ , \* $<0.05$ , \*\* $<0.01$ , \*\*\* $<0.001$ , and \*\*\*\* $<0.0001$ ).

the area under the curve (AUC) of CA-125/sarcosine, CA-125/pyruvate, CA-125/3HB, and CA-125/oxoglutaric acid was higher than that of CA-125 (Figure 5). Histology of OC was classified by CA-125/sarcosine and CA-125/pyruvate, while the classification of the clinical stage of OC was achieved by CA-125/3HB and CA-125/oxoglutaric acid. Moreover, increased ratio values of CA-125/GlycA (Supplementary Figure S6), CA-125/GlycB (Supplementary Figure S6), and CA-125/Glyc (Figure 5) within AUC analysis helped in classifying both the histology and clinical stage of OC.

### 3.4 Quantitative inflammatory parameters clearly characterize specific patterns of metabolites, lipoproteins, and CA-125 in ovarian tumor and cancer with clinical stages I–IV

K-means clustering was performed with the quantitative inflammatory parameters, where we could distinguish different inflammatory classes. In other words, quantitative inflammatory parameters varied according to each cluster (Figure 6). We then carried out sPLSDA and comparative statistics to observe the NMR-based alternations and CA-125 based on the inflammatory

classes. Each class was clearly separated along with specific and unique changes in metabolites, lipoproteins, and CA-125 (Figure 6). Moreover, the model was cross-validated with LOOCV; the error rate was 8.8% at component 1 (Supplementary Figure S10), indicating that different glycoprotein classes perform good classification.

### 3.5 Correlation of glycoprotein inflammation markers with the established cancer markers CA-125, CEA, and CA 19-9

Inflammation was positively correlated with ketone bodies (3-hydroxybutyric acid and acetoacetic acid), succinic acid, 2-hydroxybutyric acid, CA-125, and various parameters, mainly triglycerides, in lipoprotein fractions (LDLs) (Figures 7A, B). A negative correlation was observed for histidine, alanine, TPA2 (total plasma apolipoprotein A2), and subfraction of HDLs with certain lipid species, notably HDL-4 (Figure 7A). Moreover, two ketone bodies were positively correlated only with the inflammation markers and negatively correlated with alanine and sarcosine (Figures 7B, C). We also observed that the correlation between glycoprotein inflammation, CEA, and CA 19-9 antigen markers was weak (Supplementary Figures S8A, S8B).

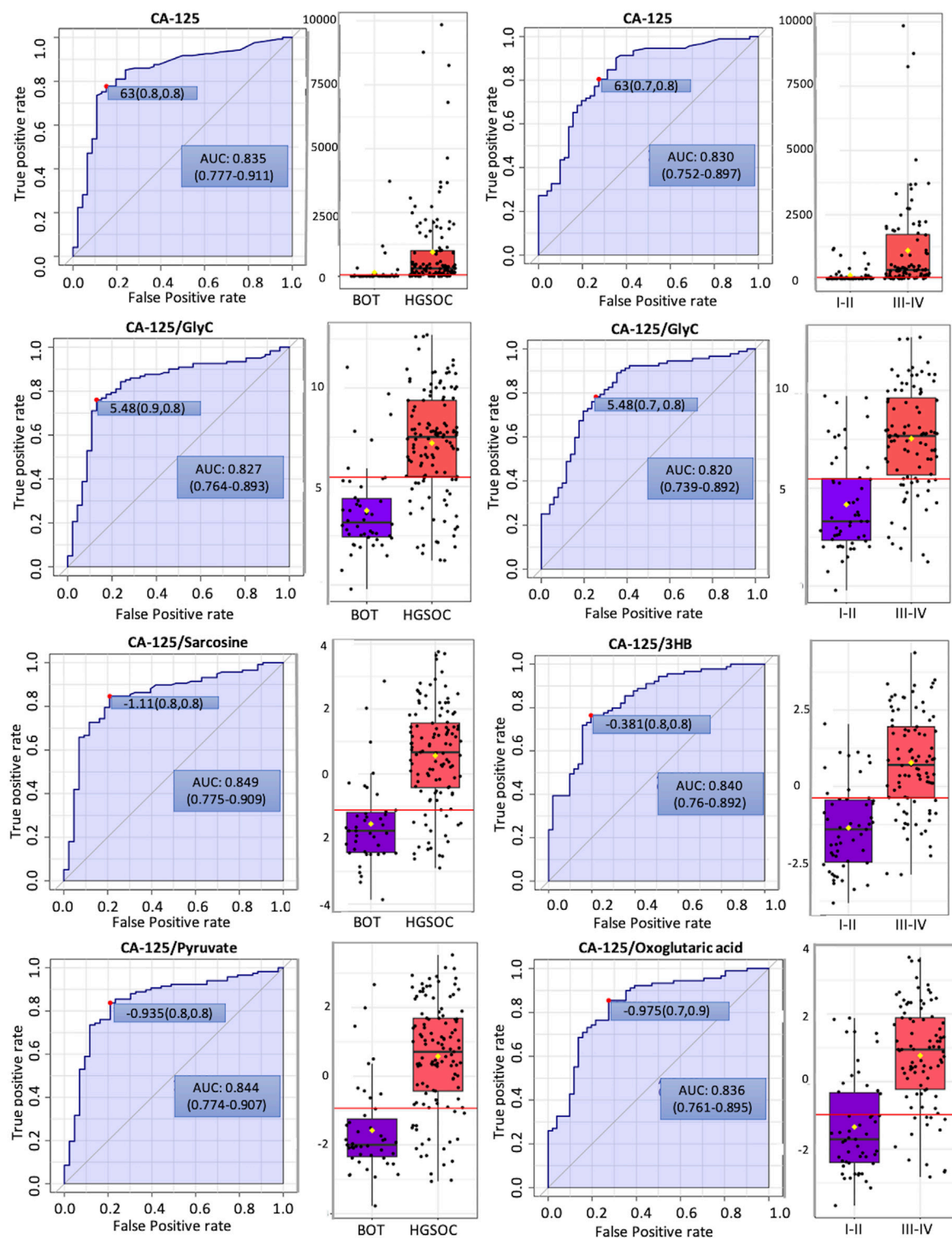
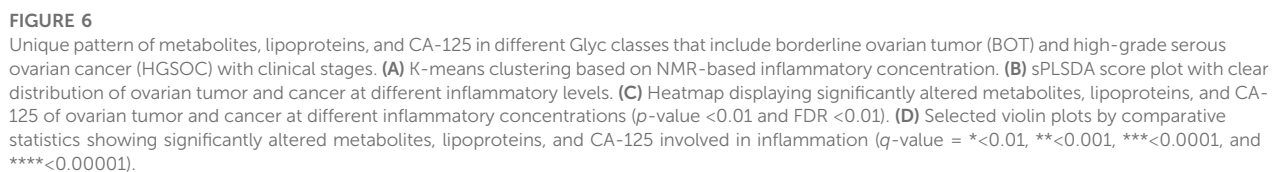


FIGURE 5

Potential biomarker candidates to cancer antigen-125 markers for ovarian cancer diagnosis and prognosis. The optimal cutoff was based on the closest to the top left corner principle and is indicated by the red dot in all the ROC curves. Black dots and yellow diamond represent the level of cancer antigen-125 and each ratio and mean concentration of cancer antigen-125 and each ratio, respectively.



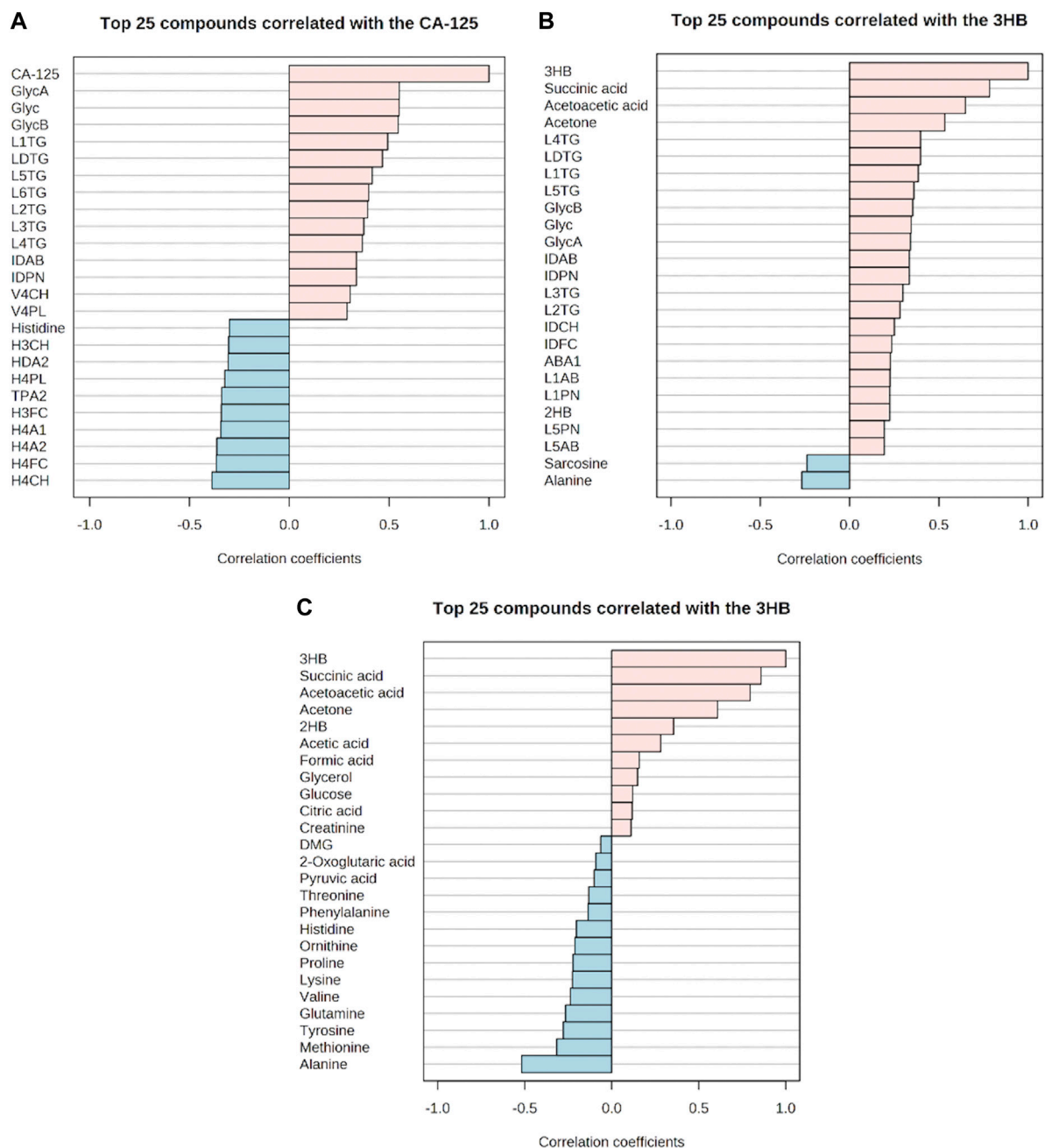


FIGURE 7

Correlation of the glycoprotein inflammation markers with metabolites, lipoproteins, and cancer antigen-125 markers. (A–C) Respective positive and negative correlations. (A) Positive and negative correlations of cancer antigen-125 with metabolite, lipoproteins, and inflammation markers. (B) Positive and negative correlations of 3-hydroxybutyric acid with metabolites, lipoproteins, and inflammation markers. (C) Positive and negative correlations of 3-hydroxybutyric acid with other metabolites.

## 4 Discussion

### 4.1 Alterations of metabolites and glycoprotein inflammation markers in borderline ovarian tumor and high-grade serous ovarian cancer clinical stages I–IV implicate critical roles in tumor development

It has been observed that malignant OC cells can disseminate to periglandular regions and the visceral omentum majus that is

basically a large layer of adipocyte tissue (Lengyel et al., 2018). By the presence of a lesion in the omentum majus, these cells can make use of free fatty acids deriving from the adipocytes and switch from the glycolytic pathway into lipid metabolism where elevated fatty acid oxidation takes place for energy supply and tumor development (Balaban et al., 2017; Wu et al., 2019). It is furthermore consistent that we observed increased ketogenesis in HGSOC along with upregulated glycerol and glutamate. Elevated ketogenesis in the OC serum implicates the utilization of fatty acid (Braicu et al., 2017; Hilvo et al., 2016), reverse



Warburg effect of circulating CAFs (Schauer et al., 2011; Ao et al., 2015), and cachexic phenotype (Pin et al., 2018), since the rate of hepatic fatty acid oxidation and fatty acid oxidation-related enzymes decreases along with hepatic ketogenesis and plasma ketone concentrations during acute phase response (Khovidhunkit et al., 2004b; Memon et al., 1992). Upregulated glycerol and glutamate represent an elevated rate of lipolysis in the adipocytes (Castelli et al., 2021; Nieman et al., 2011) and glutathione production (Aggarwal et al., 2019; Fazzari et al., 2015), respectively. As a consequence of a generally higher antioxidant capacity in the cancer cells, reactive oxygen species (ROS) do not induce apoptosis, but instead provoke inflammation, leading to facilitation in tumor development (Liou and Storz, 2010). In our results, the positive correlation of ketone bodies and highly observed NMR-based inflammatory markers of GlycA, GlycB, and Glyc in HGSOC further support this explanation.

2-Hydroxybutyric acid, a marker for insulin resistance (IR) and impaired glucose metabolism due to increased lipid oxidation and ROS (Gall et al., 2010), was higher in HGSOC. 2-Hydroxybutyrate was also higher in metastatic OC than in primary OC (Fong et al., 2011). Hence, the reason for increased glucose in HGSOC may not only be due to overexpression of GLUT1 (Lamkin et al., 2009), but it may be also attributed by IR that reduced the ability of skeletal, muscle, fat, and hepatic cells to take glucoses from the blood in response to normal circulating levels of insulin (Schwartzburd, 2019).

One of the hallmarks of cancer and key process in metastasis is the invasiveness of tumor cells (Hanahan and Weinberg, 2000). BOT has been characterized by the absence of stromal invasion and a less aggressive behavior compared to HGSOC (Brown et al., 2007); e.g., an increase in the circulating levels of formic acid or formate has been associated with an elevated rate of serine catabolism that takes place to promote invasiveness in oxidative glioblastoma multiforme cells (Meiser et al., 2018) and tumor progression in colorectal cancer (VanHook, 2022). Hence, the OC invasiveness may be facilitated by formate, which could explain why formate was higher over the clinical stages in this project.

Next, when cancer cells face genotoxic, oxidative, or nutritional stresses, they switch to amino acid metabolism guaranteeing their survival and proliferation (Wei et al., 2021). Decreased levels of alanine in HGSOC could be due to increased systemic inflammation as sustained systemic inflammation leads to hepatic glucose production followed by hyperglycemia in which the liver consumes alanine to perform gluconeogenesis and release acute phase response proteins (Gabay and Kushner, 1999; Okin and Medzhitov, 2016). Such phenomena could be linked to higher concentrations of 2-hydroxybutyric acid and glucose in HGSOC, increased phenylalanine levels in HGSOC by the systemic inflammation-induced influence of phenylalanine hydroxylase (Neurauter et al., 2008), the negative correlation between inflammation and alanine along with elevated ketogenesis, and decreased alanine levels which at the same time increased inflammation over the clinical stages. Moreover, the decreased level of alanine could reflect high glutamine uptake *via* alanine-serine-cysteine transporter 2 (ASCT2) (Guo et al., 2018).

The upregulation of excitatory amino acid (EAA) transporters is one of the characteristics of many cancers (Karunakaran et al., 2008; Saito and Soga, 2021). Decreased levels of histidine in HGSOC were

reflective of the upregulation of EAA transporters, to meet requirements for their tumor development. Histidine was not only shown to be involved in cancer progression but also to be a metabolite which possesses anti-inflammatory properties (Grohmann and Bronte, 2010). One study showed a chemokine IL-8 response in a TNF- $\alpha$ -stimulated human leukemia monocytic cell line (THP-1) which was inhibited by histidine (Hasegawa et al., 2012). Furthermore, the production of TNF- $\alpha$  and IL-6 of lipopolysaccharide-induced mouse peritoneal macrophages was affected by histidine (Andou et al., 2009). Hence, the increase in inflammation parameters could be facilitated by a low level of histidine, as observed in the clinical stage-based comparison, with a negative correlation of histidine, CA-125, and glycoprotein inflammation markers.

## 4.2 Altered lipoproteins and glycoprotein inflammation markers in borderline ovarian tumor and high-grade serous ovarian cancer with clinical stages I–IV can be used to characterize tumor development and correlate to each other

Several researchers have reported about the altered lipoprotein profile of OC and ovarian tumor (OT) compared to healthy subjects. For example, TC levels were lower in OT (Melvin et al., 2012), and also, HDLs decreased in OT (Camps et al., 2021; Gadomska et al., 2005). Furthermore TG, HDCH, CL, and LDCH decreased (Qadir and Malik, 2008) in OC patients. In this project, lipoprotein profiles were investigated based on histology and clinical stages in order to observe which lipoproteins could contribute to the development of OC.

Increased levels of VLDL in OC patients were observed by Manisha and Jindal (2019) and Tiwari et al. (2015), which is consistent with the results in this project where we identified VLPN, VLAB, V4CH, V4PL, and V4TG to be higher in HGSOC. Such increased lipoproteins indicate that CL, phospholipids, and TG were transferred to HGSOC cells. Moreover, it has been found that LDL receptors (LDLRs) are overexpressed by many tumors (Rensen et al., 2001) and upregulated in OC patients in relation to healthy subjects (Jaragh Alhadad, 2021), implicating that non-significant TG and CL may be due to elevated consumption of the tumor development.

In the clinical stages, most of the altered lipoproteins were observed in the same manner as in a histology-based comparison where V5TG and ABA1 also increased over the clinical stages. Moreover, altered HDLs were clearly shown as depicted by the levels of H3FC, H4A1, H4A2, H4FC, HDA1, HDCH, TPA1 (total plasma apolipoprotein A1), and TPA2 decreased. It has been discovered that inflammation is characterized by increased LDLs and TG, ApoB, and decreased HDLs in chronic diseases (Tsoupras et al., 2018). The reason why they decreased may be due to inflammation-associated mechanisms. First, serum amyloid A (SAA) production increases in the liver by which SAA bind to HDLs to displace apoA-1 and apoA-2 for HDL clearance (Benditt and Eriksen, 1977; Eriksen and Benditt, 1980; Hosoi et al., 1999; Ashby et al., 2001). Second, SAA decreases the level of apoA-1 and apoA-2 HDLs (Benditt and Eriksen, 1977; Eriksen and Benditt, 1980), affecting the synthesis of HDLs (Florea et al., 2022). Third, the synthesis of apoA-1 decreases in the liver, leading to a decrease in HDL



levels (Khovidhunkit et al., 2004a). Last, inflammation induces VLDL production and secretion in the liver, and decreases the hepatic clearance of TG-rich lipoproteins (Feingold et al., 2021). Indeed, such mechanisms and findings can describe the negative correlation between the Glyc inflammation markers, HDLs and TPA2. Moreover, this is in accordance with our findings that subfractions of VLDLs, IDLs, and LDLs with certain lipid species and apolipoprotein B-100 were increased in advanced OC and were positively correlated with Glyc inflammation and CA-125 markers.

Following decreased HDLs, cancer cells can maintain CL homeostasis, carry out angiogenesis, and escape immune surveillance (Ossoli et al., 2022). Additionally, oxidation of LDLs takes place more often, promoting the production of TG along with an accumulation of fatty acids in the adipocytes (Merkel et al., 2002). In other words, the transportation of fatty acids from the adipocytes to OC cells may be also facilitated by these discovered altered lipoproteins.

Another finding of this project was that ketogenesis was positively correlated with succinic acid that can be seen as increased marker during inflammation. Such correlations may indicate that OC cells utilized glutamine and fatty acids to produce glutathione and acquire ATP through the tricarboxylic acid (TCA) cycle, respectively, while potentially sparing glucose. The increase in succinate during inflammation could be due to the fact that this metabolite is a pro-inflammatory agent inducing IL-1 $\beta$  through HIF-1 $\alpha$  in macrophages (Tannahill et al., 2013). In turn, metastasis of OC cells could be facilitated by the IL-1 $\beta$ / $\beta$ 1 integrin axis (Watanabe et al., 2012), and inflammation-associated cells transformed into cancer-associated immune cells (Bent et al., 2018) that further developed OC proliferation, invasion, and metastasis.

### 4.3 The NMR-based inflammation markers GlycA, GlycB, and Glyc are potential candidates for future diagnosis, prognosis, and treatment response of ovarian cancer

We observed that NMR parameters themselves could not improve diagnostic sensitivity and specificity compared to CA-125 alone. Yet, we found that CA-125/sarcosine, CA-125/pyruvate, CA-125/3HB, and CA-125/oxoglutaric acid could be potential biomarkers. These metabolites are involved in OC proliferation (Yuan et al., 2015), invasiveness with resistance to anoikis (Caneba et al., 2012), and one-carbon metabolism (Rizzo et al., 2018). Additionally, CA-125/3HB is indeed promising, since the elevated level of 3HB is reflective of the cachexic phenotype (Pin et al., 2018) and circulating CAFs in the blood (Schauer et al., 2011; Ao et al., 2015).

We showed that NMR-based inflammation parameters increased in advanced OC serum, indicating the elevated glycosylation of the acute phase proteins, such as  $\alpha$ 1-acid glycoprotein, haptoglobin,  $\alpha$ 1-antitrypsin,  $\alpha$ 1-antichymotrypsin, and transferrin (Otvos et al., 2015). Several studies confirm that haptoglobin  $\beta$ -chain (Ahmed et al., 2004; Ahmed et al., 2005),  $\alpha$ 1-acid glycoprotein (Rodríguez, 2019),  $\alpha$ 1-antitrypsin (Normandin et al., 2010), and  $\alpha$ 1-antichymotrypsin (Saldova et al., 2007) increased, and transferrin, the negative acute phase protein, decreased in OC during inflammation (Watanabe et al., 2014). Hence, haptoglobin  $\beta$ -chain,  $\alpha$ 1-acid glycoprotein,  $\alpha$ 1-antitrypsin, and  $\alpha$ 1-antichymotrypsin could be the inflammatory proteins that may contribute to the NMR peaks of GlycA, GlycB, and Glyc in OT and

OC. Furthermore, such markers may be able to classify OC patients with and without ascites, since the presence of ascites arises by increased permeability of small vessels along with peritoneal parietal revascularization and glycoprotein production (Yung and Chan, 2011).

As observed in the results, Glyc inflammation and CA-125 markers behaved in the same way, which implicates that the effectiveness of radiotherapy and/or chemotherapy was low. Yet, CA-125 levels are influenced by a number of OC-unrelated conditions (Kobayashi et al., 2012). The cancer antigen marker is neither able to detect the early onset of OC (Journal, 2015) nor efficient in identifying asymptomatic OC patients (Skates et al., 2021), and 20% of OC have either low or completely missing presence of CA-125 (Journal, 2015). It is also observed that different kits and versions of the CA-125 test influence the absolute levels of CA-125 and test sensitivity (Kenemans et al., 1993), and the test sensitivity of OC decreases by more than 50% in the cutoff of the CA-125 level over 1,000 kU/l. (Moss et al., 2005). Of note, OC is not induced by CA-125, but inflammation. Several studies show that dysregulated inflammation is highly linked to tumor occurrence *via* angiogenesis and metastasis (Frantz et al., 2013; Qu et al., 2018; Zhao et al., 2018) and cancer-associated immune cells (Zhang et al., 2017). Moreover, the response of cancer to therapies is regulated by inflammation (Zhao et al., 2021). The response is either anti-tumor immunity *via* acute inflammation or therapy-elicited chronic inflammation along with subsequent therapeutic resistance and aggressive cancer progression (Zhao et al., 2021). In other words, Glyc inflammation markers are more reliable for cancer treatment outcomes. We could also stratify OC patients based on their quantitative inflammatory parameters, which clearly displayed specific alteration in metabolites, lipoproteins, and CA-125. Therefore, we conclude that CA-125/GlycA, CA-125/GlycB, and CA-125/Glyc, the use of both markers individually, and Glyc classes are potential for future diagnosis, prognosis, and treatment response of OC.

## 5 Conclusion

Profiles of metabolites, lipoproteins, and inflammation parameters of BOT and HGSOC serums were investigated using highly reproducible and quantitative IVDr NMR analysis. Hereby, we identified certain metabolites and lipoproteins that could be related to OC development along with acute and chronic inflammation. The NMR-based inflammation markers, GlycA, GlycB, and Glyc, were shown to be able to classify histology and early and advanced stages of ovarian cancer. Moreover, the ratios CA-125/GlycA, CA-125/GlycB, and CA-125/Glyc, the use of both markers individually, and Glyc classes could be an alternative to CA-125 alone for diagnosis, prognosis, and treatment response of EOC.

## 6 Declarations

- Ethics approval and consent to participate: 208/2021BO2
- Consent for publication: all authors read the manuscript and agree with its publication.
- Availability of data and materials: raw data are available upon request.
- Competing interests: GB, GeB, CT, NB, and SB report no competing interests.

- Funding: CT and GeB report research grants from Bruker BioSpin GmbH, Ettlingen, Germany.
- Authors' contributions: conception: CT; design of the work: GB, GeB, and CT; data acquisition: GB, GeB, CC, HS, and SB; data analysis: GB and CT; data interpretation: GB, NB, and CT; figure preparation: GB; manuscript draft: GB, GeB, and CT; and manuscript editing: GB, GeB, AK, CC, HS, SK, SB, NB, and CT. All authors approved the submitted version.
- Acknowledgments: the authors want to thank the Werner Siemens Imaging Foundation and Bernd Pichler for supporting this project. The authors also thank Daniele Bucci for excellent technical assistance.

## Data availability statement

The raw data supporting the conclusion of this article will be made available by the authors, without undue reservation.

## Ethics statement

The studies involving human participants were reviewed and approved by ethics committee of Eberhard Karls University Tübingen, study number 208/2021BO2. The patients/participants provided their written informed consent to participate in this study.

## Author contributions

Conception: CT; design of the work: GB, GeB, and CT; data acquisition: GB, GeB, CC, HS, and SB; data analysis: GB and CT; data interpretation: GB, NB, and CT; figure preparation: GB; manuscript draft: GB, GeB, and CT; and manuscript editing: GB,

GeB, AK, CC, HS, SK, SB, NB, and CT. All authors approved the submitted version.

## Funding

This research project was supported by an advanced research collaboration grant with Bruker BioSpin GmbH. The publication of this project was further financially supported by the Open Access publication funds of the Eberhard Karls University of Tuebingen, Germany.

## Conflict of interest

CT and HS were employed by Bruker BioSpin GmbH.

The remaining authors declare that the research was conducted in the absence of any commercial or financial relationships that could be construed as a potential conflict of interest.

## Publisher's note

All claims expressed in this article are solely those of the authors and do not necessarily represent those of their affiliated organizations, or those of the publisher, editors, and reviewers. Any product that may be evaluated in this article, or claim that may be made by its manufacturer, is not guaranteed or endorsed by the publisher.

## Supplementary material

The Supplementary Material for this article can be found online at: <https://www.frontiersin.org/articles/10.3389/fmolb.2023.1158330/full#supplementary-material>

## References

- Aggarwal, V., Tuli, H. S., Varol, A., Thakral, F., Yerer, M. B., Sak, K., et al. (2019). Role of reactive oxygen species in cancer progression: Molecular mechanisms and recent advancements. *Biomolecules* 9 (11), 735. doi:10.3390/biom9110735
- Ahmed, N., Barker, G., Oliva, K. T., Hoffmann, P., Riley, C., Reeve, S., et al. (2004). Proteomic-based identification of haptoglobin-1 precursor as a novel circulating biomarker of ovarian cancer. *Br. J. Cancer* 91 (1), 129–140. doi:10.1038/sj.bjc.6601882
- Ahmed, N., Oliva, K. T., Barker, G., Hoffmann, P., Reeve, S., Smith, I. A., et al. (2005). Proteomic tracking of serum protein isoforms as screening biomarkers of ovarian cancer. *Proteomics* 5 (17), 4625–4636. doi:10.1002/pmic.200401321
- Aliomar, M., Mohamed, M., Yousef, M., Farahna, M., and Alghanim, A. (2013). Assessment of ovarian tumor marker CA-125 during radiotherapy course. *J. Exp. Clin. Med.* 30 (2), 137–139. doi:10.5835/jecm.omu.30.02.010
- Andou, A., Hisamatsu, T., Okamoto, S., Chinen, H., Kamada, N., Kobayashi, T., et al. (2009). Dietary histidine ameliorates murine colitis by inhibition of proinflammatory cytokine production from macrophages. *Gastroenterology* 136 (2), 564–574.e2. doi:10.1053/j.gastro.2008.09.062
- Ao, Z., Shah, S. H., Machlin, L. M., Parajuli, R., Miller, P. C., Rawal, S., et al. (2015). Identification of cancer-associated fibroblasts in circulating blood from patients with metastatic breast cancer. *Cancer Res.* 75 (22), 4681–4687. doi:10.1158/0008-5472.CAN-15-1633
- Archid, R., Solass, W., Tempfer, C., Konigsrainer, A., Adolph, M., Reymond, M. A., et al. (2019). Cachexia anorexia syndrome and associated metabolic dysfunction in peritoneal metastasis. *Int. J. Mol. Sci.* 20 (21), 5444. doi:10.3390/ijms20215444
- Asbhy, D., Gamble, J., Vadas, M., Fidge, N., Siggins, S., Rye, K., et al. (2001). Lack of effect of serum amyloid A (SAA) on the ability of high-density lipoproteins to inhibit endothelial cell adhesion molecule expression. *Atherosclerosis* 154 (1), 113–121. doi:10.1016/s0021-9150(00)00437-8
- Balaban, S., Shearer, R. F., Lee, L. S., van Geldermalsen, M., Schreuder, M., Shtein, H. C., et al. (2017). Adipocyte lipolysis links obesity to breast cancer growth: Adipocyte-derived fatty acids drive breast cancer cell proliferation and migration. *Cancer Metab.* 5, 1. doi:10.1186/s40170-016-0163-7
- Bast, R. C., Jr, Hennessy, B., and Mills, G. B. (2009). The biology of ovarian cancer: New opportunities for translation. *Nat. Rev. Cancer* 9 (6), 415–428. doi:10.1038/nrc2644
- Benditt, E. P., and Eriksen, N. (1977). Amyloid protein SAA is associated with high density lipoprotein from human serum. *Proc. Natl. Acad. Sci. U. S. A.* 74 (9), 4025–4028. doi:10.1073/pnas.74.9.4025
- Bent, R., Moll, L., Grabbe, S., and Bros, M. (2018). Interleukin-1 beta-A friend or foe in malignancies? *Int. J. Mol. Sci.* 19 (8), 2155. doi:10.3390/ijms19082155
- Bowtell, D., Böhm, S., Ahmed, A., Aspuri, P., Bast, R., Beral, V., et al. (2015). Rethinking ovarian cancer II: Reducing mortality from high-grade serous ovarian cancer. *Nat. Rev. Cancer* 15 (11), 668–679. doi:10.1038/nrc4019
- Braicu, E. I., Darb-Esfahani, S., Schmitt, W. D., Koistinen, K. M., Heiskanen, L., Pöhö, P., et al. (2017). High-grade ovarian serous carcinoma patients exhibit profound alterations in lipid metabolism. *Oncotarget* 8 (61), 102912–102922. doi:10.18632/oncotarget.22076
- Brown, W. V. (2007). High-density lipoprotein and transport of cholesterol and triglyceride in blood. *J. Clin. Lipidol.* 1 (1), 7–19. doi:10.1016/j.jacl.2007.02.001
- Brown, J., Olson, T., and Sencer, S. (2007). "Malignancies of the ovary," in *Cancer in adolescents and young adults*, 219–236.

- Bruker.com (2022). *IVDr methods for body fluid analysis | urine screening*. Revised from 12 October 2022. Available at: <https://www.bruker.com/en/products-and-solutions/mr/nmr-clinical-research-solutions/b-i-methods.html>.
- Bruker.com (2022). *PhenoRisk PACS™*. Revised from 12 October 2022. Available at: <https://www.bruker.com/en/products-and-solutions/mr/nmr-clinical-research-solutions/phenorisk-pacs.html>.
- Butler, L. M., Perone, Y., Dehairs, J., Lupien, L. E., de Laat, V., Talebi, A., et al. (2020). Lipids and cancer: Emerging roles in pathogenesis, diagnosis and therapeutic intervention. *Adv. Drug Deliv. Rev.* 159, 245–293. doi:10.1016/j.addr.2020.07.013
- Camps, J., Castañé, H., Rodríguez-Tomás, E., Baiges-Gaya, G., Hernández-Aguilera, A., Arenas, M., et al. (2021). On the role of paraoxonase-1 and chemokine ligand 2 (C-C motif) in metabolic alterations linked to inflammation and disease. A 2021 update. *Biomolecules* 11 (7), 971. doi:10.3390/biom11070971
- Caneba, C. A., Bellance, N., Yang, L., Pabst, L., and Nagrah, D. (2012). Pyruvate uptake is increased in highly invasive ovarian cancer cells under anoikis conditions for anaplerosis, mitochondrial function, and migration. *Am. J. physiology. Endocrinol. metabolism* 303 (8), E1036–E1052. doi:10.1152/ajpendo.00151.2012
- Castelli, S., De Falco, P., Ciccarone, F., Desideri, E., and Ciriolo, M. (2021). Lipid catabolism and ROS in cancer: A bidirectional liaison. *Cancers* 13 (21), 5484. doi:10.3390/cancers13215484
- Clarke-Pearson, D. L. (2009). Clinical practice. Screening for ovarian cancer. *N. Engl. J. Med.* 361 (2), 170–177. doi:10.1056/NEJMcP0901926
- DeBerardinis, R., Lum, J., Hatzivassiliou, G., and Thompson, C. (2008). The biology of cancer: Metabolic reprogramming fuels cell growth and proliferation. *Cell. Metab.* 7 (1), 11–20. doi:10.1016/j.cmet.2007.10.002
- Desai, A., Xu, J., Aysola, K., Qin, Y., Okoli, C., Hariprasad, R., et al. (2014). Epithelial ovarian cancer: An overview. *World J. Transl. Med.* 3 (1), 1–8. doi:10.5528/wjtm.v3.i1.1
- Eriksen, N., and Benditt, E. P. (1980). Isolation and characterization of the amyloid-related apoprotein (SAA) from human high density lipoprotein. *Proc. Natl. Acad. Sci. U. S. A.* 77 (11), 6860–6864. doi:10.1073/pnas.77.11.6860
- Fantin, V., St-Pierre, J., and Leder, P. (2006). Attenuation of LDH-A expression uncovers a link between glycolysis, mitochondrial physiology, and tumor maintenance. *Cancer Cell* 9 (6), 425–434. doi:10.1016/j.ccr.2006.04.023
- Fazzari, J., Lin, H., Murphy, C., Ungard, R., and Singh, G. (2015). Inhibitors of glutamate release from breast cancer cells: new targets for cancer-induced bone-pain. *Sci. Rep.* 5 (1), 8380. doi:10.1038/srep08380
- Feingold, K. R., Bradley, A., Blackman, M. R., Boyce, A., Chrousos, G., Corpas, E., et al. (2021). “Introduction to lipids and lipoproteins,” in *Endotext*. K. R. Feingold, B. Anawalt, A. Boyce. Editors et al. (South Dartmouth (MA): MDText.com, Inc.).
- Florea, G., Tudorache, I. F., Fuior, E. V., Ionita, R., Dumitrescu, M., Fenyo, I. M., et al. (2022). Apolipoprotein A-II, a player in primary processes and diseases. *Biomedicines* 10, 1578. doi:10.3390/biomedicines10071578
- Fong, M. Y., McDunn, J., and Kakar, S. S. (2011). Identification of metabolites in the normal ovary and their transformation in primary and metastatic ovarian cancer. *PLoS One* 6 (5), e19963. doi:10.1371/journal.pone.0019963
- Frantz, S., Hofmann, U., Fraccarollo, D., Schäfer, A., Kranepuhl, S., Hagedorn, I., et al. (2013). Monocytes/macrophages prevent healing defects and left ventricular thrombus formation after myocardial infarction. *FASEB J.* 27, 871–881. doi:10.1096/fj.12-214049
- Fu, Y., Liu, S., Yin, S., Niu, W., Xiong, W., Tan, M., et al. (2017). The reverse Warburg effect is likely to be an Achilles’ heel of cancer that can be exploited for cancer therapy. *Oncotarget* 8 (34), 57813–57825. doi:10.18632/oncotarget.18175
- Gabay, C., and Kushner, I. (1999). Acute-phase proteins and other systemic responses to inflammation [published correction appears in *N Engl J Med* 1999 Apr 29;340(17):1376]. *N. Engl. J. Med.* 340 (6), 448–454. doi:10.1056/NEJM199902113400607
- Gadomska, H., Grzechocińska, B., Janecki, J., Nowicka, G., Powolny, M., and Marianowski, L. (2005). Serum lipids concentration in women with benign and malignant ovarian tumours. *Eur. J. Obstet. Gynecol. Reprod. Biol.* 120 (1), 87–90. doi:10.1016/j.ejogrb.2004.02.045
- Gall, W. E., Beebe, K., Lawton, K. A., Adam, K. P., Mitchell, M. W., Nakhle, P. J., et al. (2010). alpha-hydroxybutyrate is an early biomarker of insulin resistance and glucose intolerance in a nondiabetic population. *PLoS One* 5 (5), e10883. doi:10.1371/journal.pone.0010883
- Georgila, K., Vyrla, D., and Drakos, E. (2019). Apolipoprotein A-I (ApoA-I), immunity, inflammation and cancer. *Cancers (Basel)* 11 (8), 1097. doi:10.3390/cancers11081097
- Greten, F. R., and Grivnenkov, S. I. (2019). Inflammation and cancer: Triggers, mechanisms, and consequences. *Immunity* 51 (1), 27–41. doi:10.1016/j.immuni.2019.06.025
- Grohmann, U., and Bronte, V. (2010). Control of immune response by amino acid metabolism. *Immunol. Rev.* 236, 243–264. doi:10.1111/j.1600-065X.2010.00915.x
- Guo, H., Xu, Y., Wang, F., Shen, Z., Tuo, X., Qian, H., et al. (2018). Clinical associations between ASCT2 and p-mTOR in the pathogenesis and prognosis of epithelial ovarian cancer. *Oncol. Rep.* 40, 3725–3733. doi:10.3892/or.2018.6729
- Gupta, D., and Lis, C. G. (2009). Role of CA125 in predicting ovarian cancer survival - a review of the epidemiological literature. *J. Ovarian Res.* 2, 13. doi:10.1186/1757-2215-2-13
- Hanahan, D., and Weinberg, R. (2000). The hallmarks of cancer. *Cell* 100 (1), 57–70. doi:10.1016/s0092-8674(00)81683-9
- Hasegawa, S., Ichiyama, T., Sonaka, I., Ohsaki, A., Okada, S., Wakiguchi, H., et al. (2012). Cysteine, histidine and glycine exhibit anti-inflammatory effects in human coronary arterial endothelial cells. *Clin. Exp. Immunol.* 167 (2), 269–274. doi:10.1111/j.1365-2249.2011.04519.x
- Hilal, Z., Reznicek, G. A., Klenke, R., Dogan, A., and Tempfer, C. B. (2017). Nutritional status, cachexia, and anorexia in women with peritoneal metastasis and intraperitoneal chemotherapy: A longitudinal analysis. *J. Gynecol. Oncol.* 28 (6), e80. doi:10.3802/jgo.2017.28.e80
- Hilvo, M., de Santiago, I., Gopalacharyulu, P., Schmitt, W. D., Budczies, J., Kuhberg, M., et al. (2016). Accumulated metabolites of hydroxybutyric acid serve as diagnostic and prognostic biomarkers of ovarian high-grade serous carcinomas. *Cancer Res.* 76 (4), 796–804. doi:10.1158/0008-5472.CAN-15-2298
- Hosoi, H., Webb, N. R., Glick, J. M., Tietge, U. J., Purdom, M. S., de Beer, F. C., et al. (1999). Expression of serum amyloid A protein in the absence of the acute phase response does not reduce HDL cholesterol or apoA-I levels in human apoA-I transgenic mice. *J. Lipid Res.* 40 (4), 648–653. doi:10.1016/s0022-2275(20)32143-x
- Iyer, V. R., and Lee, S. I. (2010). MRI, CT, and PET/CT for ovarian cancer detection and adnexal lesion characterization. *AJR Am. J. Roentgenol.* 194 (2), 311–321. doi:10.2214/AJR.09.3522
- Jaragh Alhadad, L. (2021). Encapsulation and *in vitro* evaluation of low-density lipoprotein with cholesterol conjugated anti-HSP27 and HER2 proteins as drug delivery enhancement in ovarian cancer. *Biomed. J. Sci. Tech. Res.* 35 (2). doi:10.26717/bjstr.2021.35.005675
- Jia, D., Nagaoka, Y., Katsumata, M., and Orsulic, S. (2018). Inflammation is a key contributor to ovarian cancer cell seeding. *Sci. Rep.* 8 (1), 12394. doi:10.1038/s41598-018-30261-8
- Journal, B. (2015). Determination of serum CA125 and evaluate its efficiency as screening tool for early detection of ovarian tumors. *Baghdad Sci. J.* 12 (1), 55–62. doi:10.21123/bsj.12.1.55-62
- Kaku, T., Ogawa, S., Kawano, Y., Ohishi, Y., Kobayashi, H., Hirakawa, T., et al. (2003). Histological classification of ovarian cancer. *Med. Electron Microsc.* 36 (1), 9–17. doi:10.1007/s007950300002
- Karantanis, D., Allen-Auerbach, M., and Czernin, J. (2012). Relationship among glycolytic phenotype, grade, and histological subtype in ovarian carcinoma. *Clin. Nucl. Med.* 37 (1), 49–53. doi:10.1097/RLU.0b013e3182291e03
- Karunakaran, S., Umapathy, N. S., Thangaraju, M., Hatanaka, T., Itagaki, S., Munn, D. H., et al. (2008). Interaction of tryptophan derivatives with SLC6A14 (ATB0+) reveals the potential of the transporter as a drug target for cancer chemotherapy. *Biochem. J.* 414 (3), 343–355. doi:10.1042/BJ20080622
- Kenemans, P., Yedema, C. A., Bon, G. G., and von Mensdorff-Pouilly, S. (1993). CA 125 in gynecological pathology—a review. *Eur. J. obstetrics, Gynecol. reproductive Biol.* 49 (1–2), 115–124. doi:10.1016/0028-2243(93)90135-y
- Khovidhunkit, W., Kim, M. S., Memon, R. A., Shigenaga, J. K., Moser, A. H., Feingold, K. R., et al. (2004). Effects of infection and inflammation on lipid and lipoprotein metabolism: Mechanisms and consequences to the host. *J. Lipid Res.* 45 (7), 1169–1196. doi:10.1194/jlr.R300019-JLR200
- Khovidhunkit, W., Kim, M. S., Memon, R. A., Shigenaga, J. K., Moser, A. H., Feingold, K. R., et al. (2004). Effects of infection and inflammation on lipid and lipoprotein metabolism: Mechanisms and consequences to the host. *J. lipid Res.* 45 (7), 1169–1196. doi:10.1194/jlr.R300019-JLR200
- Kim, J., Park, E. Y., Kim, O., Schilder, J., Coffey, D., Cho, C. H., et al. (2018). Cell origins of high-grade serous ovarian cancer. *Cancers (Basel)* 10 (11), 433. doi:10.3390/cancers10110433
- Kobayashi, E., Ueda, Y., Matsuzaki, S., Yokoyama, T., Kimura, T., Yoshino, K., et al. (2012). Biomarkers for screening, diagnosis, and monitoring of ovarian cancer. *Cancer Epidemiol. Biomarkers Prev.* 21 (11), 1902–1912. doi:10.1158/1055-9965.EPI-12-0646
- Lamkin, D. M., Spitz, D. R., Shahzad, M. M., Zimmerman, B., Lenihan, D. J., Degeest, K., et al. (2009). Glucose as a prognostic factor in ovarian carcinoma. *Cancer* 115 (5), 1021–1027. doi:10.1002/cncr.24126
- Lengyel, E., Makowski, L., DiGiovanni, J., and Kolonin, M. G. (2018). Cancer as a matter of fat: The crosstalk between adipose tissue and tumors. *Trends Cancer* 4 (5), 374–384. doi:10.1016/j.trecan.2018.03.004
- Li, N., Zhan, X., and Zhan, X. (2019). Energy metabolism heterogeneity-based molecular biomarkers for ovarian cancer. *Mol. Med.*, 2–3. doi:10.5772/intechopen.80622
- Liou, G. Y., and Storz, P. (2010). Reactive oxygen species in cancer. *Free Radic. Res.* 44 (5), 479–496. doi:10.3109/10715761003667554
- Low, R. N., Carter, W. D., Saleh, F., and Sigeti, J. S. (1995). Ovarian cancer: Comparison of findings with perfluorocarbon-enhanced MR imaging, in-111-CYT-103 immunoscintigraphy, and CT. *Radiology* 195 (2), 391–400. doi:10.1148/radiology.195.2.7724757



- Manisha, D., and Jindal, D. (2019). Role of lipid profile in ovarian carcinoma patients. *Int. J. Med. Biomed. Stud.* 3 (8). doi:10.32553/ijmbs.v3i8.501
- Maran, L., Hamid, A., and Hamid, S. (2021). Lipoproteins as markers for monitoring cancer progression. *J. Lipids* 2021, 2–14. doi:10.1155/2021/8180424
- Mayer, A., Schmidt, M., Seeger, A., Serras, A. F., Vaupel, P., and Schmidberger, H. (2014). GLUT-1 expression is largely unrelated to both hypoxia and the Warburg phenotype in squamous cell carcinomas of the vulva. *BMC Cancer* 14, 760. doi:10.1186/1471-2407-14-760
- Meiser, J., Schuster, A., Pietzke, M., Vande Voorde, J., Athineos, D., Oziel, K., et al. (2018). Increased formate overflow is a hallmark of oxidative cancer. *Nat. Commun.* 9 (1), 1368. doi:10.1038/s41467-018-03777-w
- Melvin, J. C., Seth, D., Holmberg, L., Garmo, H., Hammar, N., Jungner, I., et al. (2012). Lipid profiles and risk of breast and ovarian cancer in the Swedish AMORIS study. *Cancer Epidemiol. Biomarkers Prev.* 21 (8), 1381–1384. doi:10.1158/1055-9965.EPI-12-0188
- Memon, R. A., Feingold, K. R., Moser, A. H., Doerfler, W., Adi, S., Dinarello, C. A., et al. (1992). Differential effects of interleukin-1 and tumor necrosis factor on ketogenesis. *Am. J. physiology* 263 (2), E301–E309. doi:10.1152/ajpendo.1992.263.2.E301
- Menendez, J., and Lupu, R. (2007). Fatty acid synthase and the lipogenic phenotype in cancer pathogenesis. *Nat. Rev. Cancer* 7 (10), 763–777. doi:10.1038/nrc2222
- Merkel, M., Heeren, J., Dudeck, W., Rinninger, F., Radner, H., Breslow, J. L., et al. (2002). Inactive lipoprotein lipase (LPL) alone increases selective cholesterol ester uptake *in vivo*, whereas in the presence of active LPL it also increases triglyceride hydrolysis and whole particle lipoprotein uptake. *J. Biol. Chem.* 277 (9), 7405–7411. doi:10.1074/jbc.M107914200
- Moss, E. L., Hollingworth, J., and Reynolds, T. M. (2005). The role of CA125 in clinical practice. *J. Clin. pathology* 58 (3), 308–312. doi:10.1136/jcp.2004.018077
- Neurauter, G., Grahmann, A. V., Klieber, M., Zeimet, A., Ledochowski, M., Sperner-Unterwieser, B., et al. (2008). Serum phenylalanine concentrations in patients with ovarian carcinoma correlate with concentrations of immune activation markers and of isoprostane-8. *Cancer Lett.* 272 (1), 141–147. doi:10.1016/j.canlet.2008.07.002
- Nichols, H. B., Trentham-Dietz, A., Hampton, J. M., Titus-Ernstoff, L., Egan, K. M., Willett, W. C., et al. (2006). From menarche to menopause: Trends among US women born from 1912 to 1969. *Am. J. Epidemiol.* 164 (10), 1003–1011. doi:10.1093/aje/kwj282
- Nieman, K. M., Kenny, H. A., Penicka, C. V., Ladanyi, A., Buell-Gutbrod, R., Zillhardt, M. R., et al. (2011). Adipocytes promote ovarian cancer metastasis and provide energy for rapid tumor growth. *Nat. Med.* 17 (11), 1498–1503. doi:10.1038/nm.2492
- Normandin, K., Péant, B., Le Page, C., de Ladurantaye, M., Ouellet, V., Tonin, P. N., et al. (2010). Protease inhibitor SERPINA1 expression in epithelial ovarian cancer. *Clin. Exp. Metastasis* 27 (1), 55–69. doi:10.1007/s10585-009-9303-6
- Okin, D., and Medzhitov, R. (2016). The effect of sustained inflammation on hepatic mevalonate pathway results in hyperglycemia. *Cell* 165 (2), 343–356. doi:10.1016/j.cell.2016.02.023
- Ossoli, A., Wolska, A., Remaley, A., and Gomaschi, M. (2022). High-density lipoproteins: A promising tool against cancer. *Biochimica Biophysica Acta (BBA) - Mol. Cell. Biol. Lipids* 1867 (1), 159068. doi:10.1016/j.bbalip.2021.159068
- Otvos, J., Shalaurova, I., Wolak-Dinsmore, J., Connelly, M., Mackey, R., Stein, J., et al. (2015). GlycA: A composite nuclear magnetic resonance biomarker of systemic inflammation. *Clin. Chem.* 61 (5), 714–723. doi:10.1373/clinchem.2014.232918
- Peres, L. C., Cushing-Haugen, K. L., Köbel, M., Harris, H. R., Berchuck, A., Rossing, M. A., et al. (2019). Invasive epithelial ovarian cancer survival by histotype and disease stage. *J. Natl. Cancer Inst.* 111 (1), 60–68. doi:10.1093/jnci/djy071
- Pin, F., Barreto, R., Kitase, Y., Mitra, S., Erne, C. E., Novinger, L. J., et al. (2018). Growth of ovarian cancer xenografts causes loss of muscle and bone mass: A new model for the study of cancer cachexia. *J. cachexia, sarcopenia muscle* 9 (4), 685–700. doi:10.1002/jcsm.12311
- Prat and FIGO Committee on Gynecologic Oncology (2014). Staging classification for cancer of the ovary, fallopian tube, and peritoneum. *Int. J. Gynaecol. Obstet.* 124 (1), 1–5. doi:10.1016/j.ijgo.2013.10.001
- Prayer, L., Stiglbauer, R., Kramer, J., Wimberger, D., Poelzeleitner, D., Schima, W., et al. (1993). Superparamagnetic particles as oral contrast medium in magnetic resonance imaging of patients with treated ovarian cancer—Comparison with plain MRI. *Br. J. Radiology* 66 (785), 415–419. doi:10.1259/0007-1285-66-785-415
- Qadir, M. I., and Malik, S. A. (2008). Plasma lipid profile in gynecologic cancers. *Eur. J. Gynaecol. Oncol.* 29 (2), 158–161.
- Qu, X., Tang, Y., and Hua, S. (2018). Immunological approaches towards cancer and inflammation: A cross talk. *Front. Immunol.* 9, 563. doi:10.3389/fimmu.2018.00563
- Rensen, P. C., de Vreeh, R. L., Kuiper, J., Bijsterbosch, M. K., Biessen, E. A., and van Berkel, T. J. (2001). Recombinant lipoproteins: Lipoprotein-like lipid particles for drug targeting. *Adv. Drug Deliv. Rev.* 47 (2–3), 251–276. doi:10.1016/s0169-409x(01)00109-0
- Rizzo, A., Napoli, A., Roggiani, F., Tomassetti, A., Bagnoli, M., and Mezzananza, D. (2018). One-carbon metabolism: Biological players in epithelial ovarian cancer. *Int. J. Mol. Sci.* 19 (7), 2092. doi:10.3390/ijms19072092
- Rodríguez, R. (2019). The relevance of alpha-1-acid glycoprotein in human cancer: A minireview. *Adv. Cancer Res. Clin. Imaging* 2 (1). doi:10.33552/acrci.2019.02.000526
- Saito, Y., and Soga, T. (2021). Amino acid transporters as emerging therapeutic targets in cancer. *Cancer Sci.* 112 (8), 2958–2965. doi:10.1111/cas.15006
- Saldova, R., Royle, L., Radcliffe, C. M., Abd Hamid, U. M., Evans, R., Arnold, J. N., et al. (2007). Ovarian cancer is associated with changes in glycosylation in both acute-phase proteins and IgG. *Glycobiology* 17 (12), 1344–1356. doi:10.1093/glycob/cwm100
- Savant, S. S., Sriramkumar, S., and O'Hagan, H. M. (2018). The role of inflammation and inflammatory mediators in the development, progression, metastasis, and chemoresistance of epithelial ovarian cancer. *Cancers (Basel)* 10 (8), 251. doi:10.3390/cancers10080251
- Schauer, I. G., Sood, A. K., Mok, S., and Liu, J. (2011). Cancer-associated fibroblasts and their putative role in potentiating the initiation and development of epithelial ovarian cancer. *Neoplasia (New York, N.Y.)* 13 (5), 393–405. doi:10.1593/neo.101720
- Schwartzburd, P. (2019). Cancer-induced reprogramming of host glucose metabolism: “Vicious cycle” supporting cancer progression. *Front. Oncol.* 9, 218. doi:10.3389/fonc.2019.00218
- Schwartz, L., Seyfried, T., Alfarouk, K. O., Veiga Moreira, DaJ., and Fais, S. (2017). Out of Warburg effect: An effective cancer treatment targeting the tumor specific metabolism and dysregulated pH. *Semin. Cancer Biol.* 43, 134–138. doi:10.1016/j.semcancer.2017.01.005
- Setiawan, V., Pike, M., Karageorgi, S., Deming, S., Anderson, K., Bernstein, L., et al. (2012). Age at last birth in relation to risk of endometrial cancer: Pooled analysis in the epidemiology of endometrial cancer consortium. *Am. J. Epidemiol.* 176 (4), 269–278. doi:10.1093/aje/kws129
- Skates, S. J., Jacobs, I. J., and Knapp, R. C. (2021). “Tumor markers in screening for ovarian cancer,” in *Ovarian cancer*, 61–73.
- Swinnen, J., Brusselmans, K., and Verhoeven, G. (2006). Increased lipogenesis in cancer cells: New players, novel targets. *Curr. Opin. Clin. Nutr. Metabolic Care* 9 (4), 358–365. doi:10.1097/01.mco.0000232894.28674.30
- Szymańska, E., Saccenti, E., Smilde, A. K., and Westerhuis, J. A. (2012). Double-check: Validation of diagnostic statistics for PLS-DA models in metabolomics studies. *Metabolomics* 8 (1), 3–16. doi:10.1007/s11306-011-0330-3
- Tannahill, G. M., Curtis, A. M., Adamik, J., Palsson-McDermott, E. M., McGettrick, A. F., Goel, G., et al. (2013). Succinate is an inflammatory signal that induces IL-1 $\beta$  through HIF-1 $\alpha$ . *Nature* 496 (7444), 238–242. doi:10.1038/nature11986
- Thuwajit, C., Ferraresi, A., Titone, R., Thuwajit, P., and Isidoro, C. (2018). The metabolic cross-talk between epithelial cancer cells and stromal fibroblasts in ovarian cancer progression: Autophagy plays a role. *Med. Res. Rev.* 38 (4), 1235–1254. doi:10.1002/med.21473
- Tiwari, S., Verma, A., Sankhwar, P., Dwivedi, A., Srivastava, R., Tripathi, D., et al. (2015). Association between lipid profile and ovarian cancer in women of north India. *Int. J. Biomed. Res.* 6 (7), 488. doi:10.7439/ijbr.v6i7.2272
- Tsoupras, A., Lordan, R., and Zabetakis, I. (2018). Inflammation, not cholesterol, is a cause of chronic disease. *Nutrients* 10 (5), 604. doi:10.3390/nu10050604
- van Nagell, J. R., Jr, and Hoff, J. T. (2013). Transvaginal ultrasonography in ovarian cancer screening: Current perspectives. *Int. J. Womens Health* 6, 25–33. doi:10.2147/IJWH.S38347
- VanHook, A. M. (2022). Formate for tumor progression. *Sci. Signal.* 15 (736), eadd1844. doi:10.1126/scisignal.add1844
- Wang, L., and Li, X. (2020). Identification of an energy metabolism-related gene signature in ovarian cancer prognosis. *Oncol. Rep.* 43 (6), 1755–1770. doi:10.3892/or.2020.7548
- Wang, L., Xiong, H., Wu, F., Zhang, Y., Wang, J., Zhao, L., et al. (2014). Hexokinase 2-mediated Warburg effect is required for PTEN- and p53-deficiency-driven prostate cancer growth. *Cell. Rep.* 8 (5), 1461–1474. doi:10.1016/j.celrep.2014.07.053
- Wang, Q., Wu, Y., Zhang, H., Yang, K., Tong, Y., Chen, L., et al. (2019). Clinical value of serum HE4, CA125, CA72-4, and ROMA index for diagnosis of ovarian cancer and prediction of postoperative recurrence. *Clin. Lab.* 65 (4). doi:10.7754/Clin.Lab.2018.181030
- Wang, Q., Zhao, L., Han, L., Fu, G., Tuo, X., Ma, S., et al. (2020). The differential distribution of bacteria between cancerous and noncancerous ovarian tissues *in situ*. *J. Ovarian Res.* 13 (1), 8. doi:10.1186/s13048-019-0603-4
- Warburg, O., Wind, F., and Negelein, E. (1927). The metabolism of tumors in the body. *J. Gen. Physiol.* 8 (6), 519–530. doi:10.1085/jgp.8.6.519
- Watanabe, T., Hashimoto, T., Sugino, T., Soeda, S., Nishiyama, H., Morimura, Y., et al. (2012). Production of IL1-beta by ovarian cancer cells induces mesothelial cell beta1-integrin expression facilitating peritoneal dissemination. *J. Ovarian Res.* 5 (1), 7. doi:10.1186/1757-2215-5-7
- Watanabe, T., Shibata, M., Nishiyama, H., Soeda, S., Furukawa, S., Gonda, K., et al. (2014). Serum levels of rapid turnover proteins are decreased and related to systemic inflammation in patients with ovarian cancer. *Oncol. Lett.* 7 (2), 373–377. doi:10.3892/ol.2013.1735

- Wei, Z., Liu, X., Cheng, C., Yu, W., and Yi, P. (2021). Metabolism of amino acids in cancer. *Front. Cell. Dev. Biol.* 8, 603837. doi:10.3389/fcell.2020.603837
- Wilson, R. B., Solass, W., Archid, R., Weinreich, F. J., Königsrainer, A., and Reymond, M. A. (2019). Resistance to anoikis in transcoelomic shedding: The role of glycolytic enzymes. *Pleura Perit.* 4 (1), 20190003. doi:10.1515/pp-2019-0003
- Wong, N., Ojo, D., Yan, J., and Tang, D. (2015). PKM2 contributes to cancer metabolism. *Cancer Lett.* 356 (2), 184–191. doi:10.1016/j.canlet.2014.01.031
- Wu, Q., Li, J., Li, Z., Sun, S., Zhu, S., Wang, L., et al. (2019). Exosomes from the tumour-adipocyte interplay stimulate beige/brown differentiation and reprogram metabolism in stromal adipocytes to promote tumour progression. *J. Exp. Clin. Cancer Res.* 38 (1), 223. doi:10.1186/s13046-019-1210-3
- Xia, J., Psychogios, N., Young, N., and Wishart, D. S. (2009). MetaboAnalyst: A web server for metabolomic data analysis and interpretation. *Nucleic Acids Res.* 37, W652–W660. doi:10.1093/nar/gkp356
- Yamamoto, Y., Oguri, H., Yamada, R., Maeda, N., Kohsaki, S., and Fukaya, T. (2008). Preoperative evaluation of pelvic masses with combined 18F-fluorodeoxyglucose positron emission tomography and computed tomography. *Int. J. Gynaecol. Obstet.* 102 (2), 124–127. doi:10.1016/j.ijgo.2008.02.019
- Yuan, L., Sheng, X., Willson, A. K., Roque, D. R., Stine, J. E., Guo, H., et al. (2015). Glutamine promotes ovarian cancer cell proliferation through the mTOR/S6 pathway. *Endocrine-related cancer* 22 (4), 577–591. doi:10.1530/ERC-15-0192
- Yung, S., and Chan, T. M. (2011). Pathophysiology of the peritoneal membrane during peritoneal dialysis: The role of hyaluronan. *J. Biomed. Biotechnol.* 2011, 180594. doi:10.1155/2011/180594
- Zhang, Q., Zhu, B., and Li, Y. (2017). Resolution of cancer-promoting inflammation: A new approach for anticancer therapy. *Front. Immunol.* 8, 71. doi:10.3389/fimmu.2017.00071
- Zhao, Y., Zou, W., Du, J., and Zhao, Y. (2018). The origins and homeostasis of monocytes and tissue-resident macrophages in physiological situation. *J. Cell. physiology* 233 (10), 6425–6439. doi:10.1002/jcp.26461
- Zhao, H., Wu, L., Yan, G., Chen, Y., Zhou, M., Wu, Y., et al. (2021). Inflammation and tumor progression: signaling pathways and targeted intervention. *Signal transduction and targeted therapy* 6 (1), 263. doi:10.1038/s41392-021-00658-5
- Zhou, Z., Wang, X., Ren, X., Zhou, L., Wang, N., and Kang, H. (2021). Disease burden and attributable risk factors of ovarian cancer from 1990 to 2017: Findings from the global burden of disease study 2017. *Front. Public Health* 9, 619581. doi:10.3389/fpubh.2021.619581



## Glossary

**Name** Extended Name

**2HB** 2-hydroxybutyric acid

**3HB** 3-hydroxybutyric acid

**ABA1** apolipoprotein-B100/apolipoprotein A1

**ApoE** apolipoprotein E

**ASCT2** alanine–serine–cysteine transporter 2

**ATP** adenosine triphosphate

**BOT** borderline ovarian tumor

**CA 19-9** cancer antigen 19-9

**CA-125** cancer antigen-125

**CAFs** cancer-associated fibroblasts

**CEA** carcinoembryonic antigen

**CL** cholesterol

**DMG** N, N-dimethylglycine

**EOC** epithelial ovarian cancer

**FC** fold change

**FDR** false discovery rate

**GlcNAc** N-acetylgalactosamine

**GLUT1** glucose transporter 1

**GlycA** glycoprotein A or glycoprotein acetylation

**H1A1** apolipoprotein-A1 HDL-1

**H1A2** apolipoprotein-A2 HDL-1

**H1CH** cholesterol HDL-1

**H1FC** free cholesterol HDL-1

**H1PL** phospholipids HDL-1

**H1TG** triglycerides HDL-1

**H2A1** apolipoprotein-A1 HDL-2

**H2A2** apolipoprotein-A2 HDL-2

**H2CH** cholesterol HDL-2

**H2FC** free cholesterol HDL-2

**H2PL** phospholipids HDL-2

**H2TG** triglycerides HDL-2

**H3A1** apolipoprotein-A1 HDL-3

**H3A2** apolipoprotein-A2 HDL-3

**H3CH** cholesterol HDL-3

**H3FC** free cholesterol HDL-3

**H3PL** phospholipids HDL-3

**H3TG** triglycerides HDL-3

**H4A1** apolipoprotein-A1 HDL-4

**H4A2** apolipoprotein-A2 HDL-4

**H4CH** cholesterol HDL-4

**H4FC** free cholesterol HDL-4

**H4PL** phospholipids HDL-4

**H4TG** triglycerides HDL-4

**HDA1** HDL-apolipoprotein A1

**HDA2** HDL-apolipoprotein-A2

**HDCH** HDL cholesterol

**HDFC** HDL-free cholesterol

**HDPL** HDL phospholipids

**HDTG** HDL triglycerides

**HGSOC** high-grade serous ovarian cancer or carcinoma

**HIF** hypoxia-inducible factor

**HK2** hexokinase 2

**IDAB** IDL-apolipoprotein-B100

**IDCH** IDL cholesterol

**IDFC** IDL-free cholesterol

**IDPL** IDL phospholipids

**IDPN** IDL particle number

**IDTG** IDL triglycerides

**IR** insulin resistance

**KNN** K-nearest neighbors

**L1AB** apolipoprotein-B100 LDL-1

**L1CH** cholesterol LDL-1

**L1FC** free cholesterol LDL-1

**L1PL** phospholipids LDL-1

**L1PN** particle number LDL-1

**L1TG** triglycerides LDL-1

**L2AB** apolipoprotein-B100 LDL-2

**L2CH** cholesterol LDL-2

**L2FC** free cholesterol LDL-2

**L2PL** phospholipids LDL-2

**L2PN** particle number LDL-2

**L2TG** triglycerides LDL-2

**L3AB** apolipoprotein-B100 LDL-3

**L3CH** cholesterol LDL-3

**L3FC** free cholesterol LDL-3

**L3PL** phospholipids LDL-3

**L3PN** particle number LDL-3

**L3TG** triglycerides LDL-3

**L4AB** apolipoprotein-B100 LDL-4

**L4CH** cholesterol LDL-4

**L4FC** free cholesterol LDL-4

**L4PL** phospholipids LDL-4

**L4PN** particle number LDL-4

**L4TG** triglycerides LDL-4

**L5AB** apolipoprotein-B100 LDL-5

**L5CH** cholesterol LDL-5

**L5FC** free cholesterol LDL-5

**L5PL** phospholipids LDL-5

**L5PN** particle number LDL-5

<b>L5TG</b> triglycerides LDL-5	<b>THP-1</b> human leukemia monocytic cell line
<b>L6AB</b> apolipoprotein-B100 LDL-6	<b>TME</b> tumor microenvironment
<b>L6CH</b> cholesterol LDL-6	<b>TPA1</b> total plasma apolipoprotein A1
<b>L6FC</b> free cholesterol LDL-6	<b>TPA2</b> total plasma apolipoprotein-A2
<b>L6PL</b> phospholipids LDL-6	<b>TPAB</b> total plasma apolipoprotein-B100
<b>L6PN</b> particle number LDL-6	<b>TPCH</b> total plasma cholesterol
<b>L6TG</b> triglycerides LDL-6	<b>TPTG</b> total plasma triglyceride
<b>LDAB</b> LDL-apolipoprotein-B100	<b>V1CH</b> cholesterol VLDL-1
<b>LDCH</b> LDL cholesterol	<b>V1FC</b> free cholesterol VLDL-1
<b>LDFC</b> LDL-free cholesterol	<b>V1PL</b> phospholipids VLDL-1
<b>LDH</b> lactate dehydrogenase	<b>V1TG</b> triglycerides VLDL-1
<b>LDHD</b> LDL-cholesterol/HDL-cholesterol	<b>V2CH</b> cholesterol VLDL-2
<b>LDLR</b> LDL receptor	<b>V2FC</b> free cholesterol VLDL-2
<b>LDPL</b> LDL phospholipids	<b>V2PL</b> phospholipids VLDL-2
<b>LDPN</b> LDL particle number	<b>V2TG</b> triglycerides VLDL-2
<b>LDTG</b> LDL triglycerides	<b>V3CH</b> cholesterol VLDL-3
<b>LOOCV</b> leave one out cross-validation method	<b>V3FC</b> free cholesterol VLDL-3
<b>LPL</b> lipoprotein lipase	<b>V3PL</b> phospholipids VLDL-3
<b>MCTs</b> lactate transporter (monocarboxylate transporter)	<b>V3TG</b> triglycerides VLDL-3
<b>NANA</b> N-acetylneuraminic acid	<b>V4CH</b> cholesterol VLDL-4
<b>OC</b> ovarian cancer	<b>V4FC</b> free cholesterol VLDL-4
<b>PCA</b> principle component analysis	<b>V4PL</b> phospholipids VLDL-4
<b>PCOS</b> polycystic ovary syndrome	<b>V4TG</b> triglycerides VLDL-4
<b>PKM2</b> pyruvate kinase type M2	<b>V5CH</b> cholesterol VLDL-5
<b>ROC</b> receiver operating characteristic	<b>V5FC</b> free cholesterol VLDL-5
<b>ROS</b> reactive oxygen species	<b>V5PL</b> phospholipids VLDL-5
<b>SAA</b> serum amyloid A	<b>V5TG</b> triglycerides VLDL-5
<b>sPLSDA</b> sparse partial least square discriminant analysis	<b>VLAB</b> VLDL-apolipoprotein-B100
<b>TBPN</b> total particle number (apolipoprotein-B100 carrying particles)	<b>VLCH</b> VLDL cholesterol
<b>TCA</b> tricarboxylic acid cycle	<b>VLFC</b> VLDL-free cholesterol
<b>TG</b> triglycerides	<b>VLPL</b> VLDL phospholipids
	<b>VLPN</b> VLDL particle number



## OPEN ACCESS

## EDITED BY

Gregorio Peron,  
University of Brescia, Italy

## REVIEWED BY

Evangelia Sarandi,  
University of Crete, Greece  
Aristidis M Tsatsakis,  
University of Crete, Greece

## \*CORRESPONDENCE

Lemin Zheng,  
✉ zhengl@bjmu.edu.cn  
Mingguo Xu,  
✉ 18938690175@163.com

<sup>†</sup>These authors have contributed equally  
to this work

RECEIVED 06 March 2023

ACCEPTED 24 April 2023

PUBLISHED 04 May 2023

## CITATION

Fan X, Li K, Guo X, Liao S, Zhang Q, Xu Y,  
Cui H, Zheng L and Xu M (2023),  
Metabolic profiling reveals altered  
tryptophan metabolism in patients with  
kawasaki disease.  
*Front. Mol. Biosci.* 10:1180537.  
doi: 10.3389/fmolb.2023.1180537

## COPYRIGHT

© 2023 Fan, Li, Guo, Liao, Zhang, Xu, Cui,  
Zheng and Xu. This is an open-access  
article distributed under the terms of the  
[Creative Commons Attribution License](#)  
(CC BY). The use, distribution or  
reproduction in other forums is  
permitted, provided the original author(s)  
and the copyright owner(s) are credited  
and that the original publication in this  
journal is cited, in accordance with  
accepted academic practice. No use,  
distribution or reproduction is permitted  
which does not comply with these terms.

# Metabolic profiling reveals altered tryptophan metabolism in patients with kawasaki disease

Xue Fan<sup>1†</sup>, Ke Li<sup>2†</sup>, Xin Guo<sup>1</sup>, Shengyou Liao<sup>3</sup>, Qi Zhang<sup>4</sup>,  
Yangkai Xu<sup>4</sup>, Hongtu Cui<sup>4</sup>, Lemin Zheng<sup>2,4\*</sup> and Mingguo Xu<sup>1\*</sup>

<sup>1</sup>Department of Pediatrics, The Third People's Hospital of Longgang District Shenzhen, Shenzhen, China, <sup>2</sup>Advanced Innovation Center for Human Brain Protection, China National Clinical Research Center for Neurological Diseases, Beijing Tiantan Hospital, Capital Medical University, Beijing, China, <sup>3</sup>Department of Clinical Medical Research Center, Guangdong Provincial Engineering Research Center of Autoimmune Disease Precision Medicine, The Second Clinical Medical College, Jinan University (Shenzhen People's Hospital), Shenzhen, China, <sup>4</sup>Key Laboratory of Molecular Cardiovascular Sciences of Ministry of Education, Health Science Center, School of Basic Medical Sciences, The Institute of Cardiovascular Sciences and Institute of Systems Biomedicine, Peking University, Beijing, China

Kawasaki disease (KD) is a childhood vasculitis disease that is difficult to diagnose, and there is an urgent need for the identification of accurate and specific biomarkers. Here, we aimed to investigate metabolic alterations in patients with KD to determine novel diagnostic and prognostic biomarkers for KD. To this end, we performed untargeted metabolomics and found that several metabolic pathways were significantly enriched, including amino acid, lipid, and tryptophan metabolism, the latter of which we focused on particularly. Tryptophan-targeted metabolomics was conducted to explore the role of tryptophan metabolism in KD. The results showed that Trp and indole acetic acid (IAA) levels markedly decreased, and that L-kynurenine (Kyn) and kynurenic acid (Kyna) levels were considerably higher in patients with KD than in healthy controls. Changes in Trp, IAA, Kyn, and Kyna levels in a KD coronary arteritis mouse model were consistent with those in patients with KD. We further analyzed public single-cell RNA sequencing data of patients with KD and revealed that their peripheral blood mononuclear cells showed Aryl hydrocarbon receptor expression that was remarkably higher than that of healthy children. These results suggest that the Trp metabolic pathway is significantly altered in KD and that metabolic indicators may serve as novel diagnostic and therapeutic biomarkers for KD.

## KEYWORDS

kawasaki disease, tryptophan metabolism, coronary arteritis, metabolomics, biomarker

## Introduction

Kawasaki disease (KD) is a vasculitis syndrome that typically affects young children under the age of five and involves multiple systems of the body. It is one of the leading causes of acquired heart diseases in children in developed countries (Newburger et al., 2016) and may lead to ischemic cardiomyopathy (Chen et al., 2016). Vascular damage during the development of KD can ultimately lead to several complications, such as coronary artery lesions (CALs), including aneurysms, and aortic root dilatation (Gordon et al., 2009). Currently, the diagnosis of KD relies on the assessment of clinical symptoms, including fever lasting five or more days, erythema of the palms and soles or edema of the hands and feet, bilateral conjunctival injection, changes in the lips and oral cavity, and cervical

lymphadenopathy (McCrindle et al., 2017). Due to a lack of specific diagnostic criteria for KD, its diagnosis requires well-trained clinicians. The ability to accurately identify KD based on improved disease characterization and prognostic models may enable clinicians to make more precise treatment decisions and initiate treatment earlier, leading to a better prognosis. In KD, biomarkers could add diagnostic value to clinical features and ultrasound. Based on their represented major pathophysiologic pathways, current biomarkers are divided into the following categories: inflammation [C-reactive protein (CRP), erythrocyte sedimentation rate (ESR)], liver dysfunction [alanine aminotransferase (ALT)], and metabolic homeostasis (albumin, serum sodium) (McCrindle et al., 2017). However, it is necessary to investigate biomarkers in other pathways to fully understand the intricate pathophysiology of the condition and improve risk assessment, and the clinical need for non-invasive biomarkers to diagnose KD remains unfulfilled.

Metabolomics is an emerging, cost-effective, quantifiable tool for biomarker discovery (Johnson et al., 2016). Metabolomics can detect underlying changes in the metabolic products of physiological processes caused by cardiovascular diseases (CVDs) and provide important information on metabolic pathways and metabolites. In addition, the effects of gene mutations and environmental changes on the body are reflected by changes in metabolites. As a result, there is increasing interest in using metabolomics to define the chemical phenotypes associated with health or disease for cardiovascular risk stratification (Newgard, 2017; Ruiz-Canela et al., 2017). For example, metabolomics has revealed that the TMAO (trimethylamine N-oxide) pathway is strongly linked to myocardial infarction (Wang et al., 2011), and PAGln (phenylacetylglutamine) has been identified as a crucial prognostic factor in cardiovascular disease (Nemet et al., 2020). However, limited metabolomics studies on KD plasma have been reported, and diagnostic and prognostic applications of metabolic alterations in KD are not yet well defined; therefore, there is an urgent need to search for biomarkers and therapeutic targets for KD from a metabolomic perspective.

Tryptophan (Trp) is an essential amino acid and, as such, must be obtained from dietary sources. Dietary Trp can undergo degradation via intestinal flora (Taleb, 2019), or it can enter the bloodstream and be carried to various tissues where it is used as a substrate in various biosynthetic pathways. Trp can be used as a precursor of serotonin in the central nervous system (Ruddick et al., 2006) and as a source of the coenzyme nicotinamide adenosine dinucleotide (NAD) (Shin et al., 1998) throughout the body. The L-kynurenine (Kyn) pathway is one of the main pathways of Trp metabolism that generates Kyn and its downstream products and participates in inflammatory and immune responses (Wang et al., 2015). The Kyn pathway has been implicated in various biological processes, including immune regulation, peripheral disorders, and central nervous system disorders (Wang et al., 2015). Additionally, Trp metabolites (Kyn, anthranilic acid, and 3-hydroxy-L-kynurenine) are associated with high CVD-related mortality (Wang et al., 2010; Mangge et al., 2014). However, limited clinical data exist on the potential prognostic value of Trp pathway metabolites in patients with KD.

Transcriptomics is widely used for studying CVDs, such as atherosclerotic diseases (Herman and Autieri, 2018), hypertension

(Nemecz et al., 2016), heart failure (Gao et al., 2015), and myocardial hypertrophy (Viereck et al., 2016), and has helped identify new biomarkers and therapeutic strategies. Single-cell transcriptome sequencing (scRNA-seq) technology can reveal subtle changes in each cell and describes the gene regulatory networks that alter physiological functions, behaviors, and phenotypes (Shaw et al., 2021). Aryl hydrocarbon receptor (AHR) is a ligand-activated transcription factor widely expressed in various immune cells, including T cells, dendritic cells, and intestinal intraepithelial lymphocytes. Trp metabolites have been shown to be capable of functioning as endogenous ligands to regulate related aryl hydrocarbon receptor expression (Hezaveh et al., 2022). Combined peripheral blood single-cell transcriptome and metabolomic analyses can better verify changes in the metabolic microenvironment in plasma.

In this study, we aimed to: 1) investigate metabolic alterations in patients with KD to identify possible novel diagnostic and prognostic biomarkers for KD; 2) validate the metabolites' change using Peripheral Blood Single-Cell Transcriptome analysis; and 3) explore changes in biomarkers in mouse KD models to support further research into therapeutic development using mouse KD models.

## Results

### Metabolite profiling of the plasma from patients with KD using untargeted metabolomics

An overview of the workflow is presented in Figure 1. To identify potential biomarker candidates, we collected plasma samples from patients as a discovery cohort. The samples from 62 participants were subjected to untargeted metabolomics analysis using ultra-high-performance liquid chromatography-quadrupole time-of-flight mass spectrometry (UHPLC-QTOF-MS). The basic characteristics (including age and gender) of all 62 individuals were similar between the KD and healthy control groups (Table 1). However, laboratory values, including routine blood tests and biochemical indices of KD patients, exhibited a higher inflammatory state.

Untargeted metabolomics was performed using ultra-performance liquid chromatography coupled with tandem mass spectrometry (UPLC-MS/MS) detectors. After instrumental analysis, peak detection, and alignment, 2,345 mass features in negative electrospray ionization (ESI-) and 2,645 in positive ESI+ were detected in the discovery cohort, 530 serum small-molecule metabolites were identified, and the annotated data matrices were used for further statistical analysis.

First, ESI- and ESI+ quality control (QC) samples were used to build principal component analysis (PCA) models to assess the quality of the metabolomics data. The QC samples clustered tightly together in both negative and positive modes, illustrating the high stability and reliability of the data (Figures 2A,B). In addition, the PCA distinguished clusters of samples from the two groups. To maximize the identification of differential metabolites in patients with KD, we constructed orthogonal projections to latent structures (OPLS-DA model) to observe the main discriminations of metabolomics between the two groups and identify significantly altered metabolites (Figure 2C). Next, we evaluated the performance

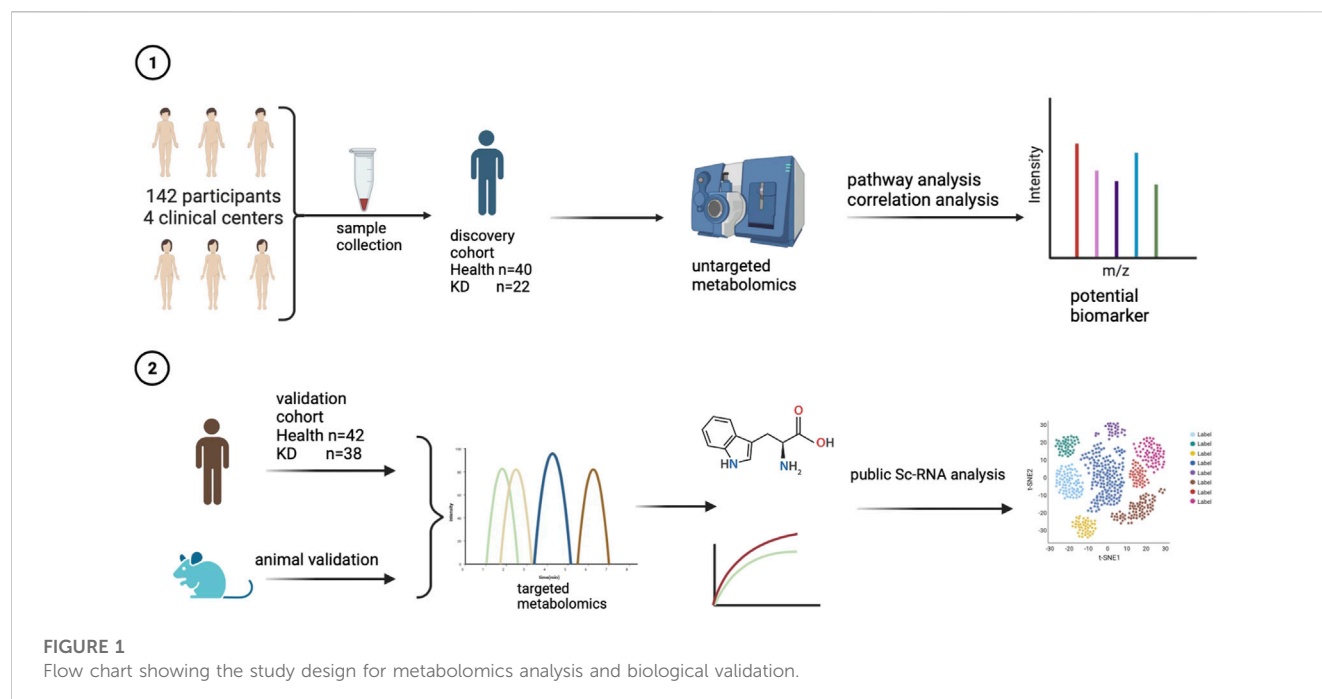


**TABLE 1** Demographic and clinical characteristics of discovery cohort individuals.

	HC	KD	<i>p</i> .Overall
	<i>N</i> = 40	<i>N</i> = 22	
Age (month)	28.0 [22.0; 40.2]	29.5 [13.2; 47.8]	0.591
Gender			0.716
Female	16 (40.0%)	7 (31.8%)	
Male	24 (60.0%)	15 (68.2%)	
WBC (10 <sup>9</sup> /L)	7.08 [5.84; 8.35]	13.8 [8.91; 16.5]	<0.001
Lymphocyte ratio (%)	58.4 [45.0; 63.0]	27.6 [16.8; 31.3]	<0.001
Neutrophils (%)	31.0 [26.5; 45.3]	65.4 [55.4; 73.1]	<0.001
Platelets (10 <sup>9</sup> /L)	284 [262; 363]	392 [315; 506]	0.002
RBC (10 <sup>12</sup> /L)	4.65 (0.34)	4.20 (0.52)	0.001
Hb (g/L)	125 (7.17)	108 (9.03)	<0.001
ALT (IU/L)	15.8 [13.0; 17.0]	36.5 [16.0; 74.2]	0.001
AST (IU/L)	33.0 [29.8; 35.0]	26.5 [24.0; 31.5]	0.001
Serum albumin (g/L)	42.8 [41.9; 43.6]	36.9 [34.5; 37.7]	<0.001
Total bilirubin (μmol/L)	6.11 [4.20; 6.90]	7.65 [5.93; 8.77]	0.100

The data are reported as either the mean ± standard deviation (SD), median with interquartile range (IQR), or percentages. A two-sided *t*-test was performed on variables represented as the mean ± SD, a Wilcoxon rank sum test was performed on variables expressed as the median with IQR, and a chi-square test was performed on variables expressed as percentages. HC, health control; KD, kawasaki disease; WBC, white blood cell; RBC, red blood cell; Hb, hemoglobin; ALT, glutamic pyruvic transaminase; AST, glutamic oxaloacetic transaminase.

of the model in correctly categorizing new samples using 7-fold cross-validation and 100 random permutation tests. The  $R^2$  and  $Q^2$  goodness-of-fit intercepts indicated that the OPLS-DA model was accurate and did not exhibit overfitting (Figures 2D,E).

The sample correlation heatmap showed that the samples between groups were scattered, and the samples within groups were significantly correlated (Figure 2F). The PCA, OPLS-DA, and the heatmap showed that KD patients were separated from



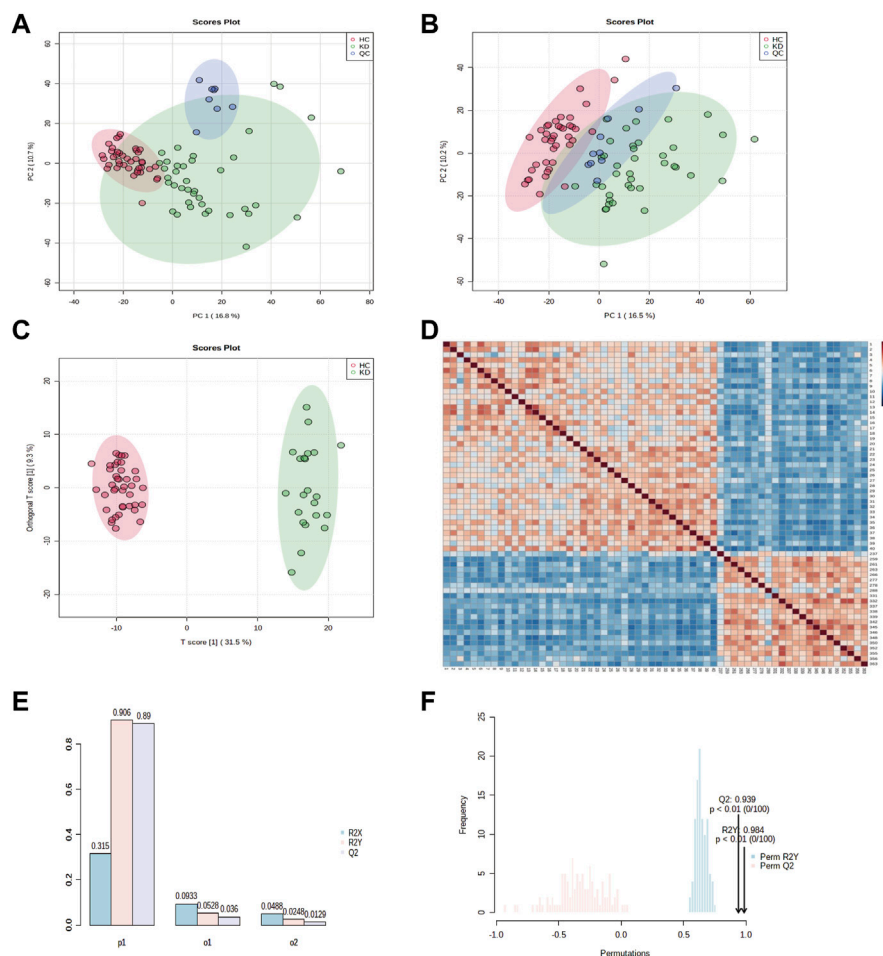


**FIGURE 2**

Principal component analysis (PCA) classification models for KD and HC in the discovery cohort. PCA score plots for patients with KD and healthy controls in (A) electrospray (ESI)+ mode and (B) ESI- mode. Healthy controls (HCs) are marked in red, patients with KD are marked in green, and quality control (QC) samples are shown in blue. The x and y axes represent the contributions of individuals to the first two principal components, PC1, and PC2, respectively. The OPLS-DA score plot shows the separation between patients with KD and healthy controls for all metabolites (C). The heat map shows the change in the abundance of metabolites in the plasma of healthy controls ( $n = 40$ ) and patients with KD ( $n = 22$ ) (D). Overview of the OPLS-DA model showing the  $R^2X$ ,  $R^2Y$ , and  $Q^2$  coefficients for the groups (E). Permutation analysis of  $R^2Y$  and  $Q^2$  coefficients repeated 200 times (F) ( $Q^2 = 0.939$  and  $R^2Y = 0.984$ ).

healthy controls and had different metabolic signatures compared with those of the healthy controls.

To investigate alterations in the metabolic pathways of all  $m/z$  features in both positive and negative ion modes, a Mummichog pathway analysis was performed. The detailed pathway enrichment results can be seen in [Supplementary Tables S1, 2](#). Tryptophan metabolism pathway ( $\text{adj}p = 0.00083892$ ) was the most drastically enriched pathway for positive-mode data using the mummichog analysis approach. Tyrosine metabolism ( $\text{adj}p = 0.00089019$ ), phenylalanine metabolism ( $\text{adj}p = 0.0012113$ ), glycerophospholipid metabolism ( $\text{adj}p = 0.0057432$ ), and fatty acid biosynthesis ( $0.019335$ ) were also significantly enriched in positive ion mode enrichment. Porphyrin and chlorophyll metabolism ( $\text{adj}p = 0.00093957$ ) and tryptophan metabolism ( $\text{adj}p = 0.0012581$ ) were the top two differently enriched pathways for negative-mode data using the mummichog analysis approach. Biosynthesis of unsaturated fatty acids ( $\text{adj}p = 0.0036836$ ), linoleic acid metabolism ( $\text{adj}p = 0.023143$ ), and

tyrosine metabolism ( $\text{adj}p = 0.027834$ ) also showed significantly differential enrichment in negative ion pattern analysis. The analysis revealed that Trp metabolism was notably enriched in both ESI+ ( $p = 0.0008$ ) and ESI- ( $p = 0.0012$ ) modes (Figures 3A,B). Furthermore, annotations based on accurate mass and tandem MS fragmentation data were subjected to traditional pathway analyses. To reduce the bias induced by pure bioinformatic analysis, we used multiple databases to increase the reliability, including SMPDB, INOH, KEGG, REACTOME, and EHMN. These aforementioned pathways, including amino acid metabolism, tyrosine metabolism, and linoleate metabolism, were also validated with the analysis using multiple databases (Figure 3C). In the discovery cohort, the relative abundance of Trp-related metabolites are presented in Figure 4A, while Figure 4B shows the differentially expressed metabolites visualized through a KEGG diagram. Pathway analysis revealed that these integrated results were generally consistent with the results of Mummichog analysis, indicating that patients with KD have significantly altered Trp metabolism.

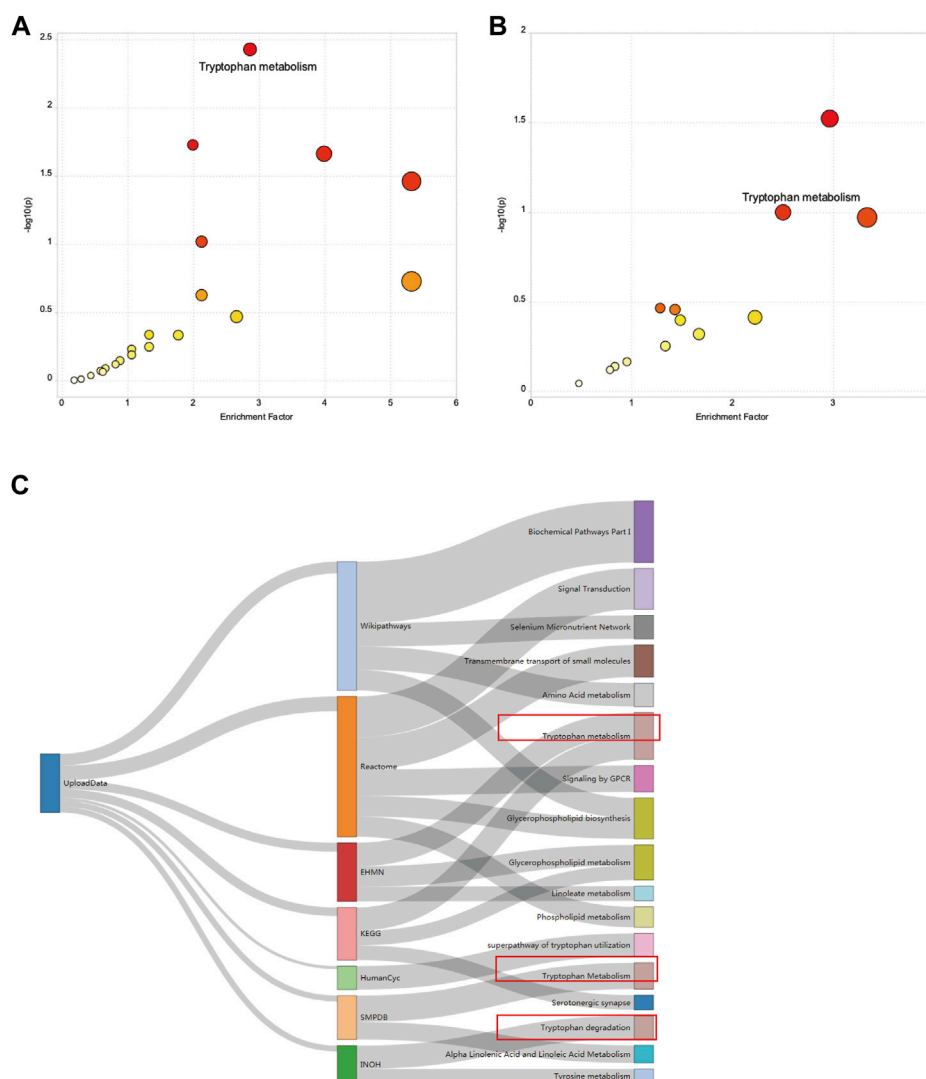


FIGURE 3

Results of the pathway enrichment analysis. A bubble chart showing the significantly enriched pathways between HCs and patients with KD from (A) electrospray (ESI)+ mode and (B) ESI- mode using Mummichog analysis before metabolite annotation. The x and y axes represent the enrichment factor of the pathway and the negative log 10 of the  $p$ -value, respectively. A Sankey diagram showing the altered metabolic pathway identified based on seven different databases (C).

## Trp-targeted metabolomic profiles in patients with KD and mice with LCWE-induced KD coronary arteritis

Untargeted metabolomic profiling demonstrated notable changes in the Trp metabolic pathway within the plasma of KD patients, suggesting that Trp metabolism may play an important role in the occurrence and development of KD. To confirm these results, serum levels of Trp, Kyn, IAA, and Kyna were quantified using a fully validated LC-MS/MS-based targeted metabolomics method, and the results were consistent with those of untargeted metabolomics. In patients with KD, compared with healthy subjects, there were significantly lower levels of Trp (65.6  $\mu$ M vs 88.0  $\mu$ M;  $p = 0.0003$ ) and IAA (0.61  $\mu$ M vs 1.18  $\mu$ M;  $p < 0.0001$ ), whereas the Kyn level was significantly higher (3.97  $\mu$ M vs 2.45  $\mu$ M;  $p < 0.0001$ ; Figure 5A). Additionally, IAA, Kyn, and Trp in patients with KD compared with

those in healthy subjects had a higher area under the curve (AUC) values (0.94,  $p < 0.0001$ ; 0.77,  $p = 0.003$ ; and 0.74,  $p = 0.001$ , respectively; Figure 5B). The combination of IAA, Trp, Kyn, and Kyna in the metabolite panel had a high AUC value (0.979, 95% CI 0.92–1; Figure 5C). Additionally, a correlation analysis of these differential metabolites and clinical characteristics was performed to better understand the relationship between the Trp metabolism panel and KD. Trp levels were only negatively associated with hemoglobin levels, indicating that the metabolism panel differs from that of existing biomarkers, such as clinical biochemical indices (Figure 5F and Supplementary Table S1).

After considering the relevance of the mouse model of KD to human disease, we used a mouse model to further examine the Trp pathways to provide evidence for identifying potential biomarkers and targeted discoveries from studies on the discovery cohort. We built a *Lactobacillus casei* cell wall extract (LCWE) induced KD model; the

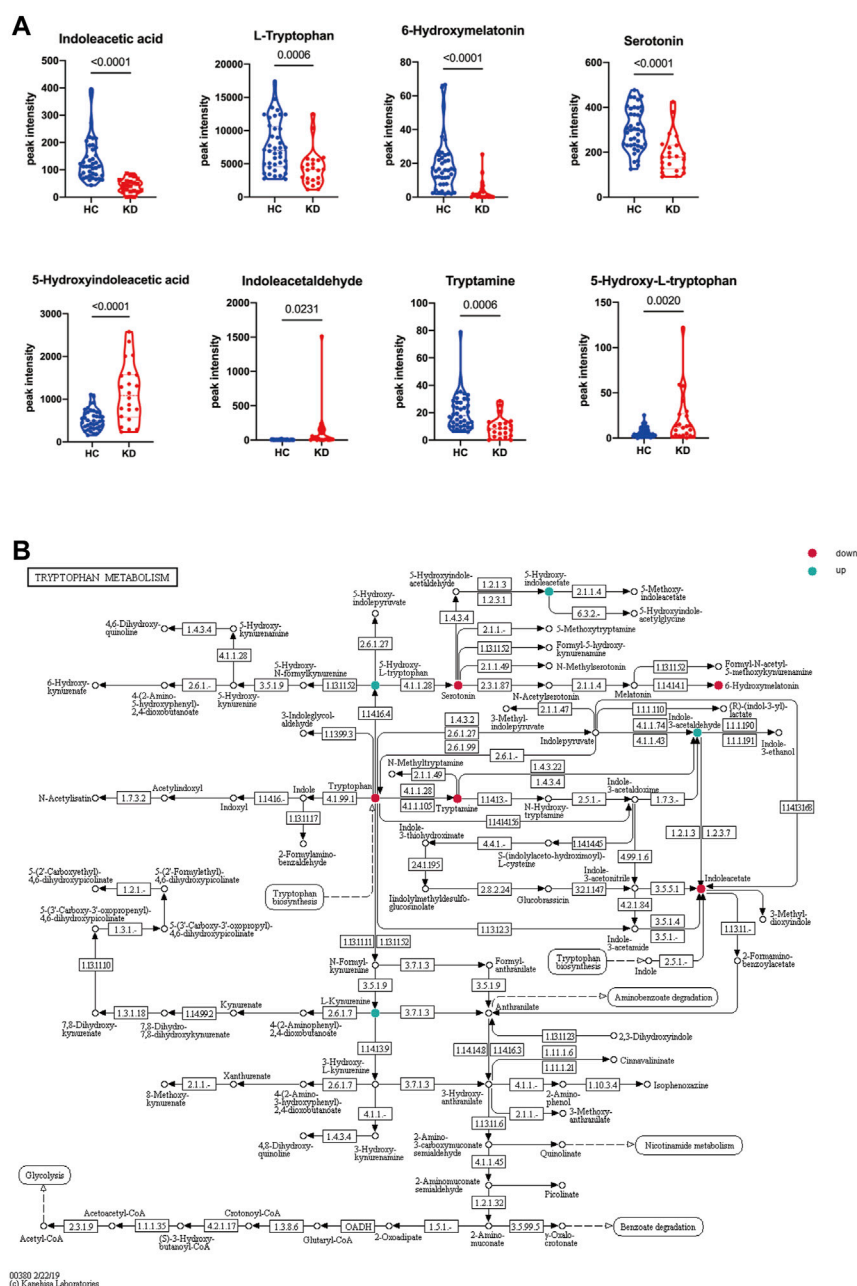


FIGURE 4

Altered tryptophan (Trp) metabolism in patients with KD. Relative abundance of Trp-related metabolites in the discovery cohort. Blue indicates HCs, and red indicates patients with KD (A). The Trp metabolic pathway was visualized by a KEGG diagram, and differentially expressed metabolites are circled (B). Red indicates downregulated metabolites, and blue indicates upregulated metabolites. Data are represented as the mean  $\pm$  standard error (SE). Statistical analysis was performed using two-tailed Student's *t*-tests.

model was shown to be successfully constructed by Hematoxylin and eosin (HE) staining, inflammation scores, and serum cytokine detection.

HE staining of myocardial tissue showed significant inflammatory cell accumulation and bleeding manifestations in the mice in the KD group (Figure 5D). Compared with the control group, the KD group exhibited significantly dilated CALs with a high concentration of infiltrating inflammatory cells, and the inner lining of the blood vessels appeared less smooth. Serum TNF- $\alpha$  and IL-1 $\beta$  levels were significantly higher in the KD mice than those

in the control mice (Figure 5G;  $p < 0.0001$ ). The mice in the KD group also had significantly higher inflammation scores than those in control mice (Figure 5H;  $p < 0.05$ ), indicating the successful creation of the KD coronary arteritis mouse model. Through targeted metabolomics focusing on Trp metabolism, we studied the changes in potential biomarkers in the plasma of mice with KD. Consistent with the observations in patients with KD, Kyna, and Kyn levels were increased, whereas Trp and IAA levels were reduced in these mice (Figure 5E).

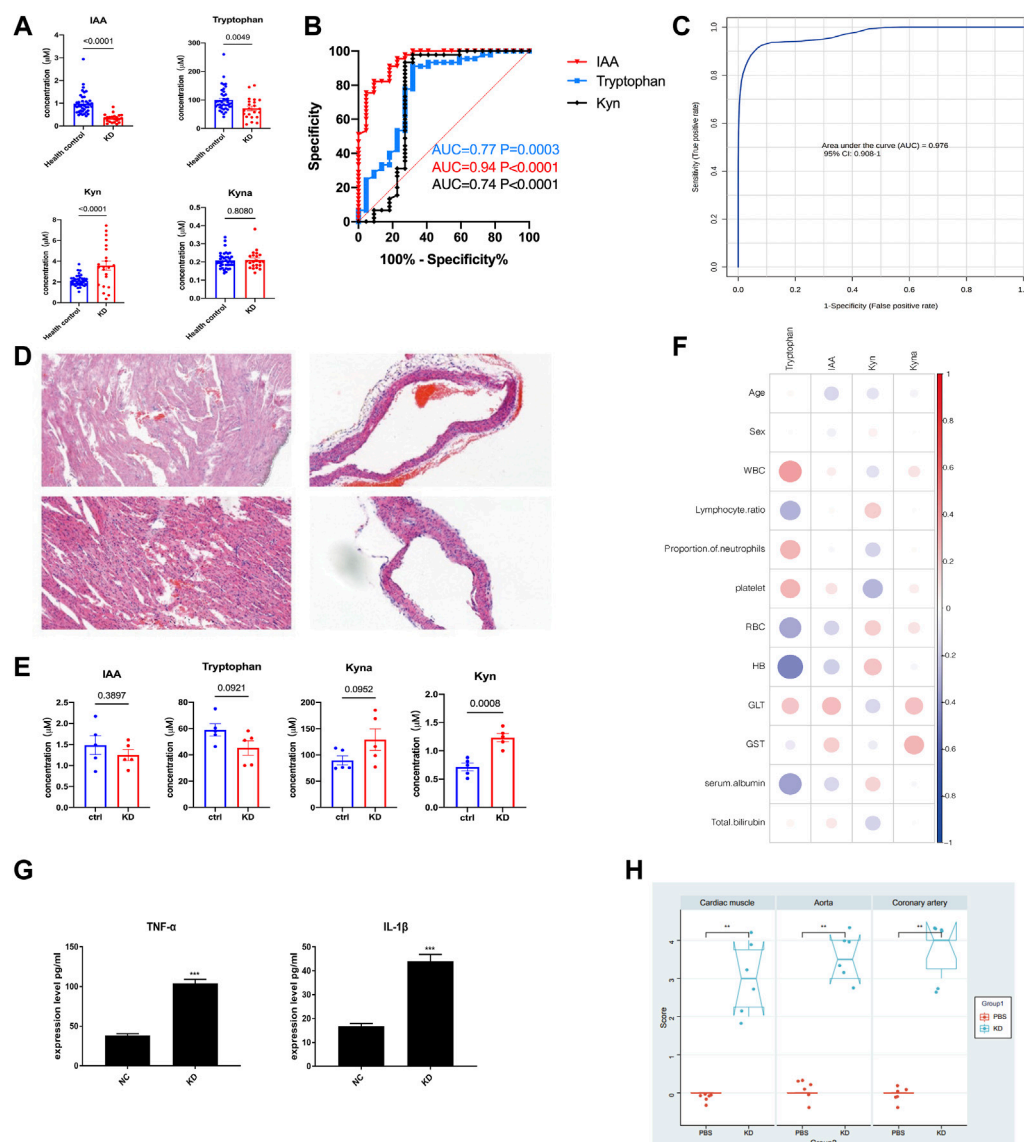


FIGURE 5

The LCWE mouse model and internal validation of metabolic alterations in patients with KD. Bar plots showing the serum levels of Trp-related metabolites in the discovery cohort (HC,  $n = 40$ ; KD,  $n = 22$ ) (A). Receiver operating characteristic (ROC) curve showing the discrimination accuracy of the three metabolites in the discovery cohort (B). ROC analysis incorporating indole acetic acid (IAA), Trp, L-kynurenine (Kyn), and kynurenic acid (Kyna) (C). Hematoxylin and eosin (HE) staining of myocardial tissue of the KD mouse model compared with that of the controls (D). Serum levels of IAA, Trp, Kyn, and Kyna in the KD mouse model (E). Correlation coefficients between serum metabolite levels and clinical characteristics in the validation cohort (F). Data were analyzed using Spearman's rank correlation test. Levels of the pro-inflammatory cytokines, tumor necrosis factor (TNF)- $\alpha$  and interleukin (IL)-1 $\beta$ , in the serum of the LCWE mouse model (G). Myocardial inflammation and heart vessel inflammation scores for each group (H). Data are represented as the mean  $\pm$  SE. Statistical analysis was performed using two-tailed Student's  $t$ -tests (A, E, G) and two-tailed Mann-Whitney U-tests (H). CI, confidence interval. \*,  $p < 0.05$ ; \*\*,  $p < 0.01$ ; \*\*\*,  $p < 0.001$ .

## External validation of altered trp metabolites in the validation cohort

To further validate the metabolic changes regarding Trp metabolism in patients with KD and identify potential biomarkers, we enrolled another set of 38 patients with KD and 42 healthy controls (validation cohort) for targeted metabolomic analysis and verification of potential biomarkers. The clinical characteristics of the validation cohort participants are presented in Table 2. There were no notable differences between the two

groups regarding sex and age. In this investigation, the profiles of Trp and its metabolites again exhibited apparent separation between the KD patients and healthy controls. The direction of changes in Trp-related metabolites was consistent with previous observations in the discovery cohort. Patients with KD had lower Trp (26.2  $\mu$ M vs 57.5  $\mu$ M,  $p < 0.0001$ ) and IAA levels (0.24  $\mu$ M vs 0.42  $\mu$ M,  $p < 0.0001$ ) but higher serum Kyna levels (0.19  $\mu$ M vs 0.12  $\mu$ M,  $p < 0.0001$ ) compared with those of control subjects (Figure 6A). No marked difference existed in the Kyn levels between the two groups in the validation cohort, whereas IAA and Trp exhibited

TABLE 2 Demographic and clinical characteristics of validation cohort individuals.

	HC	KD	<i>p</i> .Overall
	<i>n</i> = 42	<i>n</i> = 38	
Age (month)	29.0 (12.1)	24.6 (15.1)	0.161
Sex			1.000
Female	20 (47.6%)	19 (50.0%)	
Male	22 (52.4%)	19 (50.0%)	
WBC (10 <sup>9</sup> /L)	8.74 (2.07)	13.5 (3.24)	<0.001
Lymphocyte ratio (%)	33.0 (10.5)	25.9 (11.0)	0.004
Neutrophils (%)	51.0 (8.07)	67.4 (10.4)	<0.001
Platelets (10 <sup>9</sup> /L)	323 [276; 362]	463 [395; 524]	<0.001
RBC (10 <sup>12</sup> /L)	3.84 [3.50; 4.48]	4.07 [3.87; 4.26]	0.541
Hb (g/L)	104 [96.0; 111]	110 [105; 114]	0.006
Serum sodium (mmol/L)	140 [138; 142]	134 [132; 135]	<0.001
ALT (IU/L)	26.0 [19.5; 34.5]	65.5 [39.5; 86.5]	<0.001
AST (IU/L)	25.5 [15.2; 34.0]	32.0 [21.2; 54.0]	0.006
Serum albumin (g/L)	24.6 [21.6; 26.6]	35.8 [33.7; 36.8]	<0.001
Total bilirubin (μmol/L)	6.75 [5.23; 9.88]	5.40 [4.50; 7.97]	0.025

Data are presented as the mean ± standard deviation (SD) and median with interquartile range (IQR). The *p*-values are based on the two-sided *t*-test for variables expressed as the mean ± SD, Wilcoxon rank-sum test for variables expressed as median (IQR), and chi-square test for variables expressed as percentages. HC, health control; KD, kawasaki disease; WBC, white blood cell; RBC, red blood cell; Hb, hemoglobin; ALT, glutamic pyruvic transaminase; AST, glutamic oxaloacetic transaminase.

concentration level shifts in directions concordant with the results of the discovery dataset. The relative ratio of downstream Kyn metabolism to Trp metabolism was increased in both cohorts (discovery cohort, *p* = 0.0002; validation cohort, *p* < 0.0001).

Additionally, receiver operating characteristic (ROC) curve analysis showed that IAA, Trp, and Kyna had high AUC values of 0.77, 0.91, and 0.94, respectively (Figure 6B). The combination metabolite panel, including IAA, Trp, Kyn, and Kyna, had a higher AUC value of 0.943 (Figure 6C). Similarly, the levels of these different metabolites were not associated with routine blood tests or biochemical indices (Figure 6D, Supplementary Table S2).

## Expression of a Trp metabolism-related gene in peripheral blood mononuclear cells of patients with KD

The Aryl hydrocarbon receptor (AHR), a transcription factor that depends on ligands, is expressed extensively in epithelial, endothelial, and immune cells. In previous studies, cell groups were clustered into 12 cell clusters in two samples, one from a healthy child and the other from a patient with KD. Compared with the healthy child, the KD patient had low levels of naive CD8<sup>+</sup> T cells, T helper cells, and B cells; conversely, the number of immune-related T cells and natural killer T (NKT) cells was higher in the KD patient. We reanalyzed public single-cell RNA sequencing (scRNA-Seq) data from our previous study on peripheral blood mononuclear cells (PBMCs) from patients with KD (Fan et al., 2021). By comparing the gene expression of cells in each cluster and all

remaining cells, specific marker genes of the cluster were identified, and the expression of aryl hydrocarbon receptor was found to be significantly changed in most PBMC types, including NKT, secretory progenitor, and plasmacytoid dendritic cells, between patients with KD and healthy individuals, as indicated by the lattice heatmap (Figure 7). The measured changes in aryl hydrocarbon receptor expression levels were consistent with the increased levels of endogenous aryl hydrocarbon receptor ligands, such as Kyn, in the serum.

## Discussion

KD is a self-limiting systemic vasculitis that predominantly affects medium-sized arteries (Nakamura, 2018). The development of KD mainly manifests as chronic inflammation caused by immune cell infiltration and progressive remodeling of vascular tissue (Johnson et al., 2016), and its diagnosis is currently based on clinical symptoms. There is currently no recommended blood-based biomarker for diagnosing KD in medical guidelines.

A few studies have proposed the use of proteins or additional inflammatory parameters as potential biomarkers for KD. For example, Zandstra et al. reported the use of C-reactive protein (CRP), myeloid-related protein 8/14 (MRP8/14 or S100A8/9), and human neutrophil-derived elastase (HNE) for discriminating KD from infectious diseases (Zandstra et al., 2020). In another study, urine proteomic analysis revealed 43 differentially expressed proteins between patients with KD and normal controls, including serine hydroxy-methyltransferase 1, which was regarded as a hub protein (Hu et al., 2019). Based on routine



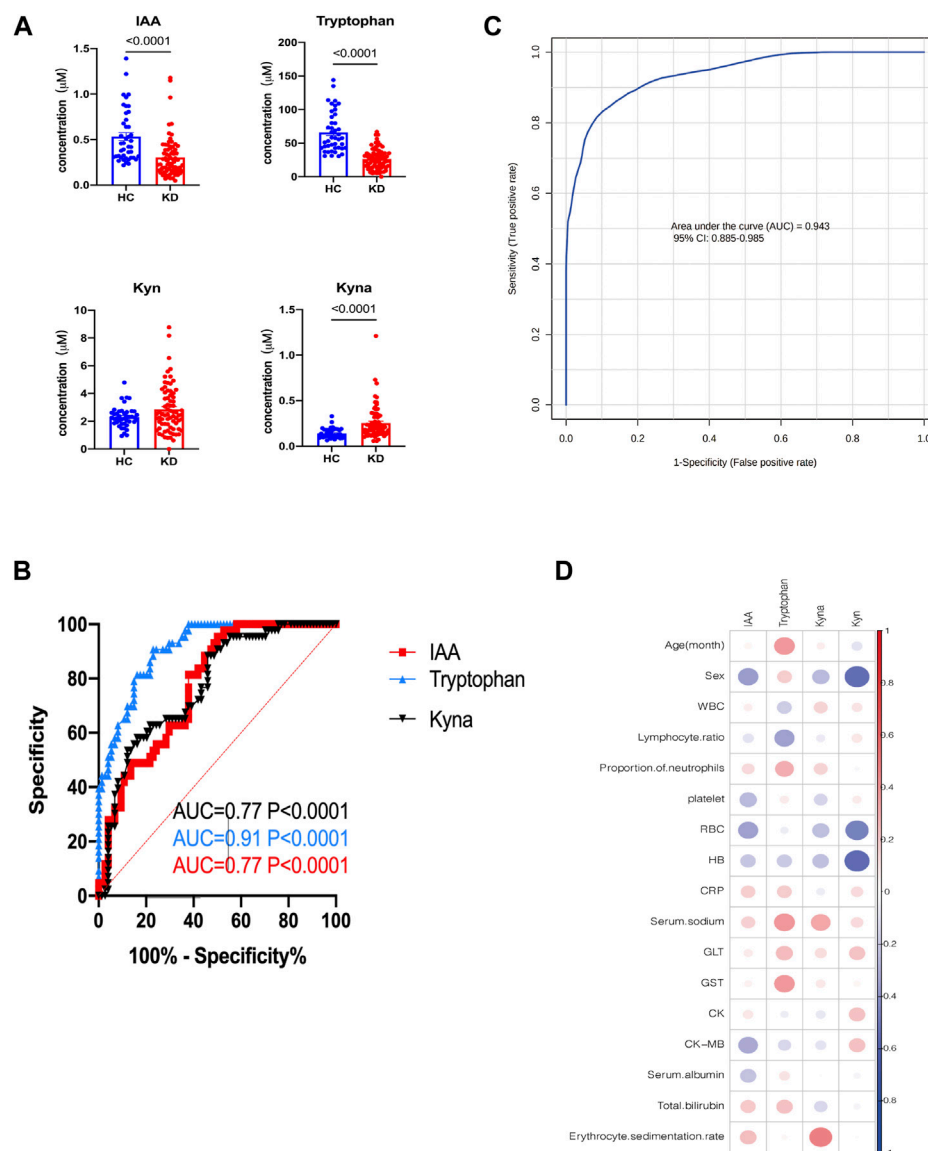


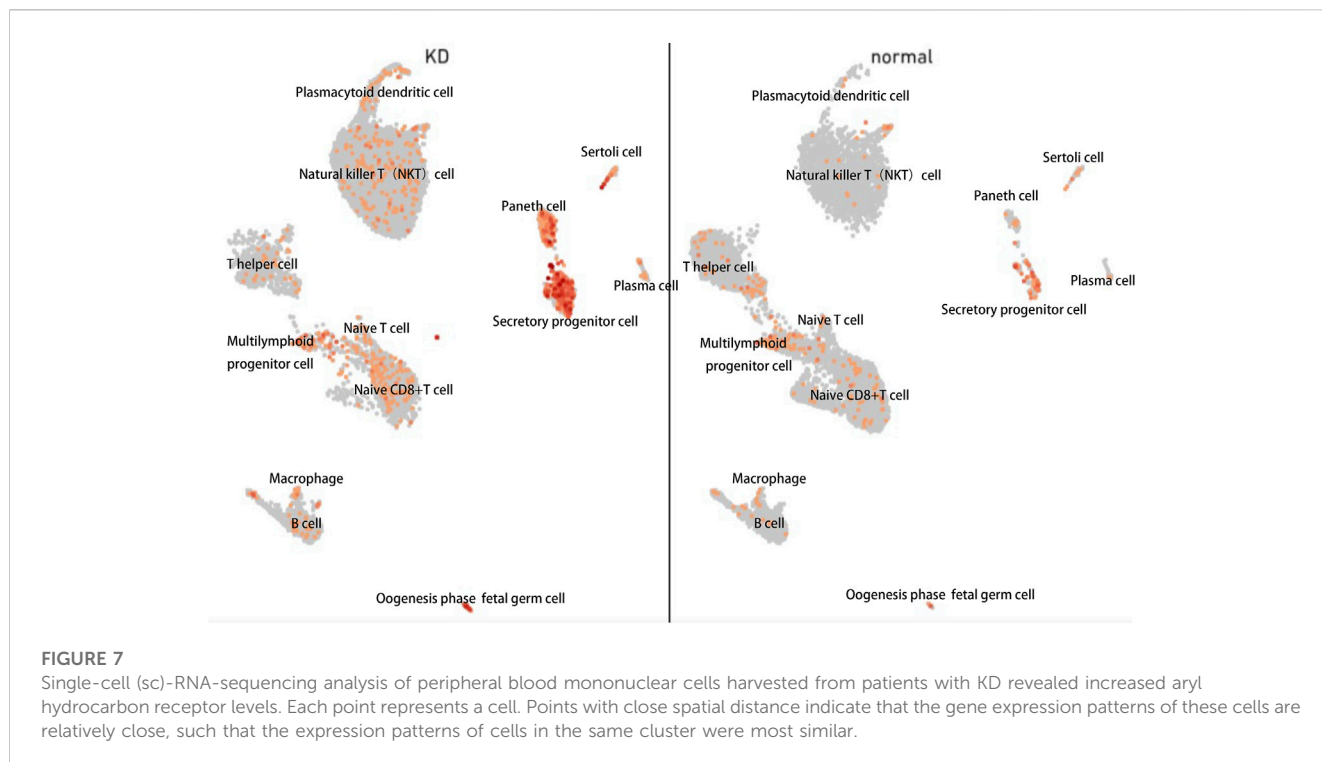
FIGURE 6

External validation of potential biomarkers for patients with KD. Bar plots showing the serum levels of Trp-related metabolites in the validation cohort (HC,  $n = 42$ ; KD,  $n = 38$ ) (A). Receiver operating characteristic (ROC) curve showing the discrimination accuracy of Trp-related metabolites in the validation cohort (B). Data represent the mean  $\pm$  SE. The  $p$ -value was calculated using two-tailed U-tests. ROC analysis incorporates IAA, Trp, Kyn, and Kyna in the validation cohort (C). Correlation coefficients between metabolite serum levels and clinical characteristics in the validation cohort (D). Association strength was assessed using Spearman's rank correlation test. IAA, indole acetic acid; Kyn, L-kynurenine; Kyna, kynurenic acid.

laboratory tests, serum ferritin may be a useful biomarker to distinguish KD from other acute febrile illnesses (Kim et al., 2021). Moreover, it has been suggested that IFN- $\gamma$ -inducible protein 10 (IP-10) can facilitate the early diagnosis of KD (Ko et al., 2015). Metabolic profiling is emerging as an efficient approach for detecting different diseases that are not easily diagnosed. However, there are limited studies exploring KD from a metabolome perspective. In the current study, we recruited a discovery and a validation cohort, established animal models of KD, and integrately analyzed the metabolome profile shift of KD using untargeted metabolomics and targeted metabolomics.

Our metabolomic analysis revealed an underlying metabolic signature in the plasma of patients with KD. We first performed pathway enrichment in the discovery cohort from MS peaks using the

well-established Mummichog. We then annotated the metabolites and comprehensively applied a variety of databases to conduct pathway analysis on the identified metabolites. The pattern of metabolic abnormalities that we found in the phospholipid oxidation pathway was consistent with that reported in a recent study by Nakashima and others (Nakashima et al., 2021). Lipid abnormalities appear in many immune disorders and different phases of the inflammatory process, such as rheumatoid arthritis (Steiner and Urowitz, 2009) and type-1 diabetes (O'Brien et al., 1998). We also observed amino acid metabolism pathways, including those of tyrosine that were enriched with metabolites that differed between KD and healthy subjects. Alterations in amino acid metabolism are widespread in metabolic disorders and participate in the immune



response caused by pathogen infection (Tomé, 2021). Among these altered metabolic pathways, the tryptophan pathway was the most significantly enriched pathway. The serum concentrations of Trp pathway metabolites were measured using targeted metabolomics because it is a more quantitatively sound approach with greater clinical utility than untargeted metabolomic assessments. The results of further targeted detection of metabolites of the tryptophan pathway replicated the non-targeted analysis results. The prognostic metabolites that were found to discriminate patients with KD from healthy individuals were from the Trp pathway, including Trp itself, IAA, Kyn, and Kyna. Tryptophan is one of the several amino acids that are essential in mammals and acts as a precursor of many signaling molecules that regulate adaptive immune responses (Liu et al., 2017). It exhibits the highest antiradical activity among all amino acids in cellular proteins. Weiss et al. suggested that Trp is a potent scavenger of the radicals that are induced by chloramine-T or hydrogen peroxide (Weiss et al., 2002). The decrease in Trp levels in patients with KD may contribute to the progression of KD symptoms, as supplementation of Trp has been shown to be beneficial (Gibson, 2018). The primary catabolic pathway of Trp in mammals is the Kyn pathway, which involves the constitutive catalysis of Trp to Kyn by three key rate-limiting enzymes—indoleamine 2,3-dioxygenase 1 and 2 (IDO1 and IDO2) and Trp 2,3-dioxygenase (Ketelhuth, 2019). Kynurenine is important to the pathogenesis of aortic diseases by contributing to inflammation in various vascular beds (Ramprasath et al., 2021). Studies have shown that Kyn exhibits pro-oxidant effects when exposed to aerobic radiation, resulting in the production of superoxide radicals, which can lead to the reduction of cytochrome C (Goda et al., 1987). Increased levels of Kyn can cause NKT cell death mediated by reactive oxygen species (ROS) (Song et al., 2011). This indicates that treatments targeting Kyn may be useful for patients with

oxidative stress-related diseases. Kynurenine acid is an intermediary in the Trp metabolic pathway and functions as a ligand for the orphan G protein-coupled receptor 35 (Wang et al., 2006). It can be generated by kynurenine aminotransferases under physiological conditions in endothelial cells (Stazka et al., 2002) and human PBMCs (Jones et al., 2015). Endothelial dysfunction is a critical process implicated in the development of KD. Indole acetic acid, which is derived from Trp, has been shown to decrease inflammation and ROS (Ji et al., 2020) by reducing the expression of pro-inflammatory cytokines (Shen et al., 2010). In the present study, the decreased concentration of IAA may be due to KD development. Overall, the identified metabolites and pathways fit the pathophysiological profile of KD.

Despite the high variability in the blood metabolome between and within individuals, the metabolic signature we constructed herein performed acceptably as a diagnostic tool for KD in two independent cohorts, with AUCs of 0.976 and 0.943. In a previous study, good intra-group repeatability was observed for the results of Kyn, Kyna, xanthurenine acid, 3-hydroxy-L-kynurenine, anthranilic acid, 3-hydroxyanthranilic acid, and the Kyn/Trp ratio in samples obtained from both the chronic heart failure and control groups, supporting the use of Trp pathway metabolites as biomarkers (Kato et al., 2010). Fortunately, KD and heart failure are uncommon, and these diseases rarely overlap.

Next, we investigated the metabolic changes of Trp metabolism in the LCWE-induced KD coronary arteritis mouse model. Consistent with our hypotheses, Trp metabolism and the correlated metabolites trended in a similar pattern as those in patients with KD. Integrating the cross-species data from humans and mice may provide more opportunities for identifying potential biomarkers and making targeted discoveries.

There are numerous interactions between circulating metabolites in plasma and blood cells. For instance, Kyn

mediates the activation of aryl hydrocarbon receptor, a ligand-activated cytoplasmic receptor and transcription factor capable of reinforcing the inflammatory state by boosting the production of interleukin-6 (Guarnieri, 2022). Hence, we performed data mining on a typical pediatric PBMC single-cell transcriptome and found that aryl hydrocarbon receptor expression was significantly altered between children with KD and healthy subjects. The stimulated Kyn metabolic pathway and aryl hydrocarbon receptor may indicate increased ligand-receptor interactions between Kyn and aryl hydrocarbon receptor. The downstream aryl hydrocarbon receptor expression changes are consistent with changes in the Trp pathway, which verified the reliability of our results—the tryptophan metabolic pathway is indeed altered in KD patients. In addition, the change in the tryptophan pathway can be used not only as a phenotype but may also play a crucial role in the regulation of the pathological development of KD by affecting transcription factors such as aryl hydrocarbon receptor. We therefore speculate on the therapeutic utility of Trp pathway metabolites in KD, but further biochemical experiments are needed to verify this assumption. Notably, increased IDO activity in the serum has been observed in patients with advanced atherosclerosis, indicating that activated kynurenine pathway may play a pivotal role in the development of vascular diseases (Ji et al., 2020). On the other hand, in the kynurenine pathway, IDO1 is the primary rate-limiting enzyme. Furthermore, several recent studies have demonstrated that the expression of IDO1 is elevated in response to inflammatory stimuli, such as type I and II interferons (Puccetti and Grohmann, 2007), prostaglandins (Jones et al., 2015), or microbial stimuli, such as lipopolysaccharides (Michaux et al., 2022). Meanwhile, IDO1 is regarded as a target gene to regulate overactive immune responses in human autoimmune diseases (Pan et al., 2008; Platten et al., 2012; Kasper et al., 2016).

Our results suggest that the Trp metabolic pathway is significantly altered in KD, particularly Trp itself, IAA, Kyn, and Kyna. Single-cell transcriptome analysis results corroborated metabolomic results to some extent. These metabolic indicators may serve as novel biomarkers and help in developing new strategies for the diagnosis and treatment of KD. Interventions in specific microorganisms targeting microbiota-ido1-aryl hydrocarbon receptor axis modulation in the host may offer innovative therapeutic strategies for treating KD.

Our study suggests that four metabolites—Trp, Kyn, Kyna, and IAA—are significantly altered in patients with KD and an LCWE-induced coronary arteritis mouse model, and that they may be potential biomarkers for diagnosing KD. However, a potential weakness of our study is that expression of the Kyn pathway increased during extensive inflammatory conditions, and it cannot be ruled out that some of the differences in metabolic profiles may be due to systemic inflammation. Thus, we should study more inflammatory disorder cohorts, such as those with measles, COVID-19, and scarlet fever, to better assess the specificity of this biomarker panel to differentiate KD. Moreover, we did not determine whether these altered levels of metabolites contribute to the inflammatory process in KD. Based on the combined metabolic analysis, we speculate that these metabolites may play key roles in the genesis and pathological development of the disease. Further studies are needed to determine the underlying mechanisms and elucidate whether these metabolites can predict the

risk of KD. Furthermore, larger and well-characterized patient cohorts are needed to validate our study.

## Materials and methods

### Human participants

A total of 142 participants from four clinical centers, including 82 healthy children and 60 KD patients, were recruited from Shenzhen Children's Hospital, Longgang District Maternal & Child Healthcare Hospital of Shenzhen City, The First Affiliated Hospital of Jinzhou Medical University, and Fushun Mining Bureau General Hospital, China, from January to October 2021. Sixty-two and eighty participants were included in the discovery and validation cohorts, respectively (Figure A). The clinical characteristics of the patients are summarized in Table 1 and Table 2. The diagnostic criteria were based on the American Heart Association guidelines for KD from 2017 (Johnson et al., 2016). The exclusion criteria included children who were not at the initial stage of the disease or had a course of disease >10 days, children with other congenital heart malformations, and those who had received treatment before admission. This study followed the guidelines of the Declaration of Helsinki and received approval from the Ethics Committees of Shenzhen Children's Hospital (protocol code 202003802) and Shenzhen Longgang Maternal & Child Healthcare Hospital (LGFYYXLLL-2022-004).

### Mice and treatments

C57/WT mice (four-to five-week-old) were purchased from the Hunan Saiké Jingda Experimental Animal Company (Changsha, China). The mice were intraperitoneally injected with a single dose of 400 µg of LCWE (day 0) to induce KD vasculitis; LCWE was prepared as previously described (Porritt et al., 2020). The mice were euthanized 14 days post-LCWE injection, and their hearts were extracted. Mouse tissues were collected for further histopathological examination, and serial sections (4 µm) were made and stained with HE. Stained sections were photographed using a fluorescence microscope (Olympus, Tokyo, Japan). Inflammation scores for coronary arteritis, aortitis, and myocarditis were assessed to evaluate the severity of inflammation. The serum levels of IL-1β and TNF-α were determined by enzyme-linked immunosorbent assay.

### Chemicals and materials for metabolomic analysis

High-performance liquid chromatography (HPLC) grade acetonitrile, methanol, formic acid was purchased from Thermo Fisher Scientific, Waltham, MA, United States, and liquid chromatography-mass spectrometry (LC-MS) grade water was purchased from A.S. Watsons Group Co., Hong-Kong, China. Unlabeled standards for targeted metabolomics were purchased from Cayman Chemical (Ann Arbor, MI, United States). The labeled standards, d4-IAA and d5-tryptophan, were purchased from Toronto Research Chemicals (Toronto, ON, Canada). All reagents and chemicals were of the

highest purity (>99%) and stored at appropriate temperatures and conditions.

## Sample collection

Blood samples were collected in heparinized tubes according to standard procedure, followed by centrifugation at 3,000 rpm at 4°C for 10 min to obtain plasma. The plasma was then aliquoted and stored at -80°C within 2 h of collection. The samples were transported to the lipid center at Capital Medical University and kept there until the end of recruitment.

## Sample preparation

The plasma samples were first mixed with three volumes of acetonitrile and incubated to precipitate proteins. The supernatant was collected after centrifugation and then evaporated under a vacuum to remove the solvent. Thereafter, the dried extracts were resuspended in a mixture of acetonitrile and water, vortexed, and centrifuged again to remove any remaining particles. Subsequently, the recovered supernatant was subjected to LC-MS analysis, and samples were injected in a randomized order during the runs to prevent bias. A quality control (QC) sample, which was a mixture of all plasma samples, was injected between every 10 sample injections to monitor consistency in the retention time and signal intensity.

## Mass spectrometry

Metabolic extracts were analyzed using reversed-phase liquid chromatography-mass spectrometry (RPLC-MS) in both positive and negative electrospray ionization modes. An AB SCIEX Triple TOF 5600 mass spectrometer (SCIEX, Framingham, MA, United States) was used to acquire data from 50 to 1,000 m/z in a 0.25 s TOF-MS scan mode. MS/MS spectra of the quality control (QC) sample was obtained using an information-dependent acquisition (IDA) method; the parameters were as follows: ion spray voltage, 5,500 V (+) and 4,500 V (-); interface heater temperature, 550°C (+) and 600°C (-); curtain gas of 35 PSI; declustering potential, 100 V (+) and -100 V (-); collision energy, 10 eV (+) and -10 eV (-). The range of m/z was set to 25–1,000, and the collision energy was 30 eV for IDA analysis. The resulting mass spectra were processed further using Progenesis QI Software (Non-linear Dynamics, Durham, NC, USA).

## Chromatographic conditions

The sample was separated using a Waters ACQUITY UPLC HSS T3 column (1.8  $\mu$ m, 2.1  $\times$  100 mm; Waters Corporation, Milford, MA, United States) with a UHPLC system (Shimadzu, Tokyo, Japan). The mobile phases consisted of water with 0.1% v/v formic acid A) and acetonitrile with 0.1% v/v formic acid B), and the column was maintained at 35°C. The separation was carried out using a linear gradient at a flow rate of 0.25 ml/min. Specifically, the gradient started at 2% B and increased to 60% B within 5 min, followed by a hold at

60% B for 5 min. Subsequently, the gradient was ramped up to 100% B for between 10 and 17 min and held at 100% B for 17–20 min. Finally, the gradient was decreased from 100% B to 2% B within 19–20.1 min. The sample volume injected was 5  $\mu$ l.

## Data preprocessing

Progenesis QI software was used for LC-MS data analysis. The software performed peak picking, alignment, and area normalization using pooled QC injections as a reference. Features that were absent in less than 10% of the pooled QC injections were removed, and an Excel file was obtained with m/z, peak retention time (RT), peak intensities, and RT-m/z pairs as identifiers for each ion. Metabolites were identified using Progenesis QI data processing software, with the aid of public databases such as HMDB and LIPID MAPS, as well as in-house databases. The Progenesis QI score, fragmentation score, and isotope similarity were reported for all annotations based on accurate mass and fragmentation data. Metabolic pathways were analyzed using MetaboAnalyst 5.0 (Chong et al., 2018).

## Targeted metabolomics and measurement of serum biomarker levels

To prepare the samples, 20  $\mu$ l of plasma was mixed with 80  $\mu$ l of an internal standard consisting of d4-IAA and d5-Trp in methanol. The mixture was vortexed for 1 min at 4°C–8°C to precipitate proteins, and the supernatant was collected by centrifugation at 20,000  $\times$  g for 10 min at 4°C. For analysis, 1  $\mu$ l of the supernatant was injected into the system, which used an analytical column (5  $\mu$ m Kinetex EVO-C18 150 mm  $\times$  4.6 mm; Phenomenex, Torrance, CA, United States) with mobile phases A (0.1% formic acid in water, v/v) and B (0.1% formic acid in acetonitrile, v/v). The column was maintained at 35°C, and all analytes were detected in the positive ion multiple reaction monitoring mode. The transitions with m/z 205.1,146 were quantified for Trp, m/z 176.04,130.02 for IAA, m/z 190,144 for Kyna, and m/z 209,94 for Kyn using a scan time of 0.1 s per transition. Chromatographic separation of the analytes was achieved using a linear and fast gradient elution program consisting of a 0–0.5-min hold at 80%, 0.5–4.5-min decrease from 80% to 10% B, 1.5-min hold at 10% B, and finally an increase to 80%. The flow rate was maintained at 0.5 ml/min.

All MS parameters were optimized by direct infusion. The declustering potential and collision energies for specific quantification and confirmation transitions were optimized to maximize the sensitivity.

## Cell clustering and differential gene expression (DGE) analysis of scRNA-seq

Seurat is a popular R package used to analyze single-cell RNA sequencing data (Hao et al., 2021). In this study, Seurat v2.0.1 was used for quality control and filtering of the single-cell data. Highly variable genes were identified using the Find Variable Genes method of the Seurat package, and 2,000 genes were selected for further analysis, including principal component analysis (PCA). Principal

components were used for cluster identification using the uniform manifold approximation and projection (UMAP) algorithm, which is a commonly used non-linear dimensionality reduction technique for visualizing high-dimensional data. Clusters were annotated to specific cell types based on the cell marker database. Finally, the FindMarkers function in Seurat was used to identify differentially expressed genes (DEGs) between healthy children and KD patients. All single-cell transcriptome data used in this study were obtained from a previous study (Shaw et al., 2021).

## Statistical analysis

All statistical analyses were performed using GraphPad Prism V.9 (GraphPad Software, San Diego, CA, United States) or SPSS version 25 (SPSS Inc., Chicago, IL, United States). Significance was assessed using one or more of the following: *t*-test, Mann–Whitney *U* test, Spearman's rank correlation test, and chi-squared test. Receiver operating characteristic (ROC) curves analysis was performed using two-tailed unpaired Student's *t*-tests (normal distribution) or Mann–Whitney *U*-tests (non-normal distribution). Comparisons between two groups for the remaining variables were performed using chi-squared or Fisher's exact tests. Statistical significance was set at  $p < 0.05$ .

## Data availability statement

The datasets presented in this study can be found in online repositories. The names of the repository/repositories and accession number(s) can be found below: <https://www.ebi.ac.uk/metabolights/>, MTBLS4983.

## Ethics statement

This research was funded by grants from several sources, including the National Nature Science Foundation of China (81870364), Shenzhen Scientific Plan (JCYJ20190809164004023), Shenzhen Longgang District Medical and Health Science and Technology Plan Project (No. LGKCYLWS2021000020), and the Guangdong Basic and Applied Basic Research Foundation (2022A1515012468).

## References

- Chen, K. Y., Curtis, N., Dahdah, N., Kowalski, R., Cheung, M., and Burgner, D. P. (2016). Kawasaki disease and cardiovascular risk: A comprehensive review of subclinical vascular changes in the longer term. *Acta Paediatr.* 105, 752–761. doi:10.1111/apa.13367
- Chong, J., Soufan, O., Li, C., Caraus, I., Li, S., Bourque, G., et al. (2018). MetaboAnalyst 4.0: Towards more transparent and integrative metabolomics analysis. *Nucleic Acids Res.* 46, W486–W494. doi:10.1093/nar/gky310
- Fan, X., Zhou, Y., Guo, X., and Xu, M. (2021). Utilizing single-cell RNA sequencing for analyzing the characteristics of PBMC in patients with Kawasaki disease. *BMC Pediatr.* 21, 277. doi:10.1186/s12887-021-02754-5
- Gao, W., Wang, Z. M., Zhu, M., Lian, X. Q., Zhao, H., Zhao, D., et al. (2015). Altered long noncoding RNA expression profiles in the myocardium of rats with ischemic heart failure. *J. Cardiovasc. Med. Hagerst.* 16, 473–479. doi:10.2459/JCM.0b013e32836499cd
- Gibson, E. L. (2018). Tryptophan supplementation and serotonin function: Genetic variations in behavioural effects. *Proc. Nutr. Soc.* 77, 174–188. doi:10.1017/S0029665117004451
- Goda, K., Hisaoka, M., and Ueda, T. (1987). Photoinduced electron transfer reaction from N-formyl-L-kynurenine and L-kynurenine to cytochrome C. *Biochem. Int.* 15, 635–643.
- Gordon, J. B., Kahn, A. M., and Burns, J. C. (2009). When children with Kawasaki disease grow up: Myocardial and vascular complications in adulthood. *J. Am. Coll. Cardiol.* 54, 1911–1920. doi:10.1016/j.jacc.2009.04.102
- Guarnieri, T. (2022). Hypothesis: Emerging roles for aryl hydrocarbon receptor in orchestrating CoV-2-related inflammation. *Cells* 11, 648. doi:10.3390/cells11040648
- Hao, Y., Hao, S., Andersen-Nissen, E., Mauck, W. M., Zheng, S., Butler, A., et al. (2021). Integrated analysis of multimodal single-cell data. *Cell* 184, 3573–3587.e29. doi:10.1016/j.cell.2021.04.048

## Author contributions

Conceptualization: XF, MX, LZ; Investigation: XF; Methodology: KL, SL, XG; Resources: XF, KL, MX, LZ; Formal Analysis: XF, KL; Writing–Original Draft: XF, KL; Writing–Review and Editing: XF, KL, HC, QZ; Funding Acquisition: MX, LZ. All authors have read and agreed to the published version of the manuscript.

## Funding

This research was funded by grants from several sources, including the National Nature Science Foundation of China (81870364), Shenzhen Scientific Plan (JCYJ20190809164004023), Shenzhen Longgang District Medical and Health Science and Technology Plan Project (No. LGKCYLWS2021000020), and the Guangdong Basic and Applied Basic Research Foundation (2022A1515012468).

## Conflict of interest

The authors declare that the research was conducted in the absence of any commercial or financial relationships that could be construed as a potential conflict of interest.

## Publisher's note

All claims expressed in this article are solely those of the authors and do not necessarily represent those of their affiliated organizations, or those of the publisher, the editors and the reviewers. Any product that may be evaluated in this article, or claim that may be made by its manufacturer, is not guaranteed or endorsed by the publisher.

## Supplementary material

The Supplementary Material for this article can be found online at: <https://www.frontiersin.org/articles/10.3389/fmolb.2023.1180537/full#supplementary-material>



- Herman, A. B., and Autieri, M. V. (2018). Cardiovascular disease, inflammation, and mRNA stability. *Aging* 10, 3046–3047. doi:10.18632/aging.101619
- Hezaveh, K., Shinde, R. S., Klötgen, A., Halaby, M. J., Lamorte, S., Ciudad, M. T., et al. (2022). Tryptophan-derived microbial metabolites activate the aryl hydrocarbon receptor in tumor-associated macrophages to suppress anti-tumor immunity. *Immunity* 55, 324–340.e8. doi:10.1016/j.immuni.2022.01.006
- Hu, H.-M., Du, H.-W., Cui, J.-W., Feng, D.-Q., and Du, Z.-D. (2019). New biomarkers of Kawasaki disease identified by urine proteomic analysis. *FEBS Open Bio* 9, 265–275. doi:10.1002/2211-5463.12563
- Ji, Y., Yin, W., Liang, Y., Sun, L., Yin, Y., and Zhang, W. (2020). Anti-inflammatory and anti-oxidative activity of indole-3-acetic acid involves induction of HO-1 and neutralization of free radicals in RAW264.7 cells. *Int. J. Mol. Sci.* 21, 1579. doi:10.3390/ijms21051579
- Johnson, C. H., Ivanisevic, J., and Siuzdak, G. (2016). Metabolomics: Beyond biomarkers and towards mechanisms. *Nat. Rev. Mol. Cell Biol.* 17, 451–459. doi:10.1038/nrm.2016.25
- Jones, S. P., Franco, N. F., Varney, B., Sundaram, G., Brown, D. A., de Bie, J., et al. (2015). Expression of the kynurenine pathway in human peripheral blood mononuclear cells: Implications for inflammatory and neurodegenerative disease. *PLoS One* 10, e0131389. doi:10.1371/journal.pone.0131389
- Kasper, S. H., Bonocora, R. P., Wade, J. T., Musah, R. A., and Cady, N. C. (2016). Chemical inhibition of kynureninase reduces pseudomonas Aeruginosa quorum sensing and virulence factor expression. *ACS Chem. Biol.* 11, 1106–1117. doi:10.1021/acschembio.5b01082
- Kato, A., Suzuki, Y., Suda, T., Suzuki, M., Fujie, M., Takita, T., et al. (2010). Relationship between an increased serum kynurenine/tryptophan ratio and atherosclerotic parameters in hemodialysis patients. *Hemodial. Int.* 14, 418–424. doi:10.1111/j.1542-4758.2010.00464.x
- Ketelhuth, D. F. J. (2019). The immunometabolic role of indoleamine 2,3-dioxygenase in atherosclerotic cardiovascular disease: Immune homeostatic mechanisms in the artery wall. *Cardiovasc. Res.* 115, 1408–1415. PMID: 30847484. doi:10.1093/cvr/cvz067
- Kim, S. H., Song, E. S., Yoon, S., Eom, G. H., Kang, G., and Cho, Y. K. (2021). Serum ferritin as a diagnostic biomarker for Kawasaki disease. *Ann. Lab. Med.* 41, 318–322. doi:10.3343/alm.2021.41.3.318
- Ko, T. M., Kuo, H. C., Chang, J. S., Chen, S. P., Liu, Y. M., Chen, H. W., et al. (2015). CXCL10/IP-10 is a biomarker and mediator for Kawasaki disease. *Circ. Res.* 116, 876–883. doi:10.1161/CIRCRESAHA.116.305834
- Liu, G., Chen, S., Zhong, J., Teng, K., and Yin, Y. (2017). Crosstalk between tryptophan metabolism and cardiovascular disease, mechanisms, and therapeutic implications. *Oxid. Med. Cell. Longev.* 2017, 1602074. doi:10.1155/2017/1602074
- Mangge, H., Stelzer, I., Reininghaus, E. Z., Weghuber, D., Postolache, T. T., and Fuchs, D. (2014). Disturbed tryptophan metabolism in cardiovascular disease. *Curr. Med. Chem.* 21, 1931–1937. doi:10.2174/0929867321666140304105526
- McCordle, B. W., Rowley, A. H., Newburger, J. W., Burns, J. C., Bolger, A. F., Gewitz, M., et al. (2017). Diagnosis, treatment, and long-term management of Kawasaki disease: A scientific statement for health professionals from the American heart association. *Circulation* 135, e927–e999. doi:10.1161/CIR.00000000000000484
- Michaux, A., Mauën, S., Breman, E., Dheur, M. S., Twyffels, L., Saelens, L., et al. (2022). Clinical grade manufacture of CYAD-101, a NKG2D-based, first in class, non-gene-edited allogeneic CAR T-Cell therapy. *J. Immunother.* 45, 150–161. doi:10.1097/JCI.0000000000000413
- Nakamura, Y. (2018). Kawasaki disease: Epidemiology and the lessons from it. *Int. J. Rheum. Dis.* 21, 16–19. doi:10.1111/1756-185X.13211
- Nakashima, Y., Sakai, Y., Mizuno, Y., Furuno, K., Hirono, K., Takatsuki, S., et al. (2021). Lipidomics links oxidized phosphatidylcholines and coronary arteritis in Kawasaki disease. *Cardiovasc. Res.* 117, 96–108. doi:10.1093/cvr/cvz305
- Nemecz, M., Alexandru, N., Tanko, G., and Georgescu, A. (2016). Role of microRNA in endothelial dysfunction and hypertension. *Curr. Hypertens. Rep.* 18, 87. doi:10.1007/s11906-016-0696-8
- Nemet, I., Saha, P. P., Gupta, N., Zhu, W., Romano, K. A., Skye, S. M., et al. (2020). A cardiovascular disease-linked gut microbial metabolite acts via adrenergic receptors. *Cell* 180, 862–877. doi:10.1016/j.cell.2020.02.016
- Newburger, J. W., Takahashi, M., and Burns, J. C. (2016). Kawasaki disease. *J. Am. Coll. Cardiol.* 67, 1738–1749. doi:10.1016/j.jacc.2015.12.073
- Newgard, C. B. (2017). Metabolomics and metabolic diseases: Where do we stand? *Cell Metab.* 25, 43–56. doi:10.1016/j.cmet.2016.09.018
- O'Brien, T., Nguyen, T. T., and Zimmerman, B. R. (1998). Hyperlipidemia and diabetes mellitus. *Mayo Clin. Proc.* 73, 969–976. doi:10.4065/73.10.969
- Pan, K., Wang, H., Chen, M., Zhang, H., Weng, D., Zhou, J., et al. (2008). Expression and prognosis role of indoleamine 2,3-dioxygenase in hepatocellular carcinoma. *J. Cancer Res. Clin. Oncol.* 134, 1247–1253. doi:10.1007/s00432-008-0395-1
- Platten, M., Wick, W., and Van den Eynde, B. J. (2012). Tryptophan catabolism in cancer: Beyond Ido and tryptophan depletion. *Cancer Res.* 72, 5435–5440. doi:10.1158/0008-5472.CAN-12-0569
- Porritt, R. A., Markman, J. L., Maruyama, D., Kocaturk, B., Chen, S., Lehman, T. J., et al. (2020). Interleukin-1 beta-mediated sex differences in Kawasaki disease vasculitis development and response to treatment. *Arterioscler. Thromb. Vasc. Biol.* 40, 802–818. doi:10.1161/ATVBAHA.119.313863
- Puccetti, P., and Grohmann, U. (2007). Ido and regulatory T cells: A role for reverse signalling and non-canonical NF-KappaB activation. *Nat. Rev. Immunol.* 7, 817–823. doi:10.1038/nri2163
- Rampasath, T., Han, Y.-M., Zhang, D., Yu, C.-J., and Zou, M.-H. (2021). Tryptophan catabolism and inflammation: A novel therapeutic target for aortic diseases. *Front. Immunol.* 12, 731701. doi:10.3389/fimmu.2021.731701
- Ruddick, J. P., Evans, A. K., Nutt, D. J., Lightman, S. L., Rook, G. A. W., and Lowry, C. A. (2006). Tryptophan metabolism in the central nervous system: Medical implications. *Expert Rev. Mol. Med.* 8, 1–27. doi:10.1017/S1462399406000068
- Ruiz-Canela, M., Hruby, A., Clish, C. B., Liang, L., Martínez-González, M. A., and Hu, F. B. (2017). Comprehensive metabolomic profiling and incident cardiovascular disease: A systematic review. *J. Am. Heart Assoc.* 6, e005705. doi:10.1161/JAHA.117.005705
- Shaw, R., Tian, X., and Xu, J. (2021). Single-cell transcriptome analysis in plants: Advances and challenges. *Mol. Plant.* 14, 115–126. doi:10.1016/j.molp.2020.10.012
- Shen, J., Yang, L., You, K., Chen, T., Su, Z., Cui, Z., et al. (2010). Indole-3-acetic acid alters intestinal microbiota and alleviates ankylosing spondylitis in mice. *Front. Immunol.* 13, 762580. doi:10.3389/fimmu.2022.762580
- Shin, M., Nakakita, S., Hashimoto, C., Sano, K., and Umezawa, C. (1998). NAD+ biosynthesis from tryptophan in the presence of nicotinic acid or vice versa by rat hepatocytes—effect of clofibrate-feeding. *Int. J. Vitam. Nutr. Res.* 68, 104–108.
- Song, H., Park, H., Kim, Y.-S., Kim, K. D., Lee, H.-K., Cho, D.-H., et al. (2011). L-kynurenine-induced apoptosis in human NK cells is mediated by reactive oxygen species. *Int. Immunopharmacol.* 11, 932–938. doi:10.1016/j.intimp.2011.02.005
- Stazka, J., Luchowski, P., Wielosz, M., Kleinrok, Z., and Urbańska, E. M. (2002). Endothelium-dependent production and liberation of kynurenine acid by rat aortic rings exposed to L-kynurenine. *Eur. J. Pharmacol.* 448, 133–137. doi:10.1016/s0014-2999(02)01943-x
- Steiner, G., and Urowitz, M. B. (2009). Lipid profiles in patients with rheumatoid arthritis: Mechanisms and the impact of treatment. *Semin. Arthritis Rheum.* 38, 372–381. doi:10.1016/j.semarthrit.2008.01.015
- Taleb, S. (2019). Tryptophan dietary impacts gut barrier and metabolic diseases. *Front. Immunol.* 10, 2113. doi:10.3389/fimmu.2019.02113
- Tomé, D. (2021). Amino acid metabolism and signalling pathways: Potential targets in the control of infection and immunity. *Nutr. Diabetes* 11, 20. doi:10.1038/s41387-021-00164-1
- Viereck, J., Kumaraswamy, R., Foinquinos, A., Xiao, K., Avramopoulos, P., Kunz, M., et al. (2016). Long noncoding RNA Chast promotes cardiac remodeling. *Sci. Transl. Med.* 8, 326ra22. doi:10.1126/scitranslmed.aaf1475
- Wang, J., Simonavicius, N., Wu, X., Swaminath, G., Reagan, J., Tian, H., et al. (2006). Kynurenine acid as a ligand for orphan G protein-coupled receptor GPR35. *J. Biol. Chem.* 281, 22021–22028. doi:10.1074/jbc.M603503200
- Wang, Q., Liu, D., Song, P., and Zou, M. H. (2015). Tryptophan-kynurenine pathway is dysregulated in inflammation, and immune activation. *Front. Biosci. (Landmark Ed.)* 20, 1116–1143. doi:10.2741/4363
- Wang, Y., Liu, H., McKenzie, G., Witting, P. K., Stasch, J. P., Hahn, M., et al. (2010). Kynurenine is an endothelium-derived relaxing factor produced during inflammation. *Nat. Med.* 16, 279–285. doi:10.1038/nm.2092
- Wang, Z., Klipfell, E., Bennett, B. J., Koeth, R., Levison, B. S., DuGar, B., et al. (2011). Gut flora metabolism of phosphatidylcholine promotes cardiovascular disease. *Nature* 472, 57–63. doi:10.1038/nature09922
- Weiss, G., Diez-Ruiz, A., Murr, C., Theur, I., and Fuchs, D. (2002). Tryptophan metabolites as scavengers of reactive oxygen and chlorine species. *Pteridines* 13, 140–143. doi:10.1515/pteridines.2002.13.4.140
- Zandstra, J., Van de Geer, A., Tanck, M. W., van Stijn-Bringas Dimitriades, D., Aarts, C. E., Dietz, S. M., et al. (2020). Biomarkers for the discrimination of acute Kawasaki disease from infections in childhood. *Front. Pediatr.* 8, 355. doi:10.3389/fped.2020.00355



## OPEN ACCESS

## EDITED BY

Donghai Lin,  
Xiamen University, China

## REVIEWED BY

Yongxia Yang,  
Guangdong Pharmaceutical University,  
China  
Xiaoxiao Ma,  
Tsinghua University, China

## \*CORRESPONDENCE

Xu Gao,  
✉ xu.gao@pku.edu.cn  
Ying Liang,  
✉ bsyliangying@126.com

<sup>†</sup>These authors have contributed equally  
to this work

RECEIVED 13 April 2023

ACCEPTED 29 June 2023

PUBLISHED 12 July 2023

## CITATION

Wang Y, Chang C, Tian S, Wang J, Gai X,  
Zhou Q, Chen Y, Gao X, Sun Y and Liang Y  
(2023), Differences in the lipid  
metabolism profile and clinical  
characteristics between eosinophilic and  
non-eosinophilic acute exacerbation of  
chronic obstructive pulmonary disease.  
*Front. Mol. Biosci.* 10:1204985.  
doi: 10.3389/fmolb.2023.1204985

## COPYRIGHT

© 2023 Wang, Chang, Tian, Wang, Gai,  
Zhou, Chen, Gao, Sun and Liang. This is  
an open-access article distributed under  
the terms of the [Creative Commons  
Attribution License \(CC BY\)](https://creativecommons.org/licenses/by/4.0/). The use,  
distribution or reproduction in other  
forums is permitted, provided the original  
author(s) and the copyright owner(s) are  
credited and that the original publication  
in this journal is cited, in accordance with  
accepted academic practice. No use,  
distribution or reproduction is permitted  
which does not comply with these terms.

# Differences in the lipid metabolism profile and clinical characteristics between eosinophilic and non-eosinophilic acute exacerbation of chronic obstructive pulmonary disease

Yating Wang<sup>1†</sup>, Chun Chang<sup>1,2†</sup>, Sifan Tian<sup>3†</sup>, Juan Wang<sup>1</sup>,  
Xiaoyan Gai<sup>1,2</sup>, Qiqiang Zhou<sup>1</sup>, Yahong Chen<sup>1,2</sup>, Xu Gao<sup>3\*</sup>,  
Yongchang Sun<sup>1,2</sup> and Ying Liang<sup>1,2\*</sup>

<sup>1</sup>Department of Respiratory and Critical Care Medicine, Peking University Third Hospital, Beijing, China,

<sup>2</sup>Research Center for Chronic Airway Diseases, Peking University Health Science Center, Beijing, China,

<sup>3</sup>Department of Occupational and Environmental Health Sciences, School of Public Health, Peking University, Beijing, China

**Objective:** In this study, we aimed to investigate the differences in serum lipid metabolite profiles and their relationship with clinical characteristics between patients with eosinophilic and non-eosinophilic AECOPD.

**Methods:** A total of 71 AECOPD patients were enrolled. Eosinophilic AECOPD was defined as blood EOS%  $\geq 2\%$  ( $n = 23$ ), while non-eosinophilic AECOPD, as blood EOS%  $< 2\%$  ( $n = 48$ ). Clinical data were collected, and serum lipid metabolism profiles were detected by liquid chromatography–mass spectrometry (LC-MS). The XCMS software package was used to pre-process the raw data, and then, lipid metabolite identification was achieved through a spectral match using LipidBlast library. Differences in lipid profiles and clinical features between eosinophilic and non-eosinophilic groups were analyzed by generalized linear regression. The least absolute shrinkage and selection operator (LASSO) was applied to screen the most characteristic lipid markers for the eosinophilic phenotype.

**Results:** Eosinophilic AECOPD patients had less hypercapnic respiratory failures, less ICU admissions, a shorter length of stay in the hospital, and a lower fibrinogen level. In the lipid metabolism profiles, 32 significantly different lipid metabolites were screened through a  $t$ -test adjusted by using FDR (FDR-adjusted  $p < 0.05$  and VIP  $> 1$ ). Nine differential lipid metabolites were found to be associated with the three clinical features, namely, hypercapnia respiratory failure, ICU admission, and fibrinogen in further integration analysis. The species of triacylglycerol (TAG), phosphatidylcholine (PC), lysophosphatidylcholine (LPC), and diacylglycerol trimethylhomoserine (DGTS) were high in these eosinophilic AECOPD. The LASSO was applied, and three lipid metabolites were retained, namely, LPC (16:0), TAG (17:0/17:2/17:2), and LPC (20:2). The logistic regression model was fitted using these three markers, and the area under the ROC curve of the model was 0.834 (95% CI: 0.740–0.929).

**Conclusion:** Patients with eosinophilic AECOPD had a unique lipid metabolism status. Species of TAGs and LPCs were significantly increased in this phenotype and were associated with better clinical outcomes.

KEYWORDS  
chronic obstructive pulmonary disease, acute exacerbation, eosinophils, lipidomics, LC-ESI-MS

1 Introduction

Chronic obstructive pulmonary disease (COPD) is a heterogeneous disease characterized by persistent respiratory symptoms and airflow limitations (Global Initiative for Chronic Obstructive Lung Disease, 2022). It is estimated that there are nearly 100 million patients with COPD in mainland China, with a prevalence of 13.7% among adults aged ≥ 40 years (Wang et al., 2018). The prevalence of COPD will continue to rise, adding a heavy economic burden to individuals and society (Global

Initiative for Chronic Obstructive Lung Disease, 2022). Additionally, acute exacerbations of COPD (AECOPD) have a significant impact on patients’ health (Wilkinson et al., 2004), contributing to hospitalization and readmission, disease progression, and increased risk of death. Eosinophilic COPD is a phenotype of airway inflammation characterized by the presence of eosinophilic inflammation in the airways, manifested by elevated peripheral blood and/or sputum eosinophil counts (Barnes, 2019). Some patients with COPD during exacerbation also have a peripheral blood eosinophilia ≥ 2% or sputum eosinophilia ≥ 3%, who are classified as eosinophilic AECOPD

TABLE 1 Demographic and clinical characteristics of the study subjects.

Characteristic	Total (n = 71)	Non-eosinophilic (n = 48)	Eosinophilic (n = 23)	p-value <sup>a</sup>
Age (years)	74.1 (9.6)	73.7 (10.3)	75.0 (8.0)	0.566
Male	62 (87.3%)	42 (87.5%)	20 (87.0%)	1.000
BMI (kg/m <sup>2</sup> )	22.0 (5.2)	22.0 (5.8)	22.1 (3.7)	0.910
Smoking status				
Never	7 (9.9%)	5 (10.4%)	2 (8.7%)	0.303
Former	42 (59.2%)	31 (64.6%)	11 (47.8%)	
Current	22 (31.0%)	12 (25.0%)	10 (43.5%)	
Smoking index (packs per year)	39.2 (29.7)	37.7 (28.1)	42.2 (33.3)	0.578
Comorbidities				
Hypertension	37 (52.1%)	27 (56.3%)	10 (43.5%)	0.451
Coronary heart disease	11 (15.5%)	8 (16.7%)	3 (13.0%)	1.000
Heart failure	4 (5.6%)	3 (6.3%)	1 (4.3%)	1.000
Diabetes	11 (15.5%)	8 (16.7%)	3 (13.0%)	1.000
Hyperlipidemia	8 (11.3%)	5 (10.4%)	3 (13.0%)	0.708
Eosinophil count (cells/μL)	115 (176)	33 (44)	287 (220)	<0.001
Eosinophil %	1.65 (2.23)	0.43 (0.50)	4.19 (2.29)	<0.001
D-dimer (μg/mL)	0.26 (0.19)	0.28 (0.21)	0.21 (0.13)	0.106
Fibrinogen (g/L)	3.97 (1.29)	4.20 (1.41)	3.48 (0.82)	0.008
Total cholesterol (mmol/L)	3.98 (0.85)	3.95 (0.89)	4.04 (0.80)	0.668
Triglyceride (mmol/L)	1.02 (0.46)	0.96 (0.40)	1.14 (0.55)	0.156
Hypercapnic respiratory failure	24 (36.9%)	22 (45.8%)	2 (8.7%)	0.004
Need for ICU admission	14 (19.7%)	13 (27.1%)	1 (4.3%)	0.027
Time to next exacerbation (months)	27.1 (13.6)	27.1 (13.6)	27.1 (13.9)	0.994

Data are presented as mean (SD) or n (%).

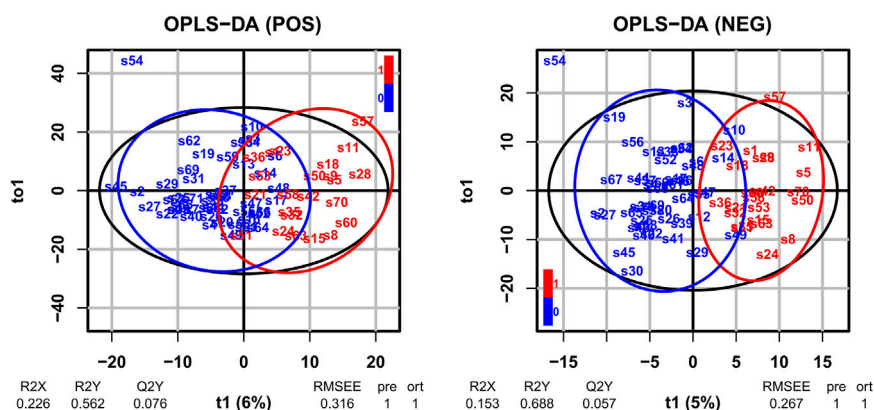


FIGURE 1

OPLS-DA of LC-MS metabolite profiles between eosinophilic AECOPD and non-eosinophilic AECOPD subjects in electrospray positive ion (ESI+) mode and electrospray negative ion (ESI-) mode, respectively. Red points represented eosinophilic AECOPD subjects, while blue points represented non-eosinophilic AECOPD subjects. OPLS-DA, orthogonal projections to latent structures-discriminate analysis; LC-MS, liquid chromatography-mass spectrometry; AECOPD, acute exacerbation of chronic obstructive pulmonary disease; POS, electrospray positive ion mode; NEG, electrospray negative ion mode.

phenotypes (Singh et al., 2014; Pascoe et al., 2015; Dai et al., 2020). These patients have specific characteristics in terms of clinical characteristics, laboratory test results, treatment, and prognosis. For instance, the risk of in-hospital mortality is lower among eosinophilic AECOPD patients, and the hospital stay is shorter (You and Shi, 2021), with better response to systemic glucocorticoid treatment (Bafadhel et al., 2014). However, the pathogenesis of the eosinophilic phenotype of COPD exacerbation is still not clear. Novel biomarkers can help clinicians recognize this phenotype and develop potential new therapeutic targets.

Lipids are important cellular components. They participate in the formation of cell membranes and are important energy storage substances, components of various hormones, and important mediators in cell signal transduction pathways. Accumulating studies have demonstrated that lipid metabolism disorders are closely related to the pathogenesis of COPD by affecting occurrence and development of the disease (Fahy et al., 2005; Chen et al., 2019; Kotlyarov and Bulgakov, 2021). For example, obesity with high amounts of triglyceride and cholesterol was associated with poorer COPD-related outcomes (lower quality of life, more dyspnea, and more severe COPD exacerbations) (Lambert et al., 2017). In addition, some species of sphingolipids were inversely associated with emphysema, while sphingosine 1-phosphate showed negative association with COPD exacerbation (Bowler et al., 2015). Phospholipids, accounting for forming cell membranes and pulmonary surfactants, were found to be decreased in patients with COPD, which may correlate with pulmonary functions (Lusuardi et al., 1992).

Lipidomics is an “omics” approach, which comprehensively analyzes the full lipid components in various biological samples and can provide significant insights into the understanding of disease pathogenesis. With this technology, fatty acid metabolism was identified to be altered in bronchial epithelial cells of asthmatic patients, leading to an increase in levels of some lipid species [phosphatidylcholine, lysophosphatidylcholine, and bis (monoacylglycerol) phosphate] (Ravi et al., 2021). Our previous study found that the levels of lysophosphatidylcholine (LPC) 18:3, lysophosphatidylethanolamine (LPE) 16:1, and

phosphatidylinositol (PI) 32:1 significantly dropped in the acute stage compared to the recovery stage in hospitalized patients with COPD exacerbation (Gai et al., 2021). In our study, we aimed to compare the serum lipid metabolite profiles between eosinophilic and non-eosinophilic AECOPD patients, and to explore the association between differential lipid metabolites and patients’ clinical and prognostic features, based on the untargeted liquid chromatography-mass spectrometry (LC-MS) lipidomics technology. We hypothesized that lipid metabolic profiles were different between these two phenotypes of AECOPD, and lipidomics analysis may help elucidate the underlying pathogenesis.

## 2. Materials and methods

### 2.1 Study subjects and data collection

Data were collected from 71 AECOPD patients hospitalized in the Department of Respiratory Medicine and Critical Care Medicine of Peking University Third Hospital from April 2017 to March 2018. These patients met the criteria for the diagnosis of acute exacerbation of COPD, according to the Global Initiative for Chronic Obstructive Lung Disease (GOLD) guidelines (Global Initiative for Chronic Obstructive Lung Disease, 2022). The exclusion criteria were as follows: subjects with other airflow limitation diseases rather than COPD, combination of pneumonia and active pulmonary tuberculosis, severe liver and kidney insufficiency, malignancies, an immunosuppressive condition due to chemotherapy or HIV infection, receiving systemic glucocorticoids due to COPD exacerbation in the past 1 month, and severe trauma or stress reaction.

The clinical data included demographic characteristics, smoking status, comorbidities, presence or absence of hypercapnic respiratory failure [arterial carbon dioxide partial pressure ( $\text{PaCO}_2$ )  $\geq 50$  mmHg], the length of stay (LOS) in the hospital, and requirement for an intensive care unit (ICU) stay or not. The time taken for the next exacerbation was also collected.

TABLE 2 Differentially expressed metabolites between eosinophilic and non-eosinophilic patients.

Metabolite	Median m/z	Median RT (s)	MS2. score	Mean non- eosinophilic	Mean eosinophilic	log2fc	p.t-test	p.t.adj	VIP
Positive-ion mode (ESI +)									
TAG (12:0/12:0/22:3)	795.611	424.092	0.876	$2.24 \times 10^{-4}$	$1.69 \times 10^{-4}$	−0.405	$5.60 \times 10^{-4}$	0.040	2.147
TAG (12:1/12:3/12:3)	647.423	155.660	0.876	$3.27 \times 10^{-6}$	$1.93 \times 10^{-6}$	−0.756	$6.50 \times 10^{-4}$	0.042	2.088
TAG (13:1/22:5/22:5)	933.671	660.639	0.880	$1.54 \times 10^{-5}$	$2.30 \times 10^{-5}$	0.576	$1.23 \times 10^{-4}$	0.022	2.469
TAG (14:0/18:2/18:2)	849.695	655.631	0.976	$4.48 \times 10^{-4}$	$6.61 \times 10^{-4}$	0.559	$6.20 \times 10^{-4}$	0.042	2.258
TAG (14:3/21:5/22:0)	934.675	659.682	0.975	$1.26 \times 10^{-5}$	$1.93 \times 10^{-5}$	0.615	$2.59 \times 10^{-4}$	0.033	2.167
TAG (15:0/20:5/20:5)	907.657	656.299	0.882	$5.00 \times 10^{-6}$	$8.04 \times 10^{-6}$	0.685	$6.48 \times 10^{-4}$	0.042	2.101
TAG (15:0/21:3/21:3)	938.819	643.019	0.515	$9.23 \times 10^{-6}$	$1.70 \times 10^{-5}$	0.878	$5.78 \times 10^{-4}$	0.040	2.092
TAG (16:0/18:1/18:2)	874.699	643.315	0.958	$1.50 \times 10^{-4}$	$2.48 \times 10^{-4}$	0.723	$4.96 \times 10^{-4}$	0.038	2.452
TAG (16:0/18:2/18:3)	870.756	660.559	0.834	$9.80 \times 10^{-4}$	$1.65 \times 10^{-3}$	0.752	$5.56 \times 10^{-4}$	0.040	2.148
TAG (16:1/16:1/18:3)	847.680	637.878	0.903	$1.17 \times 10^{-4}$	$2.03 \times 10^{-4}$	0.794	$3.54 \times 10^{-4}$	0.037	2.341
TAG (16:2/18:2/18:3)	866.673	655.307	0.577	$3.17 \times 10^{-5}$	$4.09 \times 10^{-5}$	0.369	$6.43 \times 10^{-4}$	0.042	2.306
TAG (17:0/17:2/17:2)	863.676	639.317	0.910	$2.04 \times 10^{-5}$	$3.32 \times 10^{-5}$	0.703	$3.13 \times 10^{-5}$	0.015	2.632
TAG (18:1/18:1/21:5)	941.703	660.805	0.885	$4.19 \times 10^{-5}$	$6.54 \times 10^{-5}$	0.644	$4.18 \times 10^{-4}$	0.037	2.081
TAG (20:4/22:7/22:7)	1,017.690	84.972	0.876	$2.21 \times 10^{-5}$	$3.64 \times 10^{-5}$	0.725	$4.10 \times 10^{-4}$	0.037	2.529
TAG (20:5/22:7/22:7)	1,015.664	83.199	0.876	$4.07 \times 10^{-5}$	$5.96 \times 10^{-5}$	0.552	$8.86 \times 10^{-5}$	0.021	2.903
TAG (20:6/20:6/22:5)	991.674	83.242	0.876	$6.68 \times 10^{-5}$	$1.20 \times 10^{-4}$	0.849	$9.28 \times 10^{-5}$	0.021	2.640
TAG (20:6/22:7/22:7)	1,013.656	83.220	0.876	$1.79 \times 10^{-4}$	$2.74 \times 10^{-4}$	0.610	$3.01 \times 10^{-5}$	0.015	2.962
LPC (16:0)	496.340	83.237	0.982	$9.99 \times 10^{-3}$	$1.36 \times 10^{-2}$	0.448	$3.75 \times 10^{-5}$	0.016	3.021
LPC (20:2)	548.359	112.762	0.852	$4.67 \times 10^{-5}$	$6.71 \times 10^{-5}$	0.523	$9.73 \times 10^{-5}$	0.021	2.740
PC (14:1e/22:6)	762.564	315.218	0.811	$4.35 \times 10^{-6}$	$5.89 \times 10^{-6}$	0.436	$4.74 \times 10^{-4}$	0.038	1.110
DGTS (21:1/21:1)	848.683	637.876	0.641	$6.72 \times 10^{-5}$	$1.20 \times 10^{-4}$	0.838	$1.25 \times 10^{-4}$	0.022	2.380
DGTS (26:0/16:1)	850.699	655.426	0.515	$2.63 \times 10^{-4}$	$3.83 \times 10^{-4}$	0.542	$4.42 \times 10^{-4}$	0.037	2.297
DGTS (3:0/21:0)	600.467	83.235	0.620	$1.74 \times 10^{-5}$	$2.53 \times 10^{-5}$	0.543	$7.55 \times 10^{-4}$	0.044	2.356
ACar (26:7)	526.377	112.711	0.587	$1.74 \times 10^{-4}$	$2.26 \times 10^{-4}$	0.374	$3.84 \times 10^{-4}$	0.037	2.866

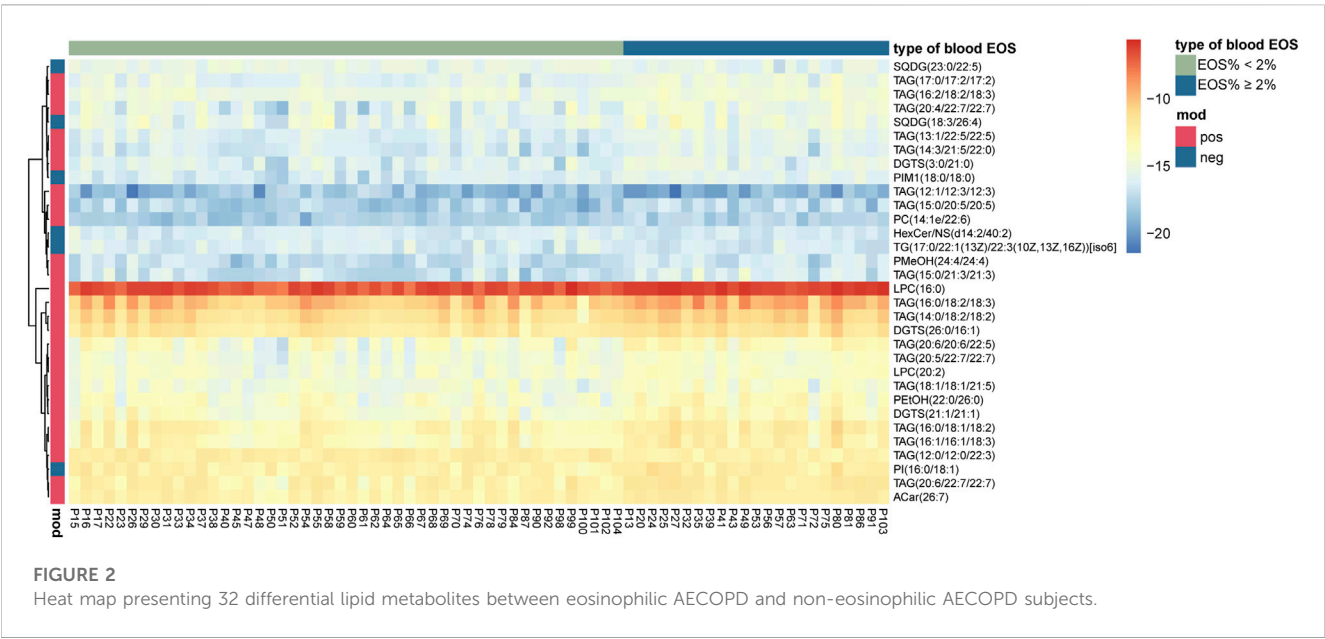
(Continued on following page)



TABLE 2 (Continued) Differentially expressed metabolites between eosinophilic and non-eosinophilic patients.

Metabolite	Median m/z	Median RT (s)	MS2. score	Mean non-eosinophilic	Mean eosinophilic	log2fc	p.t-test	p.t.adj	VIP
PEtOH (22:0/26:0)	918.755	640.810	0.796	$6.16 \times 10^{-5}$	$1.03 \times 10^{-4}$	0.747	$2.14 \times 10^{-4}$	0.029	2.037
PMeOH (24:4/24:4)	888.656	628.171	0.947	$7.93 \times 10^{-6}$	$1.21 \times 10^{-5}$	0.607	$3.80 \times 10^{-4}$	0.037	1.982
Negative-ion mode (ESI -)									
HexCer/NS (d14:2/40:2)	972.837	692.336	0.567	$1.35 \times 10^{-5}$	$1.06 \times 10^{-5}$	-0.353	$5.87 \times 10^{-3}$	0.123	2.412
PI (16:0/18:1)	835.519	273.846	0.815	$1.81 \times 10^{-4}$	$2.48 \times 10^{-4}$	0.452	$2.46 \times 10^{-3}$	0.077	1.965
SQDG (18:3/26:4)	947.607	85.781	0.826	$2.70 \times 10^{-5}$	$4.12 \times 10^{-5}$	0.611	$9.92 \times 10^{-3}$	0.156	1.799
SQDG (23:0/22:5)	965.616	449.079	0.876	$2.63 \times 10^{-5}$	$2.19 \times 10^{-5}$	-0.264	$5.88 \times 10^{-2}$	0.311	1.559
TAG [17:0/22:1 (13Z)/22:3 (10Z,13Z,16Z)] [iso6]	979.846	688.173	0.898	$1.43 \times 10^{-5}$	$1.08 \times 10^{-5}$	-0.400	$2.68 \times 10^{-2}$	0.229	2.192

RT, retention time; log2fc, log2 transformed fold change; p. t-test, p-value of the t-test; p.t.adj, FDR-adjusted p-value of the t-test; VIP, variable importance projection. Lipid metabolites: TAG, triacylglycerol; LPC, lysophosphatidylcholine; PC, phosphatidylcholine; DGTS, diacylglycerol trimethylhomoserine; ACar, acylcarnitine; PEtOH, phosphatidylethanol; PMeOH, phosphatidylmethanol; HexCer/NS, hexosylceramide non-hydroxyfatty acid-sphingosine; PI, phosphatidylinositol; SQDG, sulfoquinovosyl diacylglycerol.



A blood routine test and blood biochemical examination were performed in the clinical laboratory of our hospital. The peripheral blood cell count and classification, fibrinogen, D-dimer, total cholesterol, total triglyceride, and other laboratory parameters were recorded. Our patients were grouped according to the percentage of eosinophils (EOS) in peripheral blood. Non-eosinophilic AECOPD was defined as having blood EOS% < 2% and eosinophilic AECOPD as having blood EOS ≥ 2%.

All subjects or their close relatives participating in this study signed an informed consent before data collection. The study procedures were performed in compliance with the Declaration

of Helsinki (1964), and the study protocol was approved by the Ethics Committee of Peking University Third Hospital (M2017410).

## 2.2 LC-MS analysis

### 2.2.1 Serum sample collection and preparation

Fasting (after at least 8 h) peripheral blood samples were collected from patients using vacuum blood collection tubes. The blood samples were left at room temperature for approximately 30 min until complete clotting, and then, the samples were

**TABLE 3** Nine lipid metabolites and their association with clinical features<sup>a</sup>.

Metabolite	Preliminary screening			Eosinophil		Hypercapnic respiratory failure		Need for ICU		Fibrinogen	
	log2fc	p.t.adj	VIP	β	p.adj	OR (95% CI)	p.adj	OR (95% CI)	p.adj	β	p.adj
TAG (20:6/20:6/22:5)	0.849	0.021	2.640	1.186	0.001	0.377 (0.211, 0.675)	0.011	0.433 (0.236, 0.792)	0.028	−0.426	0.004
TAG (20:6/22:7/22:7)	0.610	0.015	2.962	0.807	0.001	0.230 (0.095, 0.554)	0.011	0.224 (0.088, 0.575)	0.023	−0.618	0.005
TAG (20:5/22:7/22:7)	0.552	0.021	2.903	0.731	0.001	0.228 (0.090, 0.578)	0.012	0.198 (0.071, 0.554)	0.023	−0.694	0.004
LPC (20:2)	0.523	0.021	2.740	0.663	0.001	0.259 (0.098, 0.685)	0.024	0.204 (0.064, 0.649)	0.028	−0.771	0.004
TAG (17:0/17:2/17:2)	0.703	0.015	2.632	0.637	0.003	0.264 (0.099, 0.703)	0.024	0.203 (0.059, 0.698)	0.036	−0.689	0.005
DGTS (3:0/21:0)	0.543	0.044	2.356	0.628	0.012	0.200 (0.075, 0.534)	0.011	0.286 (0.121, 0.672)	0.028	−0.686	0.001
LPC (16:0)	0.448	0.016	3.021	0.563	0.001	0.126 (0.036, 0.449)	0.011	0.103 (0.024, 0.439)	0.023	−0.987	0.004
ACar (26:7)	0.374	0.037	2.866	0.498	0.001	0.174 (0.050, 0.607)	0.024	0.124 (0.028, 0.548)	0.028	−1.162	0.001
TAG (16:2/18:2/18:3)	0.369	0.042	2.306	0.341	0.012	0.175 (0.043, 0.712)	0.028	0.104 (0.019, 0.570)	0.033	−0.836	0.025

a: Association of every one-fold increase of a marker with clinical features. Markers were considered the response variable for EOS, while the predictor variable for the other three clinical features.

Abbreviation: EOS, percentage of peripheral eosinophils; RF, respiratory failure; log2fc, log2 transformed fold change; p.t.adj, FDR-adjusted *p*-value for the *t*-test; VIP, variable importance projection; β, log2 transformed fold change after adjusting for age, sex, BMI, smoking status, serum total cholesterol, and triglyceride; p. adj, FDR-adjusted *p*-value.

Lipid metabolites: TAG, triacylglycerol; LPC, lysophosphatidylcholine; DGTS, diacylglycerol trimethylhomoserine; ACar, acylcarnitine.

centrifuged at 4°C at 2,500 × *g* for 15 min. The upper serum samples were extracted and then placed in frozen storage at −80°C.

## 2.2.2 Lipid metabolite extraction

After being reheated and dissolved, 100 μL of the serum sample was transferred into an EP tube, and then, 480 μL of the extract solution (methyltert-butylether: methanol = 5:1) was added to the sample. After vortexing and mixing for 30 s, the samples were sonicated in an ice water bath for 10 min. After incubating at −40°C for 1 h, the sample was centrifuged at 3,000 rpm for 15 min at 4°C. Then, 350 μL of the supernatant was transferred to a fresh EP tube and vacuum dried. A measure of 200 μL of the solution (DCM: MeOH = 1:1) was added to reconstitute the dried samples. Then, the solution was vortexed for 30 s and sonicated in an ice water bath for 10 min. A measure of 75 μL of the supernatant was placed in a fresh glass vial for LC-MS analysis. A quality control (QC) sample was prepared by mixing an equal aliquot (10 μL) of the supernatants from each subject's sample.

## 2.2.3 LC-MS analysis procedure

After lipid metabolite extraction was carried out, an ultra-high-performance liquid chromatograph (ExionLC, AB SCIEX, United States) was used to separate the target compounds using a Phenomenex Kinetex C18 (2.1 mm × 100 mm, 1.7 μm, Phenomenex, United States) liquid chromatography column. High-resolution mass spectrometry data acquisition was performed in information-dependent acquisition (IDA) mode, utilizing a triple TOF 5600 mass spectrometer (AB SCIEX, United States). The data acquisition software application (Analyst TF 1.7, AB Sciex) conducts primary acquisition, followed by automated ion selection and secondary mass spectrometry data collection based on predetermined criteria derived from primary mass spectrometry data. In each cycle, the most intensive 12 precursor ions with intensities over 100 were selected for

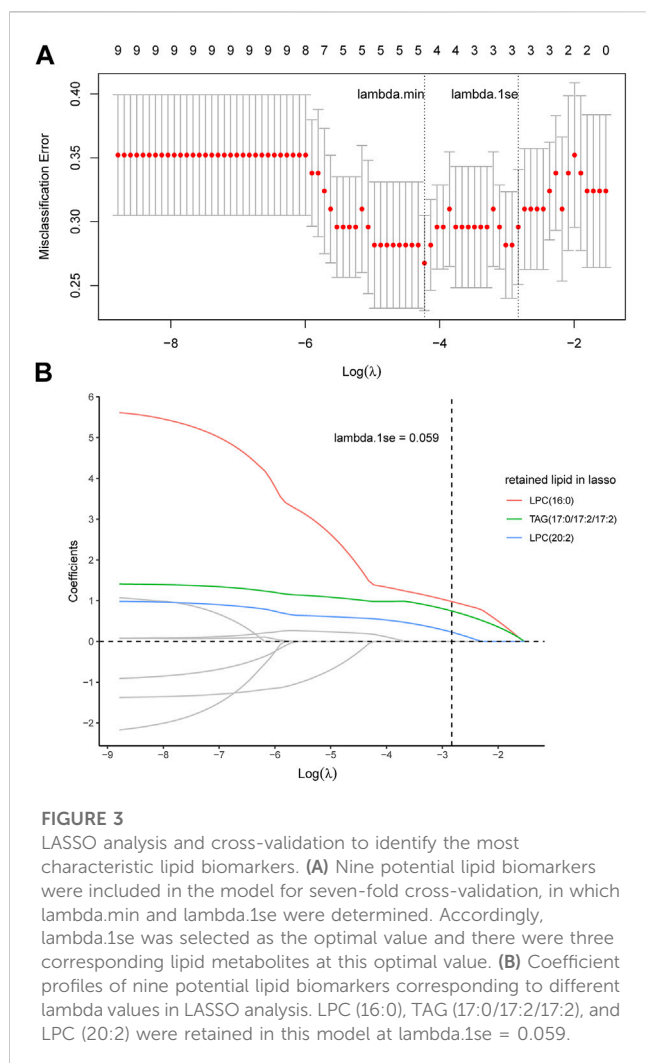
secondary mass spectrometry scanning. The energy of collision-induced dissociation was 45 eV, and the accumulation time of each secondary spectrum was 50 ms. The ion source parameters are as follows: GS1 60 psi, GS2 60 psi, CUR 30 psi, TEM 600°C, DP 100 V, ISVF 5,000 V (ESI + mode), and −3800 V (ESI − mode).

## 2.2.4 Data preprocessing and annotation

The mass-to-charge ratio (*m/z*) and retention time (RT) information of the test samples were determined by liquid chromatography–mass spectrometry (LC-MS), and then, XCMS was used for retention time correction, peak identification, peak extraction, peak integration, and peak alignment. Minfrac was set as 0.5, and the cutoff was set as 0.3. The *m/z* of the substances in the LipidBlast database was matched with RT. In the qualitative process, the score value of the secondary qualitative metabolites was calculated based on the Euclidean distance and the dot product algorithm, which improved the accuracy of the mass spectrum annotation. XCMS parameters were set as follows: centWave, ppm 10, peak width 5–20, and SN 3; prefiltering step: the metabolites could be retained only if it contained at least three peaks of intensity ≥ 1,000. The function used to calculate the *m/z* center of the chromatographic peak was wMean, which was the intensity weighted average of the *m/z* values of the peak. The minimum *m/z* dimension difference required for peaks with overlapping retention times was −0.001. Then, lipid metabolite identification was achieved through a spectral match using the LipidBlast library. Finally, a total of 2,431 lipid metabolites in the ESI + mode and 1,821 lipid metabolites in the ESI − mode were detected for further multivariate analysis.

## 2.3 Statistical analysis

The baseline data were compared between the patients with the percentage of peripheral eosinophils ≥ 2% and <2% using Student's *t*-test for continuous and Pearson's chi-squared test or Fisher's exact



test for categorical variables. The numerical variables were presented as the mean value and standard deviation (SD), while the categorical variables were expressed as numbers and percentages.

Significance of the difference between the two groups was analyzed for each lipid using Student's *t*-test, and an FDR-adjusted *p*-value < 0.05 was considered significant. The fold changes of each lipid were calculated on the basis of the average in each group. Orthogonal projections to latent structure discriminant analysis (OPLS-DA) was applied to obtain a high level of group separation and a good understanding of the variables responsible for classification, and the first principal component of the variable importance projection (VIP) was obtained. VIP values exceeding 1.0 with an adjusted *p*-value < 0.05 in the Student's *t*-test were selected to correspond to potential lipid biomarker candidates. To control the possible influences of some factors, such as age, sex, BMI, smoking status, serum total cholesterol, and triglyceride, linear regression was performed for each lipid. The lipids with an FDR-adjusted *p*-value < 0.05 from the Wald statistic were retained as potential lipid biomarkers.

We also checked the associations between the percentage of peripheral eosinophils and other clinical features. Linear regression or generalized linear regression was performed for each potential lipid biomarker and clinical features significantly associated with the

percentage of peripheral eosinophils to determine more characteristic lipid metabolites. Then, the least absolute shrinkage and selection operator (LASSO) was applied to downsize these lipid metabolites for discriminating eosinophilic and non-eosinophilic AECOPD, while the largest value of  $\lambda$ , whose corresponding misclassification error was within one standard error of the minimum misclassification error, known as “1-se”  $\lambda$ , was defined as the optimal value. A logistic regression model was fitted using these selected markers as the covariates to obtain a combined screening score. The predictability of the model was evaluated by using the area under receiver operation characteristic curve (ROC).

All the analyses were conducted using R version 4.0.5, with the following packages being used: “ropls,” “glmnet,” and “pROC”. A two-sided *p*-value of < 0.05 was considered statistically significant. All data were analyzed anonymously.

## 3 Results

### 3.1 Clinical characteristics

As shown in Table 1, the mean age of our patients was  $74.1 \pm 9.6$  years, and 87.3% of these patients were male, where 59.2% and 31.0% were former and current smokers, respectively. The age, sex proportion, body mass index, tobacco exposure, and comorbidities were not different between eosinophilic and non-eosinophilic AECOPD patients. Serum triglyceride and cholesterol levels were similar between the groups. Eosinophilic AECOPD patients had less hypercapnic respiratory failure, less ICU admission, and shorter LOS in the hospital, as well as a lower fibrinogen level. The time taken for the next exacerbation was not statistically different.

### 3.2 Lipid metabolite profiling difference between eosinophilic and non-eosinophilic AECOPD

Log2 transformation was performed before statistics analysis. First, OPLS-DA was performed. As shown in Figure 1, OPLS-DA plots both demonstrated a barely clear separation between eosinophilic and non-eosinophilic AECOPD, with most samples being within the 95% confidential interval with the exception of one non-eosinophilic sample. The  $R^2Y$  values of the OPLS-DA model in ESI + and ESI – modes were 0.562 and 0.688, respectively, and the  $Q^2Y$  values were 0.076 and 0.057, respectively. A total of 838 and 616 lipids had a VIP score > 1 in ESI + and ESI – modes, respectively. Subsequently, a *t*-test with FDR-adjusting values and fold changes was conducted to compare the difference between the mean concentrations of lipid species between the two groups. In this process, a total of 32 lipid metabolites (26 in ESI + and 6 in ESI – modes) met both FDR-adjusted *p* < 0.05 and VIP > 1, and were selected as potential candidate metabolites.

To further control the possible influencing factors, such as age, sex, BMI, smoking status, serum total cholesterol, and triglyceride, a linear regression model was structured for each candidate, and lipids with an FDR-adjusted *p*-value < 0.05 from the Wald statistic were retained in this model. It turned out that all the 32 candidate

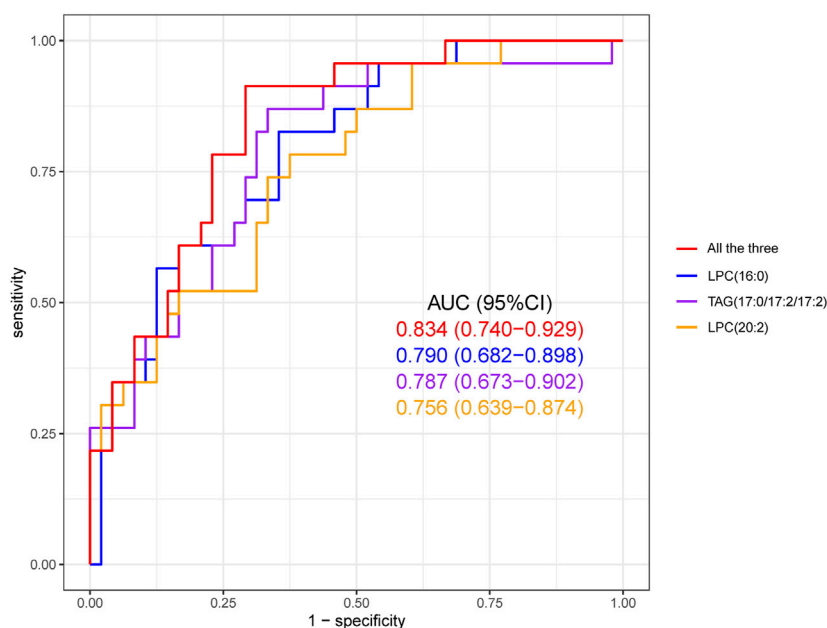


**FIGURE 4**

Receiver operating characteristic (ROC) curve of the diagnostic prediction model with three LASSO-selected markers, namely, LPC (16:0), TAG (17:0/17:2/17:2), and LPC (20:2). The combined prediction performance of these three biomarkers was superior to the individual prediction performance of each biomarker.

metabolites were retained. Therefore, a total of 32 lipid metabolites (Table 2) were selected as potential biomarkers, and they were mapped to show the clear difference between the two groups (Figure 2).

In the ESI + mode, the levels of most of triacylglycerols (TAGs), lysophosphatidylcholines (LPCs), and diacylglycerol trimethylhomoserine (DGTSS) were significantly higher in the eosinophilic AECOPD patients than those in the non-eosinophilic patients, except TAG (12:0/12:0/22:3) and TAG (12:1/12:3/12:3). In the ESI – mode, the levels of PI (16:0/18:1), PIM1 (18:0/18:0), and SQDG (18:3/26:4) were significantly higher in the eosinophilic AECOPD patients.

### 3.3 Integration analysis between clinical characteristics and differential lipid metabolites

The correlation analysis between the 32 lipid metabolites and the clinical characteristics of all the AECOPD patients is shown in Supplementary Figure 1. The most significant clinical characteristics correlated with lipid metabolites were body mass index, D-dimer, fibrinogen, total cholesterol, hypercapnic respiratory failure, and ICU admission. We further analyzed the associations between each of these 32 metabolites and the clinical features which were different between the eosinophilic and non-eosinophilic AECOPD, including hypercapnia respiratory failure, need for ICU admission, and fibrinogen. There were nine differential lipid metabolites associated with each of the three features (Table 3). Most of them have a negative association with these three features.

In order to identify the most characteristic lipid biomarkers for the eosinophilic AECOPD phenotype, LASSO regression was applied to further screen the potential biomarkers. As shown in Figure 3A, all the nine different lipid metabolites associated with the eosinophilic phenotype and clinical features were included in a 7-fold cross-validation (CV) and a CV plot was generated, in which the lambda.min and lambda.1se values were determined. Based on lambda.1se, three lipid metabolites were retained, which were LPC (16:0), TAG (17:0/17:2/17:2), and LPC (20:2) (Figures 3A, B). All of these three lipid metabolites were high in patients with eosinophilic AECOPD. Next, logistic regression models were fitted by individually using each of the three selected markers as the covariate, as well as using them together to obtain the individual screening scores and a combined score, respectively. The predictability of the models was evaluated by the area under ROC curve. As shown in Figure 4, the area under the ROC curve values of LPC (16:0), TAG (17:0/17:2/17:2), and LPC (20:2) were 0.790, 0.787, and 0.756, respectively. In addition, the AUC reached 0.834 (95% CI: 0.740–0.929) when including all the three markers together, which meant this model had an excellent discriminative capacity to distinguish eosinophilic AECOPD and non-eosinophilic AECOPD.

## 4 Discussion

Our study demonstrated the unique characteristics of lipid profiles measured using LC-MS in a group of hospitalized AECOPD patients and indicated that alterations in lipid metabolism were involved in the pathogenesis of the eosinophilic phenotype. In our study, we observed that nine lipid metabolites

were significantly associated with the difference in clinical features and prognosis between the eosinophilic and non-eosinophilic phenotypes, which were enriched in triglycerides and phospholipid metabolic pathways and were expected to be potential biomarkers for AECOPD patients and help explain the mechanisms of different clinical outcomes in the eosinophilic phenotype. Furthermore, three lipid metabolites were further screened using LASSO, including LPC (16:0), TAG (17:0/17:2/17:2), and LPC (20:2). Their combination was reliable to predict the clinical prognosis of AECOPD patients in different phenotypes.

Triglycerides are lipids containing three glyceryl groups (Fahy et al., 2005; Liebisch et al., 2020) and are mainly found in the adipose tissue (Chaurasia et al., 2016; Wu et al., 2020). Few studies have explored the characteristics and mechanisms of triglyceride metabolism of eosinophilic COPD. Our data showed that some species of TAGs were higher in those with eosinophilic AECOPD. In previous studies, high triglycerides and low HDL-C played an important role in type 2 inflammation in asthmatic patients (Barochia et al., 2017; Chanachon et al., 2022); the mechanism may be that free fatty acids released by triglycerides promoted inflammation by activating NF- $\kappa$ B signaling in mononuclear cells and enhancing reactive oxygen species generation (Tucker et al., 2020). Additionally, fatty acid synthesis or uptake and subsequent TAG synthesis were also significantly enhanced after inflammatory activation (Tucker et al., 2020). Airway inflammation in eosinophilic COPD and asthma were likely to share a similar mechanism, which could partly explain why some species of TAGs were increased in those with eosinophilic AECOPD. However, the increased levels of these species of TAGs in eosinophilic AECOPD were associated with better clinical outcomes and less systemic inflammation (a lower fibrinogen level) in our study, which seemed to contradict previous studies. A deficiency of lysosomal acid lipase could lead to disruption of triglyceride and cholesterol ester metabolism in alveolar macrophages, leading to respiratory inflammation, tissue remodeling, and emphysema (Lian et al., 2004; Lian et al., 2005). In addition, inflammation also increased the activity of angiopoietin-like protein, an inhibitor of lipoprotein lipase, which further prevented the metabolism of triglyceride-rich lipoproteins and led to elevated triglyceride levels (Lu et al., 2010). Triglycerides were associated with airflow obstruction and wheezing in asthma patients (Fenger et al., 2013; Barochia et al., 2015; Chanachon et al., 2022). However, inconsistent results between previous studies and ours may be related to different study population and disease statuses. In addition, very few studies elucidated the relevant mechanism of the effect of triglyceride species on eosinophil proliferation, activity, and function. The alteration of TAG metabolism and its role in the pathogenesis of eosinophilic COPD need to be further investigated.

Phospholipids are lipids containing phosphoric acid (Fahy et al., 2005; Liebisch et al., 2020) and are the main components of the biological membrane. Phospholipase A2 splits phospholipids into lysophospholipids (a kind of phospholipid containing a single fatty acid) and fatty acids. In our study, LPC (16:0) and LPC (20:2) were increased in eosinophilic AECOPD and associated with fewer hypercapnic respiratory failures, shorter ICU stay, and lower fibrinogen level. The physiological role of LPC in inflammation was complicated. In previous literature, LPCs could exhibit proinflammatory or anti-inflammatory activity under different

conditions. Under certain pathophysiological conditions, LPC can be used as a proinflammatory substance. The mechanism may be that LPC-dependent NADPH oxidase can stimulate the production of reactive oxygen species, thus promoting the transformation of pro-cytokines into their mature bioactive forms (such as IL-1 $\beta$ , IL-18, and IL-33), promoting the occurrence of inflammation (Schilling and Eder, 2010). However, under other conditions, some polyunsaturated LPCs (such as LPC 20:4, LPC 20:5, and LPC 22:6) can exhibit anti-inflammatory effects. The mechanism may be to downregulate the formation of pro-inflammatory mediators (such as IL-5, IL-6, NO, 12-hydroxy eicosapentaenoic acid, and LPC16:0-induced PGE2) and upregulate the expression of anti-inflammatory mediators (IL-4 and IL-10) by reducing leukocyte exosmosis and plasma leakage (Riederer et al., 2010; Hung et al., 2011; Hung et al., 2012). In our study, elevated levels of several LPCs were found to have negative correlations with fibrinogen in eosinophilic AECOPD patients, suggesting that systemic inflammatory responses may be weaker and clinical outcomes may be better, and that LPC may have a protective effect in eosinophilic AECOPD patients. Regarding the association between LPC and eosinophilic AECOPD phenotypes, we speculated the mechanism as follows: eosinophils had been demonstrated to express high levels of phospholipase A2 (Blom et al., 1998), which can cleave phosphatidylcholine into LPC and a free fatty acid and increase the level of LPC. Additionally, LPC could induce eosinophils to adhere on and infiltrate into the airway wall (Nishiyama et al., 2004; Zhu et al., 2007). However, most previous studies were based on allergic diseases, such as asthma and allergic rhinitis. The saturated or unsaturated fatty acid chains on LPC species may exhibit different effects on inflammation. Therefore, these issues should be addressed in further studies.

In our study, we also found that eosinophilic AECOPD patients had better clinical outcomes, with shorter hospital stays, fewer cases of respiratory failure, and a lower rate of ICU admission during hospitalization. These results were similar to those found in a meta-analysis. In this analysis, eosinophilic AECOPD (blood eosinophilia  $\geq 2\%$  or  $0.34 \times 10^9$  cells/L) had a better prognosis (lower risk of in-hospital mortality, shorter stay in hospital, and lower risk of arrhythmia) (You and Shi, 2021). Although studies showed a higher risk of readmission (shorter first COPD-related readmissions and an increased number of 12-month COPD-related readmissions) in eosinophilic AECOPD patients, our study did not suggest an increase in the risk of acute exacerbations again (Peng et al., 2021).

This study included the following limitations: 1) since our study results were drawn from a small sample size, further studies are needed to elucidate the relation between lipid metabolism and phenotypes of AECOPD. 2) The Q2Y value in OPLS-DA was relatively low, which meant the estimates from the model were probably on the lower side. This may be due to a possible small difference between the whole lipid profiles of the two groups and the small sample size. However, a combination of several lipids could model well in the discrimination. In future, we would verify the relationship between these lipid metabolites and disease phenotypes in a prospective study. 3) In this study, we did not observe differences in serum lipid metabolic profiles between the two groups before and after the treatment, and it would be of great significance in elucidating the mechanism if we could observe the dynamic changes in lipid metabolites with the treatment time.



In conclusion, our LC-MS analysis demonstrated that patients with eosinophilic AECOPD had a unique serum lipid metabolite profile that could be used to differentiate them from non-eosinophilic AECOPD patients. TAGs and LPCs were significantly increased in eosinophilic phenotypes and associated with less hypercapnic respiratory failure and ICU admission, as well as a lower fibrinogen level, suggesting that these lipid species can serve as biomarkers and play an important role in the pathogenesis of COPD exacerbation. Further studies regarding the mechanisms around lipid metabolism and metabolic pathways will help develop potential therapeutic targets for patients with COPD.

## Data availability statement

The raw data supporting the conclusions of this article will be made available by the authors, without undue reservation.

## Ethics statement

The studies involving human participants were reviewed and approved by the Ethics Committee of Peking University Third Hospital (M2017410). The patients/participants provided their written informed consent to participate in this study.

## Author contributions

YW, CC, XiG, YS, and YL contributed to the conception and design of the study. YW, CC, JW, YC, and YL organized the database. ST, XiG, and XuG performed the statistical analysis. YW, CC, ST, and YL wrote the first draft of the manuscript. JW, XiG, and QZ participated in writing the methods and results sections

of the manuscript. YC participated in writing the discussion section of the manuscript. All authors contributed to the article and approved the submitted version.

## Funding

This work was supported by the National Natural Science Foundation (project no. 81700039).

## Conflict of interest

The authors declare that the research was conducted in the absence of any commercial or financial relationships that could be construed as a potential conflict of interest.

## Publisher's note

All claims expressed in this article are solely those of the authors and do not necessarily represent those of their affiliated organizations, or those of the publisher, the editors, and the reviewers. Any product that may be evaluated in this article, or claim that may be made by its manufacturer, is not guaranteed or endorsed by the publisher.

## Supplementary material

The Supplementary Material for this article can be found online at: <https://www.frontiersin.org/articles/10.3389/fmolb.2023.1204985/full#supplementary-material>

## References

- Bafadhel, M., Davies, L., Calverley, P. M., Aaron, S. D., Brightling, C. E., and Pavord, I. D. (2014). Blood eosinophil guided prednisolone therapy for exacerbations of COPD—a further analysis. *Eur. Respir. J.* 44 (3), 789–791. doi:10.1183/09031936.00062614
- Barnes, P. J. (2019). Inflammatory endotypes in COPD. *Allergy* 74, 1249–1256. doi:10.1111/all.13760
- Barochia, A. V., Gordon, E. M., Kaler, M., Cuento, R. A., Theard, P., Figueroa, D. M., et al. (2017). High density lipoproteins and type 2 inflammatory biomarkers are positively correlated in atopic asthmatics. *J. Lipid Res.* 58, 1713–1721. doi:10.1194/jlr.P077776
- Barochia, A. V., Kaler, M., Cuento, R. A., Gordon, E. M., Weir, N. A., Sampson, M., et al. (2015). Serum apolipoprotein A-I and large high-density lipoprotein particles are positively correlated with FEV1 in atopic asthma. *Am. J. Respir. Crit. Care Med.* 191, 990–1000. doi:10.1164/rccm.201411-1990OC
- Blom, M. T. A., Wever, P. C., Wolbink, G. J., Brouwer, M. C., Calafat, J., Egesten, A., et al. (1998). Human eosinophils express, relative to other circulating leukocytes, large amounts of secretory 14-kD phospholipase A2. *Blood* 91 (8), 3037–3043. doi:10.1182/blood.V91.8.3037.3037\_3043
- Bowler, R. P., Jacobson, S., Cruickshank, C., Hughes, G. J., Siska, C., Ory, D. S., et al. (2015). Plasma sphingolipids associated with chronic obstructive pulmonary disease phenotypes. *Am. J. Respir. Crit. Care Med.* 191, 275–284. doi:10.1164/rccm.201410-1771OC
- Chanachon, P. N., Jotikasthira, W., Kiewngam, P., Sawatchai, A., Kanchongkittiphon, W., and Manuyakorn, W. (2022). TG/HDL-C ratio independent of obesity associates with airflow obstruction in children with asthma. *Indian J. Pediatr.* 89, 92. doi:10.1007/s12098-021-03942-y
- Chaurasia, B., Kaddai, V. A., Lancaster, G. I., Henstridge, D. C., Sriram, S., Galam, D. L., et al. (2016). Adipocyte ceramides regulate subcutaneous adipose browning, inflammation, and metabolism. *Cell Metab.* 24, 820–834. doi:10.1016/j.cmet.2016.10.002
- Chen, H., Li, Z., Dong, L., Wu, Y., Shen, H., and Chen, Z. (2019). Lipid metabolism in chronic obstructive pulmonary disease. *Int. J. Chron. Obstruct Pulmon Dis.* 14, 1009–1018. doi:10.2147/COPD.S196210
- Dai, G., Ran, Y., Wang, J., Chen, X., Peng, J., Li, X., et al. (2020). Clinical differences between eosinophilic and noneosinophilic acute exacerbation of chronic obstructive pulmonary disease: A multicenter cross-sectional study. *Mediat. Inflamm.* 2020, 1059079. doi:10.1155/2020/1059079
- Fahy, E., Subramaniam, S., Brown, H. A., Glass, C. K., Merrill, A. H., Jr., Murphy, R. C., et al. (2005). A comprehensive classification system for lipids. *J. Lipid Res.* 46, 839–861. doi:10.1194/jlr.E400004-JLR200
- Fenger, R. V., Gonzalez-Quintela, A., Linneberg, A., Husemoen, L. L., Thuesen, B. H., Aadahl, M., et al. (2013). The relationship of serum triglycerides, serum HDL, and obesity to the risk of wheezing in 85,555 adults. *Respir. Med.* 107, 816–824. doi:10.1016/j.rmed.2013.02.001
- Gai, X., Guo, C., Zhang, L., Zhang, L., Abulikemu, M., Wang, J., et al. (2021). Serum glycerophospholipid profile in acute exacerbation of chronic obstructive pulmonary disease. *Front. Physiol.* 12, 646010. doi:10.3389/fphys.2021.646010
- Global Initiative for Chronic Obstructive Lung Disease (2022). Global strategy for prevention, diagnosis and management of COPD. Available at: <https://goldcopd.org>.
- Hung, N. D., Kim, M. R., and Sok, D. E. (2011). 2-Polyunsaturated acyl lysophosphatidylethanolamine attenuates inflammatory response in zymosan A-induced peritonitis in mice. *Lipids* 46, 893–906. doi:10.1007/s11745-011-3589-2
- Hung, N. D., Sok, D. E., and Kim, M. R. (2012). Prevention of 1-palmitoyl lysophosphatidylcholine-induced inflammation by polyunsaturated acyl lysophosphatidylcholine. *Inflamm. Res.* 61, 473–483. doi:10.1007/s00011-012-0434-x

- Kotlyarov, S., and Bulgakov, A. (2021). Lipid metabolism disorders in the comorbid course of nonalcoholic fatty liver disease and chronic obstructive pulmonary disease. *Cells* 10, 2978. doi:10.3390/cells10112978
- Lambert, A. A., Putcha, N., Drummond, M. B., Boriek, A. M., Hanania, N. A., Kim, V., et al. (2017). Obesity is associated with increased morbidity in moderate to severe COPD. *Chest* 151, 68–77. doi:10.1016/j.chest.2016.08.1432
- Lian, X. Y. C., Qin, Y., Knox, L., Li, T., and Du, H. (2005). Neutral lipids and peroxisome proliferator-activated receptor- $\gamma$  control pulmonary gene expression and inflammation-triggered pathogenesis in lysosomal acid lipase knockout mice. *Am. J. Pathol.* 167 (3), 813–821. doi:10.1016/s0002-9440(10)62053-6
- Lian, X. Y. C., Yang, L., Xu, Y., and Du, H. (2004). Lysosomal acid lipase deficiency causes respiratory inflammation and destruction in the lung. *Am. J. Physiol. Lung Cell Mol. Physiol.* 286 (4), L801–L807. doi:10.1152/ajplung.00335.2003
- Liebisch, G., Fahy, E., Aoki, J., Dennis, E. A., Durand, T., Ejsing, C. S., et al. (2020). Update on LIPID MAPS classification, nomenclature, and shorthand notation for MS-derived lipid structures. *J. Lipid Res.* 61, 1539–1555. doi:10.1194/jlr.S120001025
- Lu, B., Moser, A., Shigenaga, J. K., Grunfeld, C., and Feingold, K. R. (2010). The acute phase response stimulates the expression of angiopoietin like protein 4. *Biochem. Biophys. Res. Commun.* 391, 1737–1741. doi:10.1016/j.bbrc.2009.12.145
- Lusuardi, M. C. A., Carli, S., Tacconi, M. T., Salmona, M., and Donner, C. F. (1992). Role of surfactant in chronic obstructive pulmonary disease therapeutic implications. *Respiration* 59 (1), 28–32. doi:10.1159/000196100
- Nishiyama, O., Kume, H., Kondo, M., Ito, Y., Ito, M., and Yamaki, K. (2004). Role of lysophosphatidylcholine in eosinophil infiltration and resistance in airways. *Clin. Exp. Pharmacol. Physiol.* 31, 179–184. doi:10.1111/j.1440-1681.2004.03973.x
- Pascoe, S., Locantore, N., Dransfield, M. T., Barnes, N. C., and Pavord, I. D. (2015). Blood eosinophil counts, exacerbations, and response to the addition of inhaled fluticasone furoate to vilanterol in patients with chronic obstructive pulmonary disease: A secondary analysis of data from two parallel randomised controlled trials. *Lancet Respir. Med.* 3, 435–442. doi:10.1016/s2213-2600(15)00106-x
- Peng, J., Yu, Q., Fan, S., Chen, X., Tang, R., Wang, D., et al. (2021). High blood eosinophil and YKL-40 levels, as well as low CXCL9 levels, are associated with increased readmission in patients with acute exacerbation of chronic obstructive pulmonary disease. *Int. J. Chron. Obstruct Pulmon Dis.* 16, 795–806. doi:10.2147/COPD.S294968
- Ravi, A., Goorsenberg, A. W. M., Dijkhuis, A., Dierdorp, B. S., Dekker, T., van Weeghel, M., et al. (2021). Metabolic differences between bronchial epithelium from healthy individuals and patients with asthma and the effect of bronchial thermoplasty. *J. Allergy Clin. Immunol.* 148, 1236–1248. doi:10.1016/j.jaci.2020.12.653
- Riederer, M., Ojala, P. J., Hrzenjak, A., Graier, W. F., Malli, R., Tritscher, M., et al. (2010). Acyl chain-dependent effect of lysophosphatidylcholine on endothelial prostacyclin production. *J. Lipid Res.* 51, 2957–2966. doi:10.1194/jlr.M006536
- Schilling, T., and Eder, C. (2010). Importance of lipid rafts for lysophosphatidylcholine-induced caspase-1 activation and reactive oxygen species generation. *Cell Immunol.* 265, 87–90. doi:10.1016/j.cellimm.2010.08.003
- Singh, D., Kolsum, U., Brightling, C. E., Locantore, N., Agusti, A., Tal-Singer, R., et al. (2014). Eosinophilic inflammation in COPD: Prevalence and clinical characteristics. *Eur. Respir. J.* 44, 1697–1700. doi:10.1183/09031936.00162414
- Tucker, B., Sawant, S., McDonald, H., Rye, K. A., Patel, S., Ong, K. L., et al. (2020). The association of serum lipid and lipoprotein levels with total and differential leukocyte counts: Results of a cross-sectional and longitudinal analysis of the UK Biobank. *Atherosclerosis* 319, 1–9. doi:10.1016/2020.07.11.20149310
- Wang, C., Xu, J., Yang, L., Xu, Y., Zhang, X., Bai, C., et al. (2018). Prevalence and risk factors of chronic obstructive pulmonary disease in China (the China pulmonary health [CPH] study): A national cross-sectional study. *Lancet* 391, 1706–1717. doi:10.1016/s0140-6736(18)30841-9
- Wilkinson, T. M., Donaldson, G. C., Hurst, J. R., Seemungal, T. A., and Wedzicha, J. A. (2004). Early therapy improves outcomes of exacerbations of chronic obstructive pulmonary disease. *Am. J. Respir. Crit. Care Med.* 169, 1298–1303. doi:10.1164/rccm.200310-1443OC
- Wu, Z., Bagarolo, G. I., Thoroe-Boveleth, S., and Jankowski, J. (2020). Lipidomics": Mass spectrometric and chemometric analyses of lipids. *Adv. Drug Deliv. Rev.* 159, 294–307. doi:10.1016/j.addr.2020.06.009
- You, Y., and Shi, G. C. (2021). Blood eosinophils and clinical outcome of acute exacerbations of chronic obstructive pulmonary disease: A systematic review and meta-analysis. *Respiration* 100, 228–237. doi:10.1159/000510516
- Zhu, X., Learoyd, J., Butt, S., Zhu, L., Usatyuk, P. V., Natarajan, V., et al. (2007). Regulation of eosinophil adhesion by lysophosphatidylcholine via a non-store-operated Ca<sup>2+</sup> channel. *Am. J. Respir. Cell Mol. Biol.* 36, 585–593. doi:10.1165/rcmb.2006-0391OC



## OPEN ACCESS

## EDITED BY

Gregorio Peron,  
University of Brescia, Italy

## REVIEWED BY

Xiaoshan Zhao,  
Southern Medical University, China  
Teodora Alexa-Stratulat,  
Grigore T. Popa University of Medicine and  
Pharmacy, Romania  
Francesco Vallania,  
Freemove Inc., United States

## \*CORRESPONDENCE

Feng Gao  
✉ gaofeng994512@163.com

<sup>†</sup>These authors have contributed equally to  
this work

RECEIVED 04 April 2023

ACCEPTED 23 August 2023

PUBLISHED 12 September 2023

## CITATION

Zou M, Zhang Y-S, Feng J-K, Tu H,  
Gui M-B, Wang Y-N, Yang Z-J, Yang Z-Q,  
Xu M, Wu W-Q and Gao F (2023) Serum  
metabolomics analysis of biomarkers and  
metabolic pathways in patients with  
colorectal cancer associated with spleen-  
deficiency and qi-stagnation syndrome or  
damp-heat syndrome: a prospective  
cohort study.  
*Front. Oncol.* 13:1190706.  
doi: 10.3389/fonc.2023.1190706

## COPYRIGHT

© 2023 Zou, Zhang, Feng, Tu, Gui, Wang,  
Yang, Yang, Xu, Wu and Gao. This is an  
open-access article distributed under the  
terms of the [Creative Commons Attribution  
License \(CC BY\)](https://creativecommons.org/licenses/by/4.0/). The use, distribution or  
reproduction in other forums is permitted,  
provided the original author(s) and the  
copyright owner(s) are credited and that  
the original publication in this journal is  
cited, in accordance with accepted  
academic practice. No use, distribution or  
reproduction is permitted which does not  
comply with these terms.

# Serum metabolomics analysis of biomarkers and metabolic pathways in patients with colorectal cancer associated with spleen-deficiency and qi-stagnation syndrome or damp-heat syndrome: a prospective cohort study

Min Zou<sup>1†</sup>, Yan-Sheng Zhang<sup>2†</sup>, Jin-Kai Feng<sup>3†</sup>, Hao Tu<sup>4</sup>,  
Ming-Bin Gui<sup>1</sup>, Ya-Nan Wang<sup>1</sup>, Zi-Jie Yang<sup>1</sup>,  
Zeng-Qiang Yang<sup>5†</sup>, Ming Xu<sup>1</sup>, Wei-Qiang Wu<sup>1</sup> and Feng Gao<sup>1\*</sup>

<sup>1</sup>Department of Colorectal and Anal Surgery, The 940th Hospital of Joint Logistics Support Force of Chinese People's Liberation Army, Lanzhou, China, <sup>2</sup>Department of Obstetrics and Gynecology, Gansu Provincial Maternity and Child-Care Hospital, Lanzhou, China, <sup>3</sup>Department of Hepatic Surgery VI, The Third Affiliated Hospital of Naval Medical University (Eastern Hepatobiliary Surgery Hospital), Shanghai, China, <sup>4</sup>Department of Colorectal Surgery, Chongqing Qijiang District People's Hospital, Chongqing, China, <sup>5</sup>Department of Colorectal Surgery, Gansu Provincial Central Hospital, Lanzhou, China

**Objective:** To profile the serum metabolites and metabolic pathways in colorectal cancer (CRC) patients associated with spleen-deficiency and qi-stagnation syndrome (SDQSS) or damp-heat syndrome (DHS).

**Methods:** From May 2020 to January 2021, CRC patients diagnosed with traditional Chinese medicine (TCM) syndromes of SDQSS or DHS were enrolled. The clinicopathological data of the SDQSS and DHS groups were compared. The serum samples were analyzed by liquid chromatography-mass spectrometry (LC-MS). The variable importance in the projection >1, fold change  $\geq 3$  or  $\leq 0.333$ , and  $P$  value  $\leq 0.05$  were used to identify differential metabolites between the two groups. Furthermore, areas under the receiver operating characteristic (ROC) curve > 0.9 were applied to select biomarkers with good predictive performance. The enrichment metabolic pathways were searched through the database of Kyoto Encyclopedia of Genes and Genomes.

**Results:** 60 CRC patients were included (30 SDQSS and 30 DHS). The level of alanine aminotransferase was marginally significantly higher in the DHS group than the SDQSS group ( $P = 0.051$ ). The other baseline clinicopathological characteristics were all comparable between the two groups. 23 differential serum metabolites were identified, among which 16 were significantly up-regulated and 7 were significantly down-regulated in the SDQSS group compared with the DHS group. ROC curve analysis showed that (S)-3-methyl-

2-oxopentanoic acid, neocembrene, 1-aminocyclopropanecarboxylic acid, 3-methyl-3-hydroxypentanedioate, and nicotine were symbolic differential metabolites with higher predictive power. The top five enrichment signalling pathways were valine, leucine and isoleucine biosynthesis; lysosome; nicotine addiction; fructose and mannose metabolism; and pertussis.

**Conclusion:** Our study identifies the differential metabolites and characteristic metabolic pathways among CRC patients with SDQSS or DHS, offering the possibility of accurate and objective syndrome differentiation and TCM treatment for CRC patients.

#### KEYWORDS

colorectal cancer (CRC), metabolomics, liquid chromatography-mass spectrometry (LC-MS), damp-heat syndrome (DHS), spleen-deficiency and qi-stagnation syndrome (SDQSS)

## Introduction

Colorectal cancer (CRC) is one of the most common malignant tumors, with the third highest incidence and the second highest mortality rates in the world (1). According to *Cancer Statistics in China, 2015* (2), the age-standardized morbidity and mortality rates of CRC in China were 17.81/100 000 and 8.12/100 000, ranking fourth and fifth, respectively. At present, the treatment options of CRC mainly include surgical resection, systemic chemotherapy, molecular targeted therapy, and immunotherapy. Radiation therapy with or without chemotherapy is used to treat rectal cancer (3). Due to the advance of diagnostic and treatment techniques of CRC, the long-term prognosis and quality of life of these patients are greatly improved. It has been reported that traditional Chinese medicine (TCM) treatment can inhibit tumor metastasis and growth (4, 5), accelerate postoperative rehabilitation (6), reduce postoperative complications (7), and decrease the side effects of chemotherapy in malignancies (8).

TCM is a unique medical theoretical system in China, and its therapeutic effect has been proved in clinical practice. Syndrome differentiation is the characteristic and foundation of disease diagnosis and treatment in TCM. *The Diagnosis and Treatment Guideline of Malignant Tumors Using TCM* issued by the Chinese Society of Traditional Chinese Medicine (2008 Edition) classifies TCM syndromes as 6 subtypes (9): spleen-deficiency and qi-stagnation syndrome (SDQSS), blood stasis and poison obstruction syndrome (SPOS), damp-heat syndrome (DHS), qi and blood deficiency syndrome (QBDS), spleen and kidney yang deficiency syndrome (SKYDS) and liver and kidney yin deficiency syndrome (LKYDS). Different TCM syndromes reflect various pathological features and stages of a certain disease. Conventional syndrome differentiation is mainly depended on the subjective judgment of the attending TCM physician, lacking the support of objective indicators.

Metabolomics is an integral part of systemic biology, which is a method of quantitative analysis of all metabolites in organisms

and the relative relationship between metabolites and pathophysiological changes (10). In recent years, metabolomics plays an increasingly important role in TCM syndrome differentiation of various diseases, which shows promising value in the investigation of biological essence of TCM syndromes (11). Metabolomics can be used to identify symbolic metabolic biomarkers distinctive of different TCM syndromes. Nowadays, the commonly used analytical platforms of metabolomics are comprised of nuclear magnetic resonance (NMR), mass spectrometry, high performance liquid chromatography (HPLC) and their coupling technologies, such as liquid chromatography-mass spectrometry (LC-MS), gas chromatography-mass spectrometry (GC-MS) (12, 13).

In this study, LC-MS was used to detect the serum metabolic components of CRC patients with TCM syndromes of SDQSS or DHS. We analyzed the differential metabolites of CRC patients with SDQSS or DHS by multivariate statistical analysis and receiver operating characteristic (ROC) curve analysis, and identified the significant enrichment metabolic pathways. This study provides an objective reference for syndrome differentiation and TCM treatment of CRC.

## Materials and methods

### Ethical statement

This prospective cohort study was conducted in according to the ethical guidelines of Declaration of Helsinki (as revised in 2013). This study was approved by the Medical Ethics Committee of The 940th Hospital of Joint Logistics Support Force of Chinese People's Liberation Army (approval number: 2020KYL075). Individual written informed consent was obtained from all patients. Patients' personal information have been anonymized to protect the privacy of patients.

## Patients

Patients with pathologically diagnosed CRC who were admitted to the 940th Hospital of Joint Logistics Support Force of Chinese People's Liberation Army from May 2020 to January 2021 were consecutively enrolled. These patients were divided into the SDQSS and DHS groups according to TCM syndrome differentiation. Patients' fasting peripheral venous blood was collected early in the morning and the serum was isolated and purified by centrifugation (1500 g, 10min, and 25°C) within 2h and stored at -80°C.

## Diagnostic criteria

The diagnostic criteria of CRC referred to the Chinese Colorectal Cancer Diagnosis and Treatment Guidelines (2020 edition) revised by the Chinese Society of Oncology (3). The TCM syndrome differentiation referred to the TCM Cancer Diagnosis and Treatment Guidelines (2008 edition) issued by the Chinese Association of TCM (9). The TCM syndrome of the patients was independently evaluated by two senior experts of the Department of TCM from our hospital. If the results were consistent, the TCM syndrome could be determined; otherwise, another physician participated in the differentiation until the correct TCM syndrome was obtained.

## Inclusion and exclusion criteria

The inclusion criteria included: (I) histopathologically diagnosed primary CRC; (II) age between 18 and 75 years; (III) patients' TCM syndrome classified as SDQSS or DHS; (IV) patients did not receive preoperative neoadjuvant chemotherapy or radiotherapy; and (V) patients had sufficient vital organ functions.

The exclusion criteria included: (I) patients with active infectious diseases, such as tuberculosis; (II) patients who had immunodeficiency diseases, such as AIDS; (III) cases with other benign colorectal diseases or those without pathological diagnosis of CRC; (IV) complete clinical data were not available; and (V) patients who were incapable to cooperate for syndrome differentiation.

## CRC serum sample preparation

400 µL of cold methanol was added into 100 µL of serum samples and then vortex mixed for 60s. The mixture was then centrifuged at 12000 rpm for 10min at 4°C. All supernatant from each sample was transferred and dried in vacuum. Then the supernatant was dissolved with 150 µL of 2-chlorobenzalanine and 80% methanol mixed solution; and was filtered with 0.22 µm membrane to obtain the prepared samples for LC-MS. 20 µL of each sample was mixed into QC samples to correct for systematic errors caused by the analytical instrument (14–17). The remaining samples were subjected to LC-MS detection (Panomix, Suzhou, China).

## Data processing and multivariate data analysis

The LC-MS data were processed using the Proteowizard software (version 3.0.8789) and the XCMS package from R (version 3.6.3). Multivariate data analysis was achieved on the normalized LC-MS datasets with software package SIMCA-P (version 13.0) and the R language ropls package. Principal component analysis (PCA), partial least squares discriminant analysis (PLS-DA) and orthogonal partial least squares discriminant analysis (OPLS-DA) models were constructed to overview the distribution of different samples. Variable importance in the projection (VIP) value >1, fold change (FC) value ≥3 or ≤0.333, and *P* value ≤0.05 (18) were combined used to identify the differential metabolites between the two groups. Furthermore, an area under the ROC curve (AUC) > 0.9 was applied to select symbolic metabolic biomarkers with good predictive performance. Metabolite set enrichment analysis (MSEA) was performed by using online software MetaboAnalyst 4.0 and the Kyoto Encyclopedia of Genes and Genomes (KEGG) database.

## Statistical analysis

For continuous clinical data with normal distributions, means with standard deviation (SD) were shown, and the student's *t* test was used to compare the differences. For skewed distributed continuous variables, medians with interquartile range (IQR) were expressed, and Mann-Whitney *U* test was used to compare the differences. Categorical data were exhibited as numbers and percentages, and compared using chi-square test or Fisher's exact test as appropriate. Statistical significance was set as a *P* value less than 0.05 (two-tailed). SPSS version 24.0 software (SPSS Inc., Chicago, IL) was used for statistical analysis.

## Results

### Baseline clinicopathological characteristics of the SDQSS and DHS groups

As shown in [Supplementary Figure 1](#), a total of 60 CRC patients with qualified serum samples, including 30 patients in the SDQSS group and 30 patients in the DHS group, were enrolled in this study. The baseline clinicopathological characteristics of the SDQSS and DHS groups of CRC patients are shown in [Table 1](#), including sex, age, body mass index (BMI), primary site of CRC, tumor differentiation degree and pathological stage, carcinoembryonic antigen (CEA), carbohydrate antigen 19-9 (CA199), hemoglobin (HGB), red blood cell (RBC), white blood cell (WBC), platelet counts, alanine aminotransferase (ALT), aspartate aminotransaminase (AST), albumin (ALB), total bilirubin (TBil), blood urea nitrogen (BUN), and serum creatinine (Scr). The level of ALT was marginally significantly higher in the DHS group than the SDQSS



TABLE 1 Clinicopathological characteristics of CRC patients with SDQSS or DHS.

Characteristics	SDQSS (n=30)	DHS (n=30)	P value
Sex			0.052
Male	17 (56.6%)	24 (80.0%)	
Female	13 (43.3%)	6 (20.0%)	
Age, years			0.196
≤ 65	12 (40.0%)	17 (56.7%)	
> 65	18 (60.0%)	13 (43.3%)	
BMI, kg/m <sup>2</sup>			0.271
≤ 24	18 (60.0%)	16 (53.3%)	
> 24	12 (40.0%)	14 (46.7%)	
Primary site			0.592
Colon	12 (40.0%)	10 (33.3%)	
Rectum	18 (60.0%)	20 (66.7%)	
Differentiation degree			0.100
Low	2 (6.7%)	8 (26.7%)	
Middle	26 (86.7%)	21 (70.0%)	
High	2 (6.7%)	1 (3.3%)	
pathological stage			0.073
I	1 (3.3%)	4 (13.3%)	
II	16 (53.3%)	8 (26.7%)	
III	9 (30.0%)	16 (53.3%)	
IV	4 (13.3%)	2 (6.7%)	
CEA, ng/ml			0.371
≤ 5	24 (80.0%)	21 (70.0%)	
>5	6 (20.0%)	9 (30.0%)	
CA19-9, U/ml			1.000
≤ 37	26 (86.7%)	26 (86.7%)	
>37	4 (13.3%)	4 (13.3%)	
HGB, g/L	135.5 (120.0–140.0)	137.0 (110.5–154.3)	0.589
RBC, 10 <sup>12</sup> /L	4.45 ± 0.34	4.41 ± 0.59	0.744
WBC, 10 <sup>9</sup> /L	5.89 ± 1.72	6.34 ± 2.11	0.369
PLT, 10 <sup>9</sup> /L	195.6 ± 69.9	207.6 ± 74.8	0.522
ALT, U/L	12.6 ± 6.1	16.5 ± 8.8	0.051
AST, U/L	14.0 (12.75–17.00)	16.0 (13.00–18.25)	0.229
ALB, g/L	38.3 ± 2.8	38.7 ± 3.7	0.667
TBil, umol/L	9.0 (6.60–12.63)	10.7 (7.15–14.33)	0.773
BUN, mmol/L	5.1 (4.18–6.65)	5.8 (4.38–7.45)	0.549
Scr, umol/L	69.5 (62.75–73.0)	72.5 (64.75–84.75)	0.124

CRC, colorectal cancer; DHS, damp-heat syndrome; SDQSS, spleen deficiency and Qi stagnation syndrome; BMI, body mass index; CEA, carcinoembryonic antigen; CA19-9, carbohydrate antigen 19-9; HGB, hemoglobin; RBC, red blood cell; WBC, white blood cell; PLT, platelet; ALT, alanine aminotransferase; AST, aspartate aminotransferase; ALB, albumin; TBil, total bilirubin; BUN, blood urea nitrogen; Scr, serum creatinine.

group ( $P = 0.051$ ). The other baseline clinicopathological characteristics were all comparable between the two groups.

## Quality control (QC)

Theoretically, all QC samples were identical, but systematic errors in the process of sample extraction, detection and analysis were unavoidable, which would lead to potential differences among QC samples. As shown in [Supplementary Figure 2](#), the QC samples on PCA score plots of positive and negative ion modes were clustered with good repeatability, which indicated that the data were reliable and the database building system was stable.

## PCA and PLS-DA analysis of metabolomics profiles in the SDQSS and DHS groups of CRC patients

Principal component analysis (PCA) reflects the original state of metabolomic data. The aggregation and dispersion degree of samples can be observed from PCA score plots. As shown in [Figure 1](#), the spatial distribution of principal components in metabolic spectra of SDQSS and DHS was discrete. The results demonstrated that there were obvious differences in serum metabolites between the two TCM syndrome groups.

PLS-DA can specify and group the samples during analysis, and can discriminate the differences in various samples more sensitively. As shown in PLS-DA score plot ([Figure 2A](#)), a significant separation of dots in different colors was observed, which also indicated significant differences existed in serum metabolic spectrum between the two groups.

In order to confirm there was no overfitting in the PLS-DA model, a permutation test was conducted. As shown in [Figure 2B](#), all blue Q2 points from the leftmost were lower than the rightmost original blue Q2 point, indicating that there was no overfitting in the PLS-DA model, and it could be used to identify the differentially expressed metabolites and the related metabolic pathways.

## Identification of differential metabolites among the SDQSS and DHS samples

A total of 3309 metabolites were identified by LC-MS analysis, of which 2775 were up-regulated and 534 were down-regulated. According to the selection criteria, 23 differential metabolites were screened out, among which 16 were significantly up-regulated and 7 were significantly down-regulated in the SDQSS group compared with the DHS group ([Table 2](#)). In addition, 5 differential metabolites with high predictive accuracy and diagnostic power were selected ( $AUC > 0.9$ ), including (S)-3-methyl-2-oxopentanoic acid, neocembrene, 1-aminocyclopropanecarboxylic acid, 3-methyl-3-hydroxypentanedioate, and nicotine. Among them, nicotine is the landmark metabolite of the DHS group, and (S)-3-methyl-2-oxopentanoic acid, neocembrene, 1-aminocyclopropanecarboxylic acid, 3-methyl-3-hydroxypentanedioate are the landmark metabolites of the SDQSS group. The box plots and ROC curves of these 5 metabolites are exhibited in [Figure 3](#).

## Hierarchical clustering and metabolic pathways

Hierarchical clustering is commonly used for unsupervised clustering. It is performed when taking the relative contents of metabolites under different experimental conditions as metabolic levels. The results showed that CRC patients with SDQSS or DHS syndrome could be distinguished well ([Figure 4](#)).

The possible metabolic pathways pertaining to CRC with SDQSS or DHS were analyzed with MetaboAnalyst 4.0, a free online metabolomics analysis platform on the basis of high-throughput KEGG metabolic pathways database. The pathway impact value was calculated by pathway topology analysis. For SDQSS versus DHS, the top 5 potential enrichment signalling pathways were valine, leucine and isoleucine biosynthesis; lysosome; nicotine addiction; fructose and mannose metabolism; and pertussis ([Figure 5](#)).

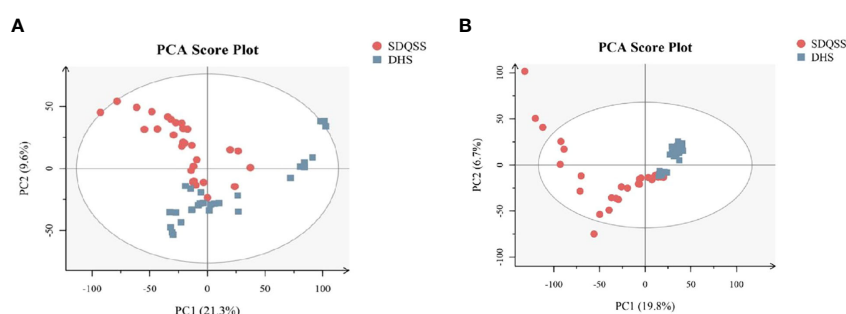


**FIGURE 1**  
PCA score plots of the SDQSS and DHS groups. **(A)** PCA in positive ion mode; **(B)** PCA in negative ion mode. PCA, principal component analysis; SDQSS, spleen-deficiency and qi-stagnation syndrome; DHS, damp-heat syndrome.

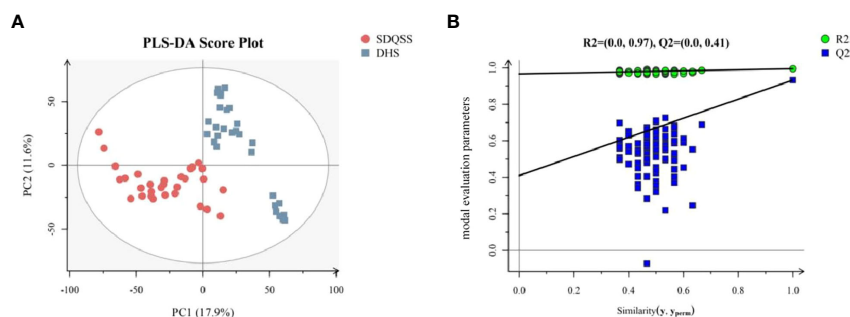


FIGURE 2

(A) PLS-DA score plots of the SDQSS and DHS groups; (B) PLS-DA permutation plot. In Figure 2B, the X-axis represents the similarity between the real grouping of samples and 100 random grouping, and the Y-axis indicates the model evaluation parameters. The cross-validation of PLS-DA permutation model mainly refers to parameters such as R2X, R2Y, and Q2. R2X is the interpretability of model X variable (independent variable), R2Y is the interpretability of model Y variable (dependent variable), and Q2 is the predictability of the model. Points R2 and Q2 in the upper right corner of Figure 2B represent the model parameters of real grouping. Usually, it is better when R2 and Q2 are both larger than 0.5, and the maximum values of R2 and Q2 are 1. When the R2 value is small, it means that the repeatability in the test set is poor (the background noise is high); when the Q2 value is small, it indicates that there is high background noise in the test set, or the model has more outlier. Permutation plot can help to effectively evaluate whether the PLS-DA model is over-fitted. The judging criteria are one of the follows: ① all blue Q2 points are lower than the rightmost original blue Q2 point from left to right; ② the intersection of the regression line at Q2 in the Y-axis is less than or equal to 0. PLS-DA, partial least squares discriminate analysis; SDQSS, spleen-deficiency and qi-stagnation syndrome; DHS, damp-heat syndrome.

TABLE 2 Differential metabolites in the serum of CRC patients with SDQSS compared with those with DHS.

Metabolite	VIP	FC	P value	FDR	Regulation direction	AUC	CI1	CI2	specificity	sensitivity
(S)-3-Methyl-2-oxopentanoic acid	1.97	4.63	3.45E-10	5.28E-08	up	<b>0.978</b>	0.936	0.995	0.87	0.93
Neocembrene	1.15	437.66	1.65E-09	1.51E-07	up	<b>0.924</b>	0.861	0.996	0.87	1.00
1-Aminocyclopropanecarboxylic acid	1.42	3.15	4.31E-08	1.81E-06	up	<b>0.914</b>	0.834	0.962	0.90	0.90
3-Methyl-3-hydroxypentanedioate	1.95	3.01	8.35E-08	2.96E-06	up	<b>0.915</b>	0.809	0.983	0.87	0.87
Triacetate lactone	1.64	4.19	2.87E-06	4.60E-05	up	0.857	0.774	0.933	0.90	0.73
Erucic acid	1.10	3.89	5.86E-06	8.07E-05	up	0.851	0.769	0.936	0.87	0.73
5-Methyl-2-furancarboxaldehyde	1.53	3.88	9.51E-06	1.17E-04	up	0.846	0.726	0.908	0.67	0.80
6-Acetyl-D-glucose	1.42	3.64	8.56E-04	3.83E-03	up	0.76	0.58	0.855	0.67	0.73
Coniferyl alcohol	1.41	3.58	1.00E-03	4.34E-03	up	0.746	0.634	0.889	0.67	0.77
(S)-beta-Tyrosine	1.46	4.52	1.68E-03	6.41E-03	up	0.76	0.68	0.844	0.63	0.83
D-erythro-3-Methylmalate	1.03	3.30	1.77E-03	6.68E-03	up	0.747	0.605	0.851	0.67	0.77
4-Hydroxycinnamic acid	1.67	3.07	7.30E-04	3.37E-03	up	0.934	0.87	0.975	0.83	0.90

(Continued)

TABLE 2 Continued

Metabolite	VIP	FC	P value	FDR	Regulation direction	AUC	CI1	CI2	specificity	sensitivity
9-OxoODE	1.75	3.85	7.60E-07	9.95E-06	up	0.889	0.772	0.939	0.87	0.87
L-Aspartate-semialdehyde	1.61	3.61	2.00E-06	2.06E-05	up	0.859	0.74	0.966	0.77	0.87
5-Aminopentanoic acid	1.07	4.14	7.74E-06	6.06E-05	up	0.842	0.759	0.927	0.80	0.80
D-Sorbose	1.00	3.18	8.56E-04	2.86E-03	up	0.753	0.622	0.864	0.60	0.83
4-Pyridoxic acid	1.89	0.19	1.04E-04	7.40E-04	down	0.802	0.664	0.896	0.93	0.77
Mannitol 1-phosphate	1.52	0.15	2.68E-04	1.57E-03	down	0.758	0.593	0.88	0.97	0.73
Nicotinic acid	1.65	0.29	6.90E-04	3.24E-03	down	0.756	0.628	0.856	0.77	0.73
O-Acetylcarnitine	1.65	0.14	1.68E-03	6.41E-03	down	0.737	0.602	0.858	0.87	0.70
Nicotine	1.65	0.06	5.97E-09	3.11E-07	down	<b>0.938</b>	0.886	0.983	0.97	0.87
D-Mannose	1.46	0.28	2.18E-05	1.39E-04	down	0.826	0.741	0.914	0.83	0.73
Gluconolactone	1.29	0.27	2.01E-04	8.52E-04	down	0.783	0.629	0.867	0.93	0.67

CRC, colorectal cancer; DHS, damp-heat syndrome; SDQSS, spleen deficiency and Qi stagnation syndrome; VIP, variable importance in the projection; FC, fold change; FDR, false discovery rate; AUC: The area under receiver operating characteristic (ROC) curves; CI1: the lower limit of 95% confidence interval; CI2: the upper limit of 95% confidence interval. AUC in bold denotes values > 0.9.

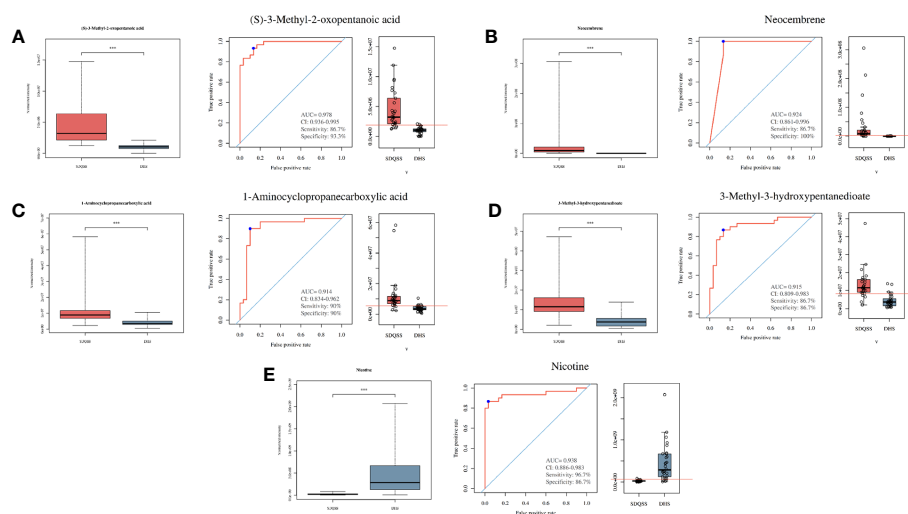
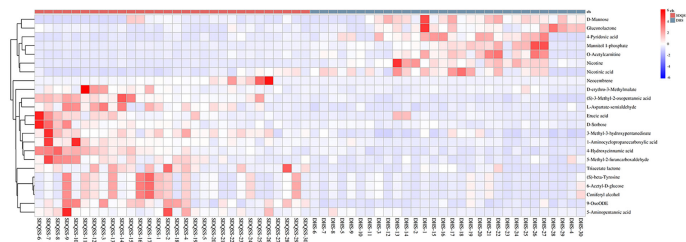


FIGURE 3

Box plots and ROC curves of 5 selected differential metabolites with AUC > 0.9. (A) (S)-3-methyl-2-oxopentanoic acid; (B) neocembrene; (C) 1-aminocyclopropanecarboxylic acid; (D) 3-methyl-3-hydroxypentanedioate; (E) nicotine. ROC, receiver operating characteristic; AUC, the area under the ROC curve; CI, confidence interval; SDQSS, spleen-deficiency and qi-stagnation syndrome; DHS, damp-heat syndrome.



**FIGURE 4**  
Hierarchical clustering heat map of differential metabolites between the SDQSS and DHS groups. SDQSS, spleen-deficiency and qi-stagnation syndrome; DHS, damp-heat syndrome.

Discussion

CRC is one of the most common malignant tumors and its incidence and mortality rates are gradually increasing in the world (1). At present, the diagnosis and treatment of CRC have developed rapidly, and the prognosis of these patients has greatly improved. TCM is a unique and long recognized theoretical system in China. TCM has been widely used as part of adjuvant therapy and comprehensive treatment for malignancies in clinical practice. The advantages of integrating TCM and Western medicine are becoming increasingly obvious, such as relief of postoperative pain, accelerating postoperative rehabilitation, and reduction of chemotherapeutic side effects. Syndrome differentiation is the foundation of TCM treatment, and the accuracy of syndrome differentiation can be interfered because of the subjectivity of attending doctors. Thus, accurate differentiation of TCM syndromes based on objective materials and quantitative biomarkers is particularly important.

TCM holds that CRC is caused by a series of internal and external negative factors, such as deficiency of vital Qi, weakness of spleen and stomach, external evils invasion, anxiety and depression, or improper diet, all of which lead to endogenous dampness and heat, qi stagnation, blood stasis and toxin stagnation. DHS and SDQSS are two basic TCM syndromes of CRC. DHS is the characteristic TCM syndrome type of early stage of CRC, with clinical manifestations of abdominal distension, mucous bloody

stool, red tongue, yellow and greasy fur, and slippery pulse. SDQSS belongs to the TCM syndrome type of relatively advanced stage of CRC. Clinically, it is mainly manifested as abdominal pain, anorexia, mental fatigue, sallow complexion, thin stool, pale tongue, thin and greasy fur, and thready pulse. There is great implications to discriminating these two TCM syndromes in clinical practice, because the TCM treatment approaches mainly depend on CRC patients' syndrome types.

Recently, an increasing number of studies have applied metabolomics to distinguish TCM syndromes of different diseases. Jiang et al. (19) used nuclear magnetic resonance (NMR) to analyze the plasma metabolites of diabetic patients with kidney-yin deficiency syndrome (KYDS), and found that the levels of creatinine, citric acid, trimethylamine oxide, phenylalanine and tyrosine were decreased, whereas the levels of alanine, glycine and taurine were increased, which can be used as the landmark metabolites for the diagnosis of KYDS. Chen et al. (20) found that phlegm-dampness stasis syndrome (PDSS) was mainly attributed to the accumulation of harmful metabolites, while LKYDS was mainly caused by the lack of protective metabolites. The serum metabolic patterns in cellular oxidation, inflammatory reaction and energy metabolism of these two syndromes were significantly different.

In this study, the clinicopathological characteristics of CRC patients in the SDQSS and DHS groups were compared. A

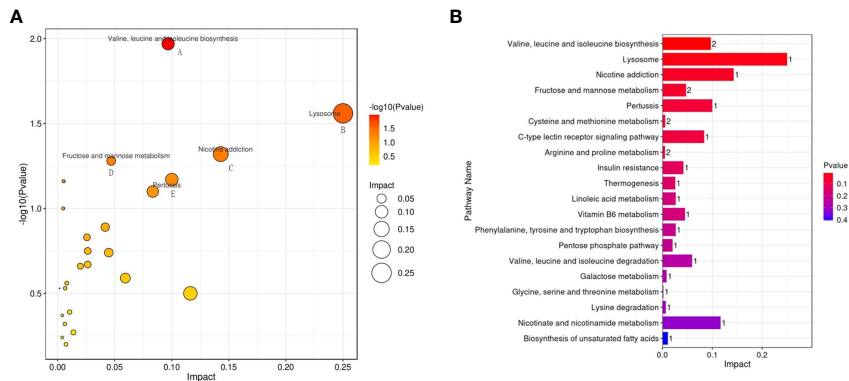


**FIGURE 5**  
Bubble diagram (A) and bar chart (B) of enriched metabolic pathways of the SDQSS and DHS groups. SDQSS, spleen-deficiency and qi-stagnation syndrome; DHS, damp-heat syndrome.



marginally significant increase of ALT was observed in the DHS group compared with the SDQSS group ( $P = 0.051$ ). Next, we used LC-MS to analyze the metabolic profiles of serum samples from CRC patients with SDQSS or DHS TCM syndrome. In our study, 23 differential metabolites were identified in the two groups. ROC curve analysis of these differential metabolites showed that areas under the ROC curves (AUC) of (S)-3-methyl-2-oxopentanoic acid, neocembrene, 1-aminocyclopropanecarboxylic acid, 3-methyl-3-hydroxypentanedioate, and nicotine were larger than 0.9, which indicated these metabolites were sensitive and specific serum biomarkers to distinguish CRC patients with SDQSS from those with DHS.

The characteristic differential metabolite with the highest discrimination ability for CRC with DHS was nicotine, which was markedly upregulated in patients with DHS compared with those with SDQSS. It was reported that 4-(methylnitrosamine)-1-(3-pyridine)-1-butanone (NNK) derived from nicotine could promote the formation of cell spheres and increase the expression of cell surface markers CD44, OCT4, C-MYC and NANOG in HCT8 and DLD-1 cells (21), while exposure to NNK could significantly enhance the proliferation and growth ability of CRC cells. Nicotine could promote the growth and metastasis of CRC through downregulation of miR-200c (21); it could also stimulate the invasion and metastasis of colon cancer cells *in vitro* by activating the downstream signalling pathways of nAChRs and p38 MAPK (22, 23). Thus, the remarkable increase of serum nicotine level in CRC patients with DHS syndrome can reflect a high risk of postoperative recurrence and metastasis. Regular monitoring of serum nicotine level in CRC patients with DHS may assist early detection of tumor recurrence and metastasis in clinical practice.

The characteristic differential metabolite that was significantly upregulated in the SDQSS group was 4-hydroxycinnamic acid, an important polyphenol in the plant manganese-containing acid biosynthetic pathway, mainly found in cereals, fruits and vegetables (24). This compound has a range of beneficial pharmacological properties, including powerful antioxidant, anti-inflammatory, anti-ulcer (25), and anti-cancer effects (26). Neog et al. (27) found that the anti-inflammatory effects of hydroxycinnamic acid were mediated through inhibition of inflammation-related proteins including nuclear factor kappa B (NF- $\kappa$ B), inducible nitric oxide synthase (iNOS) and cyclooxygenase-2 (COX-2). Ko et al. (28) investigated the effects of 4-hydroxycinnamic acid on the inflammatory response in asthma using an allergic asthma mouse model. They found that 4-hydroxycinnamic acid reduced the levels of IL-5 and IL-13 in bronchoalveolar lavage fluid (BALF), alleviated airway inflammation and mucus overproduction induced by ovalbumin exposure. In addition, 4-hydroxycinnamic acid could inhibit the increased levels of NF- $\kappa$ B, iNOS and COX-2, and also reduced matrix metalloproteinase-9 (MMP-9) activity and protein levels (28). The elevated 4-hydroxycinnamic acid level may indicate a better anti-inflammatory effect in CRC patients with SDQSS compared to patients with DHS.

On the other hand, in this study, 5 classical metabolic pathways related to 23 discriminating metabolites were found in the SDQSS

and DHS groups. These pathways suggest that severe metabolic disturbances occur during the development and progression of CRC with different TCM syndromes. The enrichment of these signalling pathways may correlate with these syndrome types.

Several limitations of our study should be acknowledged. First, the sample size of our study is insufficient. Only 30 samples were enrolled in each of the two groups, which is not large enough for the confirmative association between metabolic profiles and various TCM syndromes in CRC patients. With the sample size increased beyond 60 patients, the variables with marginally significant difference, such as ALT and pathological stage, may become statistically significantly different; hence, proper sample collection practices are needed to avoid confounding effects. Second, the detailed mechanisms underlying changes of metabolites in different CRC syndromes should be deciphered with the integration of transcriptomics and proteomics. Third, healthy participants were not included as baseline control. Last, there is a lack of metabolic profiling analysis of tumor tissues from CRC patients with different syndromes.

## Conclusion

Our study identifies the differential metabolites and characteristic metabolic pathways of CRC patients with SDQSS or DHS, TCM syndrome offering the possibility of accurate and objective syndrome differentiation and TCM treatment for CRC patients. Nevertheless, the results of this study need to be verified by further research.

## Data availability statement

The raw data supporting the conclusions of this article will be made available by the authors, without undue reservation.

## Ethics statement

The studies involving humans were approved by the Medical Ethics Committee of The 940th Hospital of Joint Logistics Support Force of Chinese People's Liberation Army (approval number: 2020KYL075). The studies were conducted in accordance with the local legislation and institutional requirements. The participants provided their written informed consent to participate in this study.

## Author contributions

Conceptualization and design: MZ and FG; Administrative support and funding acquisition: FG; Provision of study materials or patients: HT, M-BG, Y-NW, Z-JY, Z-QY, MX, and W-QW; Collection and assembly of data: MZ, HT, M-BG, Y-NW, and Z-JY; Data analysis and interpretation: MZ, Y-SZ, and J-KF; Manuscript writing and editing: MZ, Y-SZ, and J-KF. All authors contributed to the article and approved the submitted version.

## Funding

This work was supported by Natural Science Foundation of Gansu Province (20YF8FA098), the Fundamental Research Funds for the Central Universities of Northwest Minzu University (331920200016), and Science and Technology Planning Project of Gansu Province (23JRRA539).

## Acknowledgments

We would like to acknowledge Suzhou PANOMIX Biomedical Tech Co., Ltd. for providing metabolomics analysis.

## Conflict of interest

The authors declare that the research was conducted in the absence of any commercial or financial relationships that could be construed as a potential conflict of interest.

## References

- Sung H, Ferlay J, Siegel RL, Laversanne M, Soerjomataram I, Jemal A, et al. Global cancer statistics 2020: GLOBOCAN estimates of incidence and mortality worldwide for 36 cancers in 185 countries. *CA Cancer J Clin* (2021) 71(3):209–49. doi: 10.3322/caac.21660
- Chen W, Zheng R, Baade PD, Zhang S, Zeng H, Bray F, et al. Cancer statistics in China, 2015. *CA: A Cancer J Clin* (2016) 66(2):115–32. doi: 10.3322/caac.21338
- National Health Commission of the People's Republic of China. Chinese protocol of diagnosis and treatment of colorectal cancer (2020 edition). *Zhonghua Wai Ke Za Zhi* (2020) 58(8):561–85. doi: 10.3760/cma.j.cn112139-20200518-00390
- Wang K, Chen Q, Shao Y, Yin S, Liu C, Liu Y, et al. Anticancer activities of TCM and their active components against tumor metastasis. *BioMed Pharmacother* (2021) 133:111044. doi: 10.1016/j.biopha.2020.111044
- Lv J, Jia Y, Li J, Kuai W, Li Y, Guo F, et al. Gegen Qinlian decoction enhances the effect of PD-1 blockade in colorectal cancer with microsatellite stability by remodelling the gut microbiota and the tumour microenvironment. *Cell Death Dis* (2019) 10(6):415. doi: 10.1038/s41419-019-1638-6
- Cao LX, Chen ZQ, Jiang Z, Chen QC, Fan XH, Xia SJ, et al. Rapid rehabilitation technique with integrated traditional Chinese and Western medicine promotes postoperative gastrointestinal function recovery. *World J Gastroenterol* (2020) 26(23):3271–82. doi: 10.3748/wjg.v26.i23.3271
- Tan KY, Liu CB, Chen AH, Ding YJ, Jin HY, Seow-Choen F. The role of traditional Chinese medicine in colorectal cancer treatment. *Tech Coloproctol* (2008) 12(1):1–6. doi: 10.1007/s10151-008-0392-z
- Liu N, Wu C, Jia R, Cai G, Wang Y, Zhou L, et al. Traditional Chinese medicine combined with chemotherapy and cetuximab or bevacizumab for metastatic colorectal cancer: A randomized, double-blind, placebo-controlled clinical trial. *Front Pharmacol* (2020) 11:478. doi: 10.3389/fphar.2020.00478
- Chinese Society of Traditional Chinese Medicine. *Guidelines for TCM Diagnosis and Treatment of Cancer*. Beijing: China Traditional Chinese Medicine Press (2008) p. 25–9.
- Fiehn O. Combining genomics, metabolome analysis, and biochemical modelling to understand metabolic networks. *Comp Funct Genomics* (2001) 2(3):155–68. doi: 10.1002/cfg.82
- Wang X, Sun H, Zhang A, Sun W, Wang P, Wang Z. Potential role of metabolomics approaches in the area of traditional Chinese medicine: as pillars of the bridge between Chinese and Western medicine. *J Pharm BioMed Anal* (2011) 55(5):859–68. doi: 10.1016/j.jpba.2011.01.042
- Nicholson JK, Lindon JC, Holmes E. 'Metabonomics': understanding the metabolic responses of living systems to pathophysiological stimuli via multivariate statistical analysis of biological NMR spectroscopic data. *Xenobiotica* (1999) 29(11):1181–9. doi: 10.1080/004982599238047
- Vorkas PA, Abellona UM, Li JV. Tissue multiplatform-based metabolomics/metabonomics for enhanced metabolome coverage. *Methods Mol Biol* (2018) 1738:239–60. doi: 10.1007/978-1-4939-7643-0\_17
- Demurtas A, Pescina S, Nicoli S, Santi P, Ribeiro de Araujo D, Padula C. Validation of a HPLC-UV method for the quantification of budesonide in skin layers. *J chromatogr B Anal Technol Biomed Life Sci* (2021) 1164:122512. doi: 10.1016/j.jchromb.2020.122512
- Abdelhafez OH, Othman EM, Fahim JR, Desoukey SY, Pimentel-Elardo SM, Nodwell JR, et al. Metabolomics analysis and biological investigation of three Malvaceae plants. *Phytochem Anal* (2020) 31(2):204–14. doi: 10.1002/pca.2883
- Monnerat G, Seara FAC, Evaristo JAM, Carneiro G, Evaristo GPC, Domont G, et al. Aging-related compensated hypogonadism: Role of metabolomic analysis in physiopathological and therapeutic evaluation. *J Steroid Biochem Mol Biol* (2018) 183:39–50. doi: 10.1016/j.jsbmb.2018.05.005
- Smith CA, Want EJ, O'Maille G, Abagyan R, Siuzdak G. XCMS: processing mass spectrometry data for metabolite profiling using nonlinear peak alignment, matching, and identification. *Anal Chem* (2006) 78(3):779–87. doi: 10.1021/ac051437y
- Kieffer D, Piccolo B, Vaziri N, Vaziri N, Lau WL, Khazaeli M, et al. Resistant starch alters gut microbiome and metabolomic profiles concurrent with amelioration of chronic kidney disease in rats. *Am J Physiol Renal Physiol* (2016) 310(9):F857–871. doi: 10.1152/ajprenal.00513.2015
- Jiang N, Liu HF, Li SD, Zhou WX, Zhang YX, Zhang Q, et al. An integrated metabolomic and proteomic study on Kidney-Yin Deficiency Syndrome patients with diabetes mellitus in China. *Acta Pharmacol Sin* (2015) 36(6):689–98. doi: 10.1038/aps.2014.169
- Chen J, Ye C, Hu X, Huang C, Yang Z, Li P, et al. Serum metabolomics model and its metabolic characteristics in patients with different syndromes of dyslipidemia based on nuclear magnetic resonance. *J Pharm BioMed Anal* (2019) 167:100–13. doi: 10.1016/j.jpba.2018.12.042
- Lei Z, Xiaomin Y, He H, Jian C, Xiaowu X. Nicotine downregulates microRNA-200c to promote metastasis and the epithelial-mesenchymal transition in human colorectal cancer cells. *J Cell Physiol* (2019) 234(2):1369–79. doi: 10.1002/jcp.26933
- Xiang T, Fei R, Wang Z, Shen Z, Qian J, Chen W. Nicotine enhances invasion and metastasis of human colorectal cancer cells through the nicotinic acetylcholine receptor downstream p38 MAPK signaling pathway. *Oncol Rep* (2016) 35(1):205–10. doi: 10.3892/or.2015.4363
- Fu Y, Zhang Y, Cui J, Yang G, Peng S, Mi W, et al. SNP rs12982687 affects binding capacity of lncRNA UCA1 with miR-873-5p: involvement in smoking-triggered colorectal cancer progression. *Cell Commun Signal* (2020) 18(1):37. doi: 10.1186/s12964-020-0518-0

## Publisher's note

All claims expressed in this article are solely those of the authors and do not necessarily represent those of their affiliated organizations, or those of the publisher, the editors and the reviewers. Any product that may be evaluated in this article, or claim that may be made by its manufacturer, is not guaranteed or endorsed by the publisher.

## Supplementary material

The Supplementary Material for this article can be found online at: <https://www.frontiersin.org/articles/10.3389/fonc.2023.1190706/full#supplementary-material>

### SUPPLEMENTARY FIGURE 1

Study design and patients enrollment. DHS, damp-heat syndrome; SDQSS, spleen-deficiency and qi-stagnation syndrome.

### SUPPLEMENTARY FIGURE 2

PCA score plots of QC samples. (A) PCA in positive ion mode; (B) PCA in negative ion mode. PCA, principal component analysis; QC, quality control.

24. Alam MA, Subhan N, Hossain H, Hossain M, Reza HM, Rahman MM, et al. Hydroxycinnamic acid derivatives: a potential class of natural compounds for the management of lipid metabolism and obesity. *Nutr Metab (Lond)* (2016) 13:27. doi: 10.1186/s12986-016-0080-3
25. Barros MP, Lemos M, Maistro EL, Leite MF, Sousa JP, Bastos JK, et al. Evaluation of antiulcer activity of the main phenolic acids found in Brazilian Green Propolis. *J Ethnopharmacol* (2008) 120(3):372–7. doi: 10.1016/j.jep.2008.09.015
26. Sharma SH, Chellappan DR, Chinnaswamy P, Nagarajan S. Protective effect of p-coumaric acid against 1,2 dimethylhydrazine induced colonic preneoplastic lesions in experimental rats. *BioMed Pharmacother* (2017) 94:577–88. doi: 10.1016/j.biopha.2017.07.146
27. Neog MK, Joshua Pragasam S, Krishnan M, Rasool M. p-Coumaric acid, a dietary polyphenol ameliorates inflammation and curtails cartilage and bone erosion in the rheumatoid arthritis rat model. *Biofactors* (2017) 43(5):698–717. doi: 10.1002/biof.1377
28. Ko JW, Kwon HJ, Seo CS, Choi SJ, Shin NR, Kim SH, et al. 4-Hydroxycinnamic acid suppresses airway inflammation and mucus hypersecretion in allergic asthma induced by ovalbumin challenge. *Phytother Res* (2020) 34(3):624–33. doi: 10.1002/ptr.6553



## OPEN ACCESS

## EDITED BY

Gregorio Peron,  
University of Brescia, Italy

## REVIEWED BY

Zhi Tang,  
Guangdong Medical University, China  
Dawei Yang,  
Liaocheng People's Hospital, China

## \*CORRESPONDENCE

Jing Feng,  
✉ jing\_feng1985@163.com  
Lei Wang,  
✉ wangleiyes@sina.com

RECEIVED 20 September 2023

ACCEPTED 23 January 2024

PUBLISHED 07 February 2024

## CITATION

Ma S, He S, Liu J, Zhuang W, Li H, Lin C, Wang L,  
Feng J and Wang L (2024), Metabolomics  
unveils the exacerbating role of arachidonic  
acid metabolism in atherosclerosis.  
*Front. Mol. Biosci.* 11:1297437.  
doi: 10.3389/fmolb.2024.1297437

## COPYRIGHT

© 2024 Ma, He, Liu, Zhuang, Li, Lin, Wang, Feng  
and Wang. This is an open-access article  
distributed under the terms of the [Creative  
Commons Attribution License \(CC BY\)](#). The use,  
distribution or reproduction in other forums is  
permitted, provided the original author(s) and  
the copyright owner(s) are credited and that the  
original publication in this journal is cited, in  
accordance with accepted academic practice.  
No use, distribution or reproduction is  
permitted which does not comply with these  
terms.

# Metabolomics unveils the exacerbating role of arachidonic acid metabolism in atherosclerosis

Sai Ma<sup>1,2</sup>, Songqing He<sup>1,2</sup>, Jing Liu<sup>1,2</sup>, Wei Zhuang<sup>1,2</sup>, Hanqing Li<sup>1,2</sup>,  
Chen Lin<sup>1,2</sup>, Lijun Wang<sup>1,2</sup>, Jing Feng<sup>3,4\*</sup> and Lei Wang<sup>1,2\*</sup>

<sup>1</sup>Department of Cardiology, Jinling Hospital, Medical School of Nanjing University, Nanjing, China, <sup>2</sup>Department of Cardiology, The First School of Clinical Medicine, Southern Medical University, Nanjing, China, <sup>3</sup>Department of Emergency Medicine, Jinling Hospital, Medical School of Nanjing University, Nanjing, China, <sup>4</sup>Department of Emergency Medicine, The First School of Clinical Medicine, Southern Medical University, Nanjing, China

Atherosclerosis is a complex vascular disorder characterized by the deposition of lipids, inflammatory cascades, and plaque formation in arterial walls. A thorough understanding of its causes and progression is necessary to develop effective diagnostic and therapeutic strategies. Recent breakthroughs in metabolomics have provided valuable insights into the molecular mechanisms and genetic factors involved in atherosclerosis, leading to innovative approaches for preventing and treating the disease. In our study, we analyzed clinical serum samples from both atherosclerosis patients and animal models using laser desorption ionization mass spectrometry. By employing methods such as orthogonal partial least-squares discrimination analysis (OPLS-DA), heatmaps, and volcano plots, we can accurately classify atherosclerosis (AUC = 0.892) and identify key molecules associated with the disease. Specifically, we observed elevated levels of arachidonic acid and its metabolite, leukotriene B<sub>4</sub>, in atherosclerosis. By inhibiting arachidonic acid and monitoring its downstream metabolites, we discovered the crucial role of this metabolic pathway in regulating atherosclerosis. Metabolomic research provides detailed insights into the metabolic networks involved in atherosclerosis development and reveals the close connection between abnormal metabolism and the disease. These studies offer new possibilities for precise diagnosis, treatment, and monitoring of disease progression, as well as evaluating the effectiveness of therapeutic interventions.

## KEYWORDS

atherosclerosis, metabolomics, exacerbating role, metabolism, arachidonic acid

## 1 Introduction

Atherosclerosis, a widespread cardiovascular condition, exhibits a multifaceted and heterogeneous pathogenesis (Gao et al., 2016; Khambhati et al., 2018; Sharma et al., 2021). As a powerful investigative tool, Metabolomics has emerged to enhance our understanding and unravel the molecular mechanisms underlying atherosclerosis (Ren et al., 2016; Giunchi et al., 2019; Chen et al., 2021; Yang et al., 2021). Metabolomics encompasses a systematic approach that explores the metabolites within an organism, unravelling intricate associations between metabolites and diseases. This comprehensive methodology

provides profound insights into disease development and progression (Zhao et al., 2018; Tian et al., 2022; Xiao et al., 2022; Zhang et al., 2022). First, metabolomics offers comprehensive metabolic profiling by examining compositional and quantitative metabolite changes within cells, tissues, or organisms. This analytical technique unveils metabolic aberrations intimately linked to atherosclerosis, including lipid metabolism, glucose metabolism, amino acid metabolism, and other pivotal pathways crucial for comprehending atherosclerotic pathogenesis. Secondly, metabolomics analysis contributes to the identification and discovery of prospective biomarkers. Early diagnosis of atherosclerosis is of utmost importance, yet conventional clinical examination techniques have limitations. Through metabolomics research, we strive to ascertain metabolic biomarkers associated with atherosclerosis, refining the precision and sensitivity of early diagnosis. This pursuit facilitates early intervention and treatment opportunities for patients.

Matrix-assisted laser desorption/ionization (MALDI) represents an innovative metabolomics analysis approach that surpasses conventional methodologies such as liquid chromatography-mass spectrometry (LC-MS) and nuclear magnetic resonance (NMR) (Schubert and Kostrzewa, 2017; Calvano et al., 2018; Xu et al., 2019; Ashfaq et al., 2022). Initially, MALDI boasts high-throughput capabilities and exceptional sensitivity. Atherosclerosis, being a complex ailment characterized by diverse metabolic pathways and metabolites, necessitates rapid analysis of numerous samples (Ly et al., 2016; Moreno-Gordaliza et al., 2017; Duan et al., 2022). MALDI technology caters to this requirement, enabling high-throughput analysis and fostering a comprehensive understanding of metabolite composition and alterations. Furthermore, MALDI streamlines sample preparation by minimizing the steps involved in sample preprocessing. This reduction mitigates sample loss and variability, bolstering the reliability and repeatability of data. Secondly, MALDI exhibits an advantage in the analysis of small molecule metabolites. Atherosclerosis-related metabolic anomalies primarily involve small molecule metabolites such as lipid metabolites and glucose metabolites. Compared to LC-MS, MALDI excels in ionising and detecting small molecular compounds (Sun et al., 2016; Yan et al., 2017; Torata et al., 2018; Ferey et al., 2019). This attribute empowers the detection of metabolites at lower concentrations, amplifying the detection range and sensitivity of metabolites. In conclusion, MALDI, as a rapid, high-throughput, sensitive, and spatially-resolved metabolomics analysis technique, provides an effective tool for unravelling the molecular intricacies of atherosclerosis. It elucidates the associations between metabolic irregularities and disease progression, ultimately facilitating early diagnosis and treatment of atherosclerosis.

Arachidonic acid and its downstream leukotriene metabolites potentially play pivotal roles in atherosclerosis (Needleman et al., 1986; Piomelli, 1993; Zeldin, 2001). Arachidonic acid, a polyunsaturated fatty acid, generates leukotriene metabolites such as leukotriene B<sub>4</sub> (LTB<sub>4</sub>) and leukotrienes C<sub>4</sub>, D<sub>4</sub>, and E<sub>4</sub> (LTC<sub>4</sub>, LTD<sub>4</sub>, LTE<sub>4</sub>) through enzymatic catalysis (Bhatt et al., 2017; Gelfand, 2017; Wan et al., 2017). Firstly, these leukotriene metabolites exert substantial regulatory control over inflammatory reactions. Inflammation constitutes a pivotal process in atherosclerosis. The leukotriene metabolites LTC<sub>4</sub>,

LTD<sub>4</sub>, and LTE<sub>4</sub>, being potent inflammatory mediators, promote leukocyte adhesion, chemotaxis, and activation, exacerbating the inflammatory response (Gelfand, 2017; Wan et al., 2017). These inflammatory reactions, in turn, stimulate endothelial cell damage and release of inflammatory mediators, establishing a pernicious cycle that accelerates atherosclerosis progression. Secondly, leukotriene metabolites modulate platelet activation and aggregation, a crucial step in thrombus formation within atherosclerosis. The leukotriene metabolite LTB<sub>4</sub> stimulates platelet aggregation and releases platelet-activating factors, heightening the risk of thrombus formation (Bhatt et al., 2017; Gelfand, 2017; Wan et al., 2017). Platelet aggregation further intensifies endothelial damage and fosters an augmented inflammatory response, ultimately contributing to atherosclerosis development. Moreover, leukotriene metabolites influence the functionality of smooth muscle cells. Smooth muscle cell proliferation and migration are pivotal features in atherosclerotic lesion development. The leukotriene metabolites LTC<sub>4</sub>, LTD<sub>4</sub>, and LTE<sub>4</sub> facilitate smooth muscle cell proliferation and migration by binding to receptors on smooth muscle cells, leading to arterial wall thickening and plaque formation.

Hence, by employing metabolomics analysis utilizing MALDI technology, we conducted comprehensive investigations on clinical samples obtained from atherosclerosis patients and an animal model we constructed (Figures 1A,B). To uncover and analyze the metabolic alterations associated with atherosclerosis, we utilized the exceptional ionization and resolution capabilities of two-dimensional MXene materials. This advanced material, characterized by its unique two-dimensional structure, facilitated the efficient detection of small molecules involved in the metabolic processes of atherosclerosis (Figure 1C). This methodology enabled the identification of distinctive key metabolic pathways implicated in atherosclerosis. Employing strategies like volcano plots and heatmaps, we discerned potential metabolic molecules (Figure 1D). Collaborative screening analysis highlighted the critical involvement of the arachidonic acid pathway. Expanding upon the metabolomics findings, we quantitatively assessed the atherosclerotic effect of arachidonic acid by analyzing arachidonic acid inhibitors and downstream metabolites. Our aspiration is that this study provides meaningful insights into the diagnosis, treatment, and intervention of clinical atherosclerosis. Additionally, we believe that the integration of metabolomics with biological validation affords novel perspectives for researching various diseases, including cardiovascular ailments.

## 2 Materials and methods

### 2.1 Synthesis and characterization of Ti<sub>2</sub>AlN

The fabrication of Ti<sub>2</sub>AlN, a two-dimensional layered material, was accomplished through a sodium hydroxide etching process. This involved the reaction between 1 g of Ti<sub>2</sub>AlN material and 10 mL of 3M sodium hydroxide at a temperature of 40°C and a rotational speed of 500 RPM for 12 h. Subsequently, the synthesized material underwent three successive rinses with deionized water. The resulting two-dimensional material was then carefully collected and stored at a temperature of 4°C in a refrigerator for preservation.



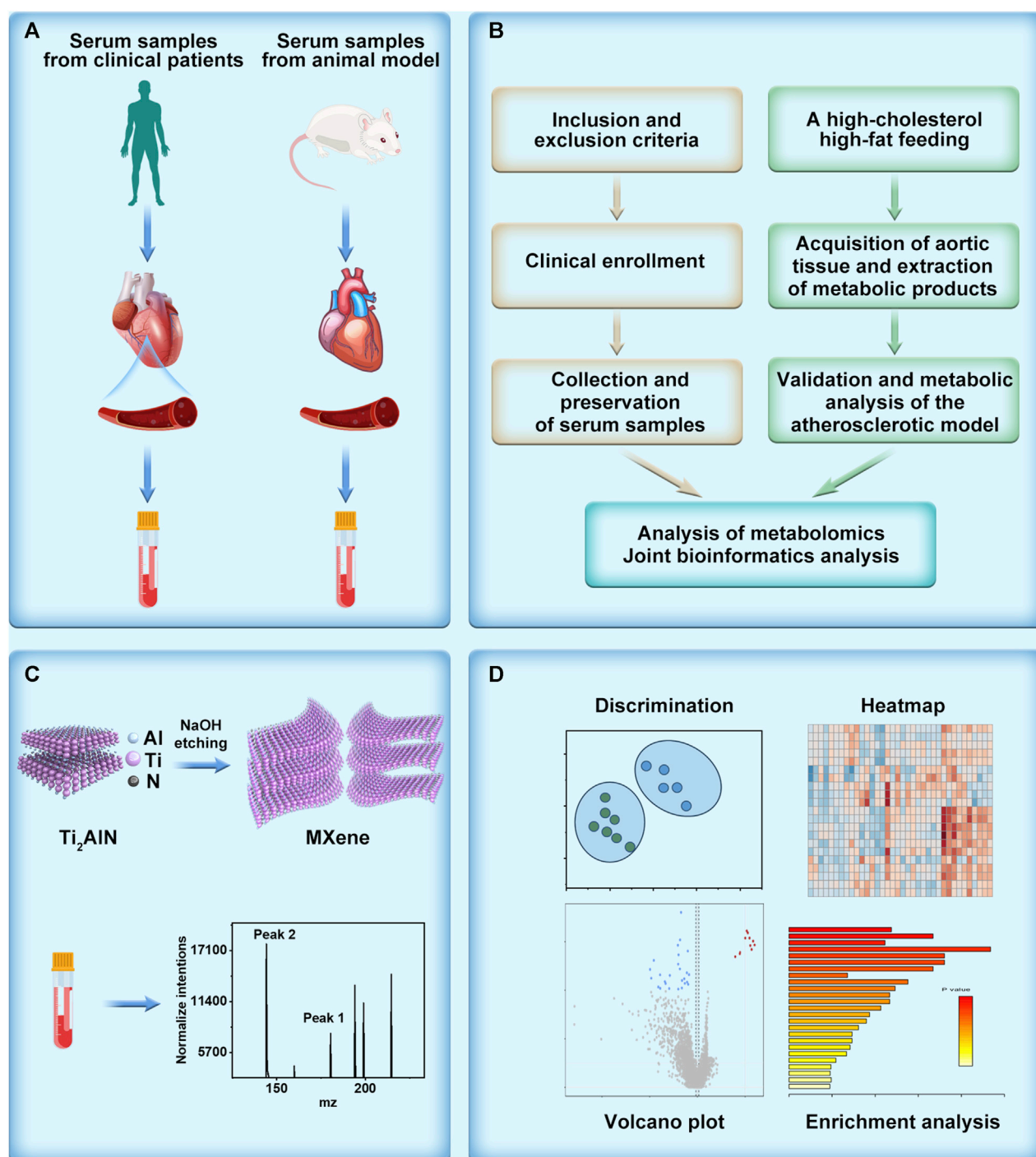


FIGURE 1

Schematic illustration of metabolomics unveils the exacerbating role of arachidonic acid metabolism in atherosclerosis. (A) Collection of serum samples derived from patients with atherosclerosis and serum obtained from an atherosclerosis model constructed using high-fat-fed APOE mice. (B) Elucidation of the mechanism of atherosclerosis through metabolomics analysis, depicted in a flowchart. (C) Illustration of the synthesis and detection of the metabolomics matrix on atherosclerosis investigation. (D) Post-metabolomics analysis, encompassing discrimination, heatmap generation, volcano plot visualization, and enrichment analysis.

To examine its microstructure, scanning electron microscopy analysis was performed using a Hitachi SU8600 instrument, operating at a voltage of 10 kV, enabling detailed characterisation of the material's features and properties.

## 2.2 Construction of AS animal model

A meticulously designed AS animal model was established, comprising 32 ApoE knock-out mice, evenly divided into control

and experimental groups. ApoE knockout mice were selected for their altered lipid metabolism genes, rendering them more susceptible to atherosclerosis, thus facilitating a simplified and time-efficient modelling process, albeit at increased expenses. The control group received no intervention, while the experimental group was subjected to a 12-week high-fat, high-cholesterol diet (SY108C) containing 20% fat and 1.25% cholesterol. After the intervention period, samples were meticulously collected from both groups, including blood and aortic tissues. For blood sampling, 2% isoflurane anaesthesia (at a flow rate of 10 mL/min, specific to the anaesthesia equipment employed) was administered, followed by the extraction of blood. The blood was allowed to clot at room temperature for 1–2 h, after which it was centrifuged at 2,500 rpm for 10 min to obtain the serum fraction, which was then stored at  $-80^{\circ}\text{C}$  for subsequent analysis. Aortic tissue collection involved carefully positioning the mice in a supine position on a dissecting table, followed by the excision of aortic tissues and their fixation in 10% paraformaldehyde solution for subsequent characterization and assessment.

### 2.3 Masson's staining, oil Red staining, sirius Red staining

Masson's staining is a histological technique employed to assess the integrity and pathological alterations of blood vessel walls. It encompasses fundamental stages, including tissue fixation (using 10% buffered formalin), tissue processing (involving dehydration and clearing), tissue embedding (using molten paraffin), tissue sectioning (at a thickness of 4–6  $\mu\text{m}$ ), and staining. The specific staining process encompasses deparaffinization (utilizing a xylene solution), dehydration (employing a descending series of ethanol concentrations, such as 100%, 95%, and 80% ethanol), staining (with Masson's staining solution encompassing acidic fuchsin, aniline blue, and orange G dyes), rinsing (using buffer solution to eliminate excess dye), dehydration (employing an ascending series of ethanol concentrations), clearing (xylene), and mounting (Canada balsam).

The steps involved in Oil Red staining are as follows: Initially, tissue sections are fixed in formaldehyde and subsequently subjected to dehydration, sequentially immersing the sections in an ethanol gradient (70%, 80%, 95%, 100%) for 10 min each, followed by transfer into a clearing agent (xylene) for clearing. Subsequently, the sections are immersed in an oil-red solution, maintained at a temperature of 60–70 $^{\circ}\text{C}$ , for 4–8 h to facilitate staining. After staining, the sections are dehydrated in the clearing agent, covered with a coverslip, and mounted.

The procedure for Sirius Red staining involves the fixation of tissue sections in paraformaldehyde, followed by dehydration. The sections are then immersed in an ethanol gradient (70%, 80%, 95%, 100%) for 10 min each and subsequently transferred to a clearing agent (such as xylene) for clearing. Next, the sections are subjected to staining with Sirius Red solution, followed by rinsing with distilled water to eliminate excess dye. The sections are further dehydrated using an increasing series of ethanol concentrations, cleared using a clearing agent, and ultimately mounted utilizing a mounting medium.

### 2.4 Q-PCR and western blotting

The procedure of Western blotting involves several intricate steps. Firstly, the samples undergo separation by SDS-PAGE electrophoresis to resolve the proteins based on their molecular weight. Subsequently, the proteins are transferred onto a polyvinylidene fluoride (PVDF) membrane, facilitating their immobilization for further analysis. Activation of the membrane is achieved through wetting with a 20% methanol solution, ensuring optimal binding efficiency. Following this, specific antibodies are applied to the membrane, facilitating the recognition and binding of the target protein of interest. To enable detection, a secondary antibody labelled with an enzyme, such as horseradish peroxidase (HRP), that exhibits affinity towards the primary antibody is employed. Finally, protein detection is accomplished utilizing sophisticated techniques, including chemiluminescence or substrate staining, which generate a measurable signal indicative of the presence and quantity of the target protein.

The q-PCR procedure entails a series of meticulous steps. Initially, RNA molecules are converted into complementary DNA (cDNA) through reverse transcription, employing the enzyme reverse transcriptase. Subsequently, specific primers and fluorescent probes designed to anneal to the target gene of interest are employed during PCR amplification. The amplification process allows for the exponential replication of the DNA region of interest. Detection of the amplified product is achieved by monitoring the fluorescence signals emitted by the fluorescent probes during PCR cycling. These signals provide a quantifiable measure of the relative expression levels of the target gene in the samples. Ultimately, the gene expression levels are determined by employing the standard curve method, which relates the fluorescence signals to the known concentrations of a reference sample.

### 2.5 Metabolomics analysis

For MALDI-TOF Analysis, initially, 1  $\mu\text{L}$  of the small molecule standard solutions or serum samples was meticulously pipetted onto a stainless steel target plate. Following air-drying at room temperature, 0.5  $\mu\text{L}$  of matrix solution was added to cover the previous spot. After another round of air-drying at room temperature, the samples underwent analysis using an Ultraflex MALDI-TOF MS (Bruker Daltonics, Billerica, MA) operating in a linear positive mode with a laser intensity set at 50%. The molecular weights of the samples, ranging from 80 to 1,000, were meticulously recorded during the analysis. Metabolomics analysis involves various analytical methods such as Principal Component Analysis (PCA), Orthogonal Partial Least Squares Discriminant Analysis (OPLS-DA), Heatmap, Volcano Plot, and Pathway Enrichment. These methods are primarily used to analyze high-throughput mass spectrometry data from both the atherosclerosis group and the control group.

## 2.6 Harvesting of clinical sample collection

Inclusion Criteria: 1) Serum samples must be obtained from patients definitively diagnosed with atherosclerosis to ensure consistency in the disease status of the study subjects; 2) Age range restrictions are applied to maintain sample uniformity while considering the characteristics of atherosclerosis across different age groups; 3) Samples are exclusively selected from patients in a stable period before treatment, minimizing the potential impact of treatment on serum biomarkers and enhancing result reliability. Exclusion Criteria: 1) Patients with other cardiovascular diseases are excluded to ensure the specificity and independence of the study results from atherosclerosis; 2) Individuals with immune system abnormalities are rejected to reduce sample variability caused by immune interference; 3) Patients with severe liver or kidney dysfunction are excluded to mitigate the impact of these factors on serum biomarkers, ensuring result accuracy (Akboga et al., 2015; Hua et al., 2023). The methodology for serum acquisition and preservation is delineated as follows: Haematological samples are meticulously obtained and deposited within receptacles devoid of anticoagulant agents. Subsequently, these samples undergo centrifugation at a velocity of 3,000 rotations per minute for 10 min, thereby resulting in the formation of a supernatant fraction that represents the coveted serum component. Lastly, the serum is diligently safeguarded within a freezer maintained at an ultra-low temperature of  $-80^{\circ}\text{C}$ . It is of paramount significance to acknowledge that the collection of clinical samples (2022-RAL-35) has been granted official endorsement by the ethics committee affiliated with the esteemed Medical School of Nanjing University.

## 2.7 Validation of the role of arachidonic acid in atherosclerosis

Aspirin is an irreversible inhibitor of cyclooxygenase (COX), which inhibits the metabolism of arachidonic acid. This inhibition leads to a reduction in the synthesis of prostaglandins (PGs), resulting in antipyretic, analgesic, and anti-inflammatory effects [29,30]. In the experimental group, the atherosclerotic mice received daily injections of aspirin at a dosage of 40 mg/kg for 1 week. The control group, on the other hand, received injections of an equivalent volume of normal saline. After 1 week, the mice from both groups were assessed using Sirius staining.

## 3 Results and discussion

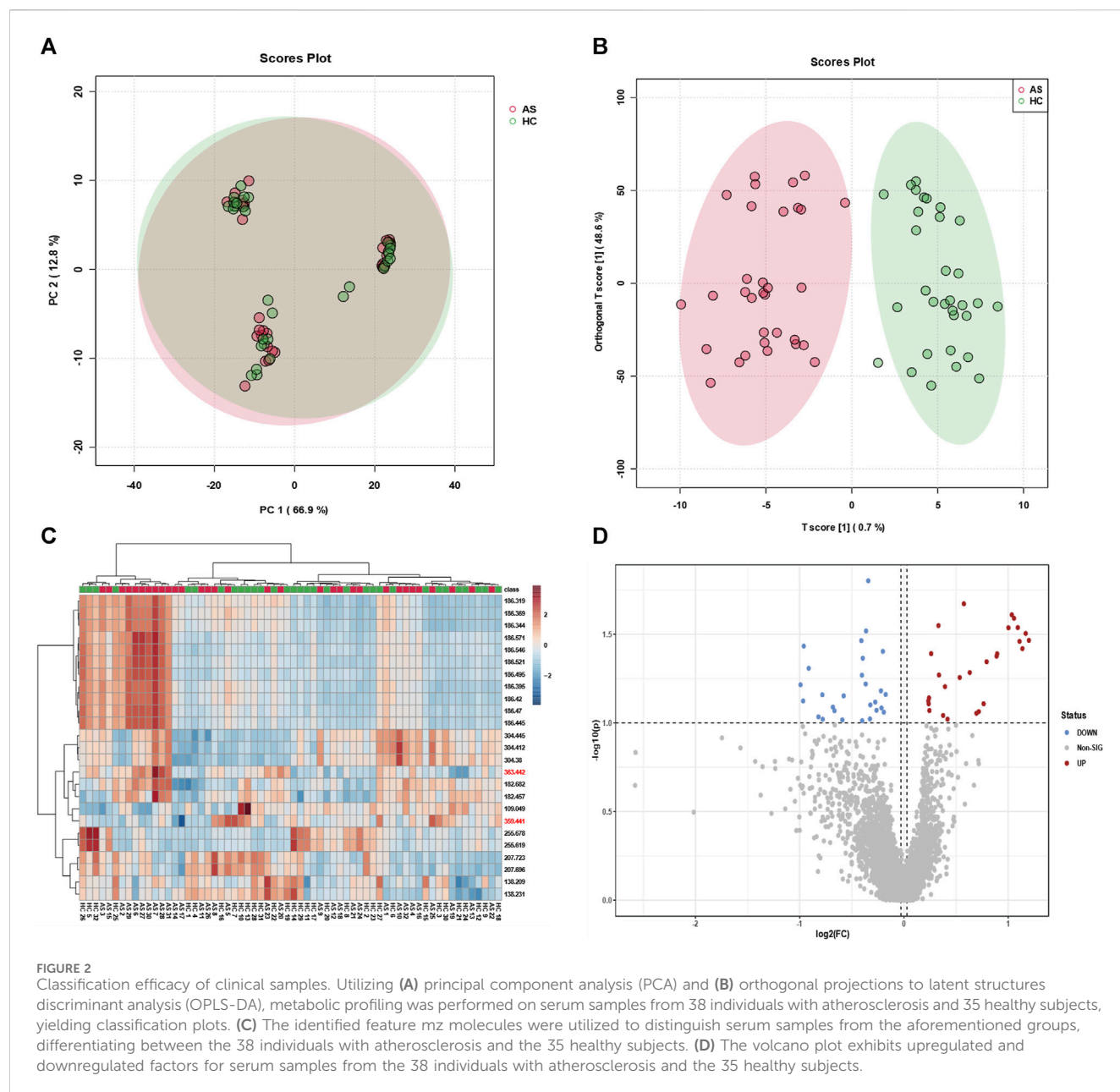
### 3.1 Metabolic fingerprinting of AS using clinical biosamples

To achieve heightened sensitivity for low-abundance metabolites in atherosclerosis samples, we synthesized a two-dimensional MXene ( $\text{Ti}_2\text{AlN}$ ) matrix, harnessing its unique advantages arising from its distinctive two-dimensional structure. This innovative matrix enabled the effective detection of low-

abundance metabolites in atherosclerosis samples, as visually depicted in [Supplementary Figure S1](#). Scanning electron microscopy vividly characterized its layered structure, affirming its unique morphology. The elemental composition of the matrix, encompassing Ti, Al, Cl, N, and O, is elucidated in [Supplementary Figure S2](#), while the elemental distribution is apparent in [Supplementary Figure S3](#). Furthermore, we conducted a comprehensive analysis and statistical evaluation of the elemental ratios, as presented in [Supplementary Table S1](#). The aforementioned meticulous morphology and elemental analysis effectively confirmed the integrity and structure of the two-dimensional material, forming a robust basis for subsequent metabolomics analysis in atherosclerosis.

To effectively screen potential biomarkers and aberrant metabolic pathways in atherosclerosis, we recruited a cohort comprising 38 atherosclerosis patients and 35 healthy individuals, from whom serum samples were collected to establish distinct groups for metabolomic profiling. Principal Component Analysis (PCA) and Orthogonal Partial Least Squares Discriminant Analysis (OPLS-DA) were employed for data analysis. While PCA focused on reducing data dimensionality and capturing overall variance, OPLS-DA proved more adept at classification and identifying discriminant features distinguishing between the groups. As demonstrated in [Figures 2A,B](#), PCA alone failed to achieve efficient discrimination between atherosclerosis and control groups; however, OPLS-DA successfully distinguished the two groups and revealed significant metabolic disparities between them. Furthermore, a heatmap analysis was performed to unveil key biomolecules implicated in the differentiation of atherosclerosis from the control group. Heatmaps, an invaluable tool in metabolomics, visually depict differences and similarities between various features, enabling rapid identification of critical metabolic pathways or biomarkers. They effectively visualize large-scale metabolic data, provide comprehensive information, and aid in identifying potential associations and trends. Additionally, they facilitate data mining and pattern recognition, expediting researchers' identification of significant metabolic features relevant to diseases or biological processes. As depicted in [Figure 2C](#), the heatmap revealed distinct metabolic profiles between the serum samples of the 38 atherosclerosis patients and 35 healthy individuals.

Subsequently, a volcano plot analysis was conducted to further scrutinize the serum samples of the 38 atherosclerosis patients and 35 healthy individuals. Volcano plots, widely employed in metabolomics, visually portray the expression differences and significance of metabolites, facilitating the identification of noteworthy metabolic changes associated with diseases or treatments. Moreover, volcano plots encompass both upregulated and downregulated metabolites, providing comprehensive information and aiding in the discovery of potential biomarkers. As depicted in [Figure 2D](#), the volcano plot unveiled key upregulated and downregulated metabolites in the serum samples of atherosclerosis patients and healthy individuals. These findings strongly indicate significant metabolic disparities between the serum samples of the 38 atherosclerosis patients and 35 healthy individuals. Through the visualization of heatmaps and volcano plots, we successfully demonstrated the differential expression of potential biomarkers



between atherosclerosis and control groups, as well as analyzed the trends of upregulation and downregulation. The aforementioned outcomes have laid a solid foundation for subsequent research endeavours. It is crucial to emphasize that our sample size of 38 vs 35 in metabolomic analysis is positioned at an intermediate level (Chinello et al., 2010; Kriegsmann et al., 2015; Laguna et al., 2021; Han et al., 2022), yet remains sufficient for decoding the metabolic fingerprint features of atherosclerosis. Furthermore, our clinical samples (38 vs 35) were meticulously collected following strict admission and exclusion criteria (Experimental section). The MALDI technique, leveraging its high-sensitivity laser desorption ionization capabilities, effectively identifies substantial differences in m/z features between the two groups (approximately 30–40 samples in each group), facilitating the screening of potential biomarkers.

### 3.2 Construction and validation of the atherosclerosis model

To conduct a more precise analysis of potential biomarkers in the metabolomic profile of atherosclerosis and explore disrupted metabolic pathways, we established an atherosclerosis animal model concurrently with a high-fat diet approach. As shown in Figure 3A, we deliberately chose not to use commonly available rodents such as SD rats, Wistar rats, C57 mice, or ICR mice, which possess normal genetic backgrounds, wider availability, lower costs, and less stringent dietary requirements. However, their cholesterol absorption and utilization rates are low, and they exhibit robust plasma cholesterol metabolism capabilities. Consequently, inducing atherosclerosis naturally, even with short-term (within 3 months) utilization of high-fat and high-cholesterol diets, poses a challenge.



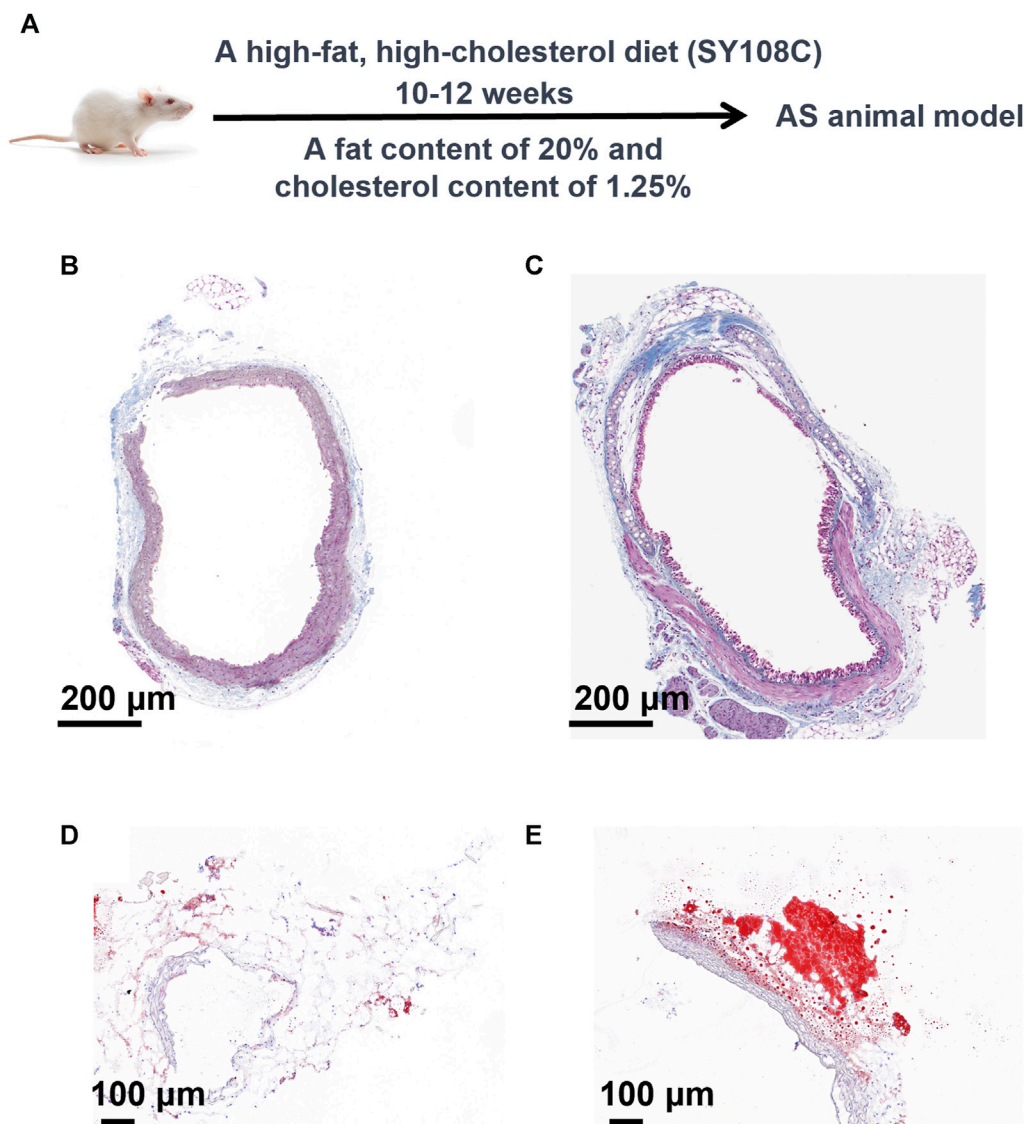


**FIGURE 3**  
Construction and validation of the atherosclerosis model. **(A)** Methodology and Procedures for Establishing Atherosclerosis. **(B)** Masson's Staining of the Control Group and **(C)** Masson's Staining of the Atherosclerosis Group. Analysis of Oil Red O staining **(D)** in the control group and **(E)** in the atherosclerosis group.

Instead, we selected ApoE mice, genetically modified to regulate their lipid metabolism and reduce their relative resistance to atherosclerosis. These genetically engineered mice simplify the modelling of atherosclerosis and significantly shorten the modelling time, albeit at a higher cost. The critical second step involved employing an appropriate high-fat feeding method. As depicted in **Figure 3A**, we adopted a strategy of administering a high-fat and high-cholesterol diet (SY108C), containing 20% fat and 1.25% cholesterol content, for 10–12 weeks to establish a stable atherosclerosis model. To validate the modelling effectiveness of atherosclerosis, we performed Masson's staining and Oil Red O staining. Masson's staining evaluates the integrity and lesions of the arterial wall by staining elastic fibers and collagen fibers, while Oil Red O staining is a lipid staining technique that highlights lipid deposition in the arterial wall, particularly lipid plaques in atherosclerotic lesions. These staining techniques provide

qualitative and quantitative pathological evaluations, aiding in the understanding of the extent and characteristics of atherosclerosis lesions, thereby offering crucial insights for related research and clinical diagnosis. As depicted in **Figures 3B,C**, noticeable differences between the atherosclerosis model and the control group are evident. Furthermore, as shown in **Figures 3D,E**, the lipid content significantly increased in the atherosclerosis group following high-fat feeding. These staining results convincingly demonstrate the success of the atherosclerosis modelling process.

Considering the association between P16, P53, and atherosclerosis, we employed Western blotting to analyze the expression of P16 and P53, as depicted in **Figure 4A**, using GAPDH as a reference protein. Glyceraldehyde-3-phosphate dehydrogenase (GAPDH), a crucial enzyme in cellular metabolic processes, exhibits stable expression levels in most cells and tissues. By detecting the expression of GAPDH as an internal reference



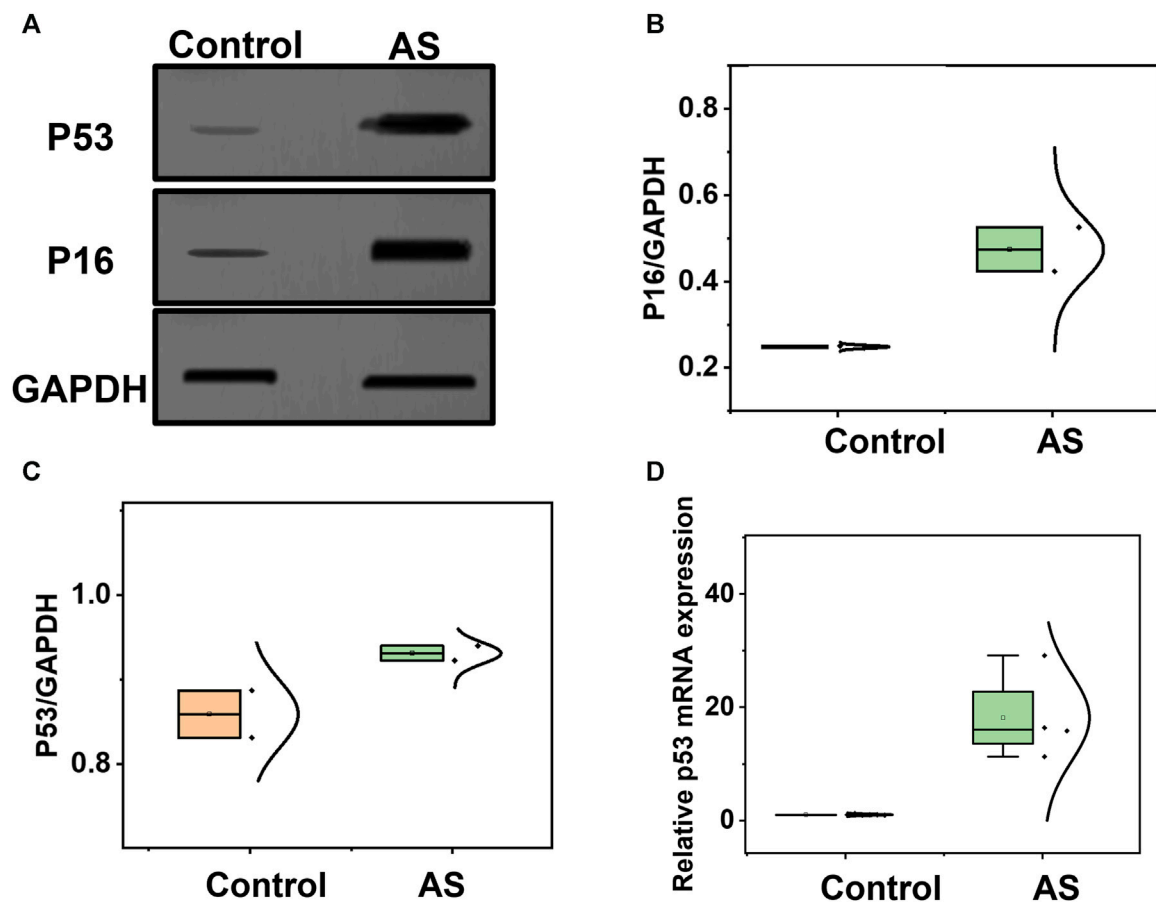


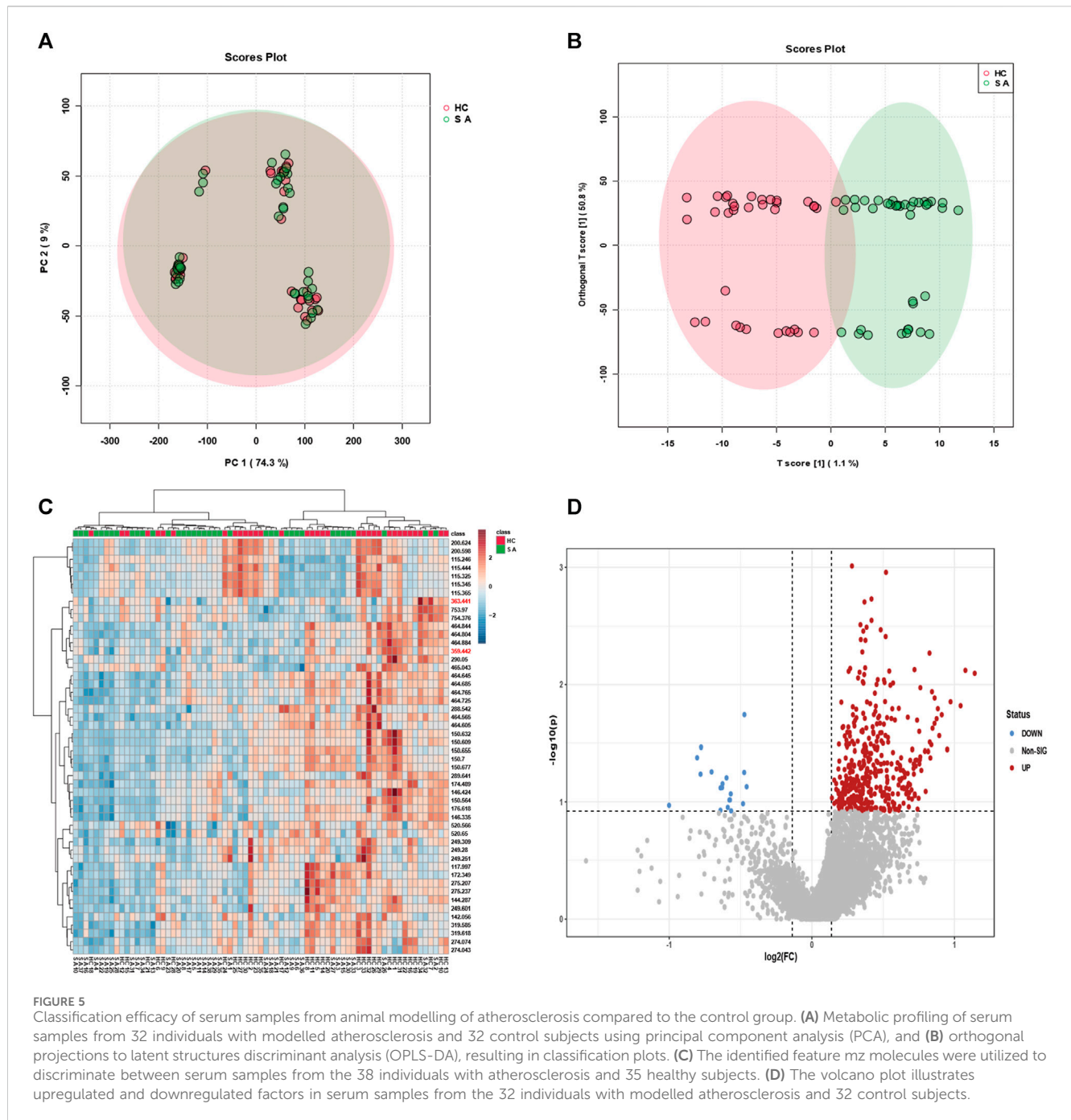
**FIGURE 4**  
Analysis of potential biomarkers before and after the development of atherosclerosis. (A) Western blotting analysis of P16 and P53 in samples from the atherosclerosis model and control group. (B) Comparison of P16, and (C) P53 between the atherosclerosis group and the control group. (D) Comparison of P53 mRNA expression levels between the atherosclerosis group and the control group.

protein, we were able to normalize protein loads in different samples, facilitating the comparison and analysis of the expression levels of the target proteins. We quantified the expression levels of P16 and P53 in atherosclerosis and control groups, as shown in [Figures 4B,C](#), indicating a significant increase in P16 and P53 during the process of atherosclerosis. Additionally, we assessed the mRNA expression levels of P16 and P53 using q-PCR technology. Based on the principles of polymerase chain reaction (PCR), fluorescently labelled probes were utilized to determine the concentration of P16 and P53 mRNA in question. The concentrations of P16 and P53 mRNA were significantly higher in atherosclerosis compared to the control group ([Figure 4D](#); [Supplementary Figure S4](#)). The aforementioned staining, Western blotting, and q-PCR characterizations confirm the successful modelling of atherosclerosis, laying the foundation for further metabolomics analysis in the atherosclerosis animal model.

### 3.3 Metabolic fingerprinting of AS using AS animal model

Expanding upon the atherosclerosis animal model, to comprehensively screen potential biomarkers and disrupted

metabolic pathways associated with atherosclerosis, a collection of 32 serum samples from atherosclerosis animal models and 32 control group samples were acquired. Principal Component Analysis (PCA) and Orthogonal Partial Least Squares Discriminant Analysis (OPLS-DA) methods were employed for classification. As depicted in [Figures 5A,B](#), PCA failed to effectively distinguish between atherosclerosis and control groups, whereas the OPLS-DA method achieved significant separation between the two groups, indicating distinctive metabolic profiles between atherosclerosis and control groups, consistently aligning with observed trends in clinical samples. Moreover, a heatmap was utilized to visualize key metabolites that differentiate the 32 atherosclerosis animal model samples from the 32 control group samples, as demonstrated in [Figure 5C](#), prominently illustrating the intergroup differences in various metabolites, thereby facilitating subsequent metabolic analyses. Additionally, a volcano plot was employed to analyse upregulated and downregulated markers in the serum samples of the 32 atherosclerosis animal models compared to the 32 control group samples, as depicted in [Figure 5D](#). The analyses conducted on the 32 atherosclerosis animal model samples and 32 control group samples, including heatmap and volcano plot analyses, in conjunction with clinical metabolomics analysis, aim to identify



potential biomarkers and disrupted metabolic pathways associated with atherosclerosis. Due to metabolic heterogeneity, there may be significant metabolic differences among patients. The advantage of animal models lies in the controllable experimental conditions, including factors such as diet, exercise, and other lifestyle variables. This controlled experimental environment helps minimize external factors' interference with metabolic analysis, ensuring more reliable results. Combining animal models with patient serum samples can provide a more extensive and comprehensive metabolic profile, which contributes to uncovering the pathogenesis of atherosclerosis. This comprehensive approach will significantly contribute to

unravelling the pathogenesis of metabolomics and provide valuable insights for the prevention, treatment, and management of atherosclerosis.

### 3.4 Screening of biomarkers and disrupted metabolic pathways associated with atherosclerosis

Expanding upon the integrated metabolomics analysis of clinical samples and animal models of atherosclerosis mentioned earlier, we have identified overlapping potential biomarkers for the diagnosis of

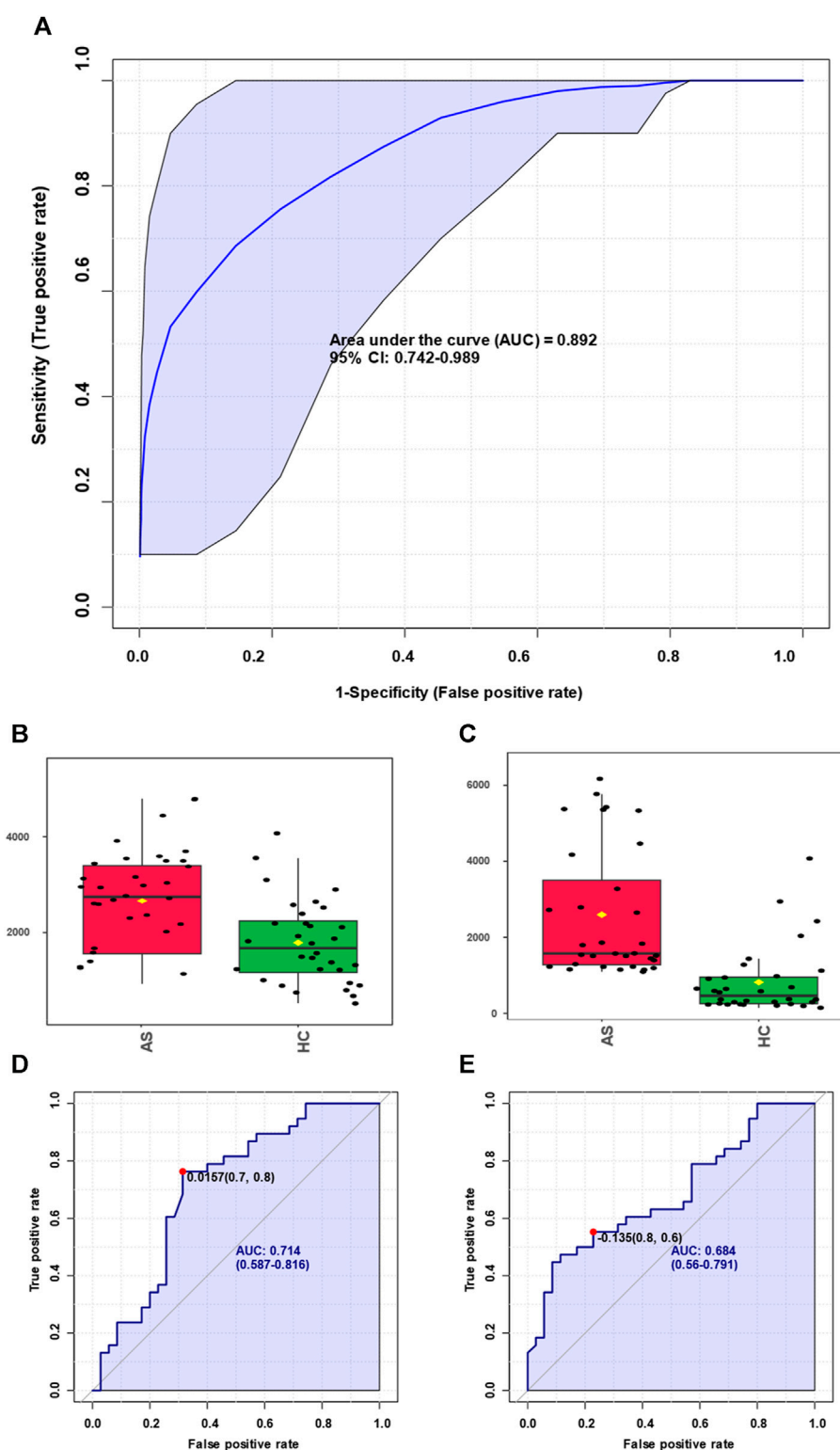


FIGURE 6

Screening of biomarkers for atherosclerosis and corresponding diagnosis capability. (A) Summarizing the selected panel of biomarkers derived from the integration of metabolomics results from clinical samples and animal models, enabling discrimination between atherosclerosis and the control group with an area under the curve (AUC) of 0.892. (B) Significant elevation of arachidonic acid molecules in atherosclerosis. (C) Arachidonic acid molecules were used for discrimination between atherosclerosis and the control group, yielding an AUC value of 0.714. (D) Marked increase of leukotriene B4 molecules in atherosclerosis. (E) Leukotriene B4 molecules were used for discrimination between atherosclerosis and the control group, resulting in an AUC value of 0.684.

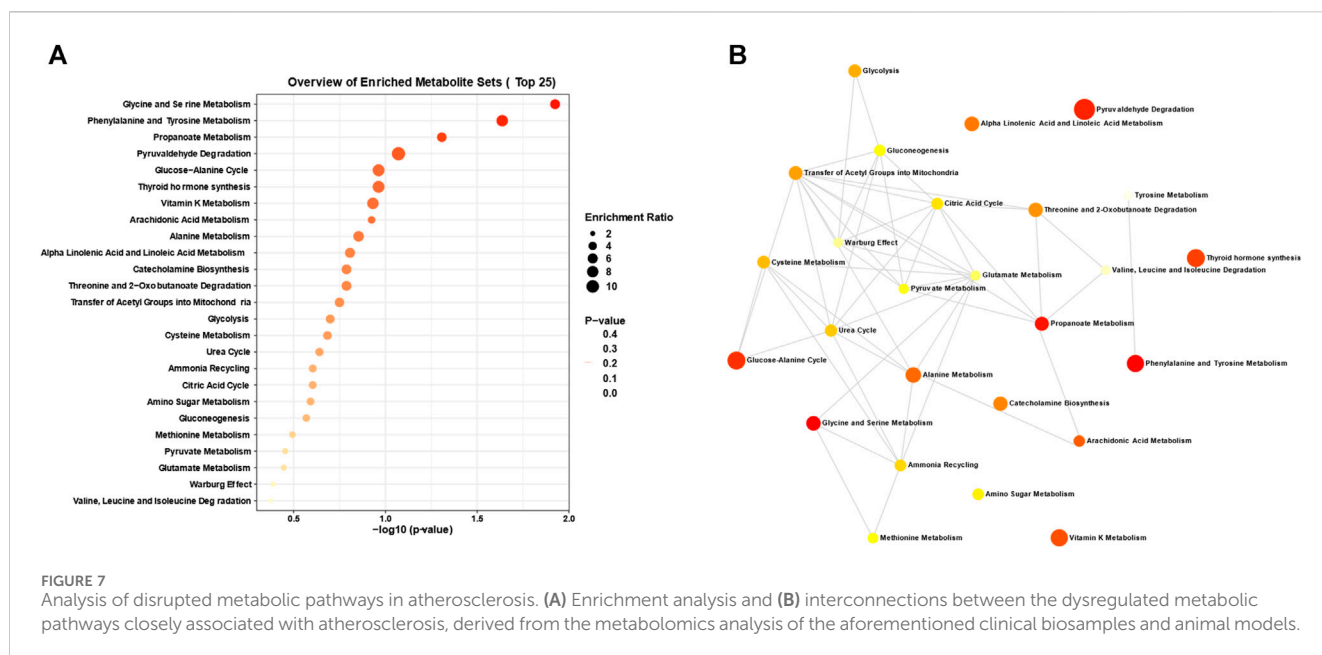


FIGURE 7  
Analysis of disrupted metabolic pathways in atherosclerosis. (A) Enrichment analysis and (B) interconnections between the dysregulated metabolic pathways closely associated with atherosclerosis, derived from the metabolomics analysis of the aforementioned clinical biosamples and animal models.

atherosclerosis. Moreover, we assessed the diagnostic efficiency using receiver operating characteristic (ROC) curves, which provide a comprehensive evaluation of the sensitivity and specificity of the diagnostic test for atherosclerosis. Sensitivity pertains to the test's ability to accurately identify patients with atherosclerosis, while specificity relates to its capacity to correctly exclude individuals without the condition. By considering both factors, the ROC curve allows us to assess the performance of the diagnostic test based on the curve's shape and the area under it, known as the area under the curve (AUC). As illustrated in Figure 6A, the obtained AUC was 0.892, indicative of high diagnostic performance and significant reference value. Furthermore, we observed significant expression of arachidonic acid in both atherosclerosis and control groups, as depicted in Figure 6B. The diagnostic efficiency of arachidonic acid alone was 0.714 (Figure 6C). Similarly, leukotriene B4 (LTB4), as a downstream product of arachidonic acid, exhibited significant expression in both atherosclerosis and control groups, as illustrated in Figure 6D. The diagnostic efficiency of LTB4 alone was 0.684 (Figure 6E). These findings suggest that integrating metabolomics analysis results from clinical samples and animal models enables the effective diagnosis of atherosclerosis. Moreover, the identification of significantly elevated levels of arachidonic acid and its downstream product, LTB4, in atherosclerosis presents opportunities for further exploration of disrupted metabolic pathways in this condition.

In our investigation of atherosclerosis, we have identified arachidonic acid and its downstream product, leukotriene B4, as potential biomarkers. To gain deeper insights, we conducted an enrichment pathway analysis, which aims to identify metabolic pathways that are significantly enriched under specific conditions. This analytical approach allows for a better understanding of the activity and regulatory mechanisms of metabolic pathways in different physiological states or disease processes. Through this exploration, we can unravel the regulatory networks and key nodes of metabolism, thus enhancing our understanding of organismal metabolic function.

As illustrated in Figure 7A, we have discovered several enriched metabolic pathways, including arachidonic acid metabolism, glycine and serine metabolism, propanoate metabolism, pyruvaldehyde degradation, the glucose-alanine cycle, thyroid hormone synthesis, and vitamin K metabolism. Notably, arachidonic acid metabolism is closely linked to both arachidonic acid and leukotriene B4. Furthermore, we analyzed the network diagram of metabolic pathways (Figure 7B), which provides a graphical representation integrating metabolic pathways, metabolites, and their interactions. This visual framework aids in comprehending the relationships and interactions between metabolic pathways, as well as the structure and functionality of the overall metabolic network. Through this analysis, we have gained valuable insights into the spatial relationships of various relevant metabolic pathways in atherosclerosis.

### 3.5 Validation of the promoting role of arachidonic acid and its downstream metabolites in atherosclerosis

The above results indicate the regulatory role of arachidonic acid and its downstream products in the process of atherosclerosis. Therefore, Sirius staining is also employed for the assessment of collagen content. When observed through a standard optical microscope, collagen fibres within tissues such as the heart and blood vessels exhibit vivid red staining, whereas muscle fibres exhibit distinct yellow staining. The accompanying Figures 8A,B illustrates the results of Sirius staining performed before and after the application of an arachidonic acid inhibitor in atherosclerosis mice (Supplementary Figure S5). In Figure 8C, the collagen area within the image was quantified using the ImageJ software and subsequently divided by the total plaque area to derive the percentage of collagen content within the plaque. A higher relative collagen content within the plaque indicates a greater degree of stability, thereby implying that the introduction of the

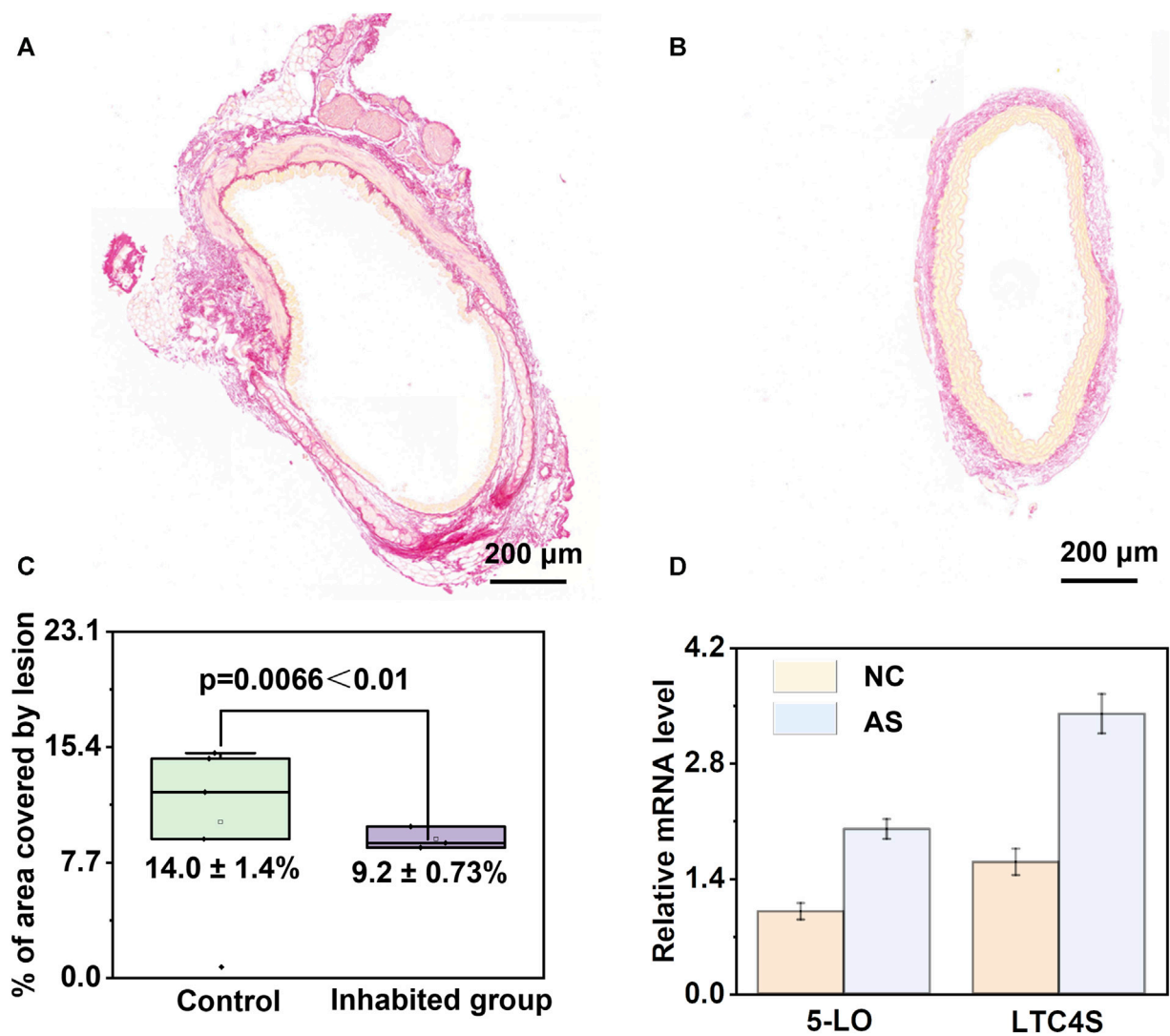


**FIGURE 8** Validation of the pivotal role of arachidonic acid metabolism disruption in atherosclerosis. (A, B) Analysis of Sirius-red staining before and after the administration of arachidonic acid inhibitor in atherosclerotic mice. (C) Analysis of plaque area before and after inhibitor administration, demonstrating effective mitigation of atherosclerosis upon inhibitor administration. (D) Significant upregulation of 5-lipoxygenase (5-LO) and LTC4 synthase (LTC4S) in the atherosclerosis group compared to the control group.

Arachidonic acid inhibitor reduces plaque stability. Additionally, we quantified the area percentage of plaques before and after applying the arachidonic acid inhibitor and found that the area decreased from  $14.0\% \pm 1.4\%$  to  $9.2\% \pm 0.73\%$ . We assessed the levels of 5-lipoxygenase (5-LO) and LTC4 synthase (LTC4S) concentrations, and intriguingly, observed a substantial upregulation in their abundance within the atherosclerosis group when compared to the control group (Figure 8D). These findings strongly imply a parallel surge in the levels of downstream metabolites derived from arachidonic acid as well. During the development of atherosclerosis, arachidonic acid participates in inflammatory responses and cellular signalling through various pathways, influencing the pathological changes in the arterial wall. Once endothelial cells in the arteries are damaged or stimulated, arachidonic acid can be released and converted into leukotriene B4 (LTB4), a potent inflammatory mediator. LTB4 can attract and activate white blood cells, leading

to the occurrence of inflammation. Therefore, we speculate that arachidonic acid and its downstream product, leukotriene B4, may promote the adhesion and migration of white blood cells to the arterial wall, thereby facilitating the formation of inflammatory cell plaques within the blood vessels. Additionally, leukotriene B4 can stimulate the release of platelet-aggregating factors and other inflammatory mediators, further accelerating plaque formation and progression. Therefore, we hypothesize that arachidonic acid and its metabolite leukotriene B4 play important regulatory and mediating roles in the pathological process of atherosclerosis.

## 4 Conclusion

In summary, our innovative metabolomics screening strategy has demonstrated remarkable efficacy in enabling precise diagnosis,



identifying biomarkers, and conducting comprehensive analysis of metabolic pathways in atherosclerosis. Our diagnostic methodology, utilizing advanced techniques such as OPLS-DA, heatmaps, and volcano plots, has achieved a high area under the curve (AUC = 0.892) for atherosclerosis classification. This has provided us with visual representations and in-depth scrutiny of the upregulation/downregulation patterns of pivotal molecules involved in the intricate processes of atherosclerotic development. Through meticulous enrichment analysis, we have discovered a significant elevation in arachidonic acid and its downstream metabolite, leukotriene B<sub>4</sub>, in atherosclerosis. Rigorous biomarker validation has yielded compelling evidence that elucidates the essential regulatory role of the arachidonic acid metabolic pathway in atherosclerosis, utilizing potent arachidonic acid inhibitors and dissecting downstream metabolites. Overall, our metabolomics approach has provided profound insights into the molecular intricacies and underlying genetic foundations of atherosclerosis, paving the way for novel avenues and promising prospects in disease prevention and therapeutic intervention. We anticipate that the widespread dissemination of our research findings will contribute to the heightened precision and efficiency of clinical medicine, offering invaluable guidance and unwavering support for the prevention, treatment, and management of related ailments.

## Data availability statement

The original contributions presented in the study are included in the article/**Supplementary Material**, further inquiries can be directed to the corresponding authors.

## Ethics statement

The studies involving humans were approved by Institutional Review Board of the Medical School of Nanjing University (2022-RAL-35). The studies were conducted in accordance with the local legislation and institutional requirements. The participants provided their written informed consent to participate in this study. The animal study was approved by Institutional Review Board of the Medical School of Nanjing University (2022-RAL-35). The study was conducted in accordance with the local legislation and institutional requirements.

## References

- Akboga, M. K., Canpolat, U., Sahinarslan, A., Alsancak, Y., Nurkoc, S., Aras, D., et al. (2015). Association of serum total bilirubin level with severity of coronary atherosclerosis is linked to systemic inflammation. *Atherosclerosis* 240, 110–114. doi:10.1016/j.atherosclerosis.2015.02.051
- Ashfaq, M. Y., Da'na, D. A., and Al-Ghouti, M. A. (2022). Application of MALDI-TOF MS for identification of environmental bacteria: a review. *J. Environ. Manage.* 305, 114359. doi:10.1016/j.jenvman.2021.114359
- Bhatt, L., Roinestad, K., Van, T., and Springman, E. B. (2017). Recent advances in clinical development of leukotriene B<sub>4</sub> pathway drugs. *Semin. Immunol.* 33, 65–73. doi:10.1016/j.smim.2017.08.007
- Calvano, C. D., Monopoli, A., Cataldi, T. R. I., and Palmisano, F. (2018). MALDI matrices for low molecular weight compounds: an endless story? *Anal. Bioanal. Chem.* 410, 4015–4038. doi:10.1007/s00216-018-1014-x
- Chen, J., Li, Y., Jiang, Y., Mao, L., Lai, M., Jiang, L., et al. (2021). TiO<sub>2</sub>/MXene-Assisted LDI-MS for urine metabolic profiling in urinary disease. *Adv. Funct. Mat.* 31. doi:10.1002/adfm.202106743
- Chinello, C., Gianazza, E., Zoppis, I., Mainini, V., Galbusera, C., Picozzi, S., et al. (2010). Serum biomarkers of renal cell carcinoma assessed using a protein profiling approach based on ClinProt technique. *Urology* 75, 842–847. doi:10.1016/j.urology.2009.09.050
- Duan, S., Li, X., Yao, Z., Zhang, X., Yao, X., Yang, J., et al. (2022). Visual authentication of steroidal saponins in *Allium macrostemon* Bge. and *Allium chinense* G. Don using MALDI-TOF imaging mass spectrometry and their structure activity relationship. *Arab. J. Chem.* 15, 104138. doi:10.1016/j.arabjc.2022.104138
- Ferey, J., Marguet, F., Laquerrière, A., Marret, S., Schmitz-Afonso, I., Bekri, S., et al. (2019). A new optimization strategy for MALDI FTICR MS tissue analysis for

## Author contributions

SM: Conceptualization, Project administration, Supervision, Writing–original draft. SH: Investigation, Writing–review and editing. JLi: Data curation, Writing–review and editing. WZ: Writing–review and editing. HL: Methodology, Writing–review and editing. CL: Writing–review and editing. LiW: Software, Writing–review and editing. JF: Data curation, Formal Analysis, Writing–review and editing. LeW: Conceptualization, Supervision, Writing–review and editing.

## Funding

The author(s) declare financial support was received for the research, authorship, and/or publication of this article. This work was financially supported by the National Natural Science Foundation of China (81900409), the PLA Youth Training Project for Medical Science (19QNP037), and the Foundation of General Hospital of Eastern Theater Command (2LCZLXJS36).

## Conflict of interest

The authors declare that the research was conducted in the absence of any commercial or financial relationships that could be construed as a potential conflict of interest.

## Publisher's note

All claims expressed in this article are solely those of the authors and do not necessarily represent those of their affiliated organizations, or those of the publisher, the editors and the reviewers. Any product that may be evaluated in this article, or claim that may be made by its manufacturer, is not guaranteed or endorsed by the publisher.

## Supplementary material

The Supplementary Material for this article can be found online at: <https://www.frontiersin.org/articles/10.3389/fmolb.2024.1297437/full#supplementary-material>

untargeted metabolomics using experimental design and data modeling. *Anal. Bioanal. Chem.* 411, 3891–3903. doi:10.1007/s00216-019-01863-6

Gao, W., Liu, H., Yuan, J., Wu, C., Huang, D., Ma, Y., et al. (2016). Exosomes derived from mature dendritic cells increase endothelial inflammation and atherosclerosis via membrane TNF- $\alpha$  mediated NF- $\kappa$ B pathway. *J. Cell. Mol. Med.* 20, 2318–2327. doi:10.1111/jcmm.12923

Gelfand, E. W. (2017). Importance of the leukotriene B<sub>4</sub>-BLT1 and LTB<sub>4</sub>-BLT2 pathways in asthma. *Semin. Immunol.* 33, 44–51. doi:10.1016/j.smim.2017.08.005

Giunchi, F., Fiorentino, M., and Loda, M. (2019). The metabolic landscape of prostate cancer. *Eur. Urol. Oncol.* 2, 28–36. doi:10.1016/j.euo.2018.06.010

Han, X., Li, D., Wang, S., Lin, Y., Liu, Y., Lin, L., et al. (2022). Serum amino acids quantification by plasmonic colloidosome-coupled MALDI-TOF MS for triple-negative breast cancer diagnosis. *Mat. Today Bio* 17, 100486. doi:10.1016/j.mtbio.2022.100486

Hua, M., Chen, W. Y., Wang, L. H., Zou, X. H., and Mao, L. L. (2023). The value of serum Lp-PLA<sub>2</sub> combined with MPO in the diagnosis of cerebral infarction caused by large artery atherosclerosis. *Clin. Neurol. Neurosurg.* 232, 107899. doi:10.1016/j.clineuro.2023.107899

Khambhati, J., Engels, M., Allard-Ratick, M., Sandesara, P. B., Quyyumi, A. A., and Sperling, L. (2018). Immunotherapy for the prevention of atherosclerotic cardiovascular disease: promise and possibilities. *Atherosclerosis* 276, 1–9. doi:10.1016/j.atherosclerosis.2018.07.007

Kriegsmann, J., Kriegsmann, M., and Casadonte, R. (2015). MALDI TOF imaging mass spectrometry in clinical pathology: a valuable tool for cancer diagnostics (review). *Int. J. Oncol.* 46, 893–906. doi:10.3892/ijo.2014.2788

Laguna, A., Xicoy, H., Tolosa, E., Serradell, M., Vilas, D., Gaig, C., et al. (2021). Serum metabolic biomarkers for synucleinopathy conversion in isolated REM sleep behavior disorder. *npj Park. Dis.* 7, 40. doi:10.1038/s41531-021-00184-9

Ly, A., Buck, A., Balluff, B., Sun, N., Gorzalka, K., Feuchtinger, A., et al. (2016). High-mass-resolution MALDI mass spectrometry imaging of metabolites from formalin-fixed paraffin-embedded tissue. *Nat. Protoc.* 11, 1428–1443. doi:10.1038/nprot.2016.081

Moreno-Gordaliza, E., Esteban-Fernández, D., Lázaro, A., Humanes, B., Aboulmagd, S., Tejedor, A., et al. (2017). MALDI-LTQ-Orbitrap mass spectrometry imaging for lipidomic analysis in kidney under cisplatin chemotherapy. *Talanta* 164, 16–26. doi:10.1016/j.talanta.2016.11.026

Needleman, P., Truk, J., Jakschik, B. A., Morrison, A. R., and Lefkowitz, J. B. (1986). Arachidonic acid metabolism. *Annu. Rev. Biochem.* 55, 69–102. doi:10.1146/annurev.bi.55.070186.000441

Piomelli, D. (1993). Arachidonic acid in cell signaling. *Curr. Opin. Cell Biol.* 5, 274–280. doi:10.1016/0955-0674(93)90116-8

Ren, S., Shao, Y., Zhao, X., Hong, C. S., Wang, F., Lu, X., et al. (2016). Integration of metabolomics and transcriptomics reveals major metabolic pathways and potential

biomarker involved in prostate cancer. *Mol. Cell. Proteomics* 15, 154–163. doi:10.1074/mcp.M115.052381

Schubert, S., and Kostrzewa, M. (2017). MALDI-TOF MS in the microbiology laboratory: current trends. *Curr. Issues Mol. Biol.* 23, 17–20. doi:10.21775/cimb.023.017

Sharma, A. R., Sharma, G., Bhattacharya, M., Lee, S.-S., and Chakraborty, C. (2021). Circulating miRNA in atherosclerosis: a clinical biomarker and early diagnostic tool. *Curr. Mol. Med.* 22, 250–262. doi:10.2174/1566524021666210315124438

Sun, N., Fernandez, I. E., Wei, M., Wu, Y., Aichler, M., Eickelberg, O., et al. (2016). Pharmacokinetic and pharmacometabolomic study of pirfenidone in normal mouse tissues using high mass resolution MALDI-FTICR-mass spectrometry imaging. *Histochem. Cell Biol.* 145, 201–211. doi:10.1007/s00418-015-1382-7

Tian, C., Qiu, M., Lv, H., Yue, F., and Zhou, F. (2022). Preliminary serum and fecal metabolomics study of spontaneously diabetic cynomolgus monkeys based on LC-MS/MS. *J. Med. Primatol.* 51, 355–366. doi:10.1111/jmp.12610

Torata, N., Kubo, M., Miura, D., Ohuchida, K., Mizuuchi, Y., Fujimura, Y., et al. (2018). Visualizing energy charge in breast carcinoma tissues by MALDI mass-spectrometry imaging profiles of low-molecular-weight metabolites. *Anticancer Res.* 38, 4267–4272. doi:10.21873/anticancer.12723

Wan, M., Tang, X., Stsiapanava, A., and Haeggström, J. Z. (2017). Biosynthesis of leukotriene B<sub>4</sub>. *Semin. Immunol.* 33, 3–15. doi:10.1016/j.smim.2017.07.012

Xiao, Y., Ma, D., Yang, Y. S., Yang, F., Ding, J. H., Gong, Y., et al. (2022). Comprehensive metabolomics expands precision medicine for triple-negative breast cancer. *Cell Res.* 32, 477–490. doi:10.1038/s41422-022-00614-0

Xu, J., Li, X., Zhang, F., Tang, L., Wei, J., Lei, X., et al. (2019). Integrated UPLC-Q/TOF-MS technique and MALDI-MS to study of the efficacy of Yixinshu capsules against heart failure in a rat model. *Front. Pharmacol.* 10, 01474. doi:10.3389/fphar.2019.01474

Yan, F., Wen, Z., Wang, R., Luo, W., Du, Y., Wang, W., et al. (2017). Identification of the lipid biomarkers from plasma in idiopathic pulmonary fibrosis by Lipidomics. *BMC Pulm. Med.* 17, 174. doi:10.1186/s12890-017-0513-4

Yang, C., Yu, H., Hu, X., Chen, H., Wu, H., Deng, C., et al. (2021). Gold-doped covalent organic framework reveals specific serum metabolic fingerprints as point of crohn's disease diagnosis. *Adv. Funct. Mat.* 31, 16163028. doi:10.1002/adfm.202105478

Zeldin, D. C. (2001). Epoxygenase pathways of arachidonic acid metabolism. *J. Biol. Chem.* 276, 36059–36062. doi:10.1074/jbc.R100030200

Zhang, H., Zhao, L., Jiang, J., Zheng, J., Yang, L., Li, Y., et al. (2022). Multiplexed nanomaterial-assisted laser desorption/ionization for pan-cancer diagnosis and classification. *Nat. Commun.* 13, 617. doi:10.1038/s41467-021-26642-9

Zhao, C., Xie, P., Yong, T., Wang, H., Chung, A. C. K., and Cai, Z. (2018). MALDI-MS imaging reveals asymmetric spatial distribution of lipid metabolites from bisphenol S-induced nephrotoxicity. *Anal. Chem.* 90, 3196–3204. doi:10.1021/acs.analchem.7b04540



## OPEN ACCESS

## EDITED BY

Jian Zhi Hu,  
Pacific Northwest National Laboratory (DOE),  
United States

## REVIEWED BY

Shi Qiu,  
Sichuan University, China  
Yuanwei Zang,  
Shandong University, China

## \*CORRESPONDENCE

Dong Hang,  
✉ hangdong@njmu.edu.cn  
Zan Fu,  
✉ fuzan1971@njmu.edu.cn

<sup>†</sup>These authors have contributed equally to  
this work

RECEIVED 06 June 2023

ACCEPTED 25 March 2024

PUBLISHED 25 April 2024



## CITATION

Huang C, Lu J, Yang J, Wang Z, Hang D and Fu Z  
(2024), Associations of serum cystatin C  
concentrations with total mortality and  
mortality of 12 site-specific cancers.  
*Front. Mol. Biosci.* 11:1209349.  
doi: 10.3389/fmolb.2024.1209349

## COPYRIGHT

© 2024 Huang, Lu, Yang, Wang, Hang and Fu.  
This is an open-access article distributed under  
the terms of the [Creative Commons Attribution  
License \(CC BY\)](https://creativecommons.org/licenses/by/4.0/). The use, distribution or  
reproduction in other forums is permitted,  
provided the original author(s) and the  
copyright owner(s) are credited and that the  
original publication in this journal is cited, in  
accordance with accepted academic practice.  
No use, distribution or reproduction is  
permitted which does not comply with these  
terms.

# Associations of serum cystatin C concentrations with total mortality and mortality of 12 site-specific cancers

Changzhi Huang<sup>1†</sup>, Jiayi Lu<sup>2†</sup>, Jing Yang<sup>2†</sup>, Zhenling Wang<sup>1</sup>,  
Dong Hang <sup>2,3\*</sup> and Zan Fu <sup>1\*</sup>

<sup>1</sup>Department of General Surgery, The First Affiliated Hospital of Nanjing Medical University, Nanjing, China, <sup>2</sup>Department of Epidemiology, School of Public Health, Nanjing Medical University, Nanjing, China, <sup>3</sup>Jiangsu Key Lab of Cancer Biomarkers, Prevention and Treatment, Collaborative Innovation Center for Cancer Medicine, Nanjing Medical University, Nanjing, China

**Purpose:** Cystatin C (CysC), beyond its biomarker role of renal function, has been implicated in various physical and pathological activities. However, the impact of serum CysC on cancer mortality in a general population remains unknown. We aimed to examine the associations of serum CysC concentrations with total mortality and mortality of 12 site-specific cancers.

**Methods:** We included 241,008 participants of the UK Biobank cohort with CysC measurements who had normal creatinine-based estimated glomerular filtration rates and were free of cancer and renal diseases at baseline (2006–2010). Death information was obtained from the National Health Service death records through 28 February 2021. Multivariable Cox proportional hazards models were used to compute hazard ratios (HR) per one standard deviation increase in log-transformed CysC concentrations and 95% confidence intervals (95% CI) for mortality.

**Results:** Over a median follow-up of 12.1 (interquartile range, 11.3–12.8) years, 5,744 cancer deaths occurred. We observed a positive association between serum CysC concentrations and total cancer mortality (HR = 1.16, 95% CI: 1.12–1.20). Specifically, participants with higher serum CysC concentrations had increased mortality due to lung cancer (HR = 1.12, 95% CI: 1.05–1.20), blood cancer (HR = 1.29, 95% CI: 1.16–1.44), brain cancer (HR = 1.19, 95% CI: 1.04–1.36), esophageal cancer (HR = 1.20, 95% CI: 1.05–1.37), breast cancer (HR = 1.18, 95% CI: 1.03–1.36), and liver cancer (HR = 1.49, 95% CI: 1.31–1.69).

**Conclusion:** Our findings indicate that higher CysC concentrations are associated with increased mortality due to lung, blood, brain, esophageal, breast, and liver cancers. Future studies are necessary to clarify underlying mechanisms.

## KEYWORDS

cancer, cystatin C, mortality, prospective cohort study, UK Biobank

# 1 Introduction

Cystatin C (CysC) is a secreted cysteine protease inhibitor abundantly expressed in body fluids (Xu et al., 2015). Due to its relatively small molecular weight (~13.3 kDa) and easy detection, CysC is commonly used in hospitals to measure the glomerular filtration rate (GFR) as an index of kidney function (Inker et al., 2012; Shlipak et al., 2013). However, emerging functional evidence suggests that CysC is directly involved in various physical and pathological activities beyond its renal function biomarker role. For example, CysC has shown the potential to regulate immune response (Pierre and Mellman, 1998), apoptosis (Mori et al., 2016), autophagy (Wang M. et al., 2021), and tumor metastasis (Kopitz et al., 2005) independently or through a potent inhibition of cysteine cathepsins. Therefore, variation in CysC levels may have additional clinical implications that warrant further investigation (Sarnak et al., 2005).

Several studies have investigated the association between circulating CysC concentrations and cancer prognosis, primarily among patients already diagnosed with malignancies, such as lung cancer (Chen et al., 2011), colorectal cancer (Kos et al., 2000), breast cancer (Decock et al., 2008), and prostate cancer (Perez-Cornago et al., 2020). Much less is known about the association in the general population, particularly those with normal renal function. Although there is evidence linking higher CysC levels to increased total cancer mortality according to the Cardiovascular Health Study (Fried et al., 2005) and the Whitehall Study (Embersson et al., 2010), the association was not replicated in two other cohort studies (Shlipak et al., 2006; Wu et al., 2010). Moreover, few studies have performed dose–response analysis or evaluated the association between CysC concentrations and site-specific cancer mortality.

In this context, leveraging data from the UK Biobank, a large prospective cohort study, we aimed to determine the association between serum CysC concentrations and mortality from common cancers among the general population. This study would improve our knowledge about the impact of circulating CysC on cancer mortality and provide novel biochemical support for the prognostic assessment of specific cancers. Such insights are crucial for developing effective strategies to reduce the risk of cancer-related deaths.

# 2 Materials and methods

## 2.1 Study population

The UK Biobank is a large prospective cohort study consisting of about half a million participants (aged 37–73 years) recruited between 2006 and 2010 across the United Kingdom (Collins, 2012). Sociodemographic, lifestyle, and health-related information was collected through self-reported questionnaires at the baseline assessment. A series of biological samples, including blood, were collected from participants to study biochemical and cellular markers (Elliott and Peakman). The ethical approval was obtained from the North West Multi-center Research Ethics Committee (11/NW/0382; 16/NW/0274), and all participants provided informed consent.

In the current study, we excluded participants who had a history of cancer or renal disease before baseline according to electronic health records and self-reported answers at baseline ( $n = 65,663$ ). Furthermore, participants who had missing data on serum CysC ( $n = 28,147$ ) or main covariates were further removed ( $n = 10,763$ ). To minimize reverse causality, we also excluded those with creatinine-based estimated glomerular filtration rates (eGFR)  $< 90$  mL/min/1.73 m<sup>2</sup>, which is considered abnormal renal function ( $n = 156,879$ ) (Stevens et al., 2013). Finally, 241,008 participants were included in the analysis (Figure 1).

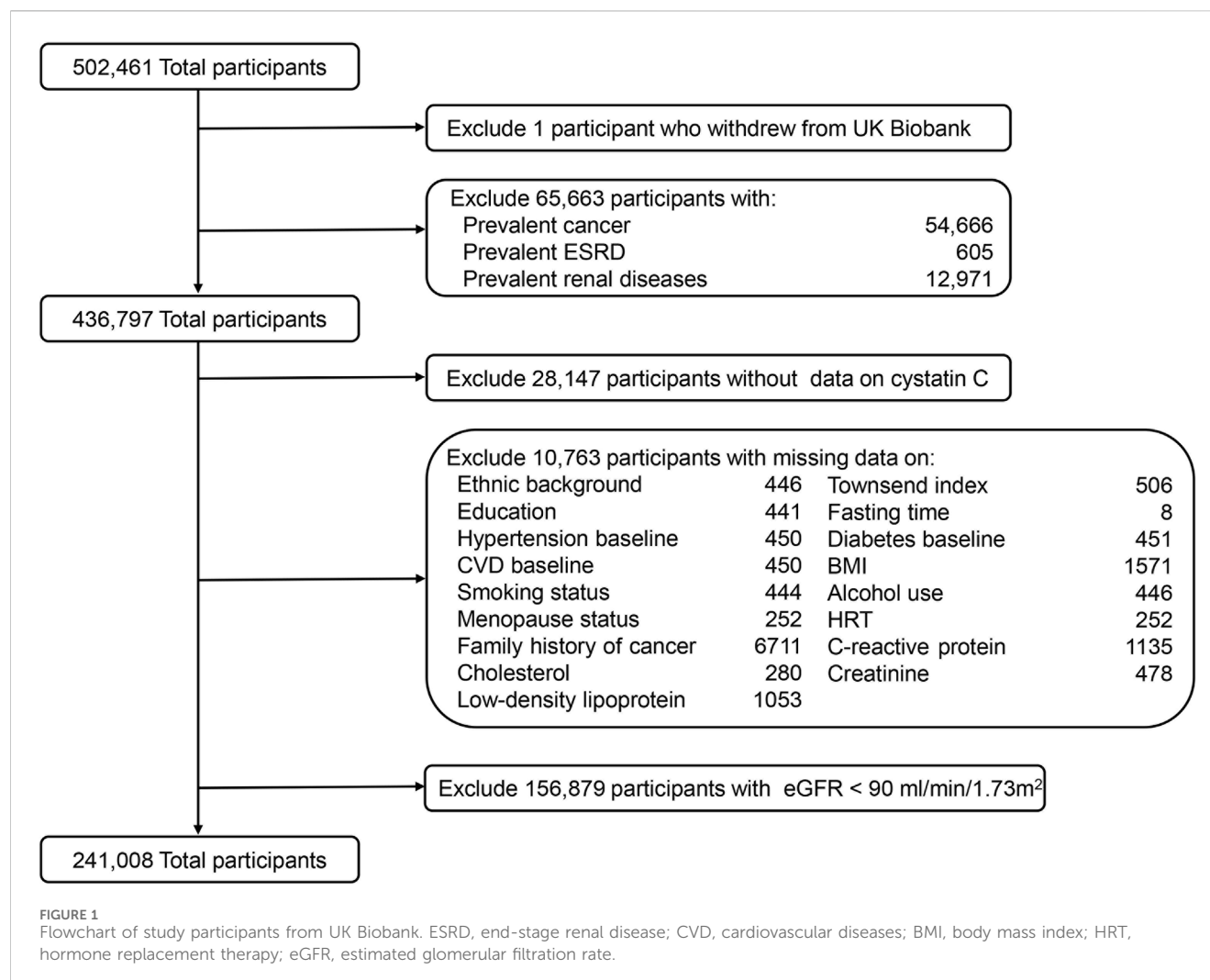
## 2.2 Biomarker measurements

An immuno-turbidimetric assay based on the Siemens Advia 1800 platform (Siemens plc) was used to measure serum CysC concentrations. The average coefficients of variation (CV) in the low- and high-level internal quality control samples of CysC were 1.36% and 0.75%, relatively. Moreover, an external quality assurance scheme was conducted to verify the assay performance, showing that 100% of participated distributions ( $n = 20$ ) were good or acceptable. In addition, serum creatinine and cholesterol concentrations were measured by enzymatic methods. C-reactive protein (CRP) concentrations were measured by an immuno-turbidimetric assay. Low-density lipoprotein (LDL) concentrations were measured by an enzymatic selective protection assay. Details about serum biomarker measurements and assay performances have been described in the online UK Biobank Showcase ([http://biobank.ndph.ox.ac.uk/showcase/showcase/docs/serum\\_biochemistry.pdf](http://biobank.ndph.ox.ac.uk/showcase/showcase/docs/serum_biochemistry.pdf)).

The eGFR was calculated based on creatinine using the Chronic Kidney Disease Epidemiology Collaboration (CKD-EPI) equation (20). CKD-EPI equation expressed as a single equation:  $GFR = 141 \times \min(Scr/\kappa, 1)^\alpha \times \max(Scr/\kappa, 1)^{-1.209} \times 0.993^{Age} \times 1.018$  (if female)  $\times 1.159$  (if black). Scr is standardized serum creatinine in mg/dL,  $\kappa$  is 0.7 for females and 0.9 for males,  $\alpha$  is  $-0.329$  for females and  $-0.411$  for males, min indicates the minimum of Scr/ $\kappa$  or 1, and max indicates the maximum of Scr/ $\kappa$  or 1. Normal creatinine-based estimated glomerular filtration rates were defined as greater than or equal to 90 mL/min/1.73 m<sup>2</sup> (CKD Work Group, 2024).

## 2.3 Covariate assessment

Information on age, sex, ethnicity, fasting status, education degree, lifestyle factors (smoking status and alcohol consumption), and medical history (medical conditions, family history of cancer, and for women, menopausal status and ever use of hormone replacement therapy) was extracted from a self-reported questionnaire at baseline. Height and body weight were measured by trained health workers, and the body mass index (BMI) was calculated as weight in kilograms divided by height in meters squared (kg/m<sup>2</sup>). The Townsend deprivation index, an indicator of socioeconomic status, was derived from data on unemployment, household overcrowding, non-home ownership, and non-car ownership (Jarman et al., 1991). Physical activity was measured as total metabolic equivalent task (MET)-hours per week for all activity, including walking, moderate, and vigorous activity (Ainsworth et al., 1993).



## 2.4 Ascertainment of cancer deaths

Death certificates were obtained from the National Health Service Information Centre (England and Wales) and the National Health Service Central Register Scotland (Scotland). The 10th revision of the World Health Organization's International Statistical Classification of Diseases (ICD-10) diagnosis codes was used to ascertain the primary cause of death. Total cancer (C00-D48) and the 12 most common cancers in the UK Biobank were assessed, which included lung cancer (C34), colorectal cancer (C18-C20), pancreatic cancer (C25), blood cancer (C81-C96), brain cancer (C71), esophageal cancer (C15), breast cancer (C50), liver cancer (C22), prostate cancer (C61), ovarian cancer (C56), stomach cancer (C16), and kidney cancer (C64) ([Supplementary Table S1](#)).

## 2.5 Statistical analysis

The follow-up time was calculated from the date of recruitment to the date of death, loss to follow-up, or the last follow-up (28 February 2021). Cancer mortality rates pertained to the number of deaths from a specific site-related cancer per a specific number of person-years of follow-up. Multivariable-adjusted

restricted cubic splines with five knots (the 5th, 27.5th, 50th, 72.5th, and 95th percentiles) were used to plot the dose-response relationship between serum CysC concentrations and cancer mortality. A likelihood ratio test was used to compare the model with both the linear and the cubic spline terms, with  $P$  for nonlinear <0.05 considered nonlinearity and  $P$  for nonlinear >0.05 &  $P$  for linear <0.05 denoting linearity. Cox proportional hazard models with age as the time scale were used to calculate hazard ratios (HR) and 95% confidence intervals (CI) for cancer mortality according to quintiles and per one standard deviation (SD) increment of the log-transformed CysC concentrations. The proportional hazard assumption was based on Schoenfeld residuals, and no violation was found in this study ([Richmond et al., 2019](#)). Model 1 was adjusted for age at baseline assessment (years), sex (female, male), ethnicity (White, not White), and fasting status (yes, no). Model 2 was additionally adjusted for the Townsend index (continuous), college or university degree (yes, no), BMI (kg/m<sup>2</sup>), smoking status (never, previous, current), pack-years of smoking (continuous), alcohol consumption (never, special occasions only, 1–3 times per month, 1–2 times per week, 3–4 times per week, daily/almost daily), physical activity (MET-hours/week), family history of cancer (yes, no), prevalent hypertension (yes, no), diabetes (yes, no), cardiovascular diseases (CVD) (yes, no), and for



TABLE 1 Baseline characteristics of UK Biobank participants with normal creatinine-based eGFR by quintile of serum cystatin C concentration<sup>a</sup>.

Characteristics	Quintile of CysC concentration, mg/L				
	Q1 (0.36–0.76)	Q2 (0.76–0.82)	Q3 (0.82–0.87)	Q4 (0.87–0.94)	Q5 (0.94–4.19)
Participants, No.	48,123	48,491	47,674	48,378	48,342
Age at assessment, year	51.1 (7.5)	53.1 (7.8)	54.2 (7.8)	55.3 (7.8)	56.6 (7.6)
Female, %	77	61	51	44	37
White race, %	92	93	94	94	93
College or university degree, %	40	38	36	33	28
Fasting when blood drawn, %	4	4	4	5	6
Townsend deprivation index	−1.4 (3.0)	−1.4 (3.0)	−1.4 (3.1)	−1.2 (3.1)	−0.7 (3.3)
Body mass index, kg/m <sup>2</sup>	25.2 (3.9)	26.2 (4.2)	27.0 (4.4)	27.8 (4.7)	29.4 (5.7)
Physical activity, MET hour/week	39.9 (31.6)	39.9 (31.9)	39.4 (31.9)	39.2 (32.4)	37.7 (31.9)
Smoking status, % <sup>b</sup>					
Never	62	59	57	53	46
Previous	31	32	32	33	32
Current	7	8	10	14	22
Alcohol consumption, % <sup>b</sup>					
Daily or almost daily	21	21	21	21	18
Three or four times a week	26	26	24	23	19
Once or twice a week	27	26	26	26	25
One to three times a month	11	11	11	11	12
Special occasions only	10	10	10	11	14
Never	6	7	7	8	11
Prevalent hypertension, %	15	19	22	26	33
Prevalent diabetes, %	4	4	4	5	7
Prevalent CVD, %	2	3	3	4	7
Postmenopausal, % <sup>c</sup>	28	30	30	28	26
Ever HRT use, % <sup>c</sup>	18	18	18	17	16
Family history of cancer, %	32	33	34	35	35
eGFR, mL/min/1.73 m <sup>2</sup>	103.8 (7.3)	100.9 (6.6)	99.5 (6.2)	98.3 (5.9)	97.0 (5.5)
C-reactive protein, mg/L	1.73 (3.26)	1.98 (3.55)	2.25 (3.86)	2.61 (4.14)	3.68 (5.42)
Cholesterol, nmol/L	5.61 (1.06)	5.71 (1.09)	5.76 (1.11)	5.76 (1.13)	5.67 (1.18)
Low-density lipoprotein, nmol/L	3.42 (0.81)	3.54 (0.83)	3.61 (0.85)	3.64 (0.86)	3.61 (0.89)

<sup>a</sup>Normal creatinine-based eGFR was defined by the CKD-EPI as  $\geq 90$  mL/min/1.73 m<sup>2</sup>. Values are expressed as means (SD) unless otherwise indicated.  
<sup>b</sup>The total did not sum to 100% because a small proportion of participants chose “prefer not to answer”.  
<sup>c</sup>Among women only.  
Abbreviations: eGFR, estimated glomerular filtration rate; CysC, cystatin C; MET, metabolic equivalent task; CVD, cardiovascular disease; HRT, hormone replacement therapy; CKD-EPI, Chronic Kidney Disease Epidemiology Collaboration; SD, standard deviation.

women, menopausal status (yes, no) and ever use of hormone replacement therapy (yes, no). Model 3 was further adjusted for serum cholesterol (mmol/L), LDL (mmol/L), CRP (mg/L), and creatinine-based eGFR (mL/min/1.73 m<sup>2</sup>).

Stratified analyses were conducted according to age at blood drawn (<55;  $\geq 55$  years), sex (male; female), BMI (<30;  $\geq 30$  kg/m<sup>2</sup>), and smoking status (non-smoker; smoker). Sensitivity analyses were performed by excluding people who died within 2 years or had

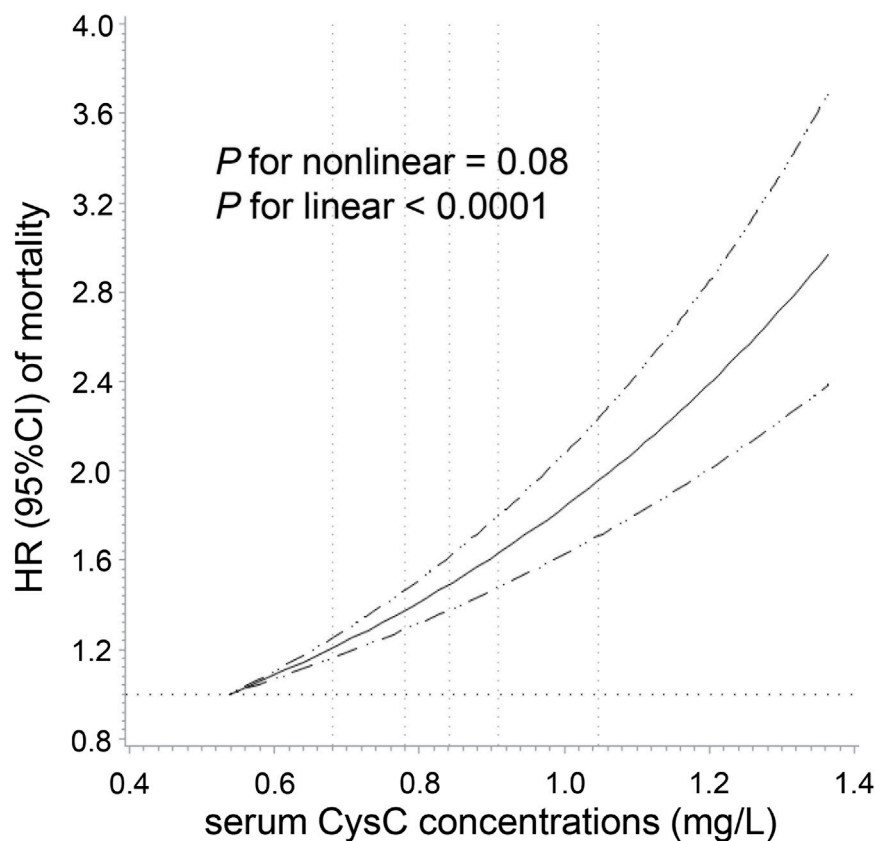


FIGURE 2

Dose-response association of serum cystatin C concentrations with total cancer mortality among participants with normal creatinine-based eGFR. Multivariable Cox regression models with restricted cubic spline analysis were performed, adjusting for the same set of covariates as in Model 3. Cystatin C concentrations above 99.9% and below 0.1% were not plotted due to wide confidence intervals at the extremes. The solid line represents estimates of hazard ratio (HR), and the dashed lines represent 95% confidence intervals (CI). The dashed lines perpendicular to the horizontal axis represent the 5th, 27.5th, 50th, 72.5th, and 95th percentiles of cystatin C, respectively. The dashed line perpendicular to the vertical axis represents the HR equal to 1. Normal creatinine-based eGFR was defined by the CKD-EPI as  $\geq 90$  mL/min/1.73 m<sup>2</sup>.

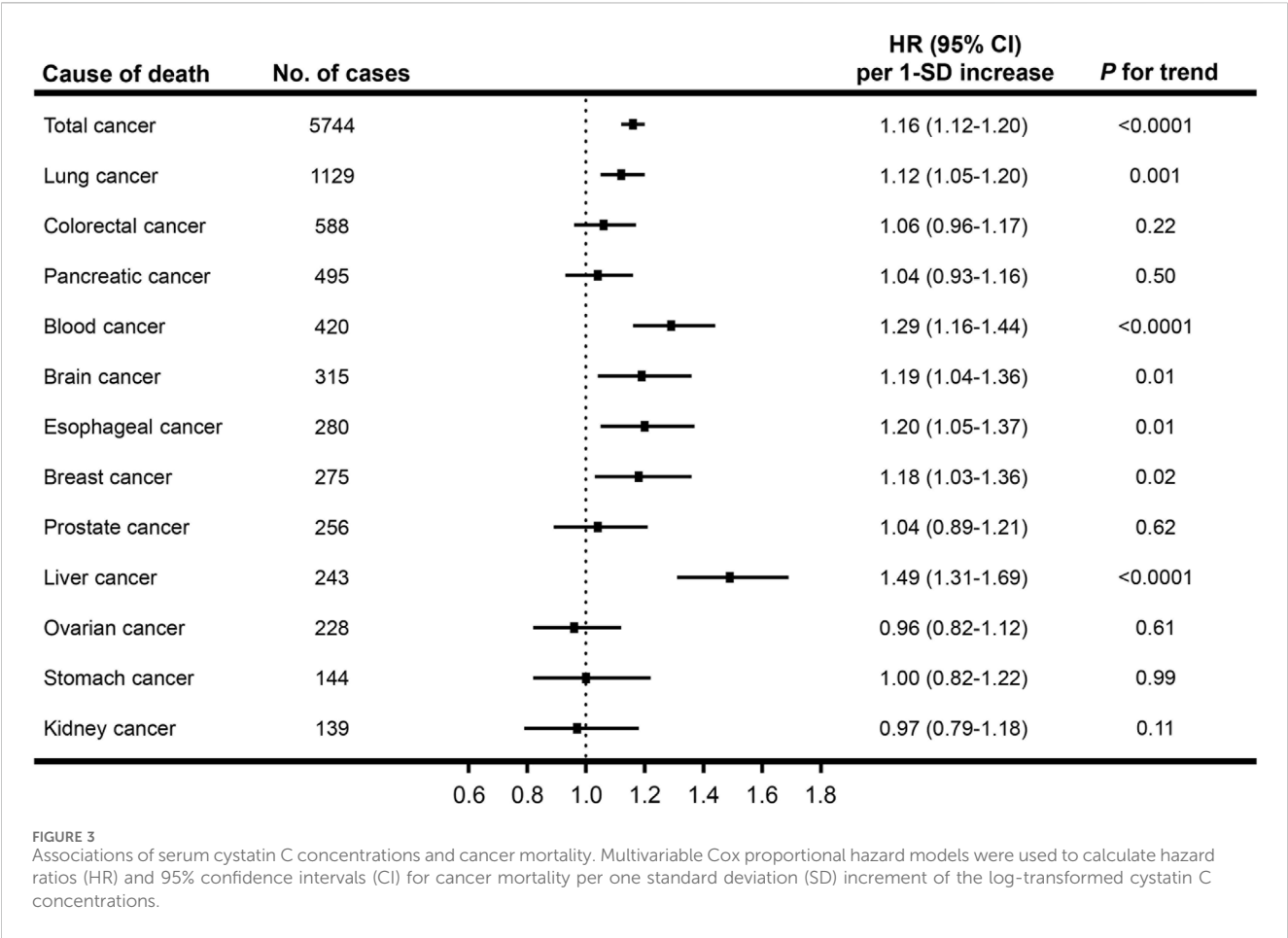
unfavorable self-assessment of overall health at baseline. Two-sided *p*-values less than 0.05 were considered statistically significant. All the statistical analyses were performed using SAS version 9.4 (SAS Institute, Cary, NC).

### 3 Results

During a total of a total of 2,860,841 person-years of follow-up (median follow-up: 12.1 years; interquartile range: 11.3–12.8 years), 5,744 of 241,008 participants died from cancer. Table 1 describes the baseline characteristics of participants according to quintiles of serum CysC concentrations. Participants with higher CysC concentrations were more likely to be older, males, current smokers, and have a higher Townsend deprivation index and BMI. In addition, they tended to have prevalent hypertension, diabetes, and CVD; they also had higher levels of CRP and LDL. The baseline characteristics of the subjects, stratified based on whether cancer death occurred, are presented in Supplementary Table S2.

We observed a positive linear relationship between CysC concentrations and total cancer mortality among participants

with normal kidney function (*P* for linear < 0.0001) after adjustment for sociodemographic information, lifestyle factors, medical history, specific biomarkers, and renal function (Figure 2). As shown in Figure 3, a per 1-SD increment of the log-transformed CysC concentrations was associated with a 16% higher risk of total cancer mortality (HR = 1.16, 95% CI: 1.12–1.20) in Model 3. In the site-specific analysis (Figure 3), CysC was positively associated with mortality from lung cancer (HR = 1.12, 95% CI: 1.05–1.20), blood cancer (HR = 1.29, 95% CI: 1.16–1.44), brain cancer (HR = 1.19, 95% CI: 1.04–1.36), esophageal cancer (HR = 1.20, 95% CI: 1.05–1.37), breast cancer (HR = 1.18, 95% CI: 1.03–1.36), and liver cancer (HR = 1.49, 95% CI: 1.31–1.69). Multivariable restricted cubic spline analysis showed that CysC had positive linear associations with mortality from the above-mentioned cancer types (*P* for linear < 0.05) (Supplementary Figure S2). However, the associations were non-statistically significant between CysC and mortality from the other types of cancer located at the colorectum, pancreas, prostate, ovarian, stomach, and kidney. The HRs and 95% CIs for mortality according to quintiles of CysC concentrations are presented in Supplementary Table S3. When compared to the lowest quintile, individuals in the highest



quintile exhibit a heightened mortality risk for lung cancer (HR = 1.36, 95% CI: 1.23–1.51), blood cancer (HR = 1.54, 95% CI: 1.05–2.26), and liver cancer (HR = 2.46, 95% CI: 1.45–4.17) after adjusting for relevant confounding variables.

In the stratified analyses by age, gender, BMI, and smoking status, the associations of serum CysC concentrations with total and site-specific cancer mortality were generally similar across subgroups despite several exceptions (Supplementary Figures S2–S5). For example, in the subgroup of younger age, the positive association with mortality of liver cancer and pancreatic cancer was stronger, while the positive association was stronger with breast cancer mortality in the older group. In addition, the association with blood cancer mortality was stronger in the subgroup of BMI <30 kg/m<sup>2</sup> (P for interaction <0.05). Sensitivity analysis showed that the associations were essentially unchanged after excluding participants who died within the first 2 years (Supplementary Table S4) or those with poor self-reported overall health at baseline (Supplementary Table S5).

4 Discussion

In this prospective cohort study of the general population, we found a positive linear association between serum CysC concentrations and cancer mortality. The site-specific analysis

further revealed the positive association with mortality from lung cancer, blood cancer, brain cancer, esophageal cancer, breast cancer, and liver cancer. Our findings suggest an independent adverse effect of CysC on the risk of cancer mortality.

4.1 Total cancer mortality

In line with our results, a cohort study including 4,673 participants from the Cardiovascular Health Study reported that compared with the lowest quartile of serum CysC concentrations, the highest quartile was associated with a 79% increased risk of cancer mortality after adjustment for known risk factors and inflammatory biomarkers (Fried et al., 2005). Another prospective cohort study incorporating 5,371 older men also showed that a 50% higher CysC concentration was associated with a 21% increased risk of cancer death (Emberson et al., 2010). However, a biracial cohort study of 3,075 Black and White ambulatory older patients (70–79 years old) with a follow-up of 6 years failed to replicate the association (Shlipak et al., 2006). Moreover, a prior study including 2,990 participants with normal eGFR reported a positive association between serum CysC concentrations and cancer mortality in univariate analysis, which was attenuated to be non-statistically significant in multivariate analysis (HR

comparing extreme deciles of CysC = 2.45, 95% CI: 0.85–7.04) (Wu et al., 2010). Generally, the studies observing no association included small numbers of cancer deaths (<350), which might have insufficient statistical power to detect the association. In the current study, which has the largest sample size to date, we ruled out individuals with renal diseases and kidney dysfunction at baseline and controlled for eGFR and other potential confounders, strongly suggesting an independent positive association of CysC concentrations with cancer mortality.

## 4.2 Site-specific cancer mortality

To the best of our knowledge, there is no epidemiologic evidence about the association between CysC concentrations and cancer-specific mortality in the general population. In support of our findings, previous case-control studies found that compared with healthy controls, elevated circulating levels of CysC were detected in patients diagnosed with lung cancer (Chen et al., 2011), esophageal cancer (Yan et al., 2017), breast cancer (Decock et al., 2008), and liver disease (Zinkin et al., 2008). In addition, several retrospective studies conducted in cancer patients have assessed the clinical prognosis significance of CysC. For example, a prior study enrolling 205 patients with small-cell lung cancer found that higher levels of serum CysC were associated with a poorer progression-free survival (Wang H. et al., 2021), and other studies reported CysC as a possible useful biomarker in clinical prognosis management of patients with breast cancer (Leto and Sepporta, 2020), non-Hodgkin B-cell lymphoma (Mulaomerovic et al., 2007), and multiple myeloma (Terpos et al., 2009).

Experimental investigations suggest that CysC plays a critical role in key events of carcinogenesis, such as cell proliferation, apoptosis, and cell adhesion, through its inhibiting activity on cysteine proteases or other cathepsin inhibition-independent mechanisms (Breznik et al., 2019). For example, cysteine proteases have shown the ability to mediate programmed cell death of lung and blood cancers (Broker et al., 2004; Sukhai et al., 2013) and to promote the maturation of antigen-presenting cells, antigen processing, and presentation to T cells (Olson and Joyce, 2015). By thwarting the effects of cysteine proteases, CysC could facilitate cancer cell growth (Leto et al., 2018) and impair T-cell-dependent-antitumor immune response (Zavasnik-Bergant et al., 2005; Magister and Kos, 2013). On the other hand, *ex vivo* and *in vitro* studies have shown a reduction in the proliferation of tumor cells with CysC knockout, indicating that CysC might directly regulate tumor growth through the p38 MAPK signaling pathway. (Završnik et al., 2017). Additional evidence shows that CysC secreted by lung cancer cells could increase the adhesion of cancer cells to the brain microvascular endothelium and result in the formation of brain metastasis (Rai et al., 2015). Moreover, CysC may be conducive to tumor cell invasion and angiogenesis by protecting matrix metalloproteinase-9 from autolysis (Mira et al., 2004; Paupert et al., 2008). Zhao et al. also reported that elevated expression of CST3, the gene encoding cystatin C, was critical for cellular polyploidization that may facilitate cancer cells to resist radiation therapy (Zhao et al., 2023).

The main strengths of this research include the large sample size, prospective design with a long-term follow-up, and accurate assessment of cancer death. Our results were robust to extensive statistical adjustments and sensitivity analyses. Nevertheless, several limitations should be addressed. First, the current study is observational and could not rule out the possibility of residual confounding. Second, a single measurement of serum CysC at baseline was used in the study, which did not take into account the change of the biomarker during the follow-up time. Third, because most of the participants in the UK Biobank were of White ethnicity, the generalization of our findings to other ethnicities should be interpreted with caution. Further independent validation is important for causal inference and would ensure that the results can be generalized to a broader population.

## 5 Conclusion

Our results suggest that serum CysC concentrations are positively associated with mortality from total and certain types of cancer in the general healthy population. Future studies are warranted to clarify the underlying mechanisms of CysC in carcinogenesis and uncover the potential of CysC as a target for cancer treatment.

## Data availability statement

The original contributions presented in the study are included in the article/Supplementary Material; further inquiries can be directed to the corresponding authors.

## Ethics statement

The ethical approval was obtained from the North West Multi-center Research Ethics Committee.

## Author contributions

Conceptualization: DH and ZF; data curation: CH, JY, and JL; formal analysis: CH, JY, and JL; methodology: CH and JY; supervision: DH and ZF; writing-original draft: CH, JY, and JL; writing-review and editing: ZW, DH, and ZF. All authors contributed to the article and approved the submitted version.

## Funding

This study was funded by the National Natural Science Foundation of China (82172956 and 81973127), the Natural Science Foundation of Jiangsu Province (BK20190083), and the Qing Lan Project of Jiangsu Province. The funders had no role in study design, data collection and analysis, decision to publish, or preparation of the manuscript.

## Conflict of interest

The authors declare that the research was conducted in the absence of any commercial or financial relationships that could be construed as a potential conflict of interest.

## Publisher's note

All claims expressed in this article are solely those of the authors and do not necessarily represent those of their affiliated

organizations, or those of the publisher, the editors, and the reviewers. Any product that may be evaluated in this article, or claim that may be made by its manufacturer, is not guaranteed or endorsed by the publisher.

## Supplementary material

The Supplementary Material for this article can be found online at: <https://www.frontiersin.org/articles/10.3389/fmolb.2024.1209349/full#supplementary-material>

## References

- Ainsworth, B. E., Haskell, W. L., Leon, A. S., Jacobs, D. R., Jr, Montoye, H. J., Sallis, J. F., et al. (1993). Compendium of physical activities: classification of energy costs of human physical activities. *Med. Sci. Sports Exerc* 25 (1), 71–80. doi:10.1249/00005768-199301000-00011
- Breznik, B., Mitrovic, A., T, T. L., and Kos, J. (2019). Cystatins in cancer progression: more than just cathepsin inhibitors. *Biochimie* 166, 233–250. doi:10.1016/j.biochi.2019.05.002
- Broker, L. E., Huisman, C., Span, S. W., Rodriguez, J. A., Kruij, F. A., and Giaccone, G. (2004). Cathepsin B mediates caspase-independent cell death induced by microtubule stabilizing agents in non-small cell lung cancer cells. *Cancer Res.* 64 (1), 27–30. doi:10.1158/0008-5472.can-03-3060
- Chen, Q., Fei, J., Wu, L., Jiang, Z., Wu, Y., Zheng, Y., et al. (2011). Detection of cathepsin B, cathepsin L, cystatin C, urokinase plasminogen activator and urokinase plasminogen activator receptor in the sera of lung cancer patients. *Oncol. Lett.* 2 (4), 693–699. doi:10.3892/ol.2011.302
- CKD Work Group (2024). KDIGO 2024 clinical practice guideline for the evaluation and management of chronic kidney disease. *Kidney Int.* 105 (4S), S117–S314. PMID: 38490803. doi:10.1016/j.kint.2023.10.018
- Collins, R. (2012). What makes UK Biobank special? *Lancet* 379 (9822), 1173–1174. doi:10.1016/S0140-6736(12)60404-8
- Decock, J., Obermajer, N., Vozelj, S., Hendrickx, W., Paridaens, R., and Jitijobm, K. (2008). Cathepsin B, cathepsin H, cathepsin X and cystatin C in sera of patients with early-stage and inflammatory breast cancer. *breast cancer* 23 (3), 161–168. doi:10.5301/bjm.2008.3270
- Elliott, P., and Peakman, T. C. The UK Biobank sample handling and storage protocol for the collection, processing and archiving of human blood and urine. *Int. J. Epidemiol.* 1464–3685.
- Embersson, J. R., Haynes, R., Dasgupta, T., Mafham, M., Landray, M. J., Baigent, C., et al. (2010). Cystatin C and risk of vascular and nonvascular mortality: a prospective cohort study of older men. *J. Intern. Med.* 268 (2), 145–154. doi:10.1111/j.1365-2796.2010.02214.x
- Fried, L. F., Katz, R., Sarnak, M. J., Shlipak, M. G., Chaves, P. H., Jenny, N. S., et al. (2005). Kidney function as a predictor of noncardiovascular mortality. *J. Am. Soc. Nephrol.* 16 (12), 3728–3735. doi:10.1681/ASN.2005040384
- Inker, L. A., Schmid, C. H., Tighiouart, H., Eckfeldt, J. H., Feldman, H. I., Greene, T., et al. (2012). Estimating glomerular filtration rate from serum creatinine and cystatin C. *N. Engl. J. Med.* 367 (1), 20–29. doi:10.1056/NEJMoa1114248
- Jarman, B., Townsend, P., and Carstairs, V. (1991). Deprivation indices. *BMJ* 303 (6801), 523. doi:10.1136/bmj.303.6801.523-a
- Kopitz, C., Anton, M., Gansbacher, B., and Kruger, A. (2005). Reduction of experimental human fibrosarcoma lung metastasis in mice by adenovirus-mediated cystatin C overexpression in the host. *Cancer Res.* 65 (19), 8608–8612. doi:10.1158/0008-5472.CAN-05-1572
- Kos, J., Krasovec, M., Cimerman, N., Nielsen, H. J., Christensen, I. J., and Brunner, N. (2000). Cysteine proteinase inhibitors stefin A, stefin B, and cystatin C in sera from patients with colorectal cancer: relation to prognosis. *Clin. Cancer Res.* 6 (2), 505–511.
- Leto, G., Crescimanno, M., and Flandina, C. (2018). On the role of cystatin C in cancer progression. *Life Sci.* 202, 152–160. doi:10.1016/j.lfs.2018.04.013
- Leto, G., and Sepporta, M. V. (2020). The potential of cystatin C as a predictive biomarker in breast cancer. *Expert Rev. Anticancer Ther.* 20 (12), 1049–1056. doi:10.1080/14737140.2020.1829481
- Levey, A. S., Stevens, L. A., Schmid, C. H., Zhang, Y. L., Castro, A. F., 3rd, Feldman, H. I., et al. (2009). A new equation to estimate glomerular filtration rate. *Ann. Intern. Med.* 150 (9), 604–612. doi:10.7326/0003-4819-150-9-200905050-00006
- Magister, S., and Kos, J. (2013). Cystatins in immune system. *J. Cancer* 4 (1), 45–56. doi:10.7150/jca.5044
- Mira, E., Lacalle, R. A., Buesa, J. M., de Buitrago, G. G., Jimenez-Baranda, S., Gomez-Mouton, C., et al. (2004). Secreted MMP9 promotes angiogenesis more efficiently than constitutive active MMP9 bound to the tumor cell surface. *J. Cell. Sci.* 117 (Pt 9), 1847–1857. doi:10.1242/jcs.01035
- Mori, J., Tanikawa, C., Funauchi, Y., Lo, P. H., Nakamura, Y., and Matsuda, K. (2016). Cystatin C as a p53-inducible apoptotic mediator that regulates cathepsin L activity. *Cancer Sci.* 107 (3), 298–306. doi:10.1111/cas.12881
- Mulaomerovic, A., Halilbasic, A., Cickusic, E., Zavasnik-Bergant, T., Begic, L., and Kos, J. (2007). Cystatin C as a potential marker for relapse in patients with non-Hodgkin B-cell lymphoma. *Cancer Lett.* 248 (2), 192–197. doi:10.1016/j.canlet.2006.07.004
- Olson, O. C., and Joyce, J. A. (2015). Cysteine cathepsin proteases: regulators of cancer progression and therapeutic response. *Nat. Rev. Cancer* 15 (12), 712–729. doi:10.1038/nrc4027
- Paupert, J., Mansat-De Mas, V., Demur, C., Salles, B., and Muller, C. (2008). Cell-surface MMP-9 regulates the invasive capacity of leukemia blast cells with monocytic features. *Cell. Cycle* 7 (8), 1047–1053. doi:10.4161/cc.7.8.5645
- Perez-Cornago, A., Fensom, G. K., Andrews, C., Watts, E. L., Allen, N. E., Martin, R. M., et al. (2020). Examination of potential novel biochemical factors in relation to prostate cancer incidence and mortality in UK Biobank. *Br. J. Cancer* 123 (12), 1808–1817. doi:10.1038/s41416-020-01081-3
- Pierre, P., and Mellman, I. (1998). Developmental regulation of invariant chain proteolysis controls MHC class II trafficking in mouse dendritic cells. *Cell.* 93 (7), 1135–1145. doi:10.1016/s0092-8674(00)81458-0
- Rai, S., Nejadhamzeeigilani, Z., Gutowski, N. J., and Whatmore, J. L. (2015). Loss of the endothelial glycocalyx is associated with increased E-selectin mediated adhesion of lung tumour cells to the brain microvascular endothelium. *J. Exp. Clin. Cancer Res.* 34, 105. doi:10.1186/s13046-015-0223-9
- Richmond, R. C., Anderson, E. L., Dashti, H. S., Jones, S. E., Lane, J. M., Strand, L. B., et al. (2019). Investigating causal relations between sleep traits and risk of breast cancer in women: mendelian randomisation study. *BMJ* 365, 12327. doi:10.1136/bmj.12327
- Sarnak, M. J., Katz, R., Stehman-Breen, C. O., Fried, L. F., Jenny, N. S., Psaty, B. M., et al. (2005). Cystatin C concentration as a risk factor for heart failure in older adults. *Ann. Intern. Med.* 142 (7), 497–505. doi:10.7326/0003-4819-142-7-200504050-00008
- Shlipak, M. G., Mattes, M. D., and Peralta, C. A. (2013). Update on cystatin C: incorporation into clinical practice. *Am. J. Kidney Dis.* 62 (3), 595–603. doi:10.1053/j.ajkd.2013.03.027
- Shlipak, M. G., Wassel Fyr, C. L., Chertow, G. M., Harris, T. B., Kritchevsky, S. B., Tylavsky, F. A., et al. (2006). Cystatin C and mortality risk in the elderly: the health, aging, and body composition study. *J. Am. Soc. Nephrol.* 17 (1), 254–261. doi:10.1681/ASN.2005050545
- Stevens, P. E., Levin, A., and Kidney Disease: Improving Global Outcomes Chronic Kidney Disease Guideline Development Work Group M, (2013). Evaluation and management of chronic kidney disease: synopsis of the kidney disease: improving global outcomes 2012 clinical practice guideline. *Ann. Intern. Med.* 158 (11), 825–830. doi:10.7326/0003-4819-158-11-201306040-00007
- Sukhai, M. A., Prabha, S., Hurren, R., Rutledge, A. C., Lee, A. Y., Sriskanthadevan, S., et al. (2013). Lysosomal disruption preferentially targets acute myeloid leukemia cells and progenitors. *J. Clin. Invest.* 123 (1), 315–328. doi:10.1172/JCI64180
- Terpos, E., Katodritou, E., Tsiftakis, E., Kastritis, E., Christoulas, D., Pouli, A., et al. (2009). Cystatin-C is an independent prognostic factor for survival in multiple myeloma and is reduced by bortezomib administration. *Haematologica* 94 (3), 372–379. doi:10.3324/haematol.2008.000638
- Wang, H., Shan, D., Dong, Y., Yang, X., Zhang, L., and Yu, Z. (2021b). Correlation analysis of serum cystatin C, uric acid and lactate dehydrogenase levels before chemotherapy on the prognosis of small-cell lung cancer. *Oncol. Lett.* 21 (1), 73. doi:10.3892/ol.2020.12334



- Wang, M., Xu, Y., Zhang, Y., Chen, Y., Chang, G., An, G., et al. (2021a). Deciphering the autophagy regulatory network via single-cell transcriptome analysis reveals a requirement for autophagy homeostasis in spermatogenesis. *Theranostics* 11 (10), 5010–5027. doi:10.7150/thno.55645
- Wu, C. K., Lin, J. W., Caffrey, J. L., Chang, M. H., Hwang, J. J., and Lin, Y. S. (2010). Cystatin C and long-term mortality among subjects with normal creatinine-based estimated glomerular filtration rates: NHANES III (Third National Health and Nutrition Examination Survey). *J. Am. Coll. Cardiol.* 56 (23), 1930–1936. doi:10.1016/j.jacc.2010.04.069
- Xu, Y., Ding, Y., Li, X., and Wu, X. (2015). Cystatin C is a disease-associated protein subject to multiple regulation. *Immunol. Cell. Biol.* 93 (5), 442–451. doi:10.1038/icb.2014.121
- Yan, Y., Zhou, K., Wang, L., Wang, F., Chen, X., and Fan, Q. (2017). Clinical significance of serum cathepsin B and cystatin C levels and their ratio in the prognosis of patients with esophageal cancer. *Onco Targets Ther.* 10, 1947–1954. doi:10.2147/OTT.S123042
- Zavasnik-Bergant, T., Repnik, U., Schweiger, A., Romih, R., Jeras, M., Turk, V., et al. (2005). Differentiation- and maturation-dependent content, localization, and secretion of cystatin C in human dendritic cells. *J. Leukoc. Biol.* 78 (1), 122–134. doi:10.1189/jlb.0804451
- Završnik, J., Butinar, M., Prebenda, M. T., Krajnc, A., Vidmar, R., Fonović, M., et al. (2017). Cystatin C deficiency suppresses tumor growth in a breast cancer model through decreased proliferation of tumor cells. *Oncotarget* 8 (43), 73793–73809. doi:10.18632/oncotarget.17379
- Zhao, Y., Lu, T., Song, Y., Wen, Y., Deng, Z., Fan, J., et al. (2023). Cancer cells enter an adaptive persistence to survive radiotherapy and repopulate tumor. *Adv. Sci. (Weinh)* 10 (8), e2204177. doi:10.1002/advs.202204177
- Zinkin, N. T., Grall, F., Bhaskar, K., Otu, H. H., Spentzos, D., Kalmowitz, B., et al. (2008). Serum proteomics and biomarkers in hepatocellular carcinoma and chronic liver disease. *Clin. Cancer Res.* 14 (2), 470–477. doi:10.1158/1078-0432.CCR-07-0586



## OPEN ACCESS

## EDITED BY

Gregorio Peron,  
University of Brescia, Italy

## REVIEWED BY

Maria Manuela Rosado,  
Hospital Physiotherapy Institutes (IRCCS), Italy  
Federica Rubbino,  
Humanitas Research Hospital, Italy  
Francois-Pierre Martin,  
H&H Group, Switzerland

## \*CORRESPONDENCE

Yuqin Li  
✉ liyuq@jlu.edu.cn

<sup>†</sup>These authors have contributed  
equally to this work and share  
first authorship

RECEIVED 01 February 2024

ACCEPTED 23 July 2024

PUBLISHED 08 August 2024

## CITATION

Li F, Wang Z, Tang T, Zhao Q, Wang Z, Han X,  
Xu Z, Chang Y, Li H, Hu S, Yu C, Chang S,  
Liu Y and Li Y (2024) From serum metabolites  
to the gut: revealing metabolic clues to  
susceptibility to subtypes of Crohn's  
disease and ulcerative colitis.  
*Front. Endocrinol.* 15:1375896.  
doi: 10.3389/fendo.2024.1375896

## COPYRIGHT

© 2024 Li, Wang, Tang, Zhao, Wang, Han, Xu,  
Chang, Li, Hu, Yu, Chang, Liu and Li. This is an  
open-access article distributed under the terms  
of the [Creative Commons Attribution License](#)  
(CC BY). The use, distribution or reproduction  
in other forums is permitted, provided the  
original author(s) and the copyright owner(s)  
are credited and that the original publication  
in this journal is cited, in accordance with  
accepted academic practice. No use,  
distribution or reproduction is permitted  
which does not comply with these terms.

# From serum metabolites to the gut: revealing metabolic clues to susceptibility to subtypes of Crohn's disease and ulcerative colitis

Fan Li<sup>1,2†</sup>, Zhaodi Wang<sup>1,2†</sup>, Tongyu Tang<sup>1,2</sup>, Qi Zhao<sup>1,2</sup>,  
Zhi Wang<sup>1,2</sup>, Xiaoping Han<sup>1,2</sup>, Zifeng Xu<sup>1,2</sup>, Yu Chang<sup>1,2</sup>,  
Hongyan Li<sup>1,2</sup>, Sileng Hu<sup>1,2</sup>, Chanjiao Yu<sup>1,2</sup>, Shiyu Chang<sup>1,2</sup>,  
Yue Liu<sup>1,2</sup> and Yuqin Li<sup>1,2\*</sup>

<sup>1</sup>Department of Gastroenterology, The First Hospital of Jilin University, Changchun, China, <sup>2</sup>Norman Bethune Health Science Center, Jilin University, Changchun, China

**Background and aims:** Inflammatory bowel disease (IBD) is a common chronic inflammatory bowel disease characterized by diarrhea and abdominal pain. Recently human metabolites have been found to help explain the underlying biological mechanisms of diseases of the intestinal system, so we aimed to assess the causal relationship between human blood metabolites and susceptibility to IBD subtypes.

**Methods:** We selected a genome-wide association study (GWAS) of 275 metabolites as the exposure factor, and the GWAS dataset of 10 IBD subtypes as the outcome, followed by univariate and multivariate analyses using a two-sample Mendelian randomization study (MR) to study the causal relationship between exposure and outcome, respectively. A series of sensitivity analyses were also performed to ensure the robustness of the results.

**Results:** A total of 107 metabolites were found to be causally associated on univariate analysis after correcting for false discovery rate (FDR), and a total of 9 metabolites were found to be significantly causally associated on subsequent multivariate and sensitivity analyses. In addition we found causal associations between 7 metabolite pathways and 6 IBD subtypes.

**Conclusion:** Our study confirms that blood metabolites and certain metabolic pathways are causally associated with the development of IBD subtypes and their parenteral manifestations. The exploration of the mechanisms of novel blood metabolites on IBD may provide new therapeutic ideas for IBD patients.

## KEYWORDS

Crohn's disease, inflammatory bowel disease, ulcerative colitis, metabolite, metabolic pathway, Mendelian randomization

# 1 Introduction

Ulcerative colitis (UC) and Crohn's disease (CD), collectively referred to as inflammatory bowel disease, are a group of chronic, recurrent autoimmune diseases. The interaction of genetic and environmental factors that influence the immune response leads to inflammatory bowel disease (1). The most common symptoms of CD or UC include diarrhea, abdominal pain, bloody stools, and weight loss. UC involvement is primarily in the colorectum, and CD can involve the entire GI tract, but primarily in the ileum. The differences between CD and UC subtypes at different sites have been debated. Dulai et al. on the basis of the differences in CD subtypes (2), suggested that a distinction should be made between ileal dominant CD and isolated colonic CD at the time of diagnosis (3). At the World Congress of Gastroenterology in Montreal in 2006, significant differences were found in patients with UC involving the rectum, left colon, and total colon based on the natural history of the disease, response to medications, risk of neoplasia, and serologic and genetic markers in patients with UC (4–6), based on which the Montreal UC Classification was popularized to differentiate between the Static severity (4). Like the subtypes at different sites, primary sclerosing cholangitis associated UC (UC-PSC) (7), CD and UC associated spondyloarthritis (CD-SpA, UC-SpA) (8) also have distinct clinical, cellular and microbiological features. These extraintestinal manifestations of UC and CD also warrant further investigation into their pathogenesis. In recent years, metabolomics has been extensively studied in patients with IBD. Single biomarker approaches cannot be considered ideal for clinical application in IBD with complex mechanisms. Metabolomics, by measuring hundreds of metabolites in biological samples, allows for the characterization of potential mechanisms specific to different disease subtypes (9). A study by Schicho et al. found that energy metabolites such as methanol, mannose, and formic acid (10), were the metabolites with the most significant increase in serum and plasma of patients with IBD, and other studies support the observation of altered energy metabolism (11, 12), including metabolites involved in amino acid cycling and TCA cycling (13). However, relatively few metabolomics studies have been conducted for the different subtypes of UC and CD.

Mendelian randomization mimics the random grouping of individuals at birth by identifying different single-nucleotide polymorphisms and identifying the causal relationship between exposure and outcome at the gene level. Since genetic differences accompany individuals throughout their lives from birth, Mendelian randomization studies effectively eliminate the effects of general confounding factors such as age, social status, and economic level, and allow for a clear direction of causality.

In this study, we explored the metabolite phenotypes responsible for the pathogenesis of 10 IBD subtypes and extraintestinal manifestations through a two-sample MR study using the 275 blood metabolite GWAS dataset. The findings of this research will guide further investigations into the diagnostic and prognostic implications of blood metabolites for IBD subtypes.

# 2 Methods

## 2.1 Data sources

We used summary data for multiple cohorts of the study. Metabolite data were derived from a genome-wide association study of 275 blood metabolites in 7,822 adults from 2 European population studies determined in 2014 by Shin et al. Hundreds of associations and their metabolic contexts reported in this study define a system-wide molecular readout atlas of human gene activity measured *in vivo* (14). We selected these metabolites into nine subclasses of lipids, fatty acids, and carbohydrates, as defined in the Kyoto Encyclopedia of Genes and Genomes (KEGG) database. The outcome data comes from FinnGen, a database that collects and analyzes genomic and health data from 500,000 Finnish Biobank participants and provides novel medical and treatment-related insights (15). It provided a GWAS dataset of UC and CD stratified diagnoses and comorbidities for us to choose from, which contained a sample size of 373,819 individuals, with a total of 15,779 patients with UC and CD. The GWAS dataset associated with gut microbiota metabolomic pathways was published by Lopera-Maya et al. in 2022. The study was based on a multidisciplinary prospective cohort study of a population residing in northern Netherlands, evaluating the impact of various exposures and lifestyles on gut microbiota composition among 167,729 individuals. This study included data from 7738 participants, encompassing 205 gut microbiota-associated metabolic pathways.

Databases of exposures and outcomes were derived from European populations and included both males and females to avoid population stratification bias (16). Details of the dataset information and stratification are shown in Table 1, and comprehensive dataset information is provided in Supplementary Table 1.

## 2.2 Research approach

In this study, we used two-sample MR (TSMR) to investigate the causal relationship between blood metabolites and IBD subtypes and their parenteral manifestations. We stratified the IBD subtypes by combining the Montreal typing and The International Classification of Diseases (ICD)-10 classification methods, details of which are shown in Table 1. We investigated single nucleotide polymorphisms (SNPs) as instrumental variables (IVs) and performed Univariate Mendelian randomization (UVMR) analyses using inverse variance weighting (IVW), MR-Egger regression, weighted median method, weighted mode method, and MR-RAPS method after screening qualified IVs, and conducted sensitivity analyses such as the MR-Egger intercept test, Cochran's Q test, and the leave-one-out test on the results to ensure that the results were robust.

## 2.3 Selection of instrumental variables

In this study, adhering to the three basic assumptions of association, independence, and exclusivity, the following steps

TABLE 1 Inclusion information and stratification details of the dataset.

Datasets	ICD-10 encoding	Montreal classification	Case	Sample Size	Year	Authors	Gender	Population	NSNP
Crohn's disease of small intestine	K50.0	L1+part of L4	2004	361931	2023	FinnGen	Males and Females	European	20167370
Crohn's disease of colon	K50.1	L2	1581	361508	2023	FinnGen	Males and Females	European	20167370
Crohn's disease of ileocolon	K50.2	L3	2098	362025	2023	FinnGen	Males and Females	European	20167370
Arthropathy in Crohn disease	M07.4*K50.9		273	373819	2023	FinnGen	Males and Females	European	20167370
Ulcerative proctitis	K51.2	E1	1773	361700	2023	FinnGen	Males and Females	European	20167370
Ulcerative rectosigmoiditis	K51.3		2487	362414	2023	FinnGen	Males and Females	European	20167370
Left-sided ulcerative colitis	K51.5	E2	4085	364012	2023	FinnGen	Males and Females	European	20167370
Ulcerative pancolitis	K51.0	E3	933	360860	2023	FinnGen	Males and Females	European	20167370
Ulcerative colitis with PSC	K83.0*K51		209	364784	2023	FinnGen	Males and Females	European	20167370
Arthropathy in ulcerative colitis	M07.5*K51.9		336	373882	2023	FinnGen	Males and Females	European	20167370
Serum level of 275 metabolites	–	–	7822	7822	2014	Shin et al.	Males and Females	European	2546774
Gut microbiota pathway of 205	–	–	7738	7738	2022	Lopera-Maya et al.	Males and Females	European	5566712

ICD, International Classification of Diseases; PSC, Primary Sclerosing Cholangitis; SNP, Single Nucleotide Polymorphism.

were performed to screen the IVs: first, SNPs significantly associated with exposure were extracted at the genome-wide significance level (threshold  $\alpha = 5 \times 10^{-8}$ ), and in order to obtain enough SNPs, we lowered the threshold to  $\alpha = 1 \times 10^{-5}$  for batches that could not be extracted. Then, the criterion of  $r^2 < 0.01$  and  $kb = 10000$  was set to remove SNPs with chained disequilibrium. The F-statistic is an indicator of the degree of association based on regression analysis, and in the instrumental variable analysis method, instrumental variables with an F-statistic of  $< 10$  are considered to be invalid weak IVs. We calculated the association F-value of each SNP with exposure and removed weak instrumental variables.

We next used PhenoScanner searches for each SNP to exclude SNPs associated with confounding factors such as serum vitamin D levels, depression, and other confounding factors to avoid the influence of confounding factors on the results (17).Next, we applied MR-PRESSO to detect hetero-SNPs and correct their horizontal pleiotropy. We also analyzed the direction of causal estimation by MR-Steiger to remove all SNPs incorrectly (18).Finally we removed SNPs directly associated with outcome according to Bonferroni correction ( $P < 0.05/n$ ,  $n$  refers to the number of remaining SNPs).The flowchart and directed acyclic diagram consisting of MR research hypotheses are shown in Figure 1.

## 2.4 Univariate MR analysis

In this study on the relationship between blood metabolites and IBD subtypes, including their extraintestinal manifestations, we employed five methods: Inverse Variance Weighted (IVW) method, MR-Egger regression, Weighted Median, Weighted Mode, and MR-Robust Adjusted Profile Score (PAPS).

The flowchart and directed acyclic graph composed of the MR study hypotheses are shown in Figure 1. IVW is characterized by a regression that does not take into account the presence of an intercept term and is fitted with the inverse of the ending variance (the quadratic of se) as weights, and its estimation can be obtained by calculating the slope of a weighted linear regression (19) (20). When the instrumental variables satisfy the three hypotheses, the IVW approach provides a robust estimate of the causal relationship between exposure and outcome and will be preferentially used for assessment (21).The MR-Egger method is similar to the IVW method except that the regression model includes an intercept term. We preferred this method to be used for assessment when there is multiple validity in the data. The weighted median and weighted mode methods are based on the majority validity assumption and the plurality validity assumption, respectively, to calculate the causal effect (21, 22).

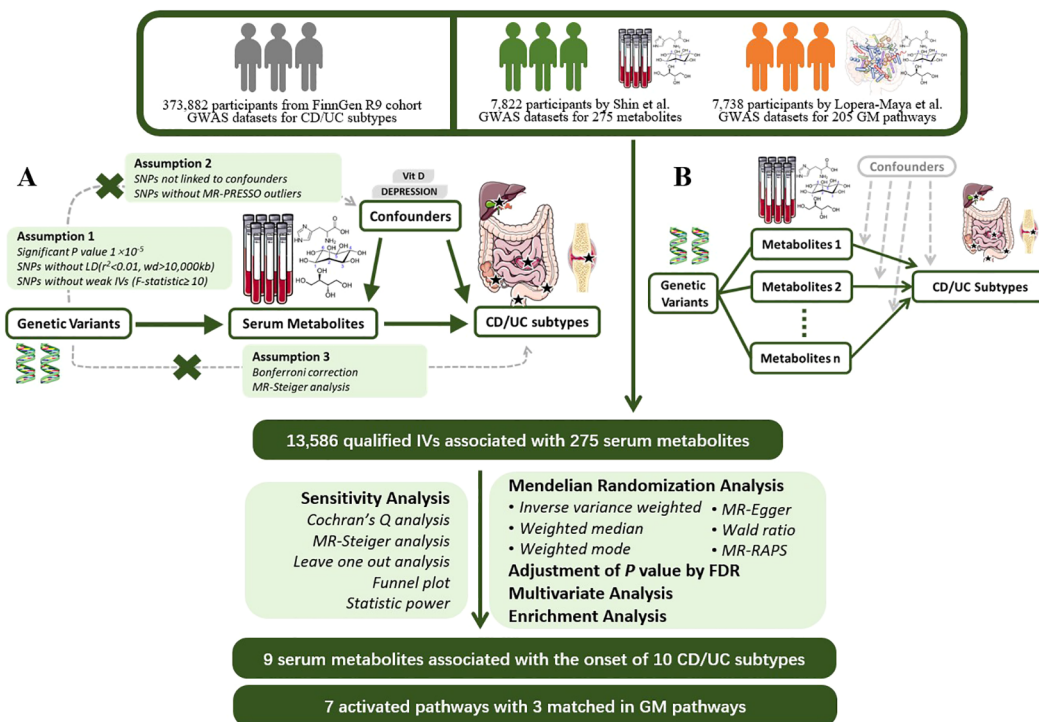


FIGURE 1

MR Study Design for the Association between Plasma Metabolites and IBD Subtypes This figure illustrates the workflow of Mendelian randomization analysis in this study. (A) Mendelian randomization three hypotheses and experimental principles; (B) Multivariable Mendelian randomization experimental principles. GWAS, Genome-Wide Association Study; CD, Crohn's Disease; UC, Ulcerative Colitis; MR, Mendelian Randomization; PRESSO, Pleiotropy RESidual Sum and Outlier; LD, Linkage Disequilibrium; IV, Instrumental Variable; RAPS, Robust Adjusted Profile Score; FDR, False Discovery Rate.

Effective IV exceeds 50%, the median of the weighted median ratio estimates will converge to the true causal effect. At less than 50%, when no larger group of invalid instrumental variables with the same ratio estimand exists, weighted mode can be used to determine the true causal effect. In the presence of heterogeneity among SNPs, the weighted median and IVW methods were required to jointly support the conclusion of significance.

The MR-RAPS method is a common modeling approach that is based on estimating causal effects based on the multiplicity of effects obeying a normal distribution centered on zero with positional variance and using a probability profile likelihood function.

In the analysis we corrected the p-values of the MR results with false discovery rate (FDR) method and inferred the causality using the corrected p-value < 0.05 as the criterion.

## 2.5 Sensitivity analysis

Therefore, in the current study we performed the Q-test for IVW and MR-Egger to evaluate the heterogeneity between IVs by calculating the weighted sum of the squared distances between the variant-specific estimates and the overall estimates, and concluded that heterogeneity existed in SNPs with a Q-test P-value < 0.05. We utilize the MR-Steiger model to estimate horizontal multinomials based on their intercepts to ensure the robustness of the results (23). The Instrument Strength Independent of Direct Effect (InSIDE) assumption and the NO Measurement Error (NOME) hypothesis

that need to be satisfied for MR-Egger regression. We constructed a funnel plot and calculated the I<sup>2</sup> statistic to ensure the validity of these assumptions. When I<sup>2</sup> < 90% and the primary analytical method is MR-Egger, a correction for causal estimates is required (24) (25). Finally, we calculated the statistical power and conducted leave-one-out sensitivity analyses using individual SNPs (26).

## 2.6 Multivariate MR analysis

After univariate MR, we performed multivariate analyses of significant metabolites using the same parameters to find independently significant plasma markers by IVW, MR-Egger, weighted median, and LASSO regression methods. Heterogeneity and pleiotropy were also analyzed by sensitivity analysis.

## 2.7 Metabolic pathway analysis

Existing metabolite sets were utilized, culminating in metabolic pathway analysis based on KEGG databases using Metabo Analyst 5.0 (<https://www.metaboanalyst.ca/>), a user-friendly online tool for streamlining metabolomics data analysis.

## 2.8 Visualization and statistical software

In this study we used scatter plots, regression plots, forest plots, and leave-one-out forest plots to present the study findings, as



detailed in [Supplementary Figures 1-4](#). The expression of the overall results is demonstrated by means of circular heat maps and forest plots. Several figures were partly generated using Servier Medical Art ([smart.servier.com](http://smart.servier.com)), provided by Servier, licensed under a Creative Commons Attribution 3.0 unported license. Statistical analyses and visualizations were performed in this study using R (version 4.1.2; R Foundation for Statistical Computing, Vienna, Austria), with the application of the “TwoSampleMR”, “MR-PRESSO”, “mr. raps”, “forestploter” packages and some basic R packages. Calculation codes are provided in [Supplementary File 1](#).

## 3 Result

### 3.1 Selection of instrumental variables

Initially, we screened a total of 16,522 SNPs associated with 275 plasma metabolites and did not find any weak variable instruments, 289 SNPs were missing from the endpoint database and were deleted, 2,027 SNPs were ambiguous SNPs, palindromic SNPs were deleted when merging the datasets, and 467 SNPs were associated with confounders such as serum vitamin D levels and depression after PhenoScanner searching, and these were deleted if they did not meet the independence assumption. The MR-PRESSO test identified 42 SNPs with horizontal pleiotropy; 111 SNPs directly associated with outcome were removed after bonferroni correction. 13,586 eligible SNPs were finally included in the study, with the number of SNPs included in significant results depicted in [Figure 2](#).

### 3.2 Causal effects of blood metabolites on 9 subtypes of IBD

We summarize the details of the MR study in the [Supplementary Information](#).

In this study, 275 plasma metabolites were included in the analysis. The number of SNPs per type of gut flora ranged from 1 to 31, and details of the IVs for 150 metabolites are listed in the [Supplementary Table](#). By univariate and multivariate MR analyses, we found that 9 metabolites had significant causal effects on IBD subtypes, of which 6 metabolites were protective against different IBD subtypes and three metabolites promoted the development of different IBD subtypes (as illustrated in [Figure 2](#)). The results of MR analysis are depicted in the circular heatmap ([Figure 3](#)), with detailed MR analysis results and the SNPs included therein provided in [Supplementary Tables 2, 3](#), while information on confounding-related SNPs is available in [Supplementary Table 4](#).

We estimated the causal associations of these 275 metabolites with 10 IBD subtypes and their extraintestinal manifestations using MR analysis, and a total of 107 associations were identified in univariate analyses, which involved 62 metabolites. Subsequent multivariate analyses were performed, and 9 metabolites were observed to have independent effects on outcome. This includes 2 metabolites from the peptide metabolism pathway, 3 metabolites from the carbohydrate pathway, 3 metabolites from the lipid metabolism pathway, and 1

metabolite from the amino acid metabolism pathway. Protection against CD subtypes was observed with three metabolites; specifically, Erythronate reduced the risk of small intestinal Crohn's disease; HWESASXX and Phenylalanylphenylalanine reduced the risk of Crohn's disease of ileocolon. The development of CD subtypes is promoted by two metabolites; 1,5-anhydroglucitol (1,5-AG) increases the risk of Crohn's disease of ileocolon, and nonanoylcarnitine increases the risk of arthritis in Crohn's disease. Against UC subtypes, three metabolites showed protective effects; 1-arachidonoylglycerophosphocholine and Myo-inositol reduced the risk of ulcerative pancolitis; and mannitol reduced the risk of ulcerative proctitis. A metabolite was found to promote the pathogenesis of UC subtypes, with 3-methylhistidine increasing the risk of ulcerative colitis with PSC.

Although the IVW approach is highly effective in inferring causal relationships between exposures and disease outcomes, it is known to be susceptible to weak instrumental variable bias. We therefore conducted sensitivity and multivariate analyses of the above data to assess whether the results were robust. With the exception of heterogeneity in the causal relationship between erythritol and small intestinal Crohn's disease (however, both the IVW method and the WM method results support a significant causal relationship), no evidence of heterogeneity or pleiotropy was found for the above significant results (as shown in [Table 2](#)). Detailed sensitivity analysis results are provided in [Supplementary Tables 5-7](#).

### 3.3 Metabolic pathway analysis

We also identified seven important metabolic pathways associated with IBD subtypes in the present study ([Table 3](#)). 3-Methylhistidine was involved in the histidine metabolic pathway ( $P=0.010$ ). Among the metabolites that passed through the UMR only, those involved in histidine metabolism, valine, leucine, and isoleucine biosynthesis, arginine biosynthesis, aminoacyl-tRNA biosynthesis, alanine, aspartate, and glutamate metabolism, phenylalanine, tyrosine, and tryptophan metabolism, phenylalanine, tyrosine, and tryptophan biosynthesis, and unsaturated fatty acid pathway biosynthesis ( $P<0.05$ ). In the metabolic pathways of gut microbiota, we identified matches with L-glutamate degradation V, super pathway of L-isoleucine biosynthesis I, and super pathway of arginine and polyamine biosynthesis ([Table 3](#), [Supplementary Table 8](#)).

## 4 Discussion

In recent years, it has been found that IBD can occur in combination with a variety of metabolic diseases, and metabolomic studies have continued to identify metabolites and metabolic pathways associated with intestinal inflammation and IBD ([11, 27](#)), and have become the focus of in-depth research. Blood is the most commonly used sample source for metabolomics identification because it contains a large number of detectable metabolites and can be easily obtained in large sample sizes to help screen for circulating biomarkers of IBD risk ([28](#)). Our study confirms the existence of an subtypes-specific metabolic profile in IBD and identifies key metabolites and

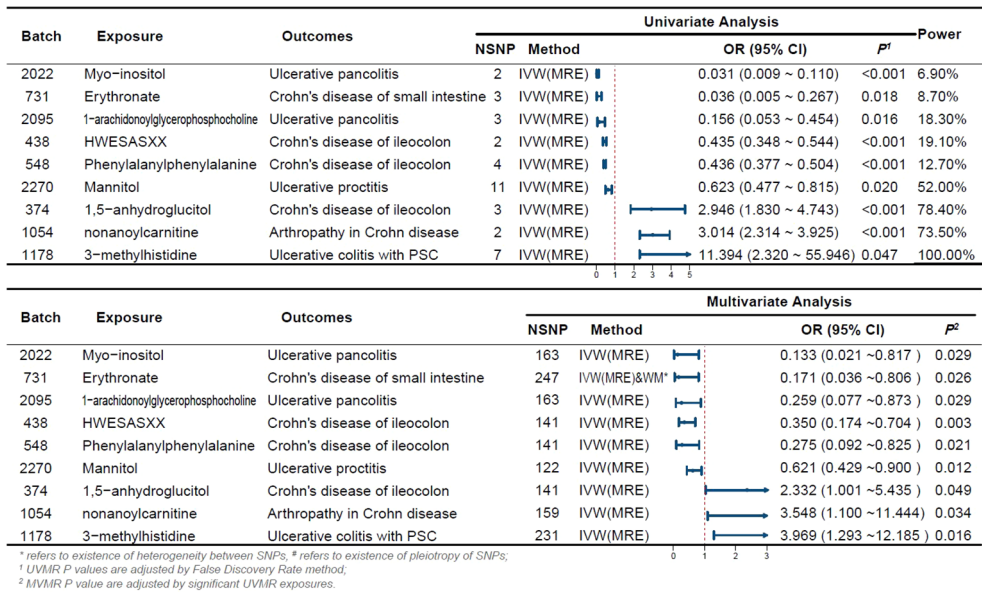


**FIGURE 2**  
Forest Plot of Significant Univariate and Multivariate MR Analyses The forest plot illustrates the results of univariable and multivariable MR analysis. \*indicates the existence of heterogeneity between SNPs, # indicates the existence of pleiotropy of SNPs; <sup>1</sup> UVMR P-values are adjusted by the False Discovery Rate method; <sup>2</sup> MVMR P-values are adjusted by significant UVMR exposures. OR, odds ratio; CI, confidence interval; PSC, primary sclerosing cholangitis; UVMR, univariable MR; MVMR, multivariable MR; NSNP, number of SNPs.

metabolic pathways associated with IBD subtypes pathogenesis and its associated phenotypes.

Table 4 summarizes the changes in metabolite levels in the bodies of patients with IBD from previous studies, as well as the effects of certain metabolites on IBD patients. Our previous studies have identified different risk factors for intestinal flora in different subtypes of CD or UC (29), and recent studies of CD subtypes have identified metabolomic differences. A mouse experiment by Baur et al. identified metabolomic differences in Crohn's disease mice with different sites of involvement (30). Whereas Schwärzler et al. found a higher inflammatory profile in patients with ileal CD rather than isolated colonic CD (31).Serum levels of sphingolipid metabolites such as S1P (Sphingosine 1 phosphate) are higher in CD patients with ileocecal involvement compared to colonic disease (32).Serum anti-Brewer's yeast antibodies better point to patients with ileal Crohn's disease (33).. The high abundance of adherent-invasive E. coli (AIEC) possessed by patients with ileal CD compared to colonic CD may differentiate the metabolomics of different subtypes of CD patients through its ability to activate the expression of innate immune/pro-inflammatory genes (34, 35). However, stratification studies of UC subtypes remain limited. Previous stratification studies have led us to stratify the subtypes and extraintestinal manifestations of UC and CD, combining multiple metabolites with different CD/UC subtypes and obtaining many reliable results.

In the amino acid metabolic pathway we identified a causal relationship between one metabolite and IBD. Amino acids are essential constituents of the human body, both for protein synthesis and through catabolism in important life activities of the body. It has been noted that the abundance of genes for the metabolism and

biosynthesis of almost all amino acids is decreased in IBD patients (36). 3-Methylhistidine (3-MH) is a histidine derivative produced by degradation of several tissues, especially skeletal muscle (37). Histidine can affect acute and chronic inflammation and modulate key events in the immune response by producing histamine through decarboxylation reactions (38). It has been shown that histidine supplementation inhibits oxidative stress in intestinal epithelial cells thereby reducing damage to the gut as well as exerting anti-inflammatory effects by inhibiting TNF- $\alpha$ -induced IL-8 secretion (39). In addition, it has been found that dietary histidine ameliorates colitis by modulating NF- $\kappa$ B activation as well as inhibiting the production of pro-inflammatory cytokines by macrophages in an IL-10-deficient cellular metastasis model of Crohn's disease (40). Decreased plasma histidine can increase the risk of recurrence in patients with ulcerative colitis in remission (41). However, our study discovered a positive causal relationship between high levels of 3-MH and the onset of ulcerative colitis with PSC, the mechanisms of which remain unknown and warrant further investigation.

Previous studies have demonstrated a strong association between foodborne bioactive peptides and the development of IBD (42).It can prevent and treat colitis by regulating four mechanisms: inflammatory cytokines, inflammatory pathways, intestinal epithelial barrier and intestinal flora balance (43). Phenylalanylphenylalanine is a peptide substance product resulting from the incomplete catabolism of proteolytic metabolism, which is strongly associated with a variety of diseases: one study found a positive correlation between Phenylalanylphenylalanine and the development of pancreatic ductal adenocarcinoma pancreatic ductal adenocarcinoma

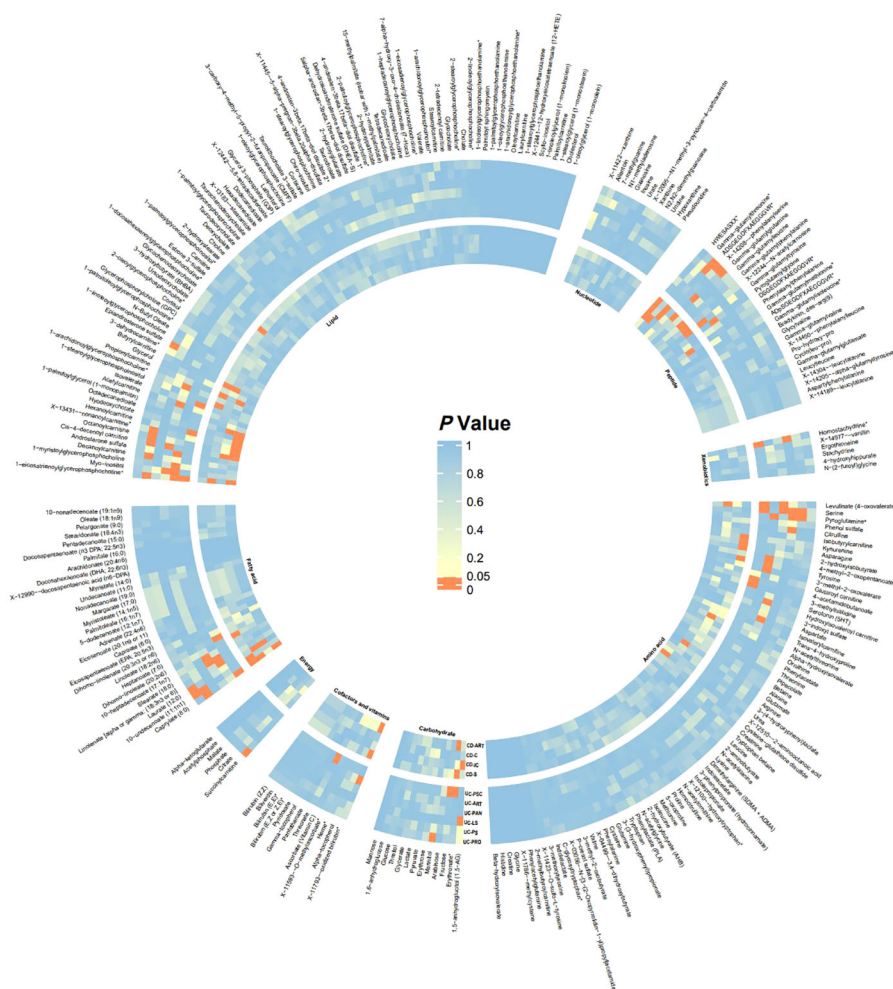


FIGURE 3

Heatmap of Significance in UVMR Analysis The heatmap displays the significance P-values of Mendelian randomization across different batches, with significant batches shown in red. From inner to outer circles are CD-ART, CD-C, CD-IC, CD-S, UC-PSC, UC-ART, UC-PAN, UC-LS, UC-PS, UC-PRO. Starting from the top left and proceeding clockwise, the groups are Lipid, Nucleotide, Peptide, Xenobiotics, Amino acid, Carbohydrate, Cofactors and vitamins, Energy, Fatty acid. CD-ART, Arthropathy in Crohn disease; CD-C, Crohn's disease of colon; CD-IC, Crohn's disease of ileocolon; CD-S, Crohn's disease of small intestine; UC-PSC, Ulcerative colitis with PSC; UC-ART, Arthropathy in ulcerative colitis; UC-PAN, Ulcerative pancolitis; UC-LS, Left-sided ulcerative colitis; UC-PS, Ulcerative rectosigmoiditis; UC-PRO, Ulcerative proctitis.

(PDAC) (44); It increases in lung cancer and decreases in tuberculosis, and can be used as a potential diagnostic marker to differentiate between lung cancer and tuberculosis (45). Phenylalanylphenylalanine and HWESASXX were also found to be causally associated with Crohn's disease of ileocolon. However, the mechanisms by which such metabolites affect IBD are not yet fully understood and further experimental explorations are needed.

Furthermore, there is a close relationship between lipid metabolism and IBD, with various fatty acids and lipid metabolites attenuating the expression of the  $TNF\alpha$  gene during the pathology of IBD, such as oleic acid, w-3 polyunsaturated fatty acids, arachidonic acid, and prostaglandins derived from phosphatidylcholine (46). Macrophages play a role in the pathogenesis of IBD through the  $cPLA2\alpha/COX-1$  pathway, which has been identified to have anti-inflammatory, immunomodulatory, intestinal microbiota-regulating, and barrier-maintaining effects (47). The existence of a causal relationship

between inositol and ulcerative proctitis may be due to the following reasons, Inositol and inositol phosphates have been shown to have a variety of health benefits such as anticancer, antidiabetic, antioxidant and anti-inflammatory (48). Specifically, inositol hexakisphosphate (IP6) reduces cell necrosis and pro-inflammatory cytokine mRNA release at sites of inflammation (49, 50), and myoIns likewise have the ability to downregulate inflammation and cytokine release (51). We hypothesized that inositol and phosphatidylinositol could protect against ulcerative proctitis by decreasing the local response to intestinal mucosal inflammation. Our study found a causal relationship between nonanoylcarnitine (nonanoylcarnitine) and IBD and related extraintestinal manifestations, and acylcarnitines were found to serve as an alternative energy source for oxidative metabolism in a study examining carnitine and its derivatives in relation to alterations in IBD flora. Acetylcarnitine dietary supplementation increases carnitine levels in the gut and promotes the recovery of

TABLE 2 Sensitivity analysis results.

Batch	Exposure	Outcomes	Univariate Analysis			Multivariate Analysis		
			$P_{\text{pleiotropy}}$	$P_{\text{heterogeneity}}$	Casual Direction	$P_{\text{pleiotropy}}$	$P_{\text{heterogeneity}}$	$P_{\text{WM}}$
2022	Myo-inositol	Ulcerative pancolitis	-	-	TRUE	0.917	0.126	0.009
731	Erythronate	Crohn's disease of small intestine	0.596	0.727	TRUE	0.811	0.082	0.041
2095	1-arachidonoylglycerophosphocholine	Ulcerative pancolitis	0.894	0.610	TRUE	0.677	0.344	0.026
438	HWESASXX	Crohn's disease of ileocolon	-	-	TRUE	0.443	0.025	0.011
548	Phenylalanylphenylalanine	Crohn's disease of ileocolon	0.980	0.998	TRUE	0.917	0.126	0.013
2270	Mannitol	Ulcerative proctitis	0.187	0.899	TRUE	0.568	0.191	0.013
374	1,5-anhydroglucitol	Crohn's disease of ileocolon	0.785	0.885	TRUE	0.811	0.082	0.154
1054	nonanoylcarnitine	Arthropathy in Crohn disease	-	-	TRUE	0.917	0.126	0.006
1178	3-methylhistidine	Ulcerative colitis with PSC	0.979	0.419	TRUE	0.265	0.871	0.173

TRUE Casual Direction indicates that the MR result passed the MR-Steiger forward causality test. Batches with less than 3 SNPs are not available for Cochran's Q test and MR-Egger intercept analysis. WM, weighted median method; PSC, Primary Sclerosing Cholangitis.

TABLE 3 Key metabolic pathways involved in the pathogenesis of IBD subtypes.

Pathway	Serum				Gut Microbiota		
	Both in MVMR and UVMR	Significant in UVMR	Outcomes	$P_{\text{Enrichment}}$	Matched pathway	Outcomes	$P_{\text{MR}}$
Histidine metabolism	3-Methylhistidine	L-Glutamic acid	UC-PSC, CD-C	0.010			
Valine, leucine and isoleucine biosynthesis	-	3-Methyl-2-oxovaleric acid, Ketoleucine	UC-ART	0.002	Super pathway of L-isoleucine biosynthesis I	UC-ART	0.002
Arginine biosynthesis	-	L-Glutamic acid, Citrulline	CD-C, UC-LS	0.007	Super pathway of arginine and polyamine biosynthesis	UC-LS	0.004
Aminoacyl-tRNA biosynthesis	-	L-Asparagine, L-Tyrosine, L-Glutamic acid	CD-C, CD-S	0.010			
Alanine, aspartate and glutamate metabolism	-	L-Asparagine, L-Glutamic acid	CD-C, CD-S	0.029	L-glutamate degradation V	CD-C	0.039
Phenylalanine, tyrosine and tryptophan biosynthesis	-	L-Tyrosine	CD-C	0.038			
Biosynthesis of unsaturated fatty acids	-	Stearic acid, Alpha-Linolenic acid	UC-ART	0.046			

CD-ART, Arthropathy in Crohn disease; CD-C, Crohn's disease of colon; CD-IC, Crohn's disease of ileocolon; CD-S, Crohn's disease of small intestine; UC-PSC, Ulcerative colitis with PSC; UC-ART, Arthropathy in ulcerative colitis; UC-PAN, Ulcerative pancolitis; UC-LS, Left-sided ulcerative colitis; UC-PS, Ulcerative rectosigmoiditis; UC-PRO, Ulcerative proctitis, UVMR, univariate MR; MVMR, multivariate MR.



TABLE 4 Evidence of the association between metabolites and IBD onset in previous literature.

Metabolites	Impact on IBD	PMID
Alanine, glutamine, histidine, leucine, phenylalanine, tyrosine, valine	Decreased levels of the aforementioned amino acids in the serum of CD and UC patients.	38156773
Omega-3 and omega-6 polyunsaturated fatty acids	Decreased levels of the aforementioned substances in the serum of CD patients. Decreased levels of ω-3 polyunsaturated fatty acids in the serum of UC patients.	37008284
Tetracosanoic acid, phosphatidylcholine (PC), lysophosphatidylcholine (LPC), sphingomyelin (SM), glycerides	Decreased levels of the aforementioned substances in the serum of colonic CD and UC patients. The levels of arachidonoyl ethanolamide, palmitoyl ethanolamide, branched fatty acid esters of hydroxy fatty acids (FAHFA), and three isomers of hexadecanoic acid (palmitoyl stearin, stearoyl palmitin, and stearin olein) were higher in colonic CD patients than in UC patients.	31368421
2-Arachidonoylglycerol	Increased levels of these substances can lead to a significant reduction in colitis and associated systemic and central inflammation.	21551239
Inositol and its phosphates	The aforementioned substances can inhibit inflammatory responses and carcinogenic effects in IBD.	33374769
1,5-Anhydroglucitol (1,5-AG), 1,5-Anhydroglucitol-6-phosphate (1,5-AG6P)	Toxic accumulation of the aforementioned substances can lead to reduced neutrophil counts, impaired neutrophil function, and a significant propensity for developing inflammatory bowel disease (IBD).	36507137

health in rodent models of enteropathogenic *Escherichia coli* infection (52). In the mouse experiments conducted by Lemons et al., it was found that consuming animal products rich in carnitine and acylcarnitines is associated with an increased risk of IBD (52). The mechanism of action here is not fully understood and still needs to be further explored.

Previous studies have indicated that 1,5-anhydroglucitol (1,5-AG) is a carbohydrate-like metabolite whose enzymatic side reaction produces 1,5-anhydroglucitol-6-phosphate (1,5-AG6P). 1,5-AG6P is a hexokinase inhibitor whose accumulation in cells inhibits the phosphorylation of glucose thereby affecting the glycolytic process. Neutrophils can suppress intestinal inflammation in IBD patients by modulating immune responses, oxidative stress, and generating pro-inflammatory cytokines, chemokines, and calprotectin (53). And since glycolysis is its only source of energy, an increase in 1,5-AG in the body may have unfavorable consequences for patients with Crohn’s disease of ileocolon through mechanisms that have not yet been clarified. Our study did confirm a causal relationship between 1,5-AG and the development of Crohn’s disease of ileocolon. Mannose, a monosaccharide *in vivo*, has been shown in mouse experiments to ameliorate colitis by strengthening tight junction proteins, inhibit

mitochondrial dysfunction during inflammation by enhancing lysosomal integrity, and limit the release of histone B for the purpose of maintaining homeostasis in the intestinal epithelium (54). Mannitol is a monosaccharide derivative, and in an *in vitro* assay conducted by Yanjun Guo et al. it was found that mannitol can induce vasorelaxation through hypertonicity as well as SKCa (Small-conductance Ca2+-activated K+ channels) and IKCa (Intermediate-conductance) mediated EDH (Endothelium dependent hyperpolarization); leading to vasorelaxation, which may play a key physiological role in enhancing postprandial small resistance vascular blood flow and thus intestinal perfusion (55). In the current study we found that mannitol reduced the risk of ulcerative proctitis, and we speculate that it may be related to the above mechanism, but further experimental verification is needed. In addition, we found that Erythronate (erythritol) as well as mannitol are causally related to IBD, but the exact mechanism is still unclear and needs to be further explored. It is noteworthy that both amino acid-related metabolites, peptide metabolites, lipid metabolites, and carbohydrate metabolites share a common pathway to exert a protective effect against IBD, i.e., modulation of different pro-inflammatory factors and inhibition of the body’s inflammatory response to exert a protective effect on the intestinal mucosa.

In the present study we also identified seven metabolic pathways associated with the 6 IBD subtypes and their extraintestinal manifestations, namely valine, leucine and isoleucine biosynthesis, arginine biosynthesis, histidine metabolism, aminoacyl-tRNA biosynthesis, alanine, aspartate and glutamate metabolism, phenylalanine, tyrosine and tryptophan biosynthesis and unsaturated fatty acid biosynthesis. Overlapping metabolic pathways between various IBD subtypes have also been identified. The arginine synthesis pathway is significantly associated with left-sided ulcerative colitis and Crohn’s disease of the large intestine. This pathway involves metabolites related to glutamate and arginine. Glutamate has been shown in previous models of inflammation to improve intestinal barrier function, alleviate inflammation, and inhibit protein degradation via the corticotropin-releasing hormone (CRH)/CRH receptor 1, toll-like receptor (TLR) 4, and nucleotide-binding oligo-structural domain protein (NOD)/NF-κB, as well as the mammalian target of rapamycin (mTOR) signaling pathways, which can exert a protective effect against IBD (56). The polyamine pathway of spermidine metabolism produces putrescine, spermidine and spermine that stimulate colonic epithelial cell growth and regulate epithelial cell apoptosis, with anti-apoptotic and pro-apoptotic effects (57). Histidine metabolism is regulated for inflammation as previously described. The biosynthesis of valine, leucine, and isoleucine is an important part of the branched-chain amino acids and may act as a modulator of intestinal development, nutrient transport, and immune-related functions, thereby improving intestinal health (58).

Epidemiologic evidence on the effect of polyunsaturated fatty acids (PUFA) on inflammatory bowel disease (IBD) is conflicting (59). In our study, we found that alpha-linolenic acid involved in this metabolic pathway had a mitigating effect on arthropathy associated with ulcerative colitis, but the results were not



sufficiently reliable and need to be verified by further studies. Pathways for histidine metabolism, aminoacyl-tRNA biosynthesis, alanine, aspartate, and glutamate metabolism, as well as biosynthesis with phenylalanine, tyrosine, and tryptophan are also present in a wide range of IBD outcomes involving glutamate, tyrosine, and aspartate.

This MR study has several strengths. First, to our knowledge, this is the first MR study to systematically assess the causal role of human blood metabolites in IBD subtypes and their parenteral manifestations. Second, we underwent rigorous instrumental variable screening and MR design, performed several sensitivity analyses and multivariate MR analyses to ensure robust results and explored independent blood metabolic markers. Finally, the dataset planning is also a major highlight, as we included datasets with European populations to minimize the error of results due to population bias. The large sample of the dataset also overcomes the sampling error brought about by the random effect. However, our study has some limitations. For example, some batches of SNP data were still pleiotropic after MR-PRESSO, and the conclusions obtained by MR-Egger may not be sufficiently robust. Second, the study population was focused on Europeans, so the conclusions cannot be generalized to larger populations for the time being. Third, since the ratio estimation method assumes linear causality, the present study cannot exclude that blood metabolites have a nonlinear relationship on outcome. Fourthly, due to the lack of relevant datasets, we stratified only by the sites of Crohn's disease, without stratifying by severity (stricturing, penetrating, perianal disease). Lastly, this study was confined to etiological exploration and did not extend to investigating the post-onset details of metabolites and IBD. Future research should follow the findings of this study to conduct prospective cohort studies with repeated measures, and dynamically monitor targeted levels of serum metabolites, in association with symptoms, CRP levels, etc., during active or remission phases, to further delineate the diagnostic and prognostic significance of specific blood metabolites.

## 5 Conclusion

Our study suggests that blood metabolites may influence the pathogenesis of inflammatory bowel disease (IBD) in a causal manner, specifically, 9 metabolites, including Erythrone, Myo-inositol, and Mannitol, may be biomarkers used in public health for screening and prevention of 10 IBD subtypes, as well as potential molecules for the study of the pathogenesis of IBD. Exploration of the Mechanisms of Novel Blood Metabolites in IBD may Provide New Diagnostic Insights for Patients with IBD.

## Data availability statement

The original contributions presented in the study are included in the article/Supplementary Material. Further inquiries can be directed to the corresponding author.

## Author contributions

FL: Writing – original draft. ZDW: Writing – original draft. TT: Writing – review & editing. QZ: Writing – review & editing. ZW: Writing – review & editing. XH: Writing – review & editing. ZX: Writing – review & editing. YC: Writing – review & editing. HL: Writing – review & editing. SH: Writing – review & editing. CY: Writing – review & editing. SC: Writing – review & editing. YL: Writing – review & editing. YL: Writing – review & editing.

## Funding

The author(s) declare financial support was received for the research, authorship, and/or publication of this article. The present study was supported by the Science and Technology Agency Jilin Province (grant nos. 20210402013GH and 20200201343JC).

## Acknowledgments

The authors would like to thank the IEU GWAS database and the FinnGen database for making the pooled data publicly available and giving us the opportunity to learn from it.

## Conflict of interest

The authors declare that the research was conducted in the absence of any commercial or financial relationships that could be construed as a potential conflict of interest.

## Publisher's note

All claims expressed in this article are solely those of the authors and do not necessarily represent those of their affiliated organizations, or those of the publisher, the editors and the reviewers. Any product that may be evaluated in this article, or claim that may be made by its manufacturer, is not guaranteed or endorsed by the publisher.

## Supplementary material

The Supplementary Material for this article can be found online at: <https://www.frontiersin.org/articles/10.3389/fendo.2024.1375896/full#supplementary-material>

### SUPPLEMENTARY TABLE 1

Dataset information included in MR studies.

### SUPPLEMENTARY TABLE 2

MR results for all batches.

### SUPPLEMENTARY TABLE 3

SNP information included in MR studies.

## SUPPLEMENTARY TABLE 4

SNP information related to confounding factors.

## SUPPLEMENTARY TABLE 5

MR-Steiger test results for SNPs.

## SUPPLEMENTARY TABLE 6

Cochrane Q-test results for all batches.

## SUPPLEMENTARY TABLE 7

Results of pleiotropic tests for all batches.

## SUPPLEMENTARY TABLE 8

MR results for GM pathway on IBD subtypes.

## SUPPLEMENTARY FILE

Calculation codes for mendelian randomization analysis.

## SUPPLEMENTARY FIGURE 1

Forest Plots.

## SUPPLEMENTARY FIGURE 2

Scatter Plots.

## SUPPLEMENTARY FIGURE 3

Leave-one-out Plots.

## SUPPLEMENTARY FIGURE 4

Funnel Plots.

## References

- Zhang YZ, Li YY. Inflammatory bowel disease: pathogenesis. *World J Gastroenterol.* (2014) 20:91–9. doi: 10.3748/wjg.v20.i1.91
- Pierre N, Salee C, Vieujean S, Bequet E, Merli AM, Siegmund B, et al. Review article: distinctions between ileal and colonic crohn's disease: from physiology to pathology. *Aliment Pharmacol Ther.* (2021) 54:779–91. doi: 10.1111/apt.16536
- Dulai PS, Singh S, Vande Castele N, Boland BS, Rivera-Nieves J, Ernst PB, et al. Should we divide crohn's disease into ileum-dominant and isolated colonic diseases? *Clin Gastroenterol Hepatol.* (2019) 17:2634–43. doi: 10.1016/j.cgh.2019.04.040
- Satsangi J, Silverberg MS, Vermeire S, Colombel JF. The montreal classification of inflammatory bowel disease: controversies, consensus, and implications. *Gut.* (2006) 55:749–53. doi: 10.1136/gut.2005.082909
- Ho GT, Nimmo ER, Tenesa A, Fennell J, Drummond H, Mowat C, et al. Allelic variations of the multidrug resistance gene determine susceptibility and disease behavior in ulcerative colitis. *Gastroenterology.* (2005) 128:288–96. doi: 10.1053/j.gastro.2004.11.019
- Joossens S, Reinisch W, Vermeire S, Sendid B, Poulain D, Peeters M, et al. The value of serologic markers in indeterminate colitis: A prospective follow-up study. *Gastroenterology.* (2002) 122:1242–7. doi: 10.1053/gast.2002.32980
- Aranake-Chrisinger J, Dassopoulos T, Yan Y, Nalbantoglu I. Primary sclerosing cholangitis associated colitis: characterization of clinical, histologic features, and their associations with liver transplantation. *World J Gastroenterol.* (2020) 26:4126–39. doi: 10.3748/wjg.v26.i28.4126
- Kumar A, Lukin D, Battat R, Schwartzman M, Mandl LA, Scherl E, et al. Defining the phenotype, pathogenesis and treatment of crohn's disease associated spondyloarthritis. *J Gastroenterol.* (2020) 55:667–78. doi: 10.1007/s00535-020-01692-w
- Aldars-Garcia L, Gisbert JP, Chaparro M. Metabolomics insights into inflammatory bowel disease: A comprehensive review. *Pharm (Basel).* (2021) 14, 1190. doi: 10.3390/ph14111190
- Schicho R, Shaykhtudinov R, Ngo J, Nazyrova A, Schneider C, Panaccione R, et al. Quantitative metabolomic profiling of serum, plasma, and urine by (1)H nmr spectroscopy discriminates between patients with inflammatory bowel disease and healthy individuals. *J Proteome Res.* (2012) 11:3344–57. doi: 10.1021/pr300139q
- Scoville EA, Allaman MM, Brown CT, Motley AK, Horst SN, Williams CS, et al. Alterations in lipid, amino acid, and energy metabolism distinguish crohn's disease from ulcerative colitis and control subjects by serum metabolomic profiling. *Metabolomics.* (2018) 14:17. doi: 10.1007/s11306-017-1311-y
- Williams HR, Willmsore JD, Cox IJ, Walker DG, Cobbold JF, Taylor-Robinson SD, et al. Serum metabolomic profiling in inflammatory bowel disease. *Dig Dis Sci.* (2012) 57:2157–65. doi: 10.1007/s10620-012-2127-2
- Dawiskiba T, Deja S, Mulak A, Zabek A, Jawien E, Pawelka D, et al. Serum and urine metabolomic fingerprinting in diagnostics of inflammatory bowel diseases. *World J Gastroenterol.* (2014) 20:163–74. doi: 10.3748/wjg.v20.i1.163
- Shin SY, Fauman EB, Petersen AK, Krumsiek J, Santos R, Huang J, et al. An atlas of genetic influences on human blood metabolites. *Nat Genet.* (2014) 46:543–50. doi: 10.1038/ng.2982
- Kurki MI, Karjalainen J, Palta P, Sipila TP, Kristiansson K, Donner KM, et al. Finngen provides genetic insights from a well-phenotyped isolated population. *Nature.* (2023) 613:508–18. doi: 10.1038/s41586-022-05473-8
- Emdin CA, Khera AV, Kathiresan S. Mendelian randomization. *JAMA.* (2017) 318:1925–6. doi: 10.1001/jama.2017.17219
- Staley JR, Blackshaw J, Kamat MA, Ellis S, Surendran P, Sun BB, et al. Phenoscanner: A database of human genotype-phenotype associations. *Bioinformatics.* (2016) 32:3207–9. doi: 10.1093/bioinformatics/btw373
- Li F, Liu Y, Wang Z, Zhao Q, Li Y, Tang T. A mendelian randomization study with populations of european ancestry rules out a causal relationship between inflammatory bowel disease and colorectal cancer. *Front Genet.* (2022) 13:949325. doi: 10.3389/fgene.2022.949325
- Thomas DC, Conti DV. Commentary: the concept of 'Mendelian randomization'. *Int J Epidemiol.* (2004) 33:21–5. doi: 10.1093/ije/dyh048
- Burgess S, Butterworth A, Thompson SG. Mendelian randomization analysis with multiple genetic variants using summarized data. *Genet Epidemiol.* (2013) 37:658–65. doi: 10.1002/gepi.21758
- Burgess S, Davey Smith G, Davies NM, Dudbridge F, Gill D, Glymour MM, et al. Guidelines for performing mendelian randomization investigations. *Wellcome Open Res.* (2019) 4:186. doi: 10.12688/wellcomeopenres.15555.2
- Bowden J, Davey Smith G, Haycock PC, Burgess S. Consistent estimation in mendelian randomization with some invalid instruments using a weighted median estimator. *Genet Epidemiol.* (2016) 40:304–14. doi: 10.1002/gepi.21965
- Hemani G, Tilling K, Davey Smith G. Orienting the causal relationship between imprecisely measured traits using gwas summary data. *PloS Genet.* (2017) 13:e1007081. doi: 10.1371/journal.pgen.1007081
- Burgess S, Thompson SG. Interpreting findings from mendelian randomization using the mr-egger method. *Eur J Epidemiol.* (2017) 32:377–89. doi: 10.1007/s10654-017-0255-x
- Bowden J, Del Greco MF, Minelli C, Davey Smith G, Sheehan NA, Thompson JR. Assessing the suitability of summary data for two-sample mendelian randomization analyses using mr-egger regression: the role of the I2 statistic. *Int J Epidemiol.* (2016) 45:1961–74. doi: 10.1093/ije/dyw220
- Burgess S. Sample size and power calculations in mendelian randomization with a single instrumental variable and a binary outcome. *Int J Epidemiol.* (2014) 43:922–9. doi: 10.1093/ije/dyu005
- Lavelle A, Sokol H. Gut microbiota-derived metabolites as key actors in inflammatory bowel disease. *Nat Rev Gastroenterol Hepatol.* (2020) 17:223–37. doi: 10.1038/s41575-019-0258-z
- Zhang T, Cao Y, Zhao J, Yao J, Liu G. Assessing the causal effect of genetically predicted metabolites and metabolic pathways on stroke. *J Transl Med.* (2023) 21:822. doi: 10.1186/s12967-023-04677-4
- He XX, Li YH, Yan PG, Meng XC, Chen CY, Li KM, et al. Relationship between clinical features and intestinal microbiota in chinese patients with ulcerative colitis. *World J Gastroenterol.* (2021) 27:4722–37. doi: 10.3748/wjg.v27.i28.4722
- Baur P, Martin FP, Gruber L, Bosco N, Brahmabhatt V, Collino S, et al. Metabolic phenotyping of the crohn's disease-like ibd etiopathology in the tnfr(Deltaare/wt) mouse model. *J Proteome Res.* (2011) 10:5523–35. doi: 10.1021/pr2007973
- Schwarzler J, Mayr L, Vich Vila A, Grabherr F, Niederreiter L, Philipp M, et al. Pufa-induced metabolic enteritis as a fuel for crohn's disease. *Gastroenterology.* (2022) 162:1690–704. doi: 10.1053/j.gastro.2022.01.004
- Danese S, Furfaro F, Vetrano S. Targeting S1p in inflammatory bowel disease: new avenues for modulating intestinal leukocyte migration. *J Crohns Colitis.* (2018) 12: S678–S86. doi: 10.1093/ecco-jcc/jjx107
- Zholudev A, Zurakowski D, Young W, Leichtner A, Bousvaros A. Serologic testing with anca, asca, and anti-omp in children and young adults with crohn's disease and ulcerative colitis: diagnostic value and correlation with disease phenotype. *Am J Gastroenterol.* (2004) 99:2235–41. doi: 10.1111/j.1572-0241.2004.40369.x
- Baumgart M, Dogan B, Rishniw M, Weitzman G, Bosworth B, Yantiss R, et al. Culture independent analysis of ileal mucosa reveals a selective increase in invasive escherichia coli of novel phylogeny relative to depletion of clostridiales in crohn's disease involving the ileum. *ISME J.* (2007) 1:403–18. doi: 10.1038/ismej.2007.52
- Darfeuille-Michaud A, Boudeau J, Bulois P, Neut C, Glasser AL, Barnich N, et al. High prevalence of adherent-invasive escherichia coli associated with ileal mucosa in crohn's disease. *Gastroenterology.* (2004) 127:412–21. doi: 10.1053/j.gastro.2004.04.061

36. Morgan XC, Tickle TL, Sokol H, Gevers D, Devaney KL, Ward DV, et al. Dysfunction of the intestinal microbiome in inflammatory bowel disease and treatment. *Genome Biol.* (2012) 13:R79. doi: 10.1186/gb-2012-13-9-r79
37. Mussini E, Cornelio F, Dworzak F, Cotellessa L, Morandi L, Colombo L, et al. Content of methylhistidines in normal and pathological human skeletal muscles. *Muscle Nerve.* (1983) 6:423–9. doi: 10.1002/mus.880060605
38. Jutel M, Akdis M, Akdis CA. Histamine, histamine receptors and their role in immune pathology. *Clin Exp Allergy.* (2009) 39:1786–800. doi: 10.1111/j.1365-2222.2009.03374.x
39. Son DO, Satsu H, Shimizu M. Histidine inhibits oxidative stress- and tnfr-alpha-induced interleukin-8 secretion in intestinal epithelial cells. *FEBS Lett.* (2005) 579:4671–7. doi: 10.1016/j.febslet.2005.07.038
40. Andou A, Hisamatsu T, Okamoto S, Chinen H, Kamada N, Kobayashi T, et al. Dietary histidine ameliorates murine colitis by inhibition of proinflammatory cytokine production from macrophages. *Gastroenterology.* (2009) 136:564–74.e2. doi: 10.1053/j.gastro.2008.09.062
41. Hisamatsu T, Ono N, Imaizumi A, Mori M, Suzuki H, Uo M, et al. Decreased plasma histidine level predicts risk of relapse in patients with ulcerative colitis in remission. *PLoS One.* (2015) 10:e0140716. doi: 10.1371/journal.pone.0140716
42. Duarte Villas Mishima M, Stampini Duarte Martino H, Silva Meneguelli T, Tako E. Effect of food derived bioactive peptides on gut health and inflammatory mediators in vivo: A systematic review. *Crit Rev Food Sci Nutr.* (2023), 1–11. doi: 10.1080/10408398.2023.2245469
43. Lv R, Sun N, Mao C, Zheng Z, Lin S. Prevention and potential repair of colitis: beneficial effects and regulatory mechanisms of food-derived anti-inflammatory peptides. *Crit Rev Food Sci Nutr.* (2023), 1–19. doi: 10.1080/10408398.2023.2197068
44. Stolzenberg-Solomon R, Derkach A, Moore S, Weinstein SJ, Albanes D, Sampson J. Associations between metabolites and pancreatic cancer risk in a large prospective epidemiological study. *Gut.* (2020) 69:2008–15. doi: 10.1136/gutjnl-2019-319811
45. Chen S, Li C, Qin Z, Song L, Zhang S, Sun C, et al. Serum metabolomic profiles for distinguishing lung cancer from pulmonary tuberculosis: identification of rapid and noninvasive biomarker. *J Infect Dis.* (2023) 228:1154–65. doi: 10.1093/infdis/jiad175
46. Astudillo AM, Rodriguez JP, Guijas C, Rubio JM, Balboa MA, Balsinde J. Choline glycerophospholipid-derived prostaglandins attenuate tnfralpha gene expression in macrophages via a cpla(2)Alpha/cox-1 pathway. *Cells.* (2021) 10, 447. doi: 10.3390/cells10020447
47. Yan D, Ye S, He Y, Wang S, Xiao Y, Xiang X, et al. Fatty acids and lipid mediators in inflammatory bowel disease: from mechanism to treatment. *Front Immunol.* (2023) 14:1286667. doi: 10.3389/fimmu.2023.1286667
48. Chatree S, Thongmaen N, Tantivejkul K, Sitticharoon C, Vucenik I. Role of inositols and inositol phosphates in energy metabolism. *Molecules.* (2020) 25, 5079. doi: 10.3390/molecules25215079
49. Silva EO, Bracarense AP. Phytic acid: from antinutritional to multiple protection factor of organic systems. *J Food Sci.* (2016) 81:R1357–62. doi: 10.1111/1750-3841.13320
50. Bizzarri M, Lagana AS, Aragona D, Unfer V. Inositol and pulmonary function. Could myo-inositol treatment downregulate inflammation and cytokine release syndrome in sars-cov-2? *Eur Rev Med Pharmacol Sci.* (2020) 24:3426–32. doi: 10.26355/eurrev\_202003\_20715
51. Chen C, Chen K, Su T, Zhang B, Li G, Pan J, et al. Myo-inositol-1-phosphate synthase (Ino-1) functions as a protection mechanism in corynebacterium glutamicum under oxidative stress. *Microbiologopen.* (2019) 8:e00721. doi: 10.1002/mbo3.721
52. Lemons JMS, Conrad M, Tanes C, Chen J, Friedman ES, Roggiani M, et al. Enterobacteriaceae growth promotion by intestinal acylcarnitines, a biomarker of dysbiosis in inflammatory bowel disease. *Cell Mol Gastroenterol Hepatol.* (2024) 17:131–48. doi: 10.1016/j.jcmgh.2023.09.005
53. Li G, Lin J, Zhang C, Gao H, Lu H, Gao X, et al. Microbiota metabolite butyrate constrains neutrophil functions and ameliorates mucosal inflammation in inflammatory bowel disease. *Gut Microbes.* (2021) 13:1968257. doi: 10.1080/19490976.2021.1968257
54. Dong L, Xie J, Wang Y, Jiang H, Chen K, Li D, et al. Mannose ameliorates experimental colitis by protecting intestinal barrier integrity. *Nat Commun.* (2022) 13:4804. doi: 10.1038/s41467-022-32505-8
55. Guo Y, Lu C, Zhang L, Wan H, Jiang E, Chen Y, et al. Nutrient-induced hyperosmosis evokes vasorelaxation via trpv1 channel-mediated, endothelium-dependent, hyperpolarization in healthy and colitis mice. *Br J Pharmacol.* (2021) 178:689–708. doi: 10.1111/bph.15322
56. Liu Y, Wang X, Hu CA. Therapeutic potential of amino acids in inflammatory bowel disease. *Nutrients.* (2017) 9, 920. doi: 10.3390/nu9090920
57. Li JY, Guo YC, Zhou HF, Yue TT, Wang FX, Sun F, et al. Arginine metabolism regulates the pathogenesis of inflammatory bowel disease. *Nutr Rev.* (2023) 81:578–86. doi: 10.1093/nutrit/nuac070
58. Nie C, He T, Zhang W, Zhang G, Ma X. Branched chain amino acids: beyond nutrition metabolism. *Int J Mol Sci.* (2018) 19, 954. doi: 10.3390/ijms19040954
59. Jia X, Hu C, Wu X, Qi H, Lin L, Xu M, et al. Evaluating the effects of omega-3 polyunsaturated fatty acids on inflammatory bowel disease via circulating metabolites: A mediation mendelian randomization study. *Metabolites.* (2023) 13, 1041. doi: 10.3390/metabo13101041

# Frontiers in Molecular Biosciences

Explores biological processes in living organisms  
on a molecular scale

Focuses on the molecular mechanisms  
underpinning and regulating biological processes  
in organisms across all branches of life.

## Discover the latest Research Topics

[See more →](#)

### Frontiers

Avenue du Tribunal-Fédéral 34  
1005 Lausanne, Switzerland  
[frontiersin.org](https://frontiersin.org)

### Contact us

+41 (0)21 510 17 00  
[frontiersin.org/about/contact](https://frontiersin.org/about/contact)



### Frontiers in Molecular Biosciences

